ROLL PRESSURE DISTRIBUTION IN STRIP ROLLING

by

STEPHEN ROBERT BRADBURY B.Sc

A thesis submitted to the COUNCIL FOR NATIONAL ACADEMIC AWARDS

in partial fulfilment for the degree of DOCTOR OF PHILOSOPHY

Sponsoring Establishment: Department of Mechanical and
Production Engineering
Sheffield City Polytechnic
Sheffield 1

Collaborating Establishment: Davy McKee Plc
Prince of Wales Road
Sheffield 9

December 1986

ABSTRACT

ROLL PRESSURE DISTRIBUTION IN STRIP ROLLING

S R Bradbury

The determination of the pressure distribution generated along the arc of contact between the rolls and workpiece during the rolling process has been a subject of interest to researchers for many years. Existing rolling theories make assumptions and include simplifications which are not often substantiated by direct measurement techniques in which pressure transducers are located within the roll surfaces. Such techniques are effective but prohibitively expensive since they render the rolls useless for rolling.

A technique has been developed in which the pressure distribution and roll separating load are determined from consideration of the elastic deformation of the rolls during operation. By interrupting a rolling pass before completion, the shapes of the deformed rolls are imparted to the workpiece surface. Accurate measurement of the imparted profiles at several sections across the width of the workpiece allows the extent of the elastic deformation of the roll to be determined. An analytical solution based on solid body contact theory was used to determine the pressure distribution responsible for the elastic deformation along each section. The solution incorporates experimentally determined parameters and functions relating to specific mill-stands and schedules.

Initial experimental work was undertaken in which the proposed technique was applied to the quasi-static indentation of flat and inclined strip specimens. Having established the basic features of the method relating to these modes of deformation the technique was then applied to the cold rolling process in the form of interrupted rolling passes.

Tests were undertaken using a two-high laboratory rolling mill reducing the thickness of mild steel strip workpieces. Comparisons between the predicted pressure profiles using the technique developed and those determined by others using pressure transducers show close similarities. A comparison between the predicted roll separating loads and those determined experimentally show a reasonable correlation.

ACKNOWLEDGEMENTS

The author wishes to express his gratitude to Dr M S J Hashmi, Director of Studies, for his encouragement and helpful supervision during the course of this project. Thanks are also expressed to Dr M S Ali and Mr D R Howard for their constructive suggestions and comments.

The technical assistance offered by Mr R Teasdale and his staff was much appreciated and in particular the author wishes to thank Messrs M Jackson, S Leigh, R Sidebottom and R Wilkinson for their valued contributions at various stages of this work.

Finally to Mrs S Saunby for typing the thesis.

ABSTRACT

ROLL PRESSURE DISTRIBUTION IN STRIP ROLLING

S R Bradbury

The determination of the pressure distribution generated along the arc of contact between the rolls and workpiece during the rolling process has been a subject of interest to researchers for many years. Existing rolling theories make assumptions and include simplifications which are not often substantiated by direct measurement techniques in which pressure transducers are located within the roll surfaces. Such techniques are effective but prohibitively expensive since they render the rolls useless for rolling.

A technique has been developed in which the pressure distribution and roll separating load are determined from consideration of the elastic deformation of the rolls during operation. By interrupting a rolling pass before completion, the shapes of the deformed rolls are imparted to the workpiece surface. Accurate measurement of the imparted profiles at several sections across the width of the workpiece allows the extent of the elastic deformation of the roll to be determined. An analytical solution based on solid body contact theory was used to determine the pressure distribution responsible for the elastic deformation along each section. The solution incorporates experimentally determined parameters and functions relating to specific mill-stands and schedules.

Initial experimental work was undertaken in which the proposed technique was applied to the quasi-static indentation of flat and inclined strip specimens. Having established the basic features of the method relating to these modes of deformation the technique was then applied to the cold rolling process in the form of interrupted rolling passes.

Tests were undertaken using a two-high laboratory rolling mill reducing the thickness of mild steel strip workpieces. Comparisons between the predicted pressure profiles using the technique developed and those determined by others using pressure transducers show close similarities. A comparison between the predicted roll separating loads and those determined experimentally show a reasonable correlation.

CONTENTS **Page**

INDEX TO FIGURES

INDEX TO PLATES

CHAPTER 1

INTRODUCTION

1.1 The Rolling Process

Rolling is one of the most widely used forming processes for both the hot and cold working of metals and alloys and by far the most commonly used process for producing strips and plates.

In its most fundamental form, the process involves passing a workpiece between two hard cylindrical rolls, revolving with the same angular velocities but in opposite directions. The distance between the rolls is somewhat less than the thickness of the workpiece and consequently plastic deformation of the workpiece ensues as it passes through the gap between the rolls. For the process to operate effectively the rolls must 'bite' the workpiece material when it is fed into the roll gap, thus, unlike most other forming processes, a certain amount of frictional constraint must be present at the tool and workpiece interface. As reduction is implemented, pressure distributions are generated along the interfaces between the rolls and workpiece which attempt to separate rolls. This action has been schematically represented in figure 1.1.

The primary purposes of the rolling process are:

(i) The reduction of workpieces to desired gauge thicknesses with high repeatability.

(ii) The attainment of a satisfactory surface finish.

(iii) The attainment of desired metallurgical properties.

The implementation of (i) is constrained by the maximum operating load of a mill-stand, hence when attaining large reductions or when rolling hard materials it necessitates passing the material through several mills with progressively reducing roll gaps.

The mill operator endeavours to make the transformations from stock material to the finished strip or plate by the most economical method. This generally means that each pass is executed at the maximum safe operating load of each mill-stand, so obtaining the total reduction by the minimum number of passes. Application of these optimised conditions necessitates prior knowledge of the roll separating force required to produce a known reduction in a given material by a specific mill-stand. The roll separating force is normally derived from the pressure distribution at the interface between the rolls and workpiece.

1.2 Historical Development of Analytical and Numerical Solutions to the Rolling Process

Since the early years of this century, considerable efforts have been made by many researchers in the quest to accurately analyse both the hot and cold rolling processes. In 1925, von Karman[(1)*] published the first noteworthy mathematical analysis of the rolling process in which he considered the equilibrium of an element of workpiece material within the roll bite. His analysis included the assumptions that:

(i) The arcs of contact between the rolls and stock material remain circular in profile.

(ii) The coefficient of friction remains constant over the whole contact region.

* Numbers in brackets as superscripts refer to references found at the end of the text.

(iii) Elastic compression within the deformation zone is negligible.

(iv) Plane strain compression conditions ensue.

(v) The yielding of the workpiece material obeys von Mises yield criterion.

(vi) Stress is independent of workpiece thickness.

Research derived from the von Karman equations included notable work by Hitchcock(2), published in 1935 and by Nadai(3), published in 1939, whose investigations produced refinements to the analysis with regard to the length of contact arc and frictional behaviour, respectively.

Orowan(4), in his paper published in 1943, suggested that all previous authors had undermined the validity of their work by including unsubstantiated mathematical approximations. In developing his numerical and graphical techniques for determining the pressure distribution along the arc of contact between the rolls and workpiece, he discarded as many approximations as possible. He developed two analytical techniques:

(i) Simplified analysis including assumptions of homogenous deformation and slipping friction.

(ii) Comprehensive analysis including a compensatory factor for inhomogenous deformation.

Correlation with experimentally determined data was slightly improved with (ii), however its practical applicability was severely limited by the excessive computations required for solution.

Work by authors such as Bland, Ford and Sims and their collaborators[5-13] between 1948 and 1956 attempted to hasten the calculating process but their simplified approaches did not significantly improve accuracy.

Simulation of inhomogenous deformation of the workpiece between the rolls was attempted using a slip-line field approach[14-18] but reliable solutions proved unobtainable.

In a review of rolling analyses in 1975, Sansome[19] concluded that there were reasonable methods available for calculating the roll separating force for a wide range of rolling conditions, however, because of the number of variables and the rapidity at which these variables change during the rolling process, a purely analytical solution would be unlikely to be derived which would be adequate for continuous control.

In recent years the technological advancement of both computer hardware and software has enabled the mathematical modelling of the rolling process to be approached in greater depth. In 1972, Alexander[20] published a comprehensive solution to von Karman's equations[1] using a Runge-Kutta process. The advent of large deformation elastic-plastic finite element computer programs/ packages has enabled the study of various aspects of the rolling process to be undertaken in detail. Many workers have devised or adapted elastic-plastic, rigid-plastic, visco-plastic and elasto-visco-plastic finite element techniques to simulate aspects of the rolling process in one, two and three dimensions.[21-39] However two considerable disadvantages are associated with this form of numerical solution:

(i) The need for expensive computing facilities with back-up services.

(ii) The wide ranging variability of the rolling parameters from the considered conditions.

1.3 Historical Development of Empirical Solutions to the Rolling Process

Resulting from experimental investigations pioneered by Siebel and Leug[40] et al and their collaborators between 1925 and 1935, the measurement of the pressure distribution between roll and strip was achieved by inserting a 2 x 2mm piezo-electric crystal into the surface of the roll. Despite requiring substantial correction factors, the results were used by notable authors such as Orowan[4] to assess the merits of their analytical solutions.

Other pioneering investigations considered strain distributions within the workpiece material during the rolling process. MacGregor and his co-researchers analysed this topic by experiments in which grids were scribed onto the surface of the workpiece preceeding deformation,[41] and by attaching electrical resistive strain gauges.[42]

In 1952, Smith et al[43] applied a photoelastic technique to determine the pressure distribution across the roll gap by using a photoelastic dynamometer fitted to a 0.7mm radial pin. These investigations were used to determine the errors associated with pin protrusion, exemplified within the works of Siebel and Leug.[40] Other relevant photoelastic techniques involved the analysis of epoxyresin rolls when rolling epoxyresin strip (Ohashi et al[44] in 1964) and lead strip (Khyyat and Lancaster[45] in 1969).

In 1967, Matsuura and Motomura[46] updated the direct measurement techniques developed by Siebel and Leug[40] by inserting smaller and more reliable pressure transducers into the roll surface. The pressure distribution profiles and lengths of contact arc showed considerable discrepancies with theoretically derived values. An investigation by Al-Salehi et al[47] in 1973 arrived at similar conclusions.

The merits of the purely analytical theories were brought further into question by Kobasa and Schultz[48] whose high-speed photographic technique showed large discrepancies between the photographed and evaluated lengths of contact arc derived from Hitchcock's analysis.[2]

Recent investigations have included visio-plastic analysis of photographed grids on the sides of strip specimens by Thompson[49] in 1982; and analysis of the variation of the coefficient of friction within the roll gap using an optical method of reflected caustics (light reflected from a grid on plexiglas rolls and projected onto a reference screen) by Theocaris et al[50] in 1982. Neither of these techniques have achieved success to date.

1.4 Scope of the Present Work

A general assessment of the purely analytical approaches to modelling the pressure distribution and separating load generated during the rolling process suggest that further refinements are required to improve correlation with direct measurement techniques over a wider range of rolling conditions. However, a widely applicable analytical solution remains unlikely due to the complexity and variability of the parameters involved (ie friction, geometric configuration and material properties).

Direct measurement techniques in which pressure transducers are located in the roll surfaces, appear the only reliable method of determining the pressure distribution. A series of tests would provide valid results for a certain roll size, but the roll could no longer be used for strip production. Consequently, applying such a technique to a complete range of rolls would be prohibitively expensive.

A technique for estimating the pressure distribution and separating load which includes aspects of both analytical and empirical forms of approach, is under investigation by the present author in association with the research and development section of Davy McKee Plc of Sheffield. An analytical solution is used which incorporates empirical functions derived from non-destructive tests relating to a specific mill stand or rolling schedule. This technique should enable the determination of the required parameters to reasonable accuracies without destroying the rolls, and consequently be of real value in both research and production activities.

The investigation considers the elastic deformation of the rolls at the interface with the deforming workpiece. Interruption of a rolling pass before completion would result in the basic shapes of the elastically deformed rolls being retained in the workpiece surfaces. By accurate measurement of the imparted profiles along the arcs of contact at different sections across the width of the upper and lower surfaces of the workpiece, and correcting for the elastic recovery of the material, deformed roll profiles would be established. The extent of the elastic deformation along each section can be established in a discretised form by superposition of the rigid roll profile. Solid body contact theory used by Timoshenko and Goodier[51] can be adapted and applied to determine the magnitudes of the individual pressure bands directly responsible for part of the displacement at each element, and the influential displacements of neighbouring elements.

Implementation of the analysis requires that initial tests be undertaken to determine the extent of the inter-element influences relating to specific configurations and loading conditions. Values derived from the tests (in the form of constants) can be correlated and presented as empirical relationships. These relationships will be capable of estimating the appropriate values when considering process conditions the same, or similar to those of the tests. By relating such tests to a specific mill configuration or rolling schedule empirical relationships can be derived and be incorporated in a computer program to predict the pressure distributions and separating loads appertaining to the same or similar rolling conditions.

The current investigation has been approached by considering the following modes of deformation:

(i) Quasi-static indentation of flat strip specimens by a cylindrical indentor under vertical loading.

(ii) Quasi-static indentation of inclined strip specimens by a cylindrical indentor under vertical loading.

(iii) Deformation of workpieces by interrupting passes during cold strip rolling.

Each mode is schematically illustrated in figures 1.2(a) to (c).

It was considered by the present author that the development of the methods relating to conditions (i) and (ii) would be valuable when establishing the techniques required to simulate the pressure behaviour in (iii).

The principal objectives of the work programme related to each deformation mode are to:

(i) Formulate an analytical solution based on the theory of solid body contact mechanics to estimate the pressure distributions and separating loads generated at the interface between the tool and workpiece.

(ii) Develop and implement the experimental techniques necessary for the determination of the influence constant values.

(iii) Formulate computer programs for the determination of influence constant values, and the prediction of pressure distributions and separating loads.

(iv) Assess the capabilities of the computer programs.

(v) In relation to the interrupted rolling pass deformation mode, an assessment of the overall capabilities of the technique and the potential practical applicability.

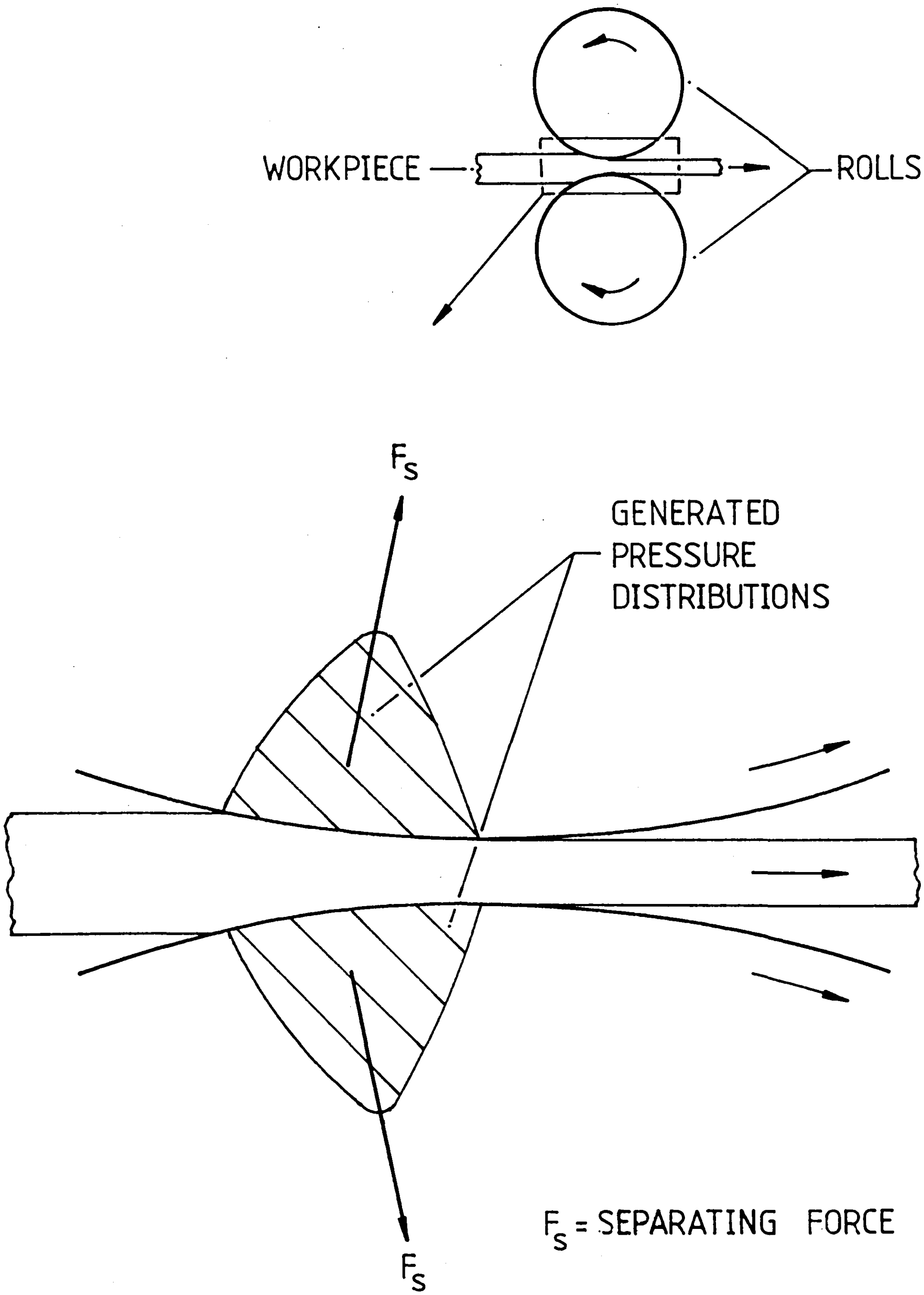

FIG 1.1 : SCHEMATIC REPRESENTATION OF PRESSURE GENERATION DURING THE COLD ROLLING PROCESS

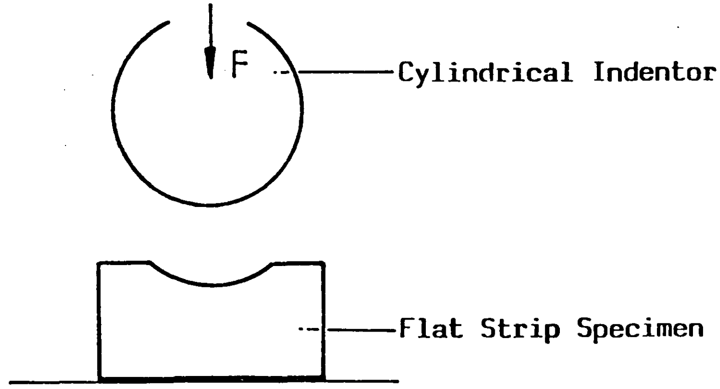

FIG 1.2(a) : SCHEMATIC REPRESENTATION OF THE MODE FOR THE INDENTATION OF FLAT SPECIMENS

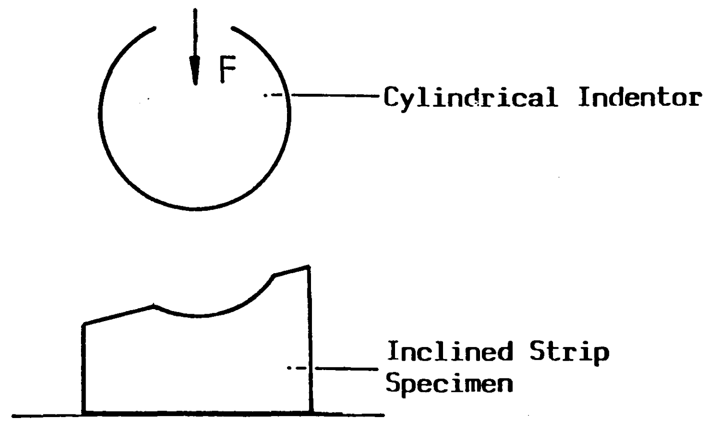

FIG 1.2(b) : SCHEMATIC REPRESENTATION OF THE MODE FOR THE INDENTATION OF INCLINED SPECIMENS

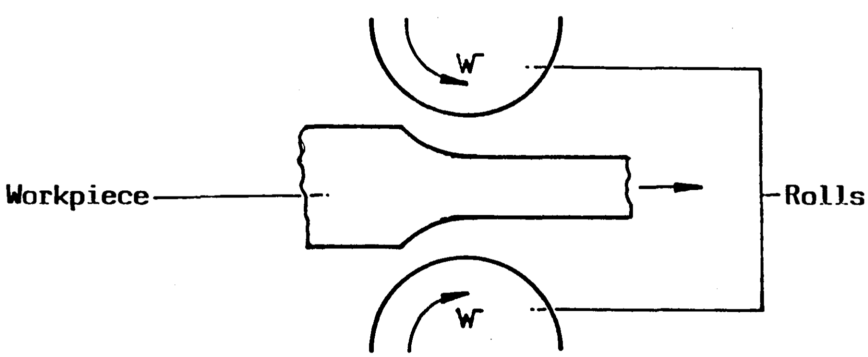

FIG 1.2(c) : SCHEMATIC REPRESENTATION OF THE MODE FOR THE INTERRUPTED-PASS ROLLING TESTS

CHAPTER 2

DESCRIPTION AND OPERATION OF THE EXPERIMENTAL EQUIPMENT

2.1 The Static Indentation Experiments

2.1.1 Introduction to the Experimental Equipment

The indentation of both the flat and inclined strip specimens were carried out using a standard Denison Servo-Hydraulic Universal Testing Machine of 500kN capacity (tensile or compressive), fitted with a jig purposefully designed for the experimentations. The principal functions of the jig were to guide and transmit a compressive force generated by the Denison through to the interface between the strip specimen and a cylindrical indentor. During each test, the application of the force resulted in the plastic deformation of the strip material and the elastic deformation of the indentor material along the contact interface.

The jig contains a rigid rectangular frame screwed onto a base plate. The base plate is covered by a hardened steel plate onto which the undeformed strip specimen is centrally located by aligning with scribed lines. Slots machined vertically in opposing sides of the frame allow a selected indentor to be inserted to rest directly upon the specimen. The indentor is restrained by a solid block (ram), which in turn is constrained by the sides of the machined slots and centrally locates onto the ram of the

Denison. The configuration of the jig is schematically illustrated in figure 2.1, and the direction of each moving part is shown.

The applied load was directly read from the load indicator on the Denison. During the tests values ranged from a minimum of 100kN to a maximum of 450kN.

The vertical displacement of the indentor, and the recovered displacement of the indentor and strip were measured by inductive displacement transducers located at each end of the indentor. Plates 2.1, 2.2 and 2.4 pictorially illustrate the test equipment during operation.

2.1.2 Description and Fabrication of the Jig Body Assembly

The configuration of the jig body is illustrated in figure 2.1 and plate 2.2. En8 mild steel was used for fabrication apart from the ram and base plate cover which are made from the appreciably harder En24 steel (VPN249) so as to minimise deformation of these parts during operation.

In fabricating the jig body, extra care was taken with the following features:

(a) Grinding the upper and lower surfaces of the base plate and base plate cover parallel in order to ensure that the test specimens were located normal to the direction of applied load.

(b) Machining the slots in the frame sides perpendicular to the edge affixed to the base plate to ensure a normal approach by the ram.

(c) Boring the recess centrally and ensuring that the arms of the ram were symmetrical to ensure balanced loading of the ram.

Figures 2.2 and 2.3 show dimensional details of the jig frame and ram.

2.1.3 Description and Fabrication of the Indentor Assemblies

Initial static indentation tests were carried out using a 75mm diameter and a 100mm diameter En9 steel indentor (Surface Hardness VPN193). Each cylindrical indentor had two smaller cylindrical necks protruding axially from the main body. Holes drilled and tapped axially into the necks allow extension pins to be inserted, onto which the pins of the displacement transducers locate. Figures 2.4(a) and 2.4(b) show the dimensional details of the indentor assemblies.

In fabricating the indentor assemblies, care was taken with the following features:

(a) Grinding of the final diameter to be accomplished to within a tolerance of ± 0.02mm with a smooth finish.

(b) Roundness and cylindricality of each indentor.

The initial roundness errors associated with the indentor bodies were found to be less than 3μm and are chronicled in figures 2.5(a) and (b).

Roundness tests were carried out using a Taylor Hobson roundness tester (type Talyrond with reference computer). In establishing the uniformity of roundness along the length of an indentor body measurements were taken at three sections; centrally and close to both ends.

To ensure that the roundness condition did not significantly deteriorate during testing, measurements were repeated following every ten tests.

2.1.4 Description and Preparation of the Specimens

Annealed En43A steel strip was used for both the flat and inclined specimens (Surface hardness VPN104-119). The strip was annealed to increase the difference in hardness with the indentor material.

In preparing the specimens the following guidelines were adhered to:

(a) Grinding of both the upper and lower surfaces of each specimen to a parallel and smooth finish to aid profile measurement (Chapter 3) and to attain the specified angle of inclination to within a small tolerance. (The angle of each inclined specimen is measured optically using an Angle Dekkor).

(b) Grinding the upper surface by taking cuts fine so as not to radically alter the micro-structural properties of the strip material.

A selection of deformed and undeformed strip specimens are shown in plate 2.3 and they are dimensionally detailed in figures 2.6(a) and (b).

2.1.5 Description of the Displacement Measuring System

Inductive displacement transducers (Sangamo-Weston type DG1, 2mm stroke, linearity 0.1%) were used to monitor the vertical movement at each end of the indentor during testing. A displacement transducer and housing assembly is illustrated pictorially in plate 2.4. Activated by an operational source voltage of 10 Volts, each transducer is connected to a digital voltmeter from which the displacement values are interpolated, using a calibrated conversion factor (volts to millimeters).

2.1.6 Modifications to the Rig

The indentation of flat strip specimens have been satisfactorily implemented using the rig as described in sections 2.1.1 to 2.1.5. Related analyses presented in this study are based on experiments employing the rig in this format.

For the indentation of inclined strip specimens three significant modifications were enforced:

(a) The nature of the reaction between the indentor and inclined specimen surface would produce a horizontal component of force. This would physically move the specimen if the frictional forces at the interface between the specimen and base plate cover were overcome. To prevent this possibility a thin strip of metal (referred to in the text as the stopper plate) was secured to the base plate cover. During operation the specimen abuts the stopper plate, restraining lateral movement of the lower surface while allowing strain displacements associated with the deformation zone on the upper surface to continue unimpeded.

(b) The thickness of the strip material was increased from approximately 9mm to 20mm. This reduced any influential effects which the reactions between the specimen and base plate cover (and stopper plate) may have had upon the development of the indentor profiles.

(c) Following the flat specimen tests the surface condition and roundness of the indentors were deemed unsatisfactory for further usage. New indentors were fabricated to similar dimensions using En24 steel. Initial roundness analyses for the indentors are shown in figures 2.7(a) and (b).

The different indentor material properties will have a minimal effect since the analyses only require knowledge of the Young's modulus and Poisson's ratio. The small variations between the values of these elastic properties corresponding to the En9 and En24 steels are insignificant when considered in the context of the total analysis. Consequently, comparative assessments between the results obtained from flat and inclined indentation tests will remain valid.

2.1.7 Experimental Procedure for the Static Indentation Tests

The experimental work associated with the indentation of flat and inclined specimens were carried out in three distinct stages. Methods adopted during each stage are fully itemized below:

(a) Location of the specimen within the jig and connection to the displacement measuring system.

(i) Remove ram from the jig body.

(ii) Place the undeformed specimen on the base plate cover. For flat specimens align the centre markings with those on the plate surface. Let inclined specimens butt against the stopper plate.

(iii) Adjust the specimen until centred with respect to the jig sides.

(iv) Semi-rigidly secure the specimen with strips of plasticine (this ensures no accidental movement of the specimen prior to loading).

(v) Place the required indentor into the recess in the jig body so that it rests upon the specimen.

(vi) Replace the ram so that its arm rests centrally upon the indentor necks.

(vii) Screw the extension pins into the indentor necks.

(viii) Place the inductive displacement transducers into their respective housings; allow their pins to rest upon the extension pins.

(ix) Connect the displacement transducers to the digital voltmeters and supply voltage source.

(b) Location of the rig upon the Denison anvil and the final adjustments.

(i) Place the loaded rig upon the Denison anvil.

(ii) Lock the Denison strain advance wheel (turn clockwise) and reduce the pace setting slider to zero.

(iii) Select the required loading scale (maximum 50kN, 100kN, 250kN or 500kN) ensuring that the required scale is 'locked' correctly.

(iv) Switch on power.

(v) Advance pace setting slider, lowering the Denison platform towards the rig.

(vi) When the Denison ram is approximately 2mm above the ram, halt the advance of the pace setting slider.

(vii) Accurately place the recess in the ram beneath the Denison ram.

(viii) Slowly lower the Denison ram into the recess. Halt before load is applied to the ram.

(ix) Adjust and secure both displacement transducers such that the voltmeter readings are equal (+2V for zero roll displacement).

(c) Indentation and removal of the specimen.

(i) Slowly advance the pace setting slider until the required load is reached.

(ii) Read and note the applied load from the indicator on the Denison.

(iii) Read and note the voltages from the digital voltmeters.

(iv) Release the load (turn strain advance wheel anticlockwise) and raise the Denison arm a sufficient distance so as to remove the rig.

(v) Disconnect and remove the displacement transducers.

(vi) Remove the ram.

(vii) Remove the extension pins and indentor.

(viii) Remove and examine the indented test specimen.

(ix) Mark the specimen with the appropriate identification code.

Following the final test, raise the upper platform of the Denison to its maximum limit and switch power off.

2.2 The Interrupted-Pass Rolling Experiments

2.2.1 The Experimental Equipment

The interrupted-pass rolling tests were carried out using a Farmer Norton two-high laboratory reversing mill (type 683BE), powered by a 230V, 80HP d.c. motor. The mill is fitted with a pair of tempered steel cold rolls, 304.8mm (12 inches) wide and 254mm (10 inches) in diameter. The general layout of the mill is shown in plate 2.5.

During the experimental testing, the separating force acting on the upper roll was measured for a controlled reduction in the strip thickness. The strip thickness was monitored by an indicator of the Taylor Hobson flying micrometer type. The separating force was measured by strain gauge type load cells, which are located below the mill screws above each end of the upper roll.

2.2.2 Instrumentation of the Load Cells

The layout of the instrumentation used to monitor the signals from the load cells is shown in plate 2.6, and a schematic block diagram of the system is shown in figure 2.8. The signal from each load cell was fed into a Mini-balance and a Mini-amplifier unit (types Fylde 492BBS and 251GA, respectively), with the strain gauges being activated by a 5V d.c. supply. The signal from each load cell was balanced at no load conditions so that the output is zero for zero load. The output from the strain gauges in each load cell were in milli-volts and so the mini-amplifiers were used to increase the strength of the signals by a gain of 1000. The amplified signals were fed through two channels of a chart recorder (type Rikadenki Multi-Pen Recorder R-10 series) which produces a load/time trace for each load cell. A typical load/time trace is shown in figure 2.9. It was possible to determine the values of load from such traces, when using suitable calibration curves.

2.2.3 Calibration of the Load Cells and Strip Thickness Indicator

Before testing, the load cells and instrumentation were removed from the mill and calibrated using a 500kN Denison Servo-Hydraulic Universal Testing Machine. The calibration curves for both load cells are shown in figure 2.10.

The strip thickness indicator was calibrated in situ on the mill. A strip of similar dimensions to those under investigation was deformed at the required reductions. The indicator setting and the actual reduced strip thickness values were compared. The calibration curves are shown in figure 2.11.

2.2.4 The Preparation and the Deformed Shape of the Strip Specimens

Annealed En2 steel strip was used for the test specimens (surface hardness VPN85-117), and are dimensionally detailed in figure 2.12. The upper and lower surfaces have a ground surface finish to aid the measurement of the partially deformed profiles.

During the experimental testing each strip was subjected to a series of interrupted reductions. The resulting deformation patterns along a strip are illustrated in plate 2.7, and compared with an undeformed strip. The experimental procedure adopted in carrying out these reductions are discussed in the following sub-section.

2.2.5 Experimental Procedures for the Interrupted-Pass Rolling Tests

The procedure adopted for the interrupted reductions of a single strip is listed below. However, at each strip thickness setting a series of strips with varying widths were reduced.

(i) Balance the output signal from each load cell.

(ii) Set the strip thickness indicator to the required reduction.

(iii) Start the forward rotation of the rolls.

(iv) Start the load/time trace.

(v) Feed the strip between the rolls and advance to terminal position.

(vi) Stop, then reverse the direction of rotation of the rolls and remove the strip.

(vii) Stop the rolls and the load/time trace.

(viii) Measure the reduced strip thickness with a micrometer, and measure the surface hardness.

(ix) Repeat stages (ii) to (viii) for the remaining reductions, taking care to separate the pass terminal positions.

(x) Separate each terminal region along the strip length, and identify it .

Displacement Measuring
Assembly Omitted

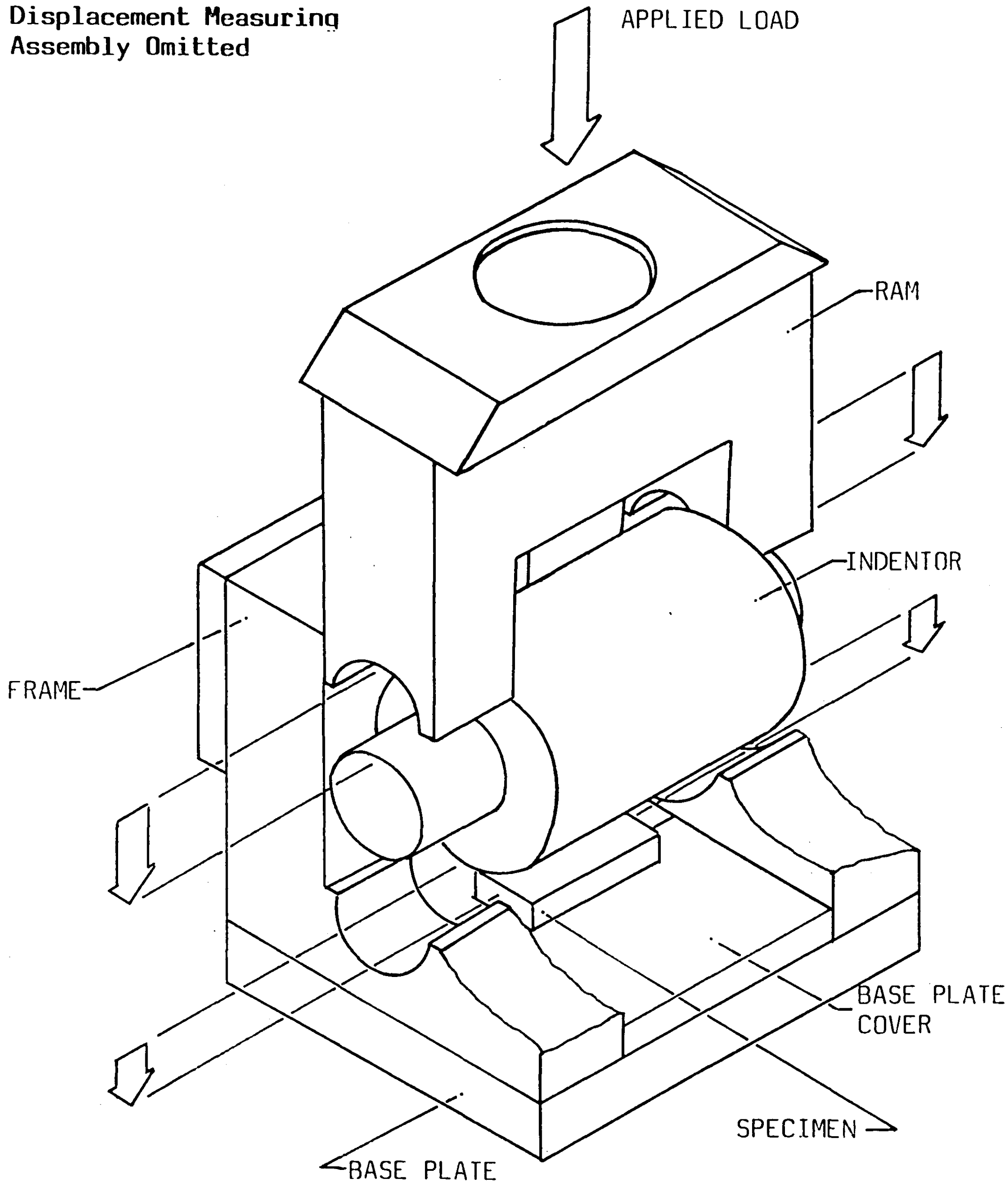

FIG 2.1 : STATIC INDENTATION RIG ASSEMBLY

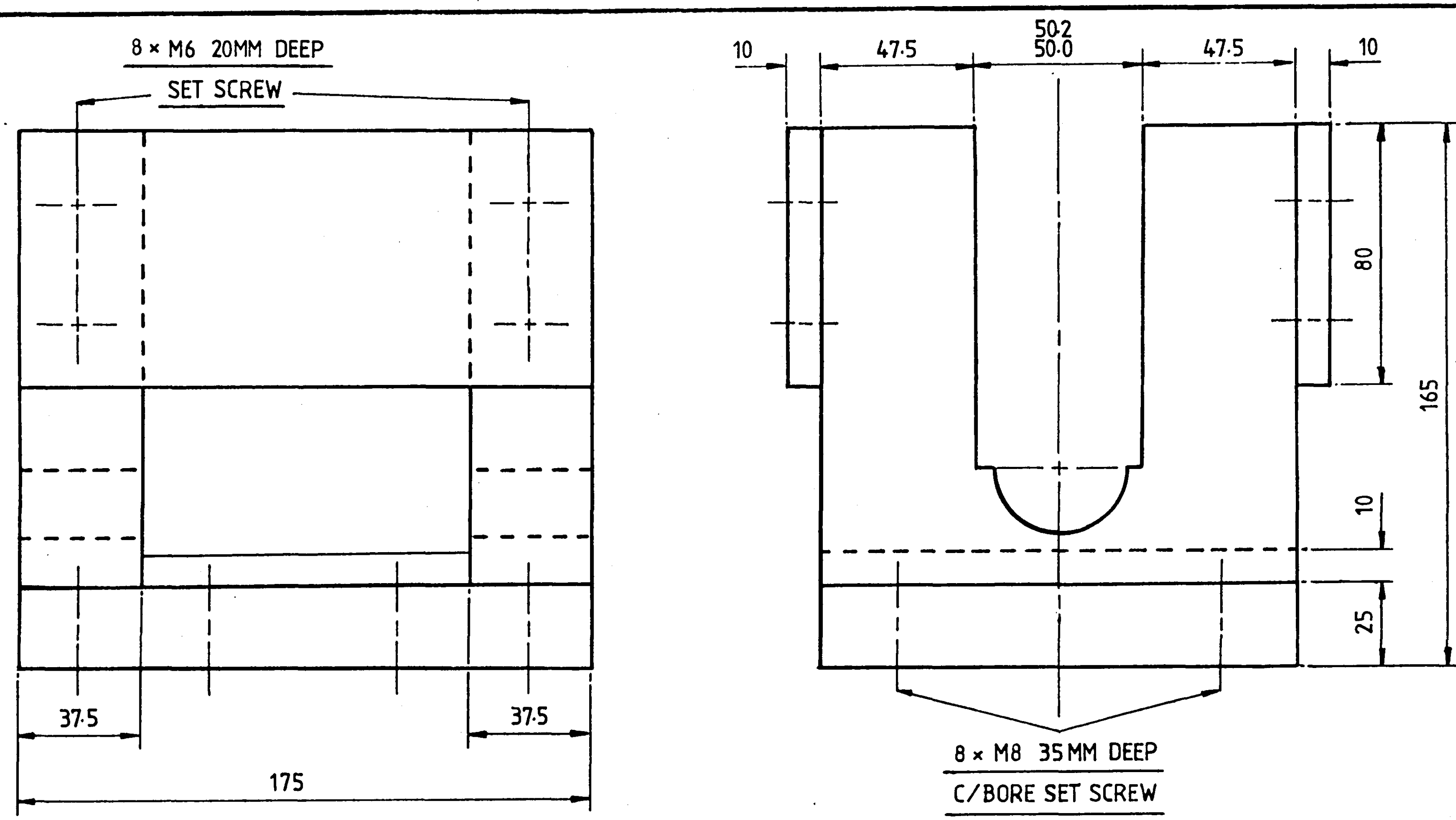

FIG 2.2 : STATIC INDENTATION JIG FRAME

All Dimensions in mm

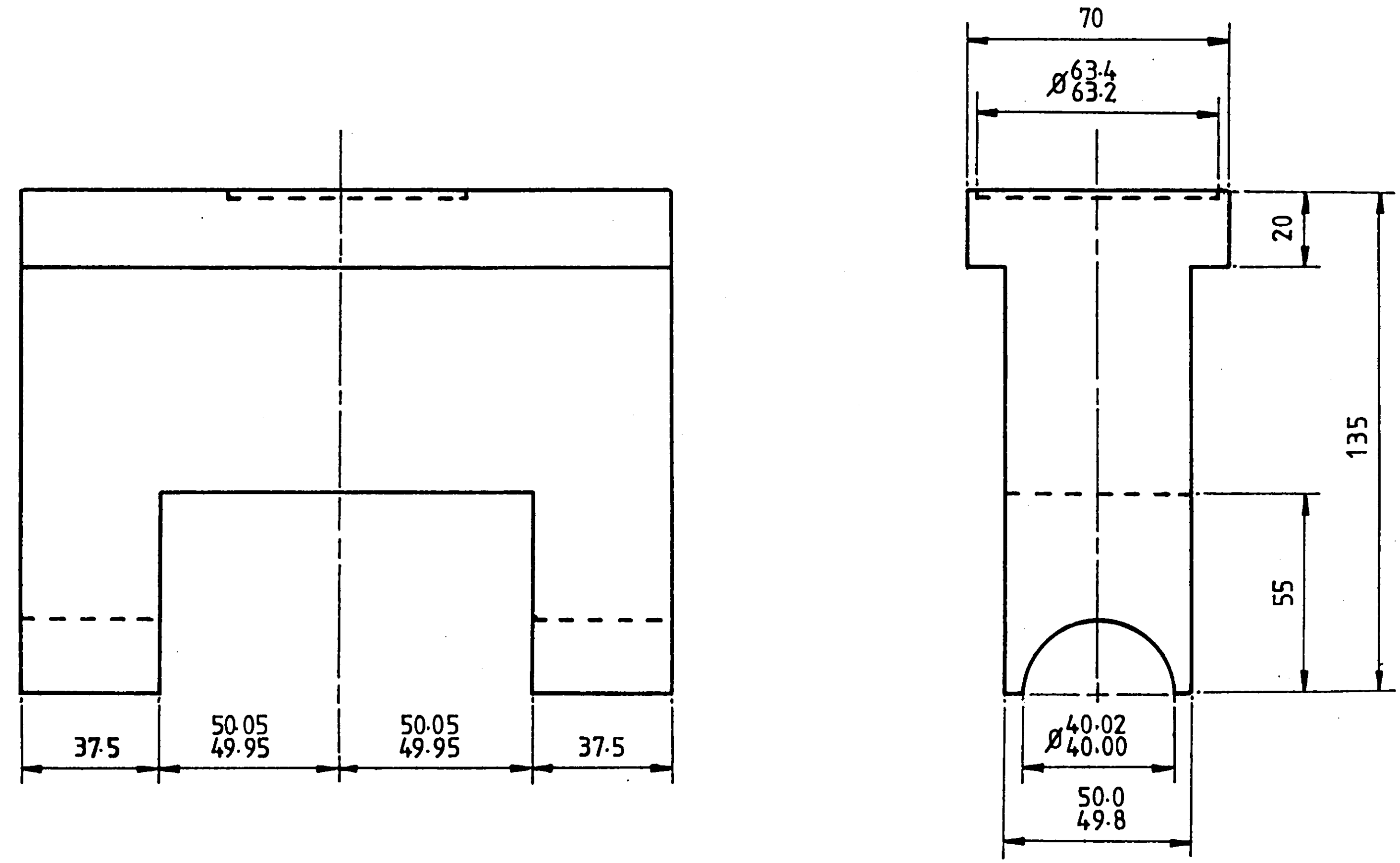

FIG 2.3 : STATIC INDENTATION RAM

All Dimensions in mm

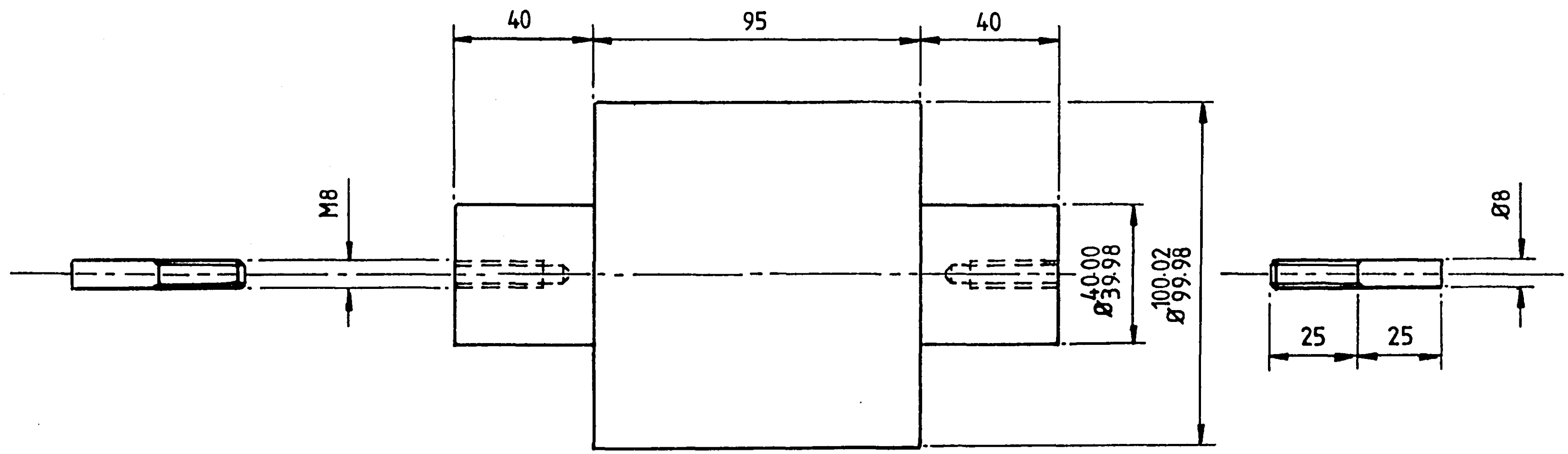

FIG 2.4(a) : 100mm Ø STATIC INDENTOR ASSEMBLY

All Dimensions in mm

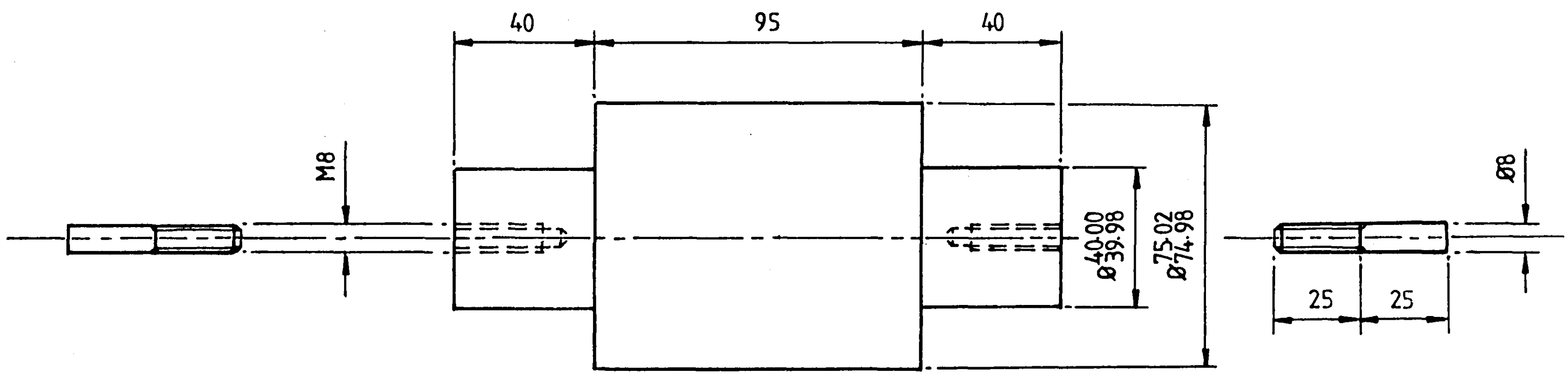

FIG 2.4(b) : 75mm Ø STATIC INDENTOR ASSEMBLY

All Dimensions in mm

FIG 2.5(a) : INITIAL ROUNDNESS PROFILES OF THE 100mm Ø En9 STEEL INDENTOR

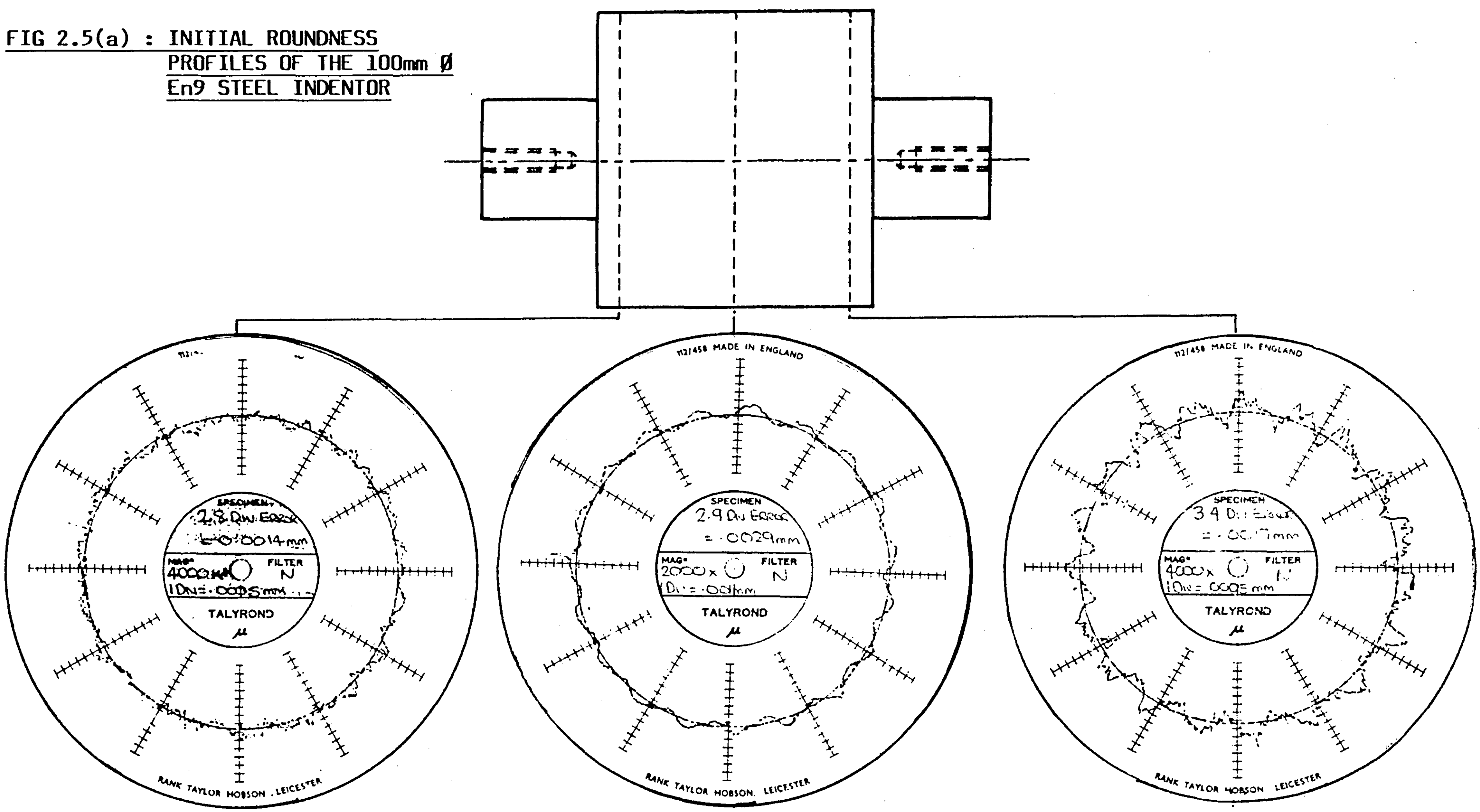

FIG 2.5(b) : INITIAL ROUNDNESS PROFILES OF THE 75mm O En9 STEEL INDENTOR

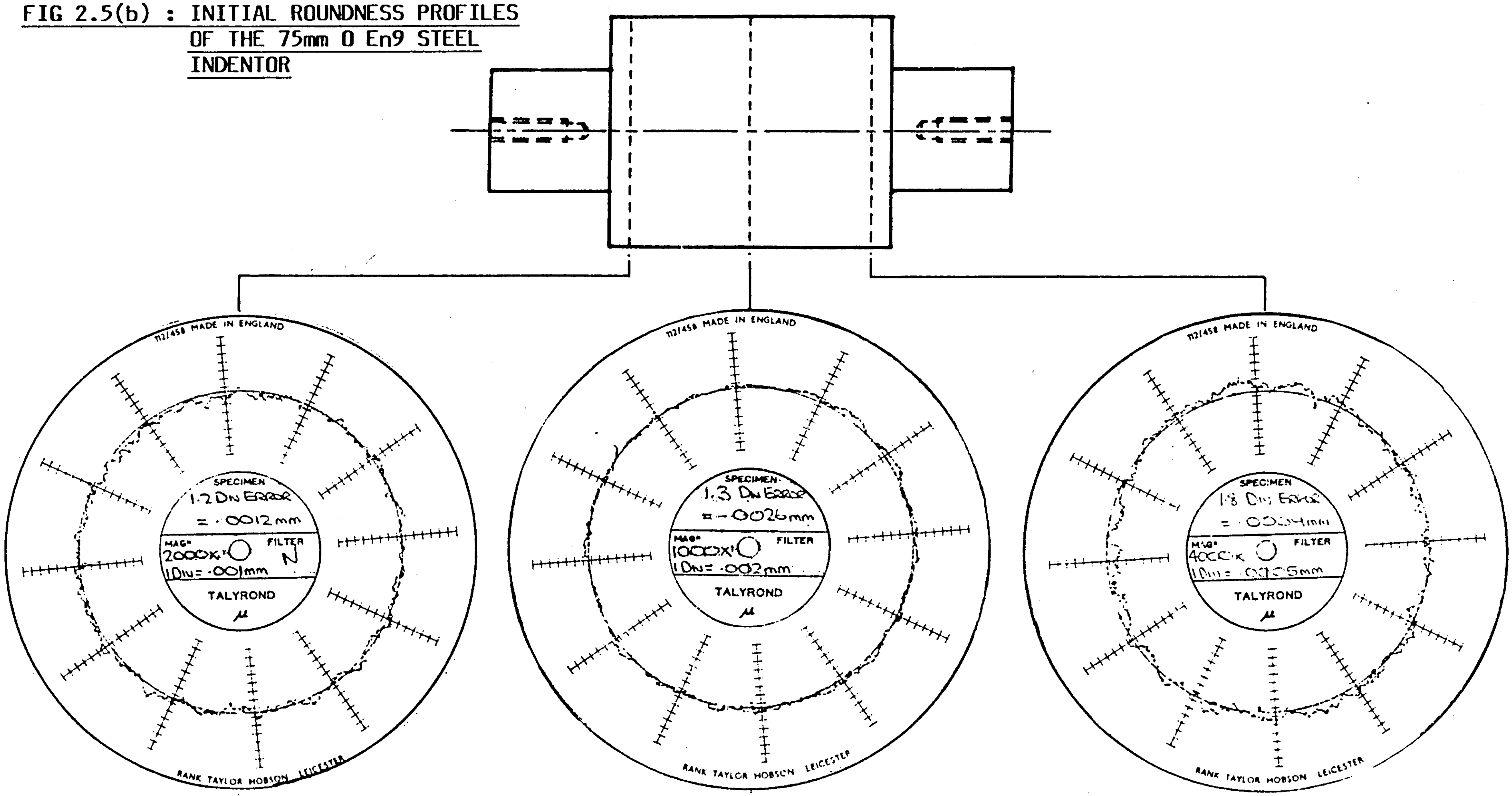

FIG 2.6(a) : FLAT STRIP SPECIMENS

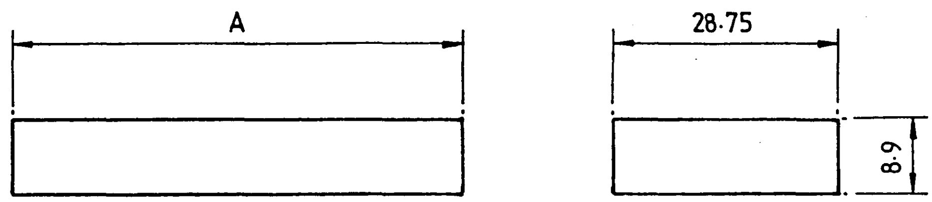

DIMENSION A = 30-70

All Dimensions in mm

FIG 2.6(b) : INCLINED STRIP SPECIMENS

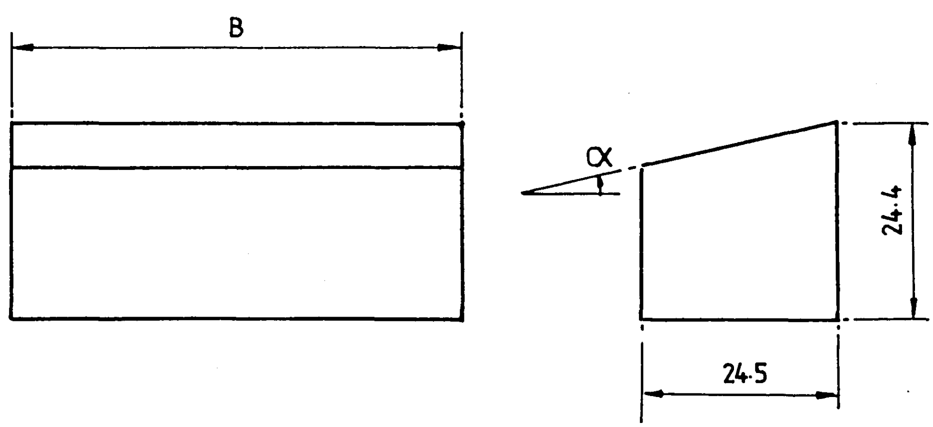

DIMENSION B = 30-60 (Increment 10)

ANGLE α = 5°-15° (Increment 5°)

All Dimensions in mm

FIG 2·7(a) : INITIAL ROUNDNESS PROFILES OF THE 100mm Ø En24 STEEL INDENTOR

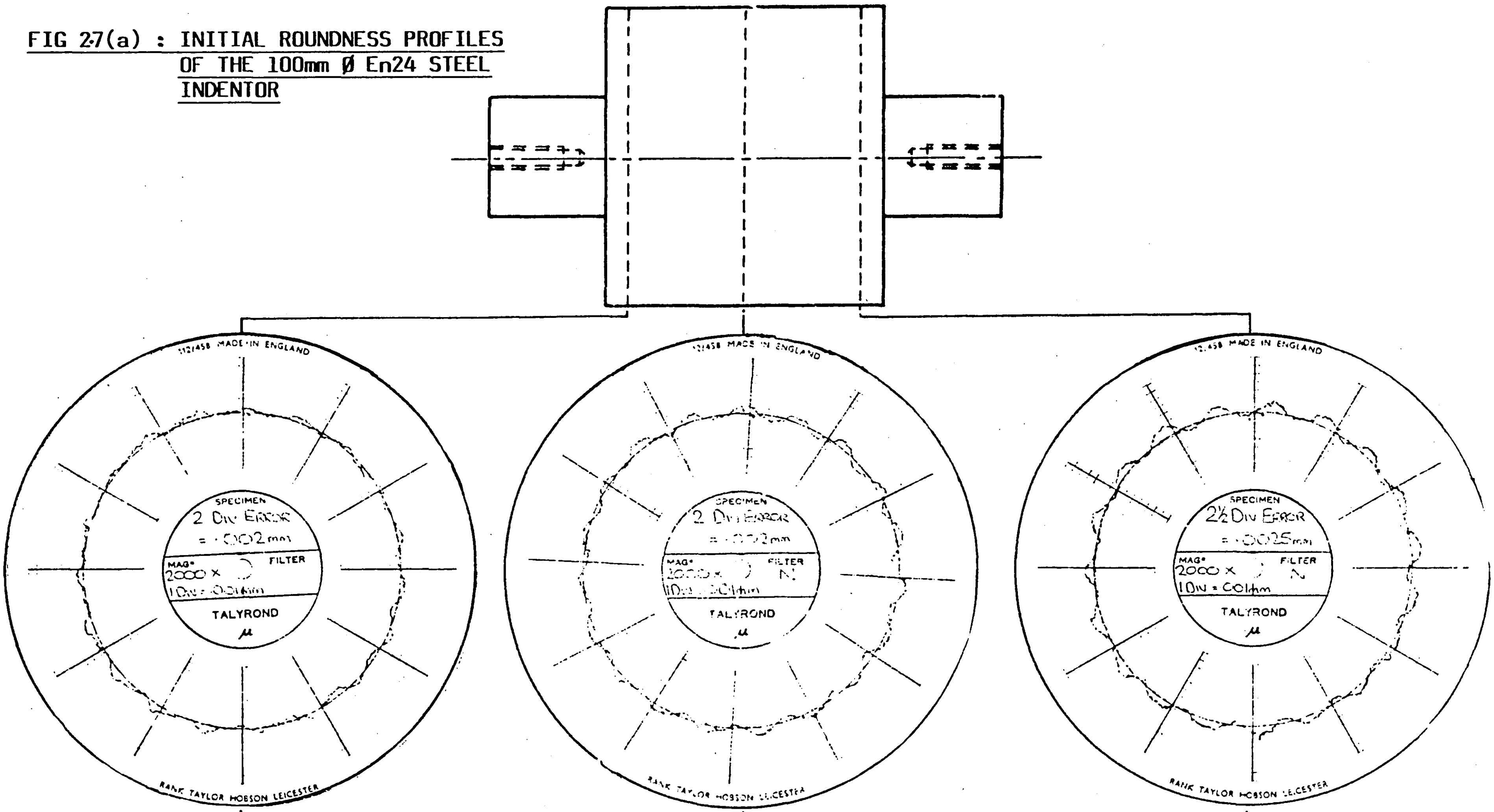

FIG 2.7(b) : INITIAL ROUNDNESS PROFILES OF THE 75mm Ø En24 STEEL INDENTOR

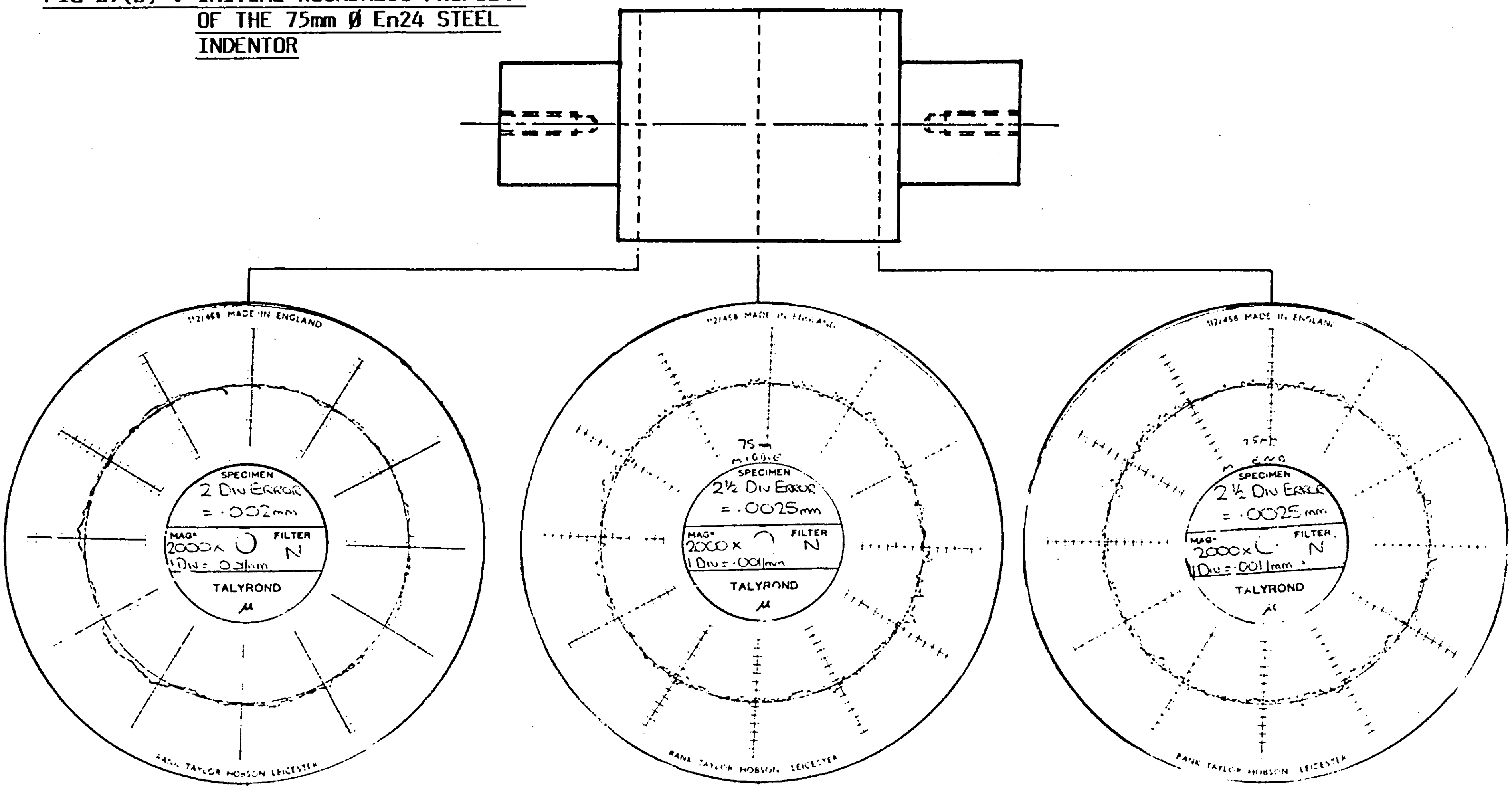

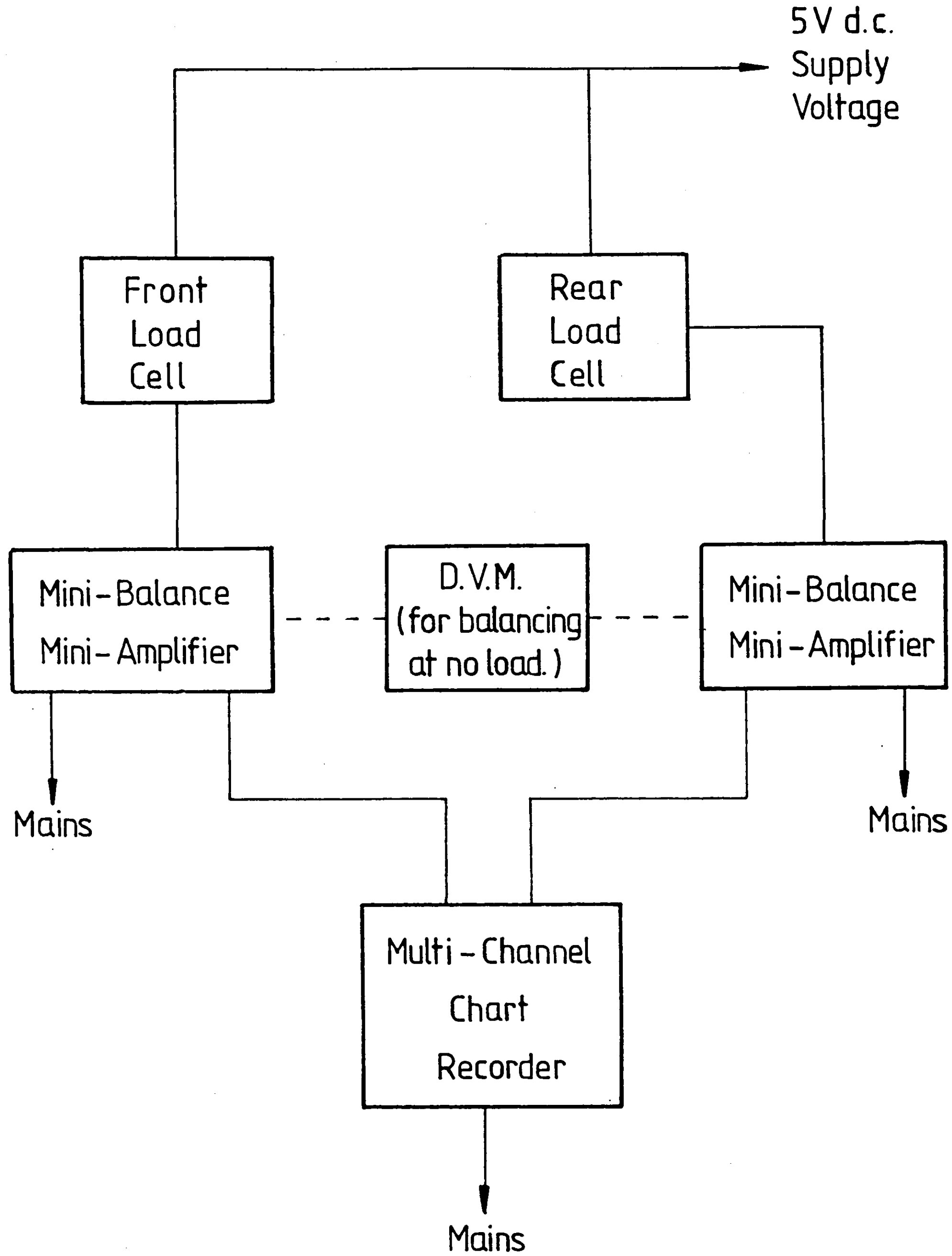

FIG 2.8 : SCHEMATIC BLOCK DIAGRAM OF INSTRUMENTATION FOR INTERRUPTED-PASS ROLLING TESTS

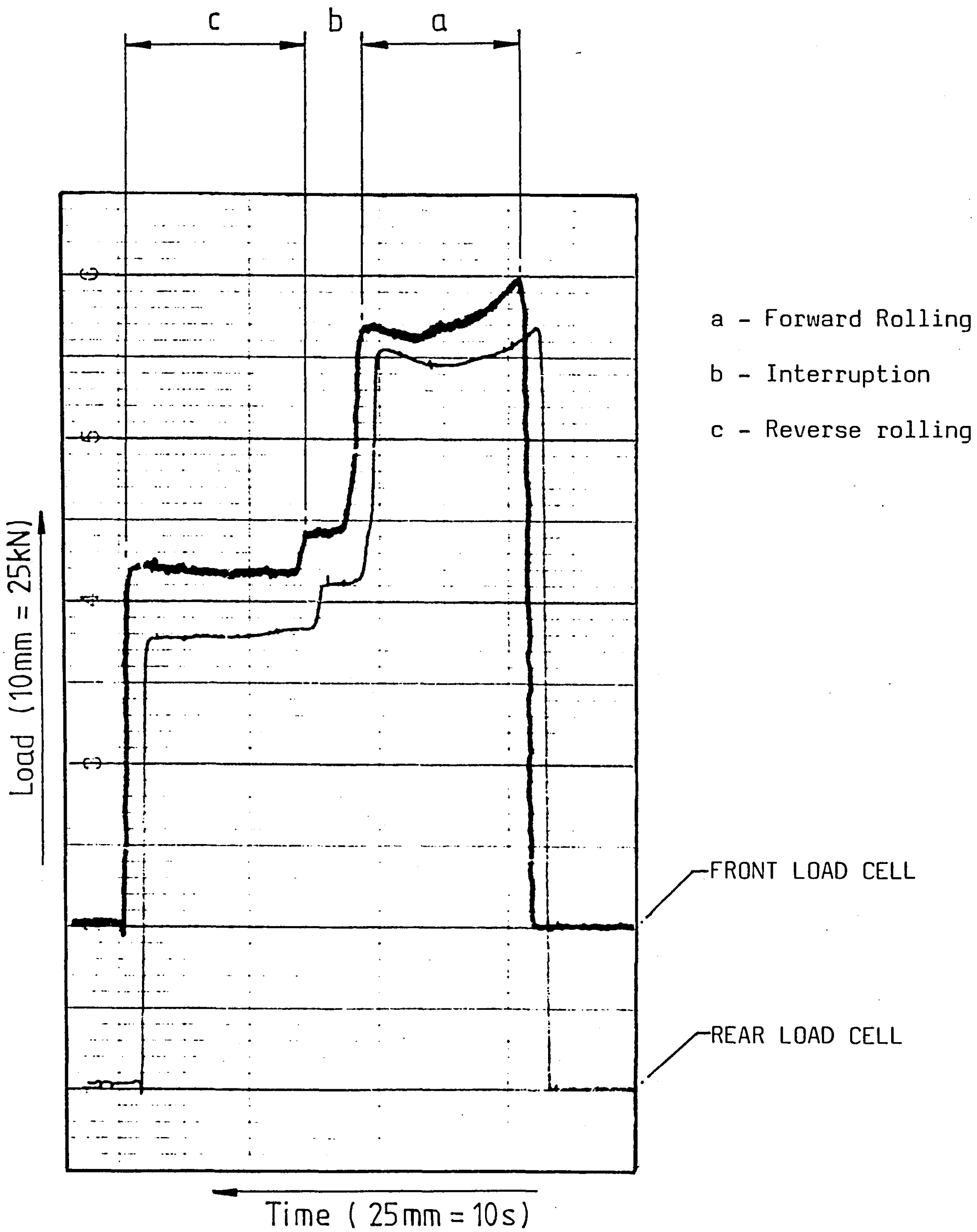

FIG 2.9 : TYPICAL LOAD/TIME TRACE FOR AN INTERRUPTED-PASS ROLLING TEST

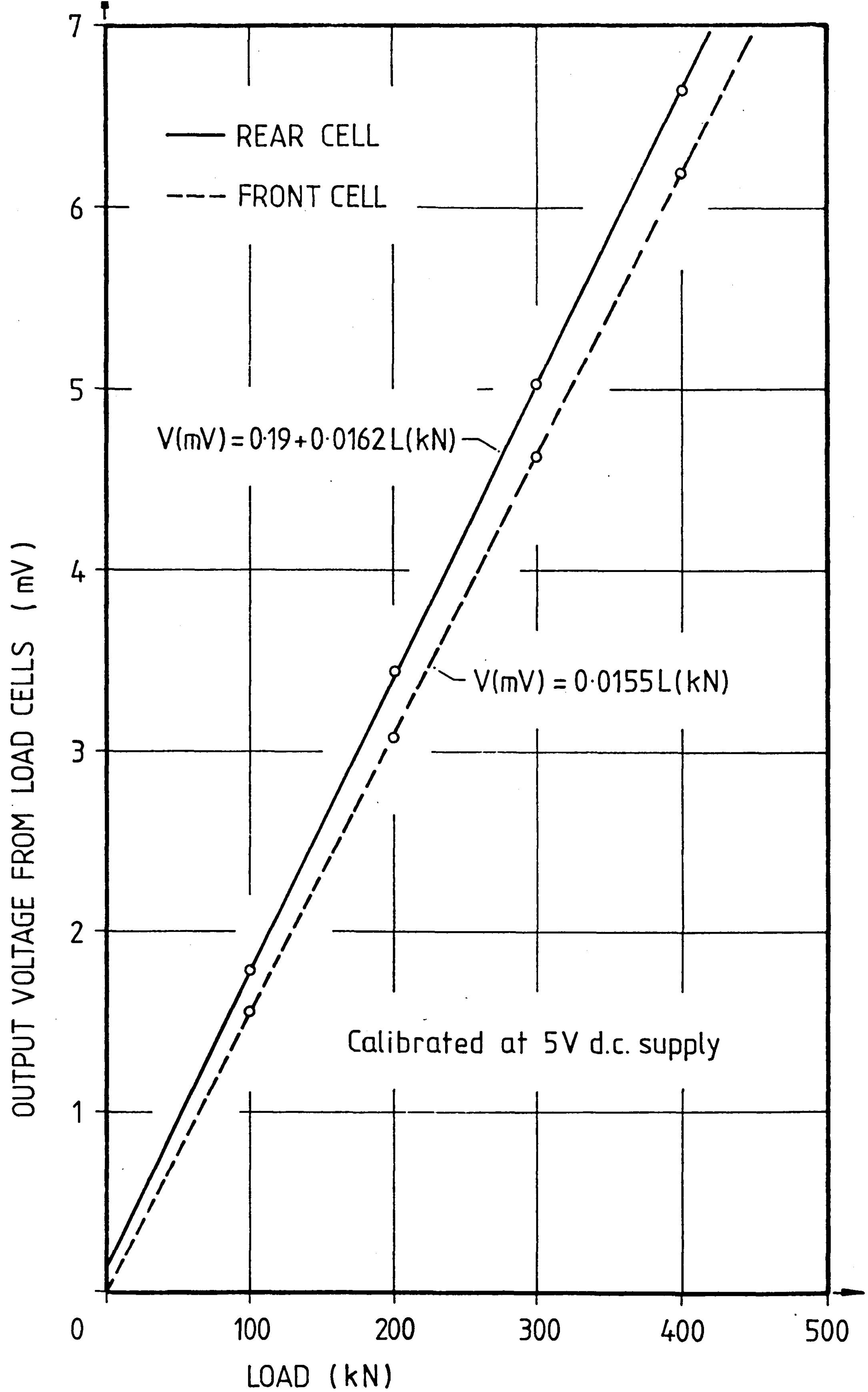

FIG 2.10 : CALIBRATION OF INSTRUMENTATION TO MEASURE LOAD FOR INTERRUPTED-PASS ROLLING TESTS

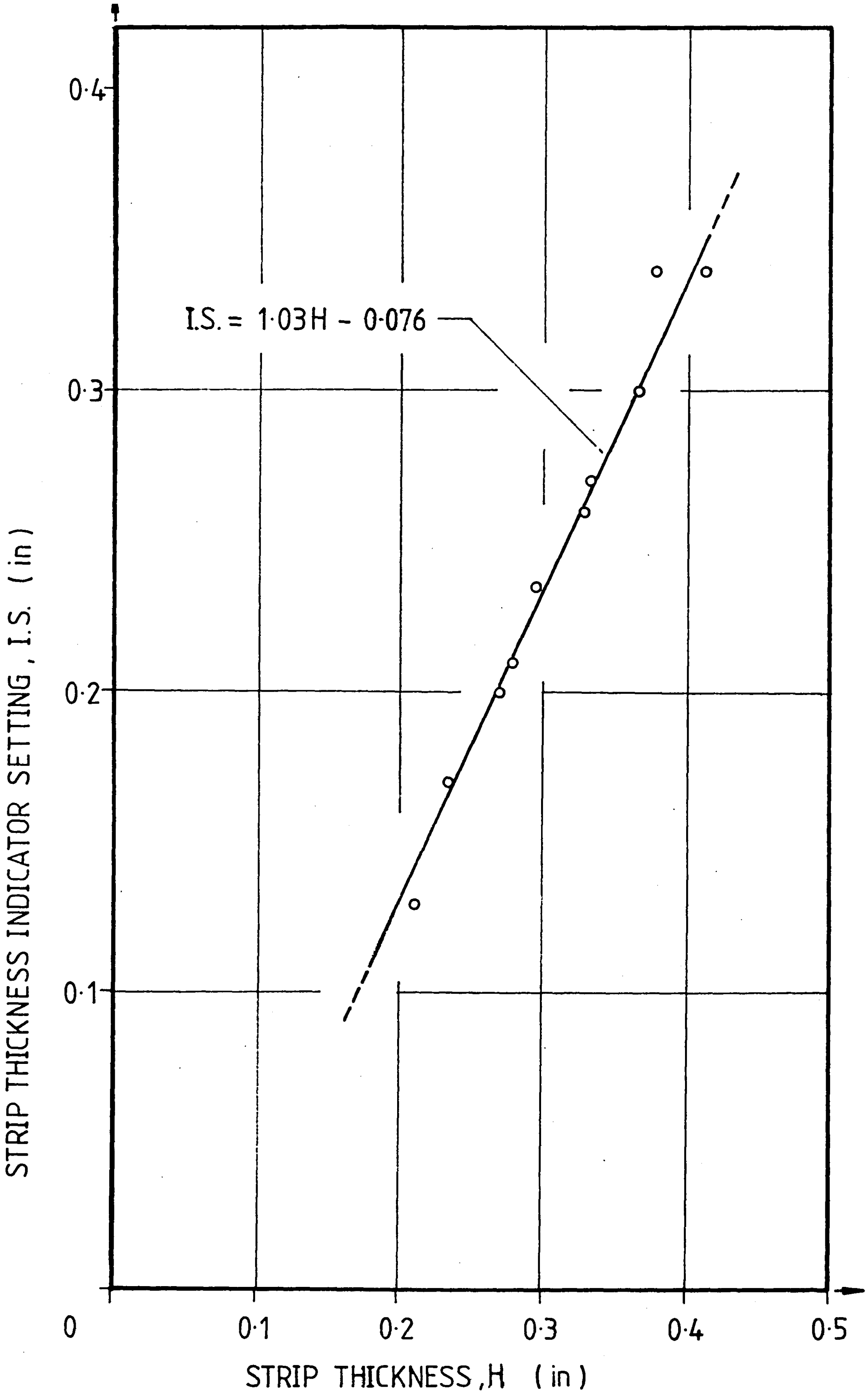

FIG 2.11 : CALIBRATION OF STRIP THICKNESS INDICATOR FOR INTERRUPTED-PASS ROLLING TESTS

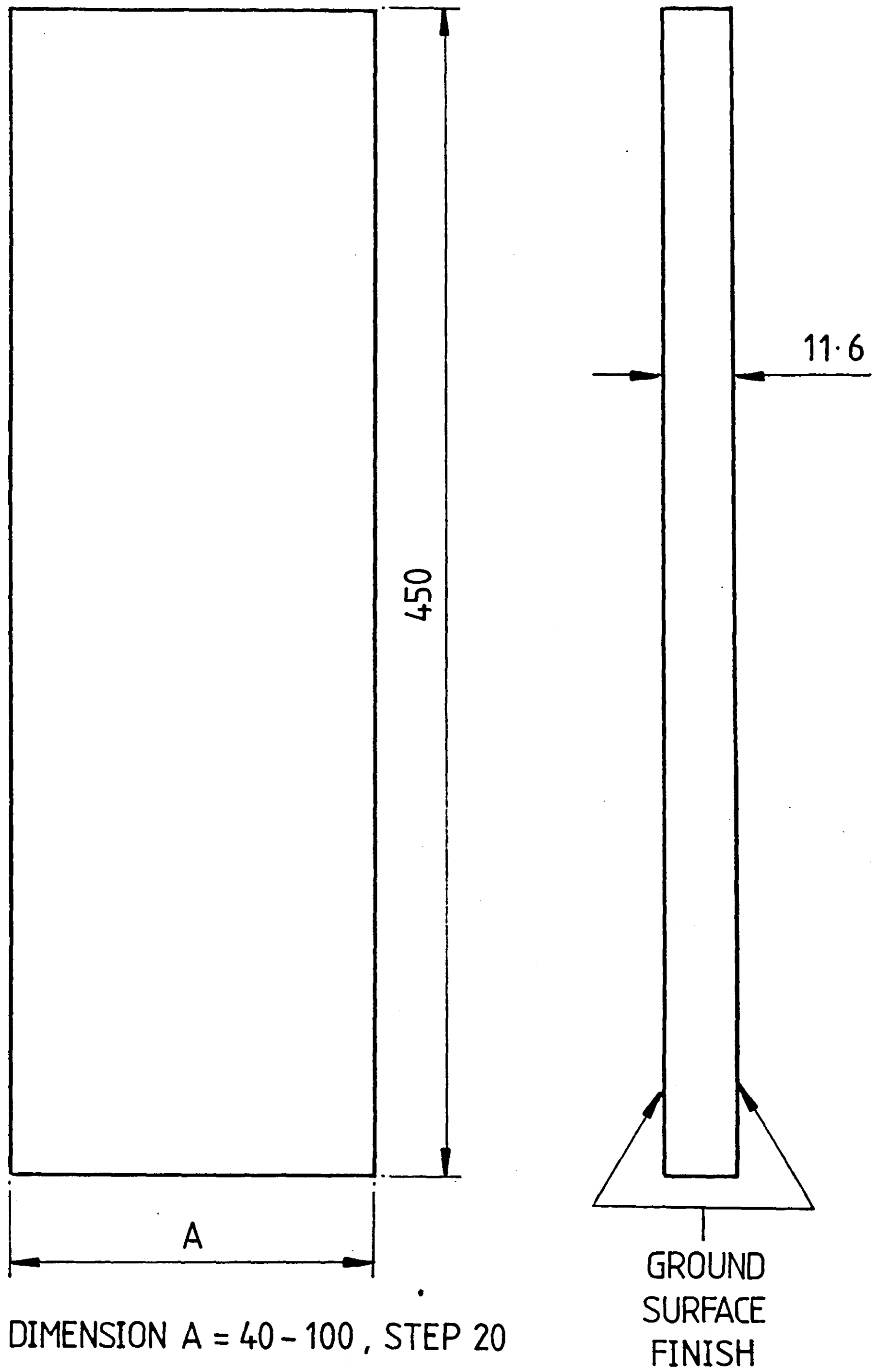

DIMENSION A = 40 – 100 , STEP 20

Not Drawn to Scale : All Dimensions in mm.

FIG 2.12: STRIP WORKPIECES

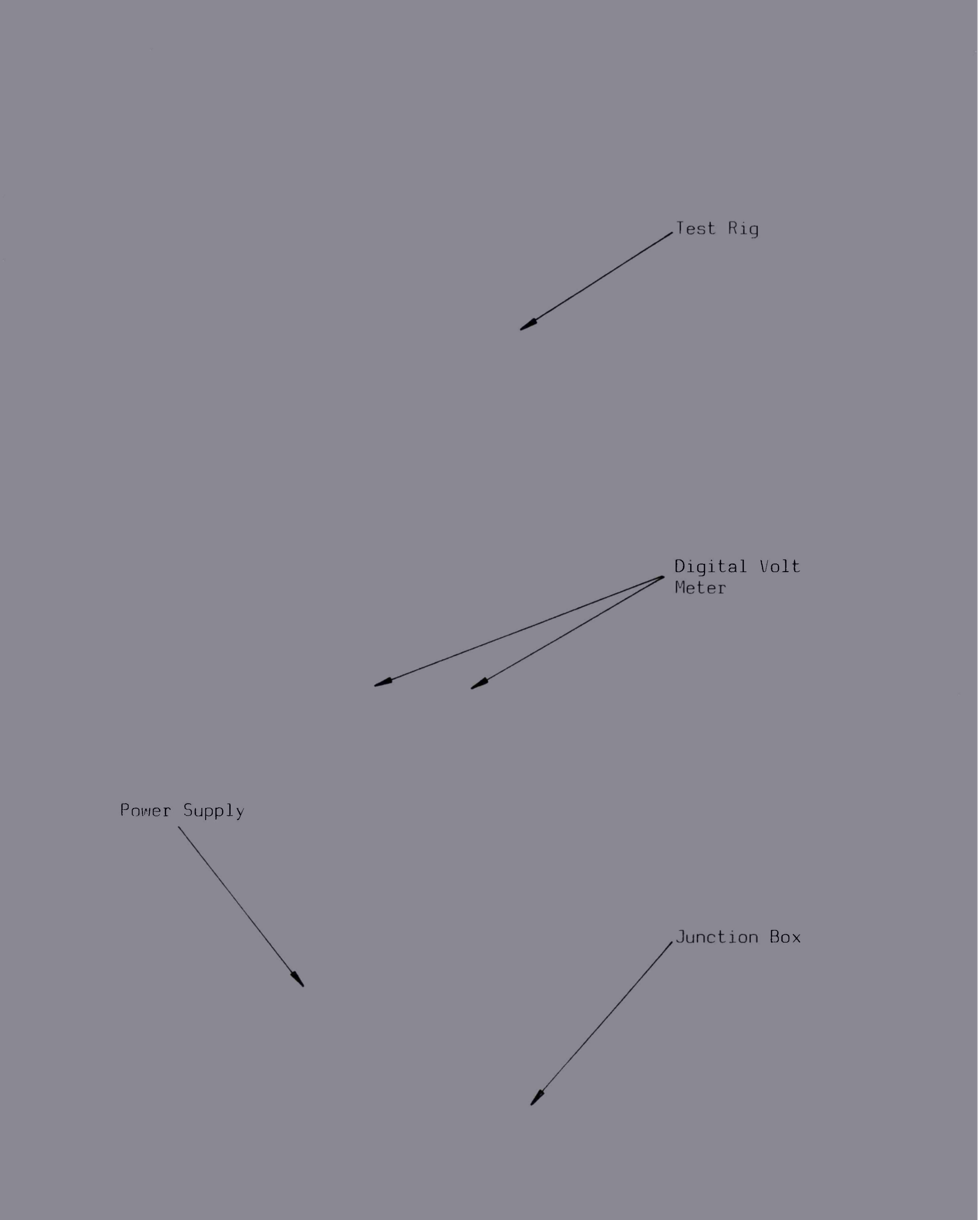

PLATE 2.1 : LAYOUT OF THE INSTRUMENTATION FOR THE STATIC INDENTATION TESTS

Test Rig

Digital Volt
Meter

Power Supply

Junction Box

PLATE 2.1 : LAYOUT OF THE INSTRUMENTATION FOR THE STATIC
INDENTATION TESTS

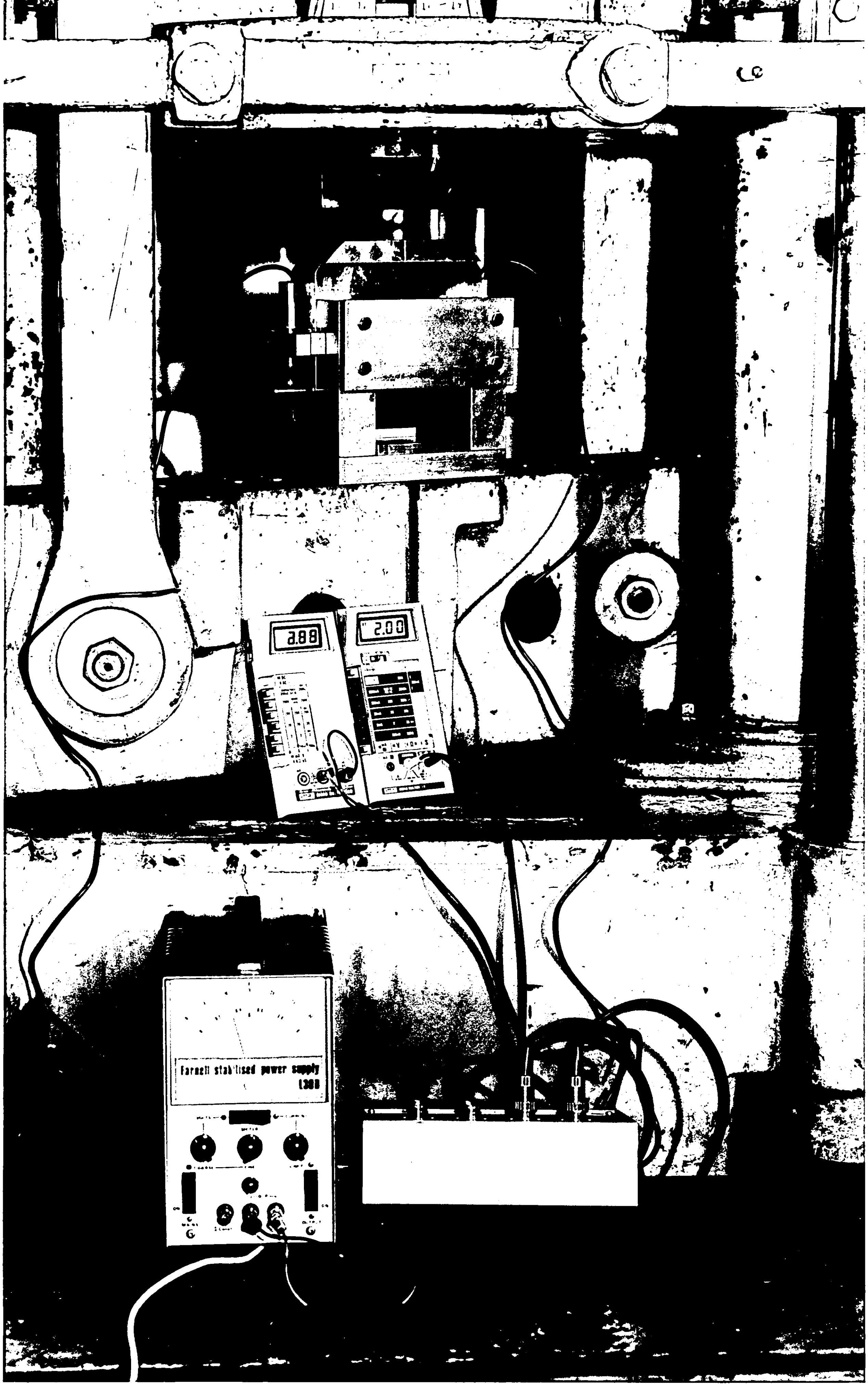
2.00
Farnell stabilised power supply
L30B

PLATE 2.2 : THE STATIC INDENTATION RIG

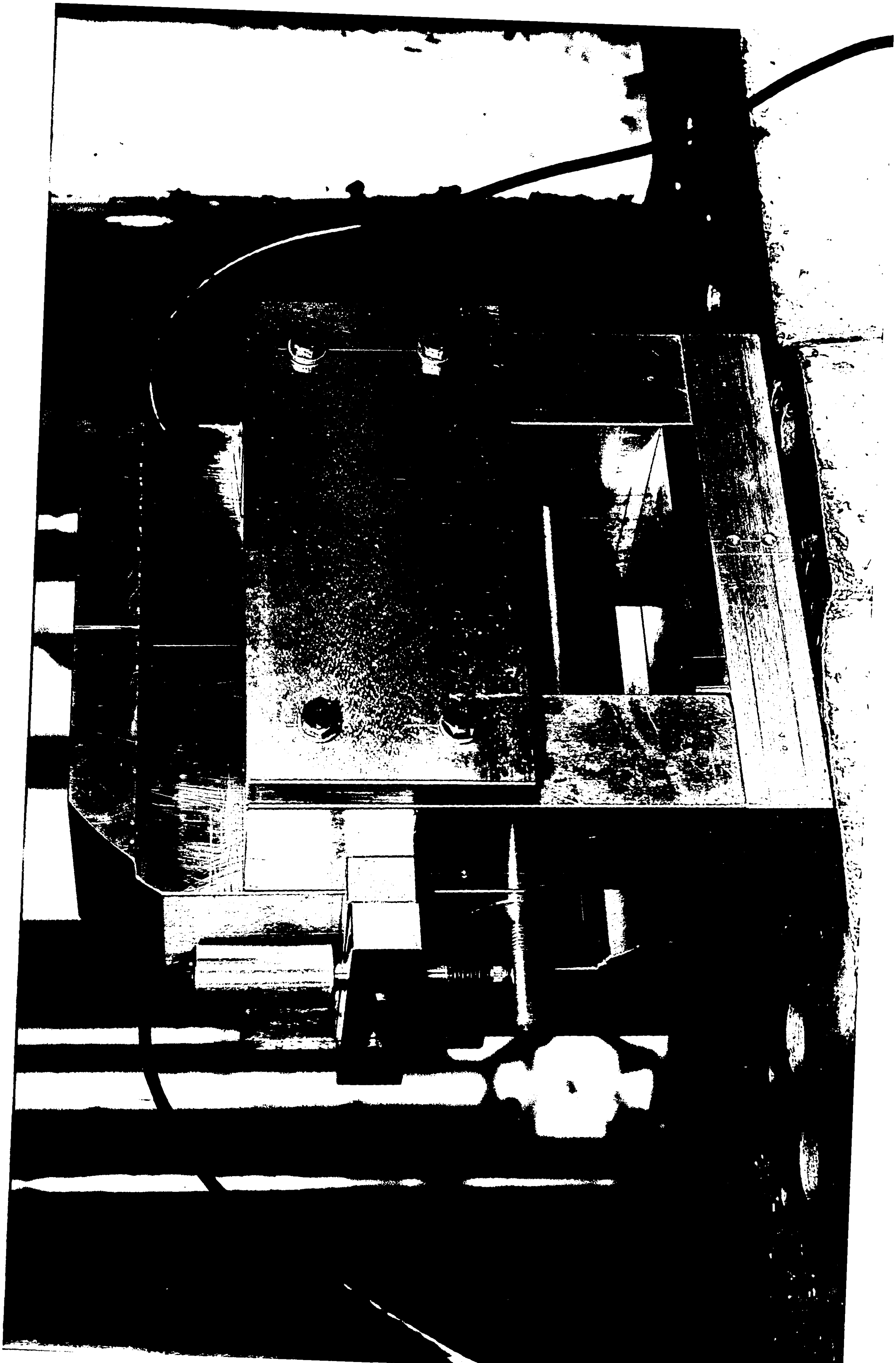

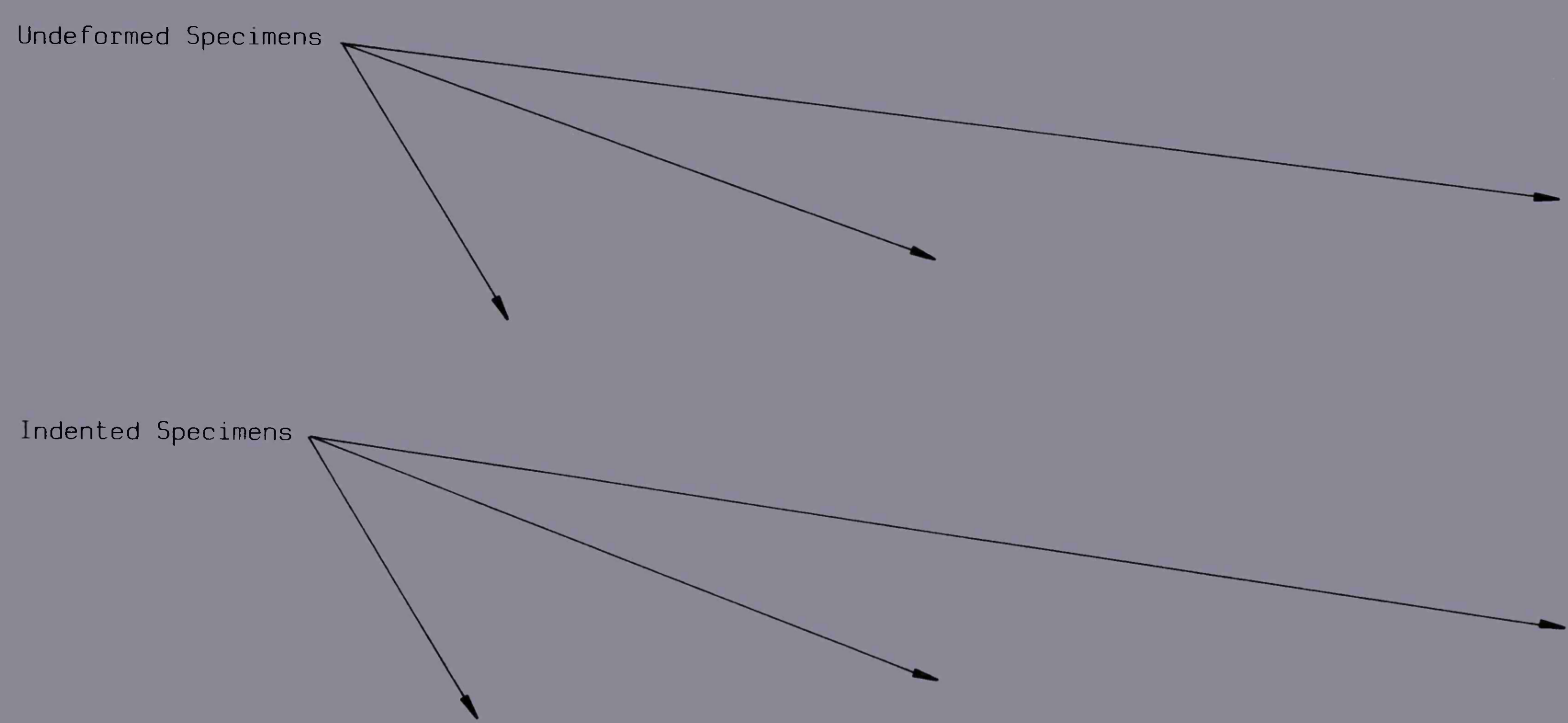

PLATE 2.3 : SELECTION OF FLAT AND INCLINED STRIP SPECIMENS

Undeformed Specimens

Indented Specimens

PLATE 2.3 : SELECTION OF FLAT AND INCLINED STRIP SPECIMENS

PLATE 2.4 : POSITIONING OF THE DISPLACEMENT TRANSDUCERS

PLATE 2.4 : POSITIONING OF THE DISPLACEMENT TRANSDUCERS

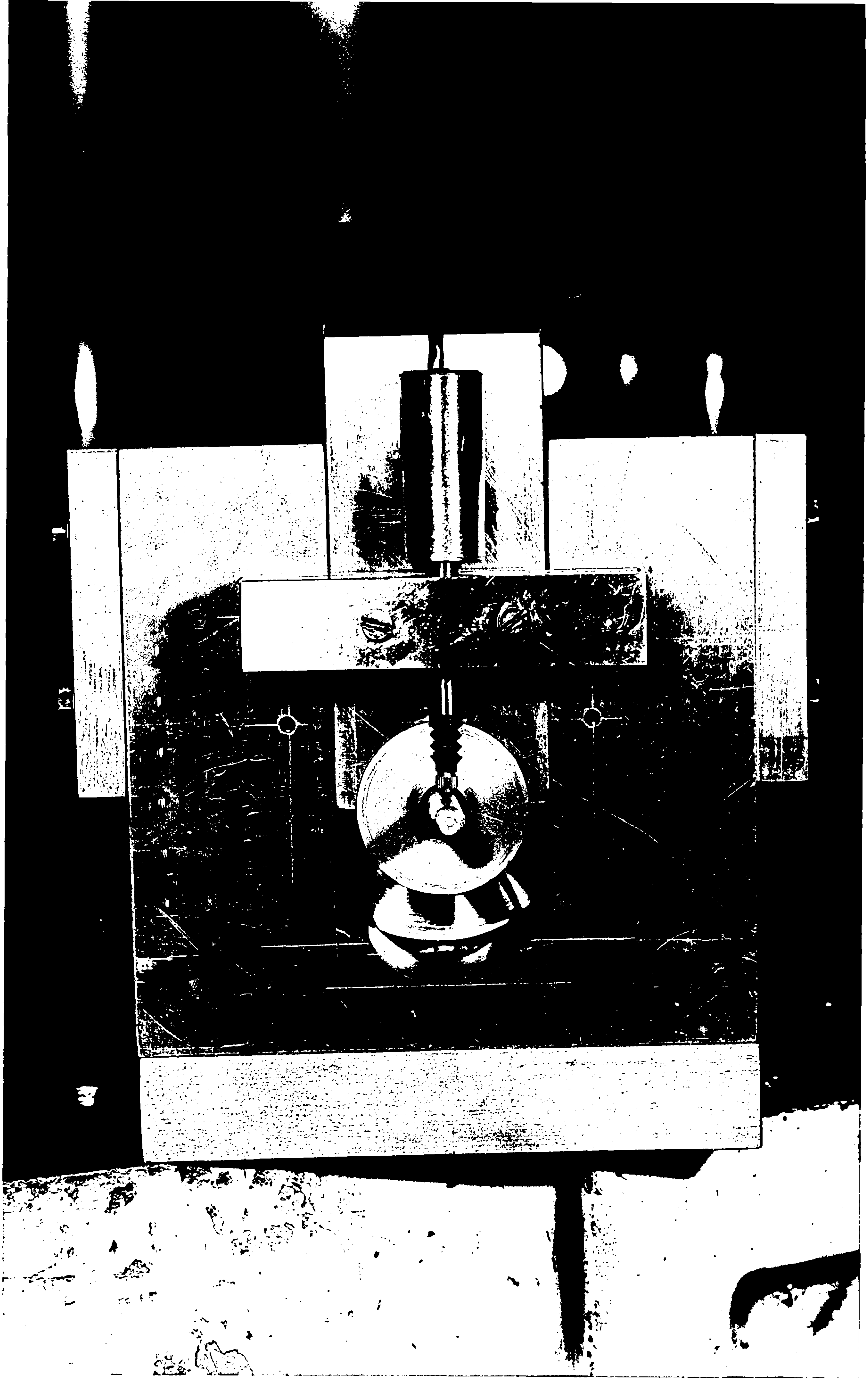

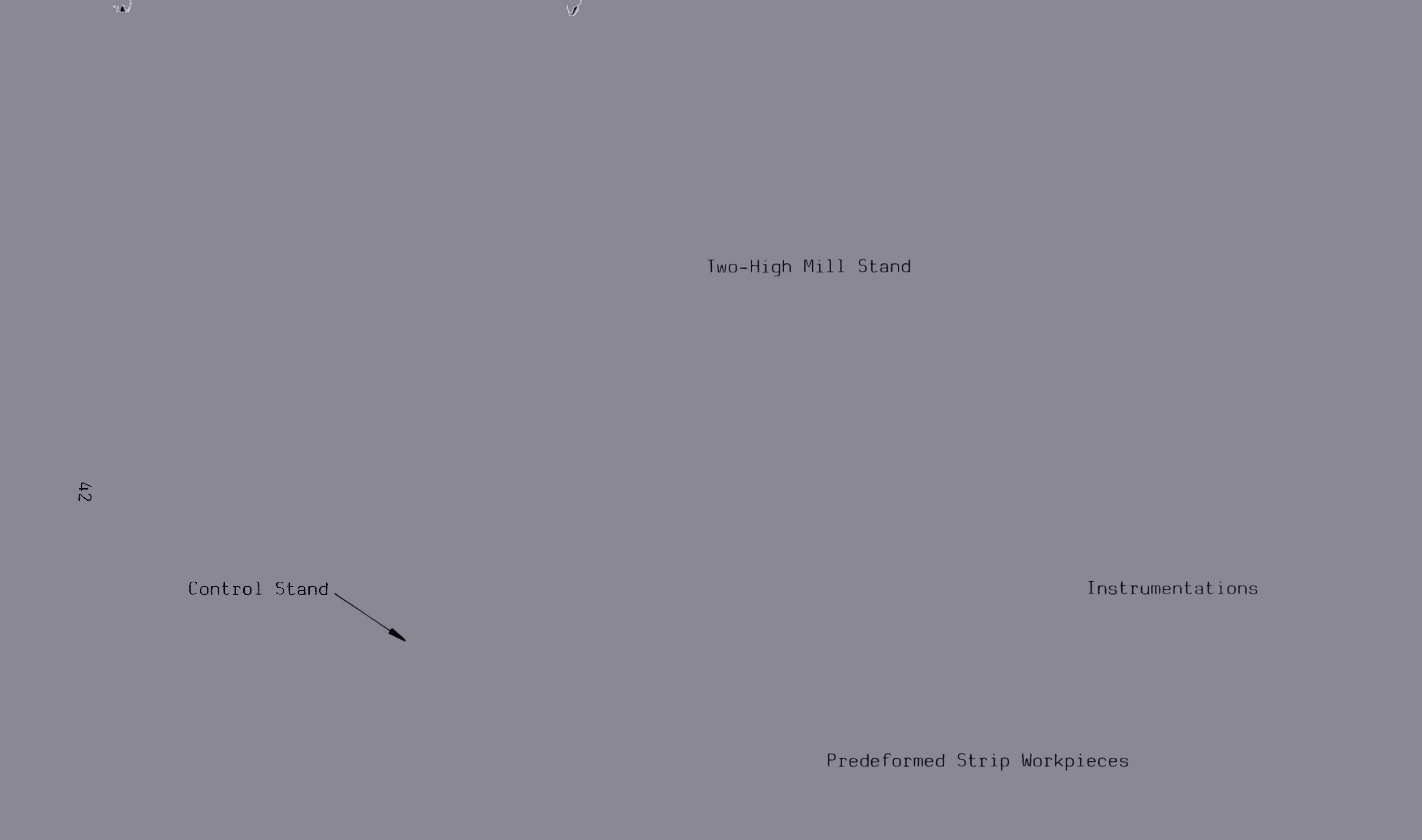

PLATE 2.5 : GENERAL VIEW OF THE LABORATORY ROLLING MILL

Two-High Mill Stand

Instrumentations

Control Stand

Preformed Strip Workpieces

PLATE 5.2 : GENERAL VIEW OF THE LABORATORY ROLLING MILL

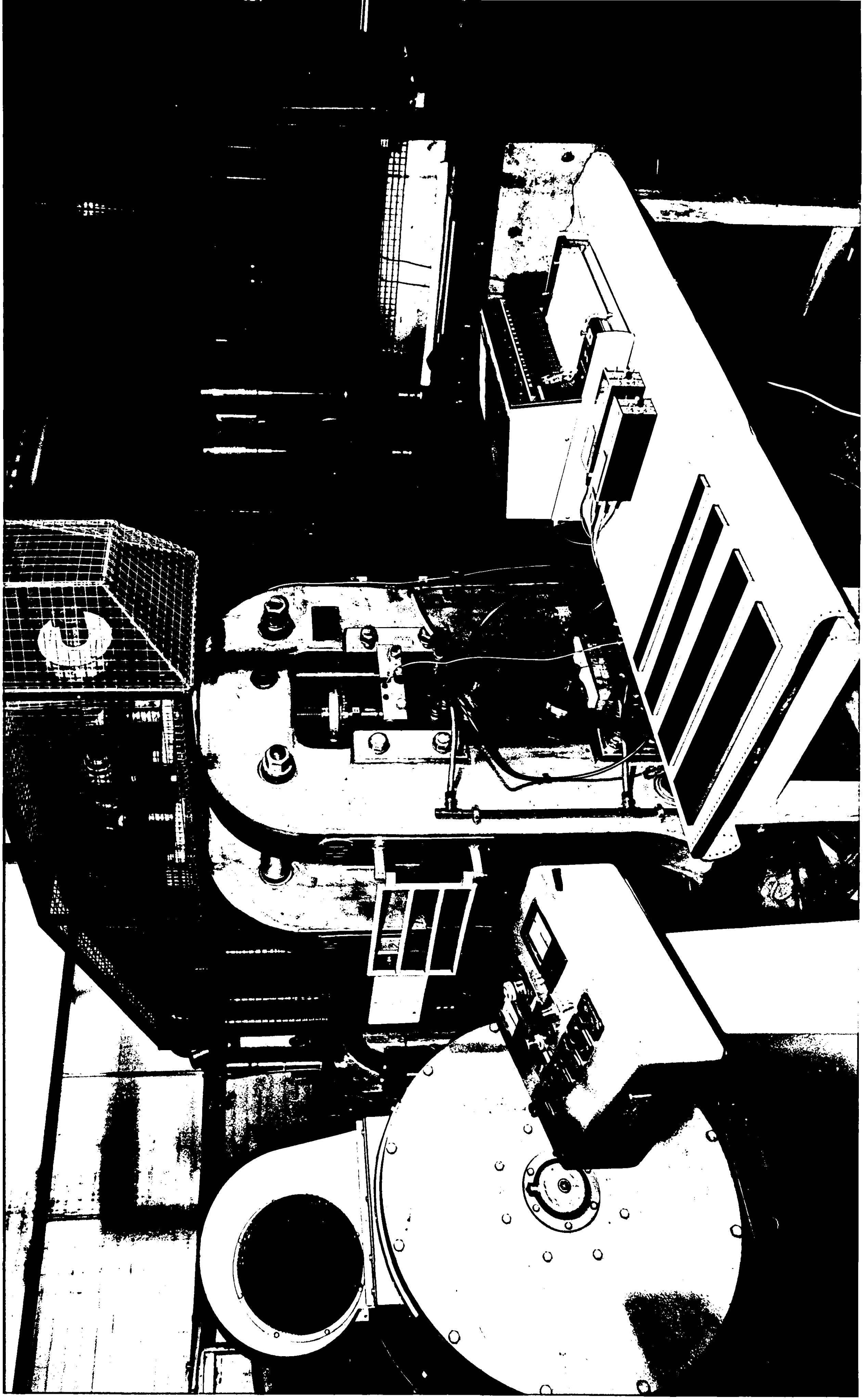

Load Cell

Strip thickness
indicator

Mini-Amp/
Mini-Balance

Chart Recorder

PLATE 2.6 : LAYOUT OF THE INSTRUMENTATION FOR THE INTERRUPTED-PASS ROLLING TESTS

Load Cell

Strip thickness
indicator

Chart Recorder

Mini-Amp/
Mini-Balance

PLATE 2.6 : LAYOUT OF THE INSTRUMENTATION FOR THE INTERRUPTED-PASS ROLLING TESTS

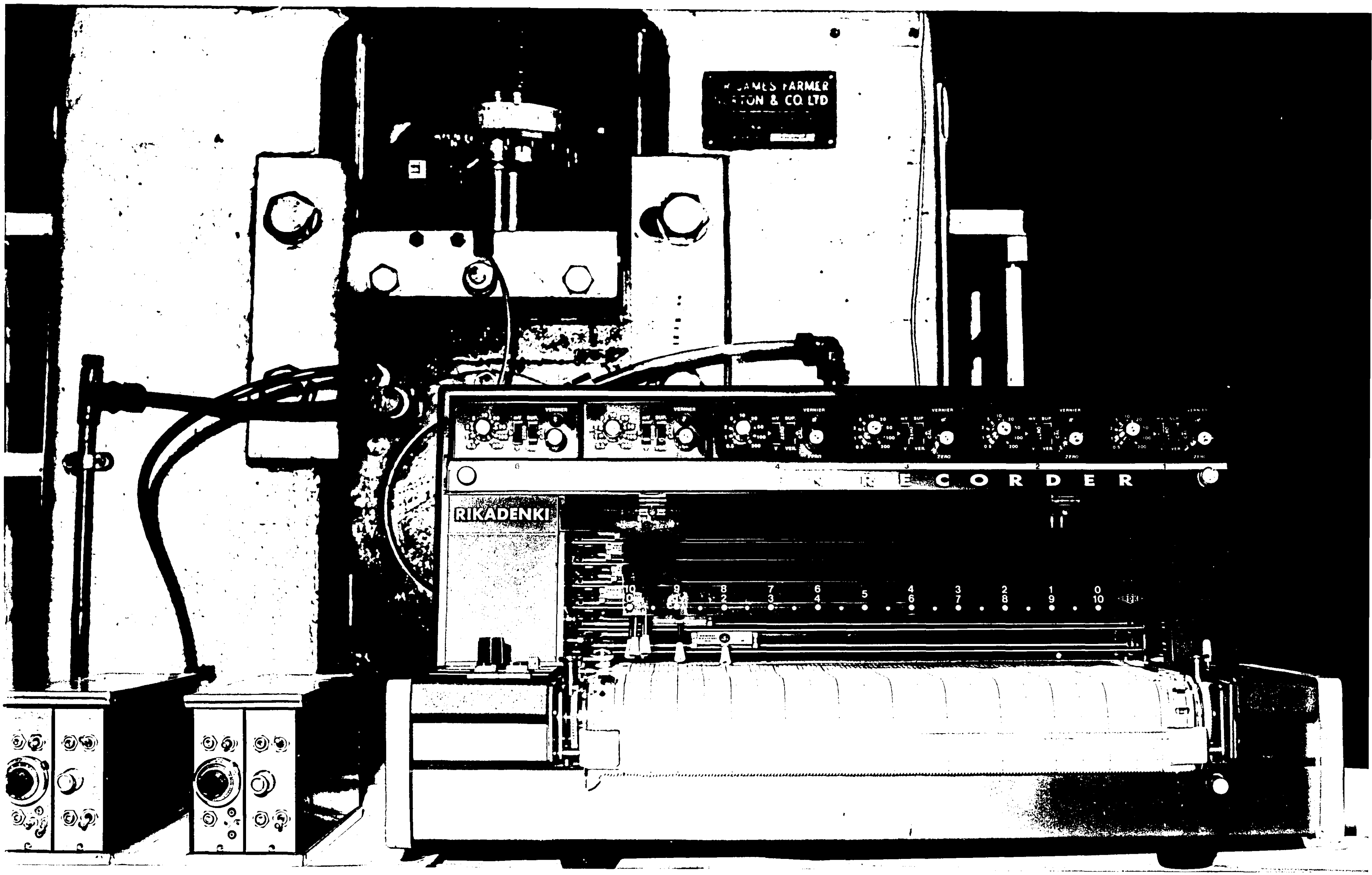
RIKADENKI
RECORDER
JAMES FARMER
& CO LTD

Deformed Workpiece

Undeformed Workpiece

PLATE 2.7 : CONFIGURATION OF THE DEFORMED AND UNDEFORMED STRIP WORKPIECES

Deformed Workpiece

Undeformed Workpiece

PLATE 2.7 : CONFIGURATION OF THE DEFORMED AND UNDEFORMED STRIP WORKPIECES

CHAPTER 3

PROFILE MEASUREMENT

3.1 Introduction

Precise nodal measurements were established along the arcs of contact at different sections across the width of each deformed workpiece after unloading. Each series of measurements were used in the determination of the roll or indentor profiles along the respective sections during deformation.

Along the arc of contact at each section, the relative positions of a series of points were established in cartesian co-ordinates. The position of each point was determined with both high precision and repeatability.

Initially, an optical technique was devised employing a S.I.P. Universal Measuring Machine (type MU412B). This entailed focussing a locating microscope at each position on the workpiece surface, then reading the corresponding positional settings.

The recent acquisition of a Ferranti Metrology System (type Merlin 750M) provided an alternative measurement system. This computer assisted machine established each nodal position by probing the workpiece surface with a spherically ended stylus.

Both instruments and the operational procedures adopted for profile measurement are detailed in this chapter.

3.2 Description of the SIP Universal Measuring Machine

This instrument provides a measurement system in three rectangular axes, and is shown in plate 3.1. It is best suited for the inspection of workpieces produced in small batches to close limits of precision.

Measurements in the horizontal plane (X, Y) are established by the relative displacements of the longitudinal carriage on which the workpiece is located (X) and the transverse carriage onto which the locating devices are mounted (Y). Micrometer microscopes fixed above built-in precision standard scales enable the positions of either carriage to be read directly to 0.1μm, however, settings to a resolution of 1μm are established.

Measurements in the vertical axis (Z) are effected by the vertical slide of the part of the transverse carriage which carries the tool holder and locating microscope. A point measurement is taken by focussing the locating microscope on the specimen surface, and reading the positional settings on the appropriate micrometer microscopes.

An evaluation of the uncertainties associated with a single point measurement are detailed in Appendix I.

3.3 Profile Measurement Procedures using the SIP Universal Measuring Machine

3.3.1 Profile Measurement for the Static Indentation Tests

The following procedure was adopted for the profile measurements of both flat and inclined strip specimens which had been indented under quasi-static loading conditions. The inclined specimens were mounted on angle gauges prior to measurement so that the orientation of the indented surfaces became horizontal. The configuration of a typical horizontal indented surface and measurement sequence are schematically shown in figure 3.1. The denoted nomenclature applies only to this figure and the following procedural list:

(i) Check for and remove all irregularities from beneath the specimen.

(ii) Place inside the controlled environment several hours before inspection to allow for stabilisation at standard temperature, 20°C.

(iii) Lightly secure the flat specimen, or inclined specimen and angle gauge to the worktable with strips of plasticine. Approximately align the axis across the indentation with the transverse axis of the instrument.

(iv) Accurately align in the transverse axis by observing and equating the longitudinal carriage settings at positions A and B, 1mm along the indentation lip from the edges. Firmly secure with plasticine.

(v) Determine the specimen width at the indentation centre by taking settings of the transverse carriage at positions C and D. Repeat for an increased assurance of accuracy.

(vi) Select the profile measurement sections across the indentation width relative to C. Move the transverse carriage to the setting of the first section.

(vii) Focus the locating microscope at a point E*, beneath the indentation lip and note the vertical setting z_1. Re-focus and compare values until satisfactory correlation is attained. Note the longitudinal carriage setting, x_1.

(viii) Locate the corresponding focussed point F on the opposite side of the indentation (retaining a constant z setting) and note the longitudinal carriage setting, x_n.

(ix) Determine the distance between longitudinal settings x_1 and x_n and discretise into an even number of between 10 and 30 elements (ensuring a centrally located node).

(x) Traverse the longitudinal carriage to each node in succession and focus the locating microscope. Note the vertical and longitudinal settings at each point, (x_1, z_1), (x_2, z_2), (x_3, z_3) ... (x_n, z_n). Repeat each measurement on a reverse pass along the section.

(xi) Repeat stages (vii) to (x) for all remaining sections.

3.3.2 Profile Measurement for the Interrupted-Pass Rolling Tests

The following procedure was adopted for the profile measurement of both sides of a strip workpiece following an interrupted rolling pass. The configuration of a typical deformed surface and measurement sequence are

---

* In figure 3.2 the profile inspection is shown along the third section.

schematically shown in figure 3.2. The denoted nomenclature applies only to this figure and the following procedural list:

(i) Repeat the preliminary inspection and temperature stabilisation practices described in the previous sub-section.

(ii) Place the specimen on strips of plasticine located across the worktable on the longitudinal carriage. Position the surface which was in contact with the upper roll uppermost, aligning the axis across the deformed arc with the transverse axis of the instrument. Lightly secure with plasticine.

(iii) Accurately align in the transverse axis (Y) by observing and equating the longitudinal settings at positions A and B, 1mm along the lip from each side. Firmly secure with plasticine.

(iv) Determine the strip width along the lip by taking settings of the transverse carriage at positions C and D.

(v) Select the sections across the width where the profile measurements are to be taken. Move the transverse carriage to the setting of the first section and traverse the longitudinal carriage until the locating microscope is positioned above the arc, E.*

(vi) Estimate the length of arc available for measurement and discretise into between 10 and 30 elements.

---

* In figure 3.3 the profile inspection is shown along the third section.

(vii) Traverse the longitudinal carriage to each point in succession and focus the locating microscope. Note the vertical and longitudinal settings at each point, (x_1, z_1), (x_2, z_2), (x_3, z_3) ... (x_n, z_n). Repeat each measurement on a reverse pass along the section.

(viii) Repeat stages (vi) to (vii) for all remaining sections across the strip width.

(ix) Repeat stages (ii) to (viii) for the profile measurement of the lower deformed surface. Reversal of the direction of the sectional sequence ensures that corresponding sections on both surfaces follow an ascending order, ie sections 1 and 6, 2 and 7, ... 5 and 10.

3.4 Description of the Ferranti Merlin 750M Metrology System

This machine provides a measurement system in three rectangular axes, a vertical probe column (Z : travel length 500mm), a horizontal bridge (X : travel 750mm) and a longitudinal granite worktable (Y : travel 750mm). All axes are fitted with air bearings for precision of movement and accurate optical scales which allow measurements to be determined to a resolution of 0.5µm.

A Micro 900 microprocessor is fitted onto the worktable and operates as a combined counter and data processing unit. This helps guide the operator through inspection routines and uses standard data processing facilities for functional requirements such as alignment, change of working plane, probe calibration, datum locations and others.

A Hewlett and Packard HP Series 200 microcomputer and printer extends the system range to establish a part-programming capability. Plate 3.2 shows the machine and ancillary equipments.

Positional locations along the surface of a typical workpiece are established by probing with a spherically ended stylus. This operation can be performed manually under joystick control, or computerised using the part-programming facility. When carrying out repetitive inspection routines, the formulation of a suitable part-program for controlling the measurement sequence is desirable. The co-ordinates relating to each positional measurement are displayed by the microprocessor, and can be sent to the printer. The measurement uncertainties associated with a series of positional locations along a typical arc profile are detailed in Appendix I. The configuration of the equipments on the worktable during a typical inspection are shown in Plate 3.3.

3.5 Profile Measurement Procedure using the Merlin 750M

The following procedure was adopted for the measurement of arc profiles across each side of a deformed strip workpiece having been subjected to an interrupted rolling pass. An outline of the part-program used to control the measurement sequence is also detailed. Figure 3.3 schematically represents the sequence by which each surface was measured. The directions referred to in the proceeding text adhere to the axis system shown in this figure.

(a) Preparation and positioning of the workpiece:

   (i) Subject each workpiece to the preliminary inspection and temperature stabilisation practices adopted for previous techniques.

(ii) Clamp the workpiece to the worktable. Align the upper surface lip (ridge across the width of the workpiece, established when the pass was terminated) with the longitudinal axis (Y) of the machine. Ensure that all regions to be inspected remain unobstructed.

(b) Initialisation of systematic and positional functions:

(i) Calibrate the probe stylus : probe at five locations on a precision sphere, the diameter being evaluated and displayed by the microprocessor.

(ii) Establish localised planes : probe at three locations on the entry plane of the workpiece and align and level the resulting data-fit (constant Z). Probe at two locations on the workpiece side and align the resulting data-fit (constant Y).

(iii) Establish datums : probe at a location on the workpiece side close to the lip; save as master datum in Y direction. Probe at a location on the entry plane at the position in X of each initial sectional measurement; save as master datum in X and Z directions.

(iv) Determine strip width along lip : probe at a location on the opposite side of the workpiece (to the Y datum) close to the lip; note the y-value displayed.

(v) Change working plane to X-Z, so that during operation the machine increments in the X and Y directions and probes in the Z direction.

(c) Operation and structure of the part-program:

(i) Input of the operational variables : input of the strip width along the lip, the number of sections to be inspected and the onset from each side enables the sectional locations to be established. Input of the scan length and incremental step determines the measurement positions along each section. Note that the scan length and increment are judged by the operator and remain constant for all sections across a surface.

(ii) Execute the part-program : the principal features of the part-program are presented in the form of a flow chart in figure 3.4

Apart from calibration of the probe stylus, the procedure is repeated for the inspection of the lower surface of the workpiece.

Consideration of the listings of positional measurement relating to each section proceeds. Points sited on the entry and exit planes are disregarded. Such points are established by considering the differences in depth (Z) of successive measurements.

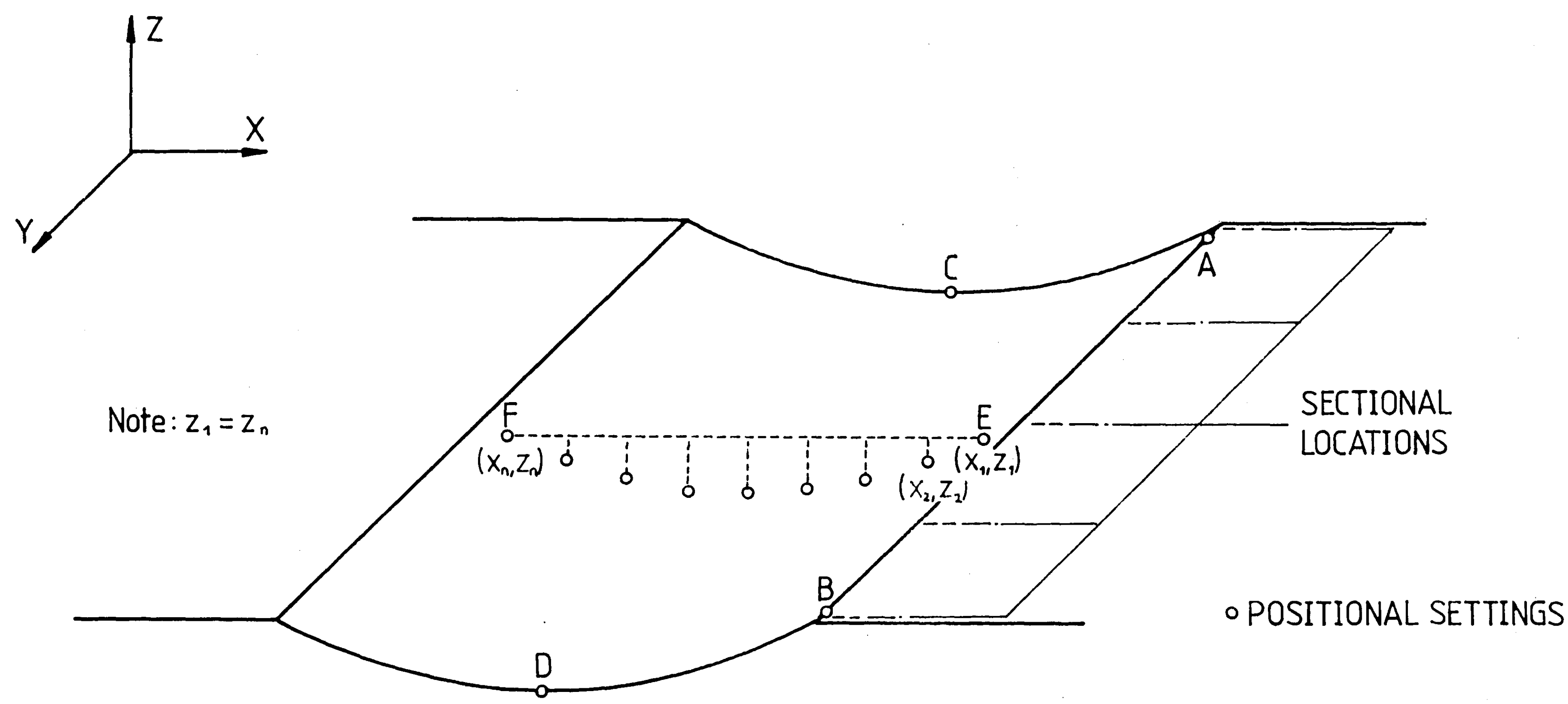

FIG 3.1 : SCHEMATIC REPRESENTATION OF MEASUREMENT SEQUENCE : INDENTED WORKPIECES INSPECTED BY THE S.I.P.

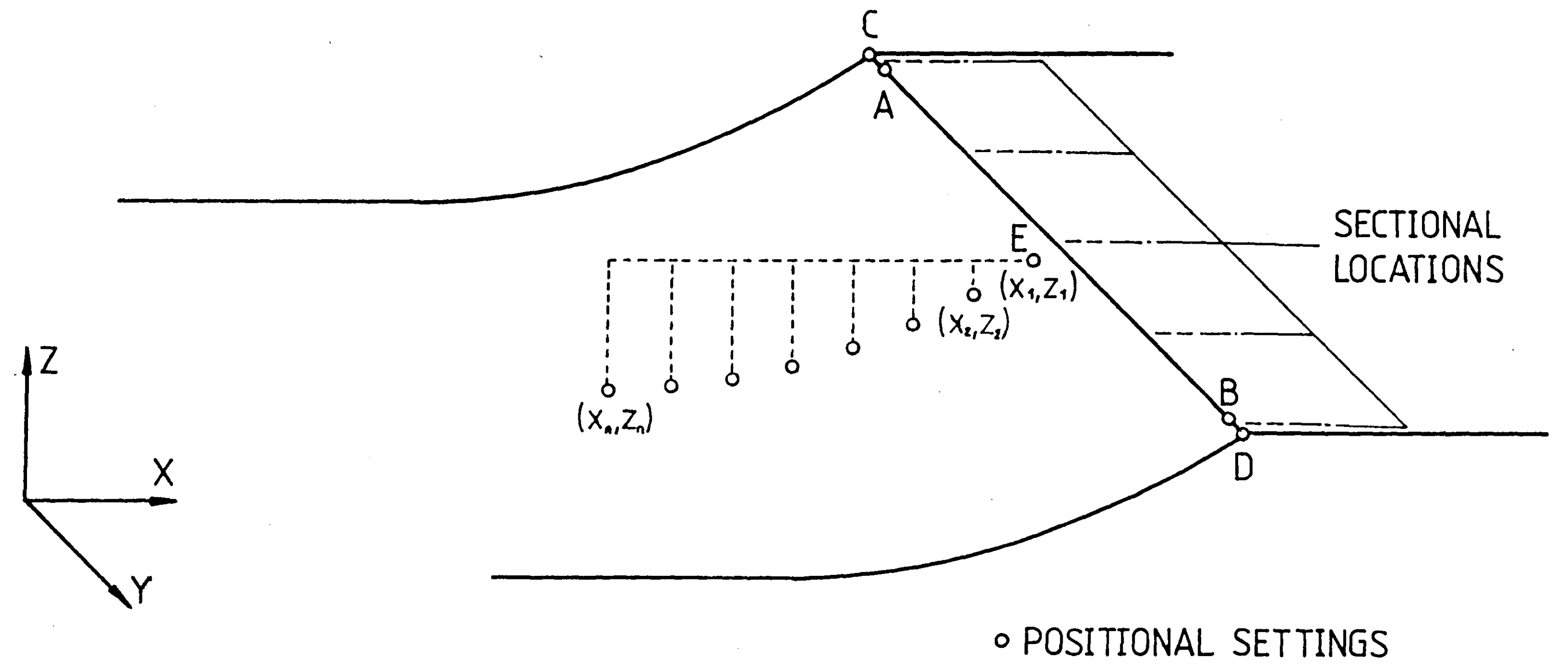

FIG 3.2 : SCHEMATIC REPRESENTATION OF MEASUREMENT SEQUENCE : INTERRUPTED-PASS WORKPIECES INSPECTED BY THE S.I.P.

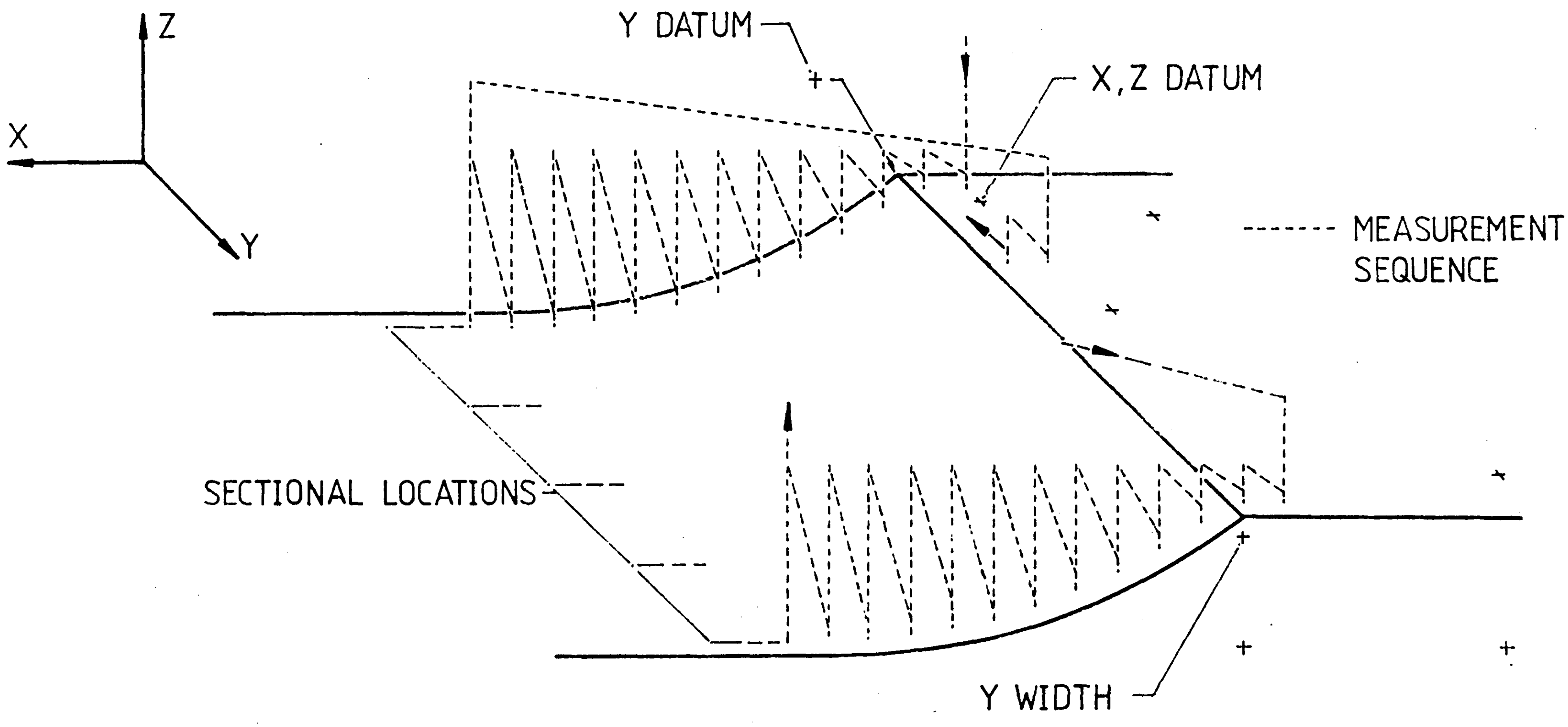

FIG 3.3 : SCHEMATIC REPRESENTATION OF MEASUREMENT SEQUENCE : INTERRUPTED-PASS WORKPIECES INSPECTED BY THE MERLIN

FIG 3.4 : FLOW CHART OF THE PART-PROGRAM USED TO INSPECT INTERRUPTED-PASS WORKPIECES BY THE MERLIN

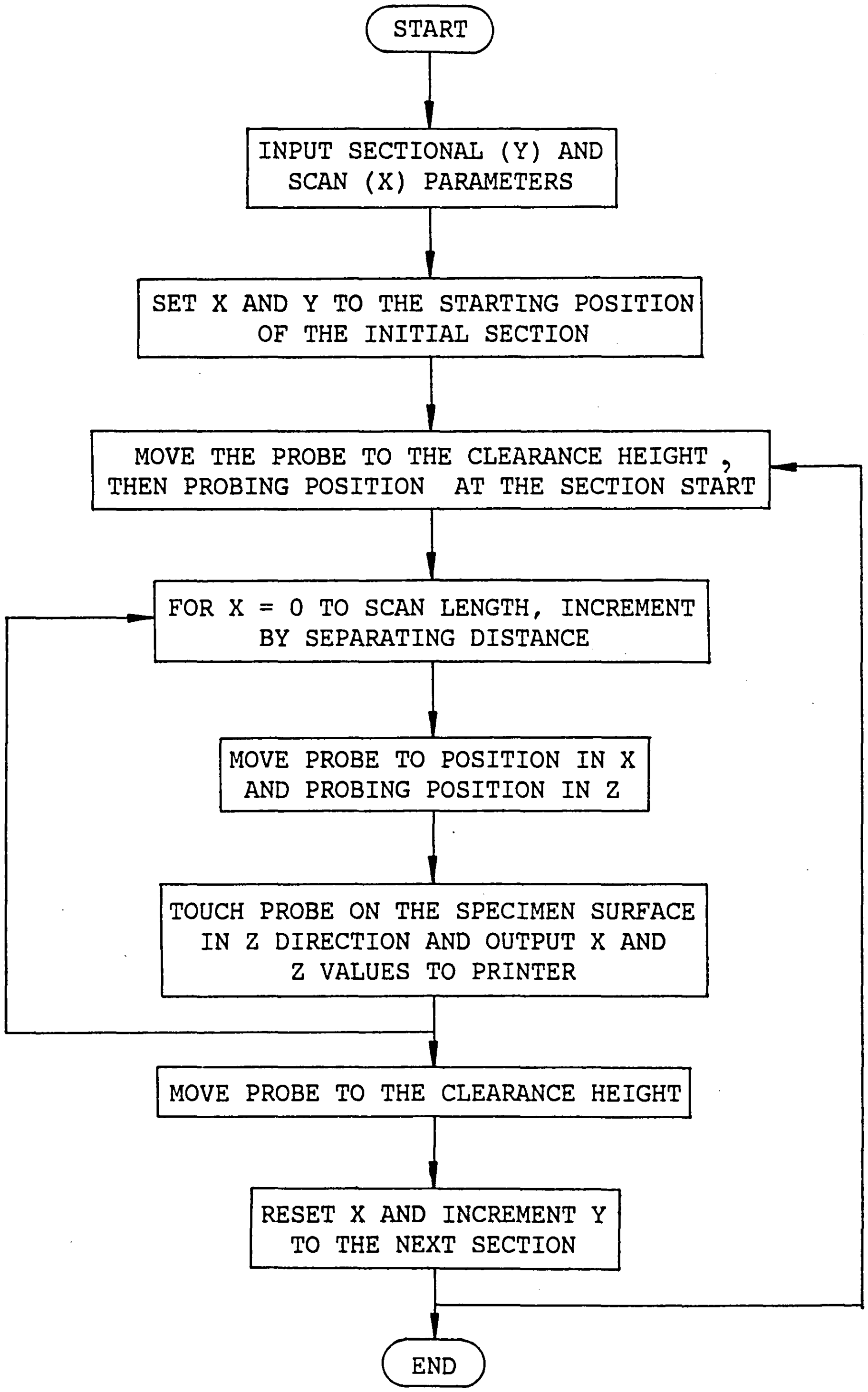

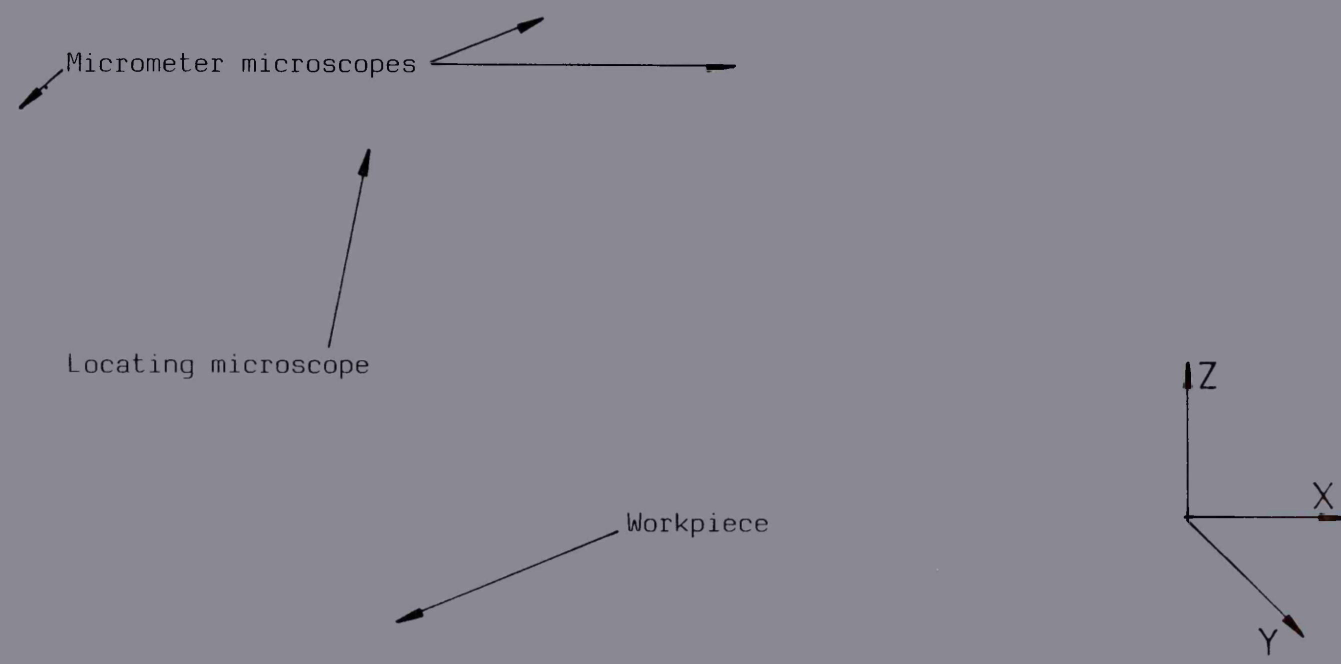

PLATE 3.1 : THE SIP UNIVERSAL MEASURING MACHINE

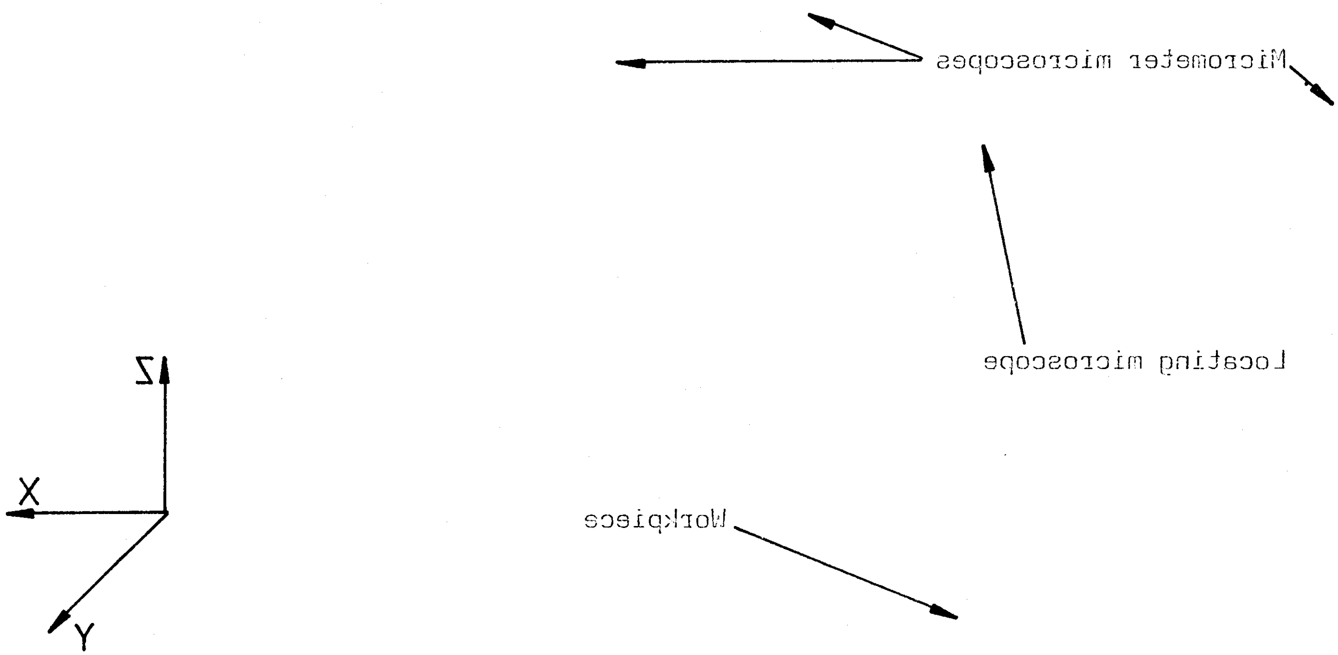

PLATE 3.1 : THE SIP UNIVERSAL MEASURING MACHINE

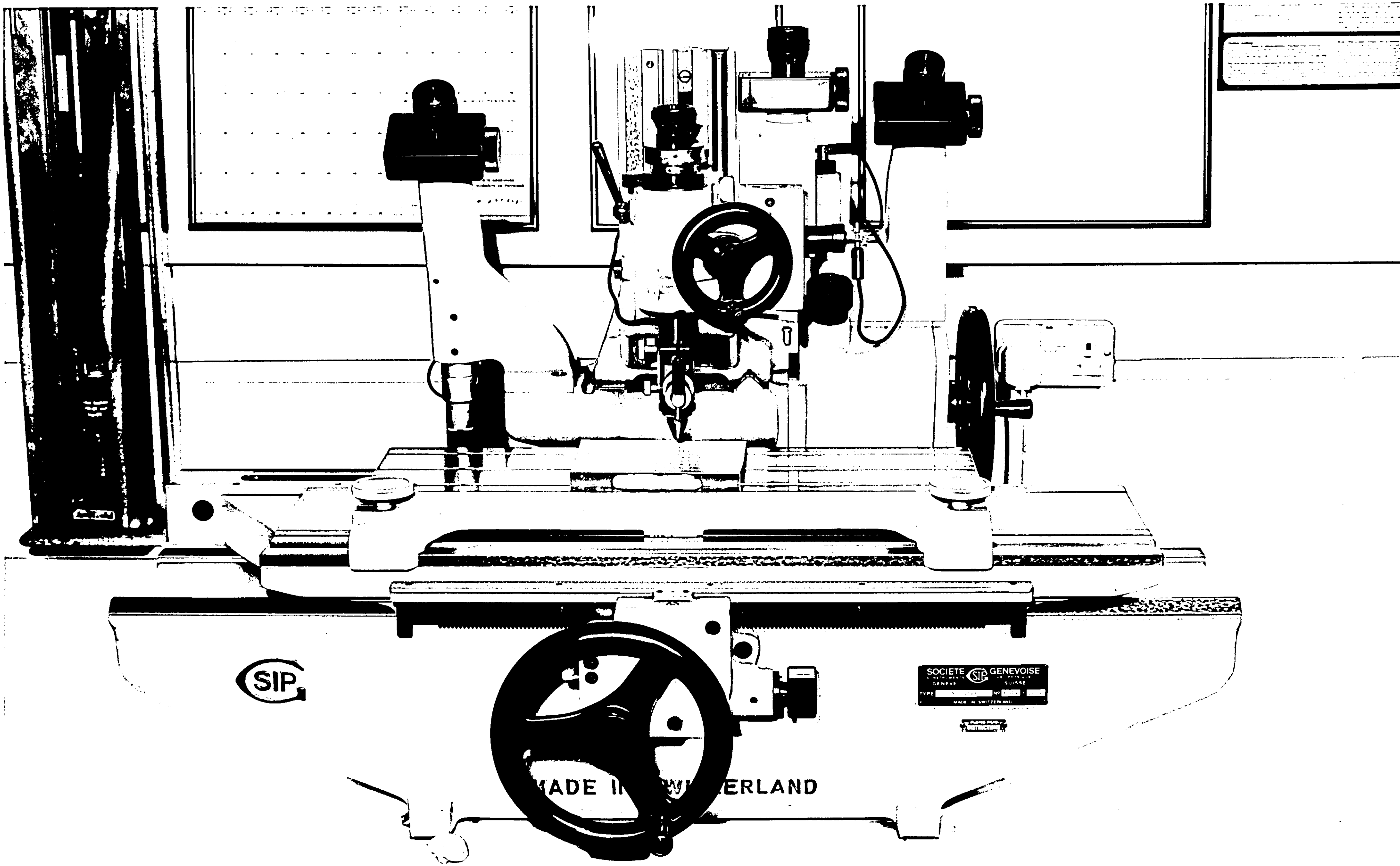
SIP
SOCIETE GENEVOISE
GENEVE
SUISSE
TYPE
MADE IN SWITZERLAND

Measuring Machine

Microcomputer and Printer

Microprocessor

PLATE 3.2 : THE FERRANTI MERLIN 750M METROLOGY SYSTEM

PLATE 3.2 : THE FERRANTI MERLIN 750M METROLOGY SYSTEM

Measuring Machine

Microprocessor

Microcomputer and Printer


FERRANTI
Metrology Systems
MERLIN

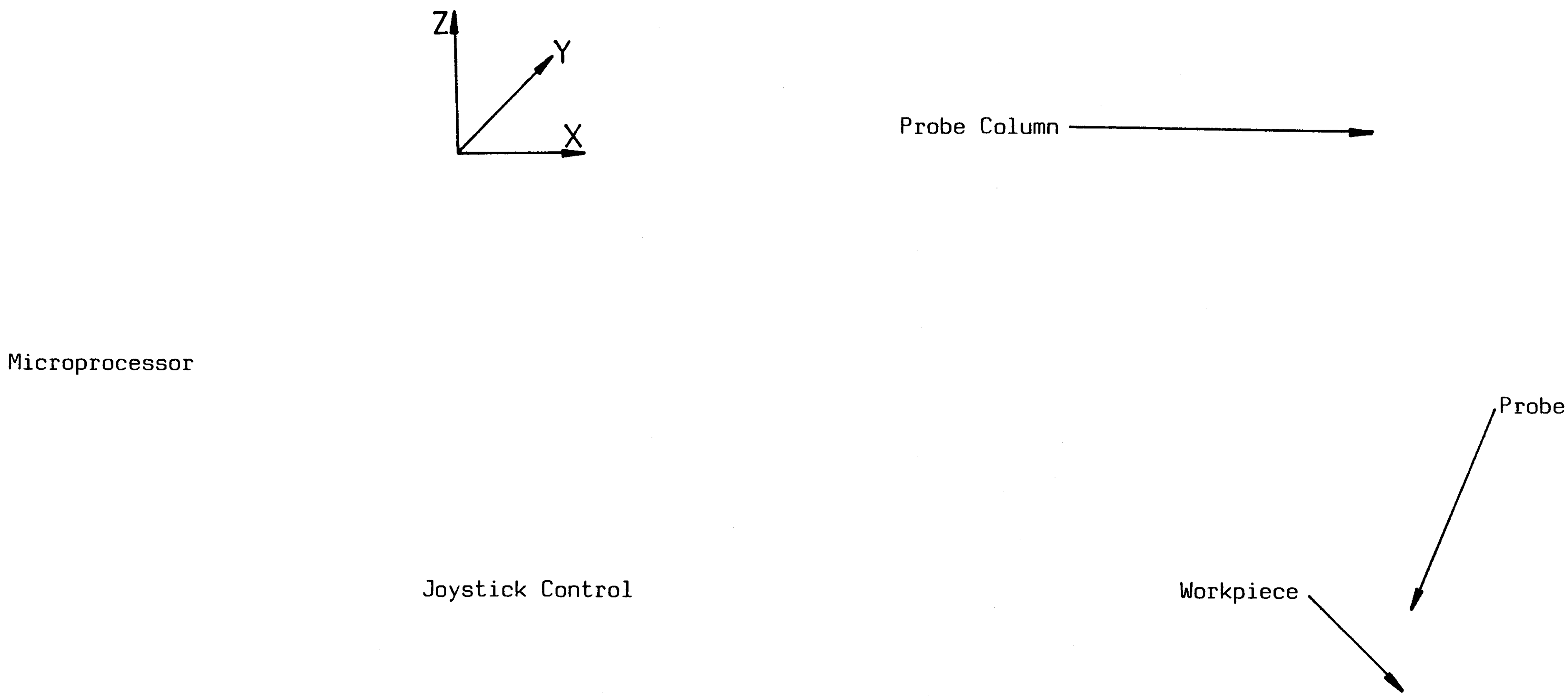

PLATE 3.3 : MERLIN 750M WORKTABLE DURING INSPECTION

PLATE 5.3 : MERLIN 750M WORKTABLE DURING INSPECTION

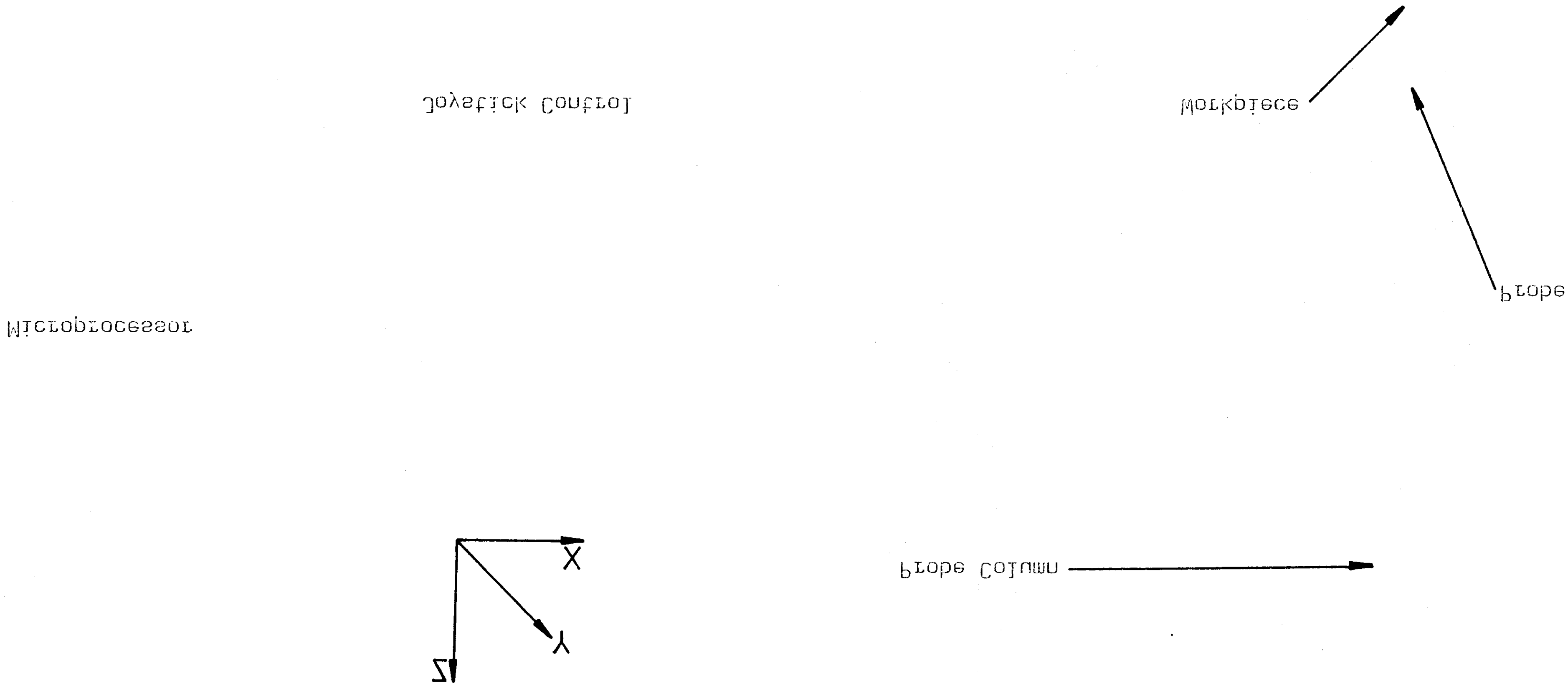

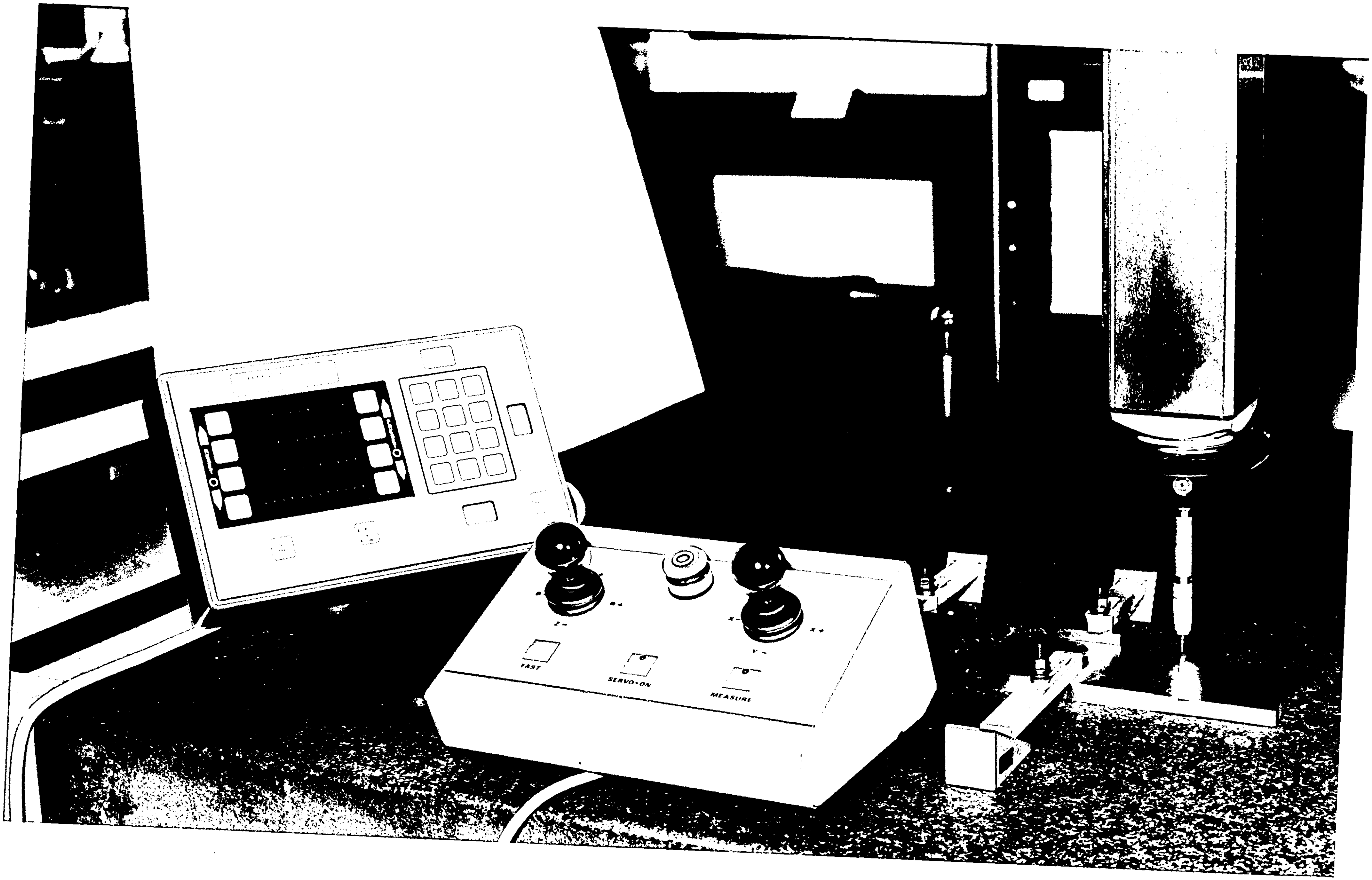
FAST
SERVO-ON
MEASURE

CHAPTER 4

ANALYSIS

4.1 Requirements and Inadequacies of Analyses for Predicting the Pressure Distribution in the Cold Rolling Process

Published literature shows that until recently the modelling of the pressure distribution between the rolls and stock material has tended to be analytical, with some analyses requiring numerical techniques to solve non-linear equations. Some models have been verified by limited experimental results which related to specific rolling conditions but most required correction factors to extend their applicability to practical situations. This is understandable since:

(i) the extent of variability of parameters in the rolling process is extreme;

(ii) the inherent inadequacies of most analytical solutions due to mathematical assumptions.

The recent advent of finite element analysis techniques have considerably aided and increased the scope of analytical investigations but have limited practical applicability due to high running costs and extremely long solution times.

The most reliable method for determining the pressure distribution between rolls and stock material in the cold rolling process is through direct measurement using pressure transducers.[40, 46,47] Such tests ascertain accurate results but are costly since the rolls cannot be used again for strip production.

For smaller companies with limited R and D facilities the application of analytical models incorporating empirical functions, determined from non-destructive tests, present an attractive and adequate solution. Although not completely accurate, results compare well with those determined using the alternative methods. To minimise inherent inaccuracies within the models, correction factors relating to each specific mill are necessary.

The principal advantages of such models are:

(i) Probably inexpensive in terms of manpower and expertise required for application.

(ii) Equations developed may be easily understood by users.

(iii) Model may be incorporated within a CAE process control program.

(iv) Checks, verifications and adjustments may be quickly made to the model to avoid excessive scrap.

(v) Models may also be developed for the hot rolling process.

The work undertaken in the present investigation adapts this form of solution to a novel technique for determining the pressure distribution in the cold rolling process. Empirical relationships are included to estimate indeterminable parameters and to minimise inaccuracies within the models.

4.2 Development of Analysis

The static indentation and interrupted rolling models are formulated by adopting the theory of solid body contact mechanics, see Timoshenko and Goodier.[51]

The analysis develops the point loading of a horizontal straight boundary of a semi-infinite body into a format which enables the pressure distribution acting between roll or indentor and strip specimen to be evaluated. The proposed model includes the following assumptions:

(i) The interface between the roll or indentor and the stock material is considered straight as the radius of the roll or indentor is considerably greater than the length of contact arc.

(ii) The roll or indentor surface is divided into a number of elements within the contact zone: the elastic displacement of each element is considered to be partly due to a uniformly distributed pressure activity acting across its breadth, and that acting across neighbouring elements.

(iii) Each section is considered independent of the displacement influences of neighbouring sections and the loaded indentor necks.

The cumulative effects of the assumptions are smoothed when formulating empirical functions for usage with each program. The functions apply to specific deformation conditions.

4.2.1 Concentrated Force Acting at a Point along a Straight Boundary

Consider a concentrated vertical force F acting at a point on a horizontal straight boundary A-B of an infinitely large plate of uniform thickness (F denotes the load per unit width), diagramatically illustrated in figure 4.1. Stress distribution within the plate may be determined by considering the effect of the force acting at a typical element C, a distance r from the point of application. Element C will be subjected to a radially compressive force satisfied by the stress component value:

$$\sigma_r = -k \frac{F\cos\Theta}{r} \quad , \tag{4.1}$$

where k is a constant adjusted to satisfy boundary conditions.

The radial stress acting at element C over an arc length of $d\Theta$ (unit width) and at an angle of Θ will give :

$$\sigma_r \cos\Theta \, r d\Theta = -F \quad . \tag{4.2}$$

Substituting for σ_r from equation (4.1) and simplifying:

$$-kF\cos^2\Theta \, d\Theta = -F \quad . \tag{4.3}$$

Radial stress acting over the whole arc at a distance r from the point of application becomes:

$$-2kF\int_0^{\frac{\pi}{2}} \cos^2\Theta d\Theta = -F \quad .$$

By integrating and simplifying we obtain:

$$-kF\frac{\pi}{2} = -F \quad ,$$

hence:

$$k = \frac{2}{\pi} \quad . \tag{4.4}$$

Substituting for k into equation (4.1), the stress components become:

$$\sigma_r = \frac{-2F}{\pi}\frac{\cos\Theta}{r} \quad ,$$

and by inspection: (4.5)

$$\sigma_\Theta = 0; \quad \tau_{r\Theta} = 0 \quad .$$

Since tangential stress σ_Θ and shearing stress $\tau_{r\Theta}$ are both zero throughout the enclosed region, equilibrium conditions are directly satisfied.

Boundary conditions along A-B are also satisfied except at the point of load application where σ_r becomes infinite.

The stress components can be derived from the stress function:

$$\emptyset = \frac{-F}{\pi} r\Theta \sin\Theta \quad . \tag{4.6}$$

Compatability requirements are satisfied by inserting the stress function into the compatibility equations below, obtaining:

$$\sigma_r = \frac{1}{r}\frac{\partial\Theta}{\partial r} + \frac{1}{r^2}\frac{\partial^2\Theta}{\partial\Theta^2} = \frac{-2F}{\pi}\frac{\cos\Theta}{r} \quad , \tag{4.7(a)}$$

$$\sigma_\Theta = \frac{\partial^2\Theta}{\partial r^2} = 0 \quad , \tag{4.7(b)}$$

$$\tau_{r\Theta} = -\frac{\partial}{\partial r}\left[\frac{1}{r}\frac{\partial\emptyset}{\partial\Theta}\right] \quad . \tag{4.7(c)}$$

Having satisfactorily established the validity of the stress component values, the radial (u) and tangential (v) displacements at points within the plate may be evaluated from the relationships:

$$\varepsilon_r = \frac{\sigma_r}{E} - \frac{\nu\sigma_\theta}{E} = \frac{du}{dr} \quad , \tag{4.8(a)}$$

$$\varepsilon_\theta = \frac{\sigma_\theta}{E} - \frac{\nu\sigma_r}{E} = \frac{u}{r} + \frac{dv}{rd\Theta} \quad , \tag{4.8(b)}$$

$$\gamma_{r\theta} = \frac{\tau_{r\theta}}{G} = \frac{rdu}{d\Theta} + \frac{dv}{dr} - \frac{v}{r} \quad . \tag{4.8(c)}$$

Substituting stress component values from equation (4.5), equations 4.8(a), (b) and (c) give :

$$\frac{\partial u}{\partial r} = \frac{-2F}{\pi E}\frac{\cos\Theta}{r} \quad , \tag{4.9(a)}$$

$$\frac{u}{r} + \frac{\partial v}{r\partial\Theta} = \frac{\nu 2F}{\pi E}\frac{\cos\Theta}{r} \quad , \tag{4.9(b)}$$

and $$\frac{r\partial u}{\partial\Theta} + \frac{\partial v}{\partial r} - \frac{v}{r} = 0 \quad . \tag{4.9(c)}$$

By integrating equation 4.9(a), we obtain:

$$u = \frac{-2F}{\pi E}\cos\Theta \,\ell n\, r + f(\Theta) \tag{4.10(a)}$$

where $f(\Theta)$ is a function of Θ only.

Substituting for u in equation 4.9(b) and integrating it can be shown that:

$$v = \frac{2\nu F}{\pi E}\sin\Theta + \frac{2F}{\pi E}\,\ell n r \sin\Theta - \int f(\Theta)d\Theta + F(r), \tag{4.10(b)}$$

where $F(r)$ is a function of r only.

Substituting expressions for u and v in equation 4.9(c) integrating and simplifying, we conclude that:

$$f(\Theta) = -\frac{(1-\nu)}{\pi E}F\Theta\sin\Theta + A\sin\Theta + B\cos\Theta \quad ,$$

$$\text{and } F(r) = Cr \quad , \tag{4.11}$$

where A, B and C are constants of integration.

Substituting expressions for $f(\Theta)$ and $F(r)$ into equations 4.10(a) and 4.10(b), expressions for radial and tangential displacements within the plate become:

$$u = \frac{-2F}{\pi E}\cos\Theta \ln r - \frac{(1-\nu)}{\pi E}F\Theta\sin\Theta + A\sin\Theta + B\cos\Theta \quad , (4.12(a))$$

and

$$v = \frac{2\nu F}{\pi E}\sin\Theta + \frac{2F}{\pi E}\ln r \sin\Theta - \frac{(1-\nu)}{\pi E}F\sin\Theta + \frac{(1-\nu)}{\pi E}F\Theta\cos\Theta$$
$$+ A\cos\Theta - B\sin\Theta + Cr \ . \qquad (4.12(b))$$

Constants of integration A, B and C are evaluated by implementing boundary conditions:

(i) All points along the line of action of the concentrated load will have no lateral displacement, hence $v = 0$ when $\Theta = 0$. By substituting these values into equation 4.12(b) we obtain the expression:

$$0 = A + Cr \quad ,$$

which can only be satisfied when $A = C = 0$

(ii) By including values for the constants of integration A and C, the downward displacement ($\Theta = 0$) at any point along the horizontal straight boundary will be obtained by substituting into equation 4.12(a):

$$u_{(\Theta = 0)} = \frac{-2F}{E}\ln r + B \quad .$$

By considering a point on the horizontal boundary a distance d from the point of the applied load with no downward movement ($u = 0$), the value of integration constant B can be determined:

$$B = \frac{2F}{\pi E}\ell n d \quad .$$

Substituting values for the constants of integration into equations 4.12(a) and 4.12(b), the expressions for radial and tangential displacements within the plate become:

$$u = -\frac{2F}{\pi E}\cos\Theta \, \ell n r - \frac{(1-\nu)}{\pi E}F\Theta\sin\Theta + \frac{2F}{\pi E}\ell n d \cos\Theta \quad , \qquad (4.13(a))$$

and

$$v = \frac{2\nu F}{\pi E}\sin\Theta + \frac{2F}{\pi E}\ell n r \sin\Theta - \frac{(1-\nu)}{\pi E}F\Theta\cos\Theta + \frac{(1-\nu)}{\pi E}F\Theta\sin\Theta - \frac{2F}{\pi E}\ell n d \sin\Theta \quad . \qquad (4.13(b))$$

Displacements along the horizontal boundary relative to the point of load application are determined by substituting $\theta = \pm\frac{\pi}{2}$ into equations 4.13(a) and 4.13(b).

Expressions for radial displacements, parallel to the boundary give

$$u_{(\Theta = \frac{\pi}{2})} = u_{(\Theta = -\frac{\pi}{2})} = -\frac{(1-\nu)F}{2E} \quad . \qquad (4.14(a))$$

The first two equations ensure that points along the boundary equidistant from the point of load application are subjected to constant horizontal displacement directed towards the point of application.

Expressions for tangential displacements;i.e. perpendicular to the boundary :

$$v_{(\Theta = -\frac{\pi}{2})} = -v_{(\Theta = \frac{\pi}{2})} = \frac{2F}{\pi E} \ln \frac{d}{r} - \frac{(1+\nu)F}{\pi E} \quad . \qquad (4.14(b))$$

At points along the boundary equidistant from the point of load application the vertical displacement is the same. At the point of load application the equation calculates an infinitely large displacement which may be excluded by excluding a semi-cylindrical portion of material in this region.

4.2.2 Uniform Loading of a Straight Boundary

Consider a uniform load distribution of length l, acting vertically over a section of a horizontal straight boundary of a semi-infinite plate with uniform width , diagramatically illustrated by figure 4.2.

The distribution is divided into a number of elements of length dr (unit width), each subject to a load of intensity q. The vertical displacement at a point '0' (equivalent to the tangential displacement relative to the point of load application) on the horizontal straight boundary at a distance r from the element will be evaluated by expressing the load as qdr and substituting into equation 4.14(b) to give:

$$v_0 = \frac{2q}{\pi E} \ln \frac{d}{r} \, dr - \frac{(1+\nu)}{\pi E} \, qdr \quad . \qquad (4.15)$$

By applying equation 4.15, the vertical displacement at any point along the initially straight boundary may be determined:

(i) External to the load distribution:

As the distributed load is uniform with intensity q, equation 4.15 may be rewritten:

$$v_o = \frac{2q}{\pi E} \int_x^{\ell+x} \ln\frac{d}{r}\, dr - \frac{(1+\nu)q}{\pi E} \int_x^{\ell+x} dr \quad .$$

By integrating and rearranging, we obtain:

$$v_o = \frac{2q}{\pi E}\left[(\ell+x)\ \ln\frac{d}{(\ell+x)} - x\ln\frac{d}{x}\right] + \frac{(1-\nu)\ell q}{\pi E} \quad . \qquad (4.16)$$

(ii) Within the load distribution:

Equation 4.15 may be rewritten:

$$v_o = \frac{2q}{\pi E} \int_x^{\ell-x} \ln\frac{d}{r}\, dr - \frac{(1+\nu)q}{\pi E} \int_x^{\ell-x} dr \quad .$$

By integrating and rearranging, we obtain:

$$v_o = \frac{2q}{\pi E}\left[(\ell-x)\ \ln\frac{d}{(\ell-x)} + x\ \ln\frac{d}{x}\right] + \frac{(1-\nu)}{\pi E}\ \ell q \quad . \qquad (4.17)$$

4.2.3 Uniform Loading of Elements Along a Straight Boundary

Consider the displacement of a series of elements along a straight boundary of a semi-infinite body of uniform depth, which result from a uniform pressure P, acting at a single element as illustrated in figure 4.3. Equations 4.16 and 4.17 are adjusted to include the uniform pressure distribution over the loaded element since this parameter equates to the product of the load intensity q, and the element surface area, to give:

$$V = \frac{2P}{\pi E}\left[(\ell+x)\ln\frac{d}{(\ell+x)} - x\ \ln\frac{d}{x}\right] + \frac{(1-\nu)P\ell}{\pi E} \quad , \qquad (4.18)$$

for the unloaded elements, and:

$$V = \frac{2P}{\pi E}\left[(\ell-x)\ell n\frac{d}{(\ell-x)} + \ell n\frac{d}{x}\right] + \frac{(1-\nu)P\ell}{\pi E} \quad , \qquad (4.19)$$

for the loaded element.

By rearranging we obtain:

$$V = P\left[\frac{2}{\pi E}\left[(\ell+x)\ \ell n\frac{d}{(\ell-x)} - x\ \ell n\ \frac{d}{x}\right] + \frac{(1-\nu)\ell}{\pi E}\right] \quad , \qquad (4.20)$$

and

$$V = P\left[\frac{2}{\pi E}\left[(\ell-x)\ \ell n\frac{d}{(\ell-x)} + x\ \ell n\ \frac{d}{x}\right] + \frac{(1-\nu)\ell}{\pi E}\right] \quad , \qquad (4.21)$$

respectively.

Equation 4.20 or 4.21 then may be applied to each element to determine the deflection caused by the active pressure band.

Considering a series of elements along a straight boundary, each subjected to a uniformly distributed pressure of varying intensity, the total displacement of each element can be determined by summing the deflection due to the directly impinging pressure distribution and the deflections associated with the pressure distributions active on neighbouring elements. These may be expressed as a series of simultaneous equations of the form:

$$V_i = P_j\ \Sigma a_{ij} \quad ,$$

or in matrix form as:

$$[V] = [P]\,[A_{ij}] \quad . \tag{4.22}$$

For cases in which the element displacements are known, the magnitude of the corresponding pressure distributions can be determined by establishing the inverse of the matrix of coefficients $[A_{ij}]$. Consequently, equation 4.22 is rearranged to:

$$[P] = [A_{ij}]^{-1}\,[V] \quad . \tag{4.23}$$

To implement equations 4.20 and 4.21 in the form of equation 4.23, it is necessary to determine the distance from each element to its limit of its influence. It is considered that the distance d, adheres to the form:

$$d = C \times \ell \quad , \tag{4.24}$$

where C is an influence constant and ,

ℓ the element breadth .

Evaluation of influence constant C depends upon the formulation of empirical relationships to satisfy boundary conditions relating to specific applications.

The present study considers the elastic deformation of elements of an indentor or roll within the contact interface during deformation of strip specimens. By including empirical relationships to determine the influence constant, the associated pressure distributions can be estimated by the described analysis.

By arranging the pressure values $\bar{P}$, and the contact lengths $\overline{CL}$, across the strip width W, the separating force F_S, may be determined by:

$$F_s = \bar{P} \times \overline{CL} \times W \tag{4.25}$$

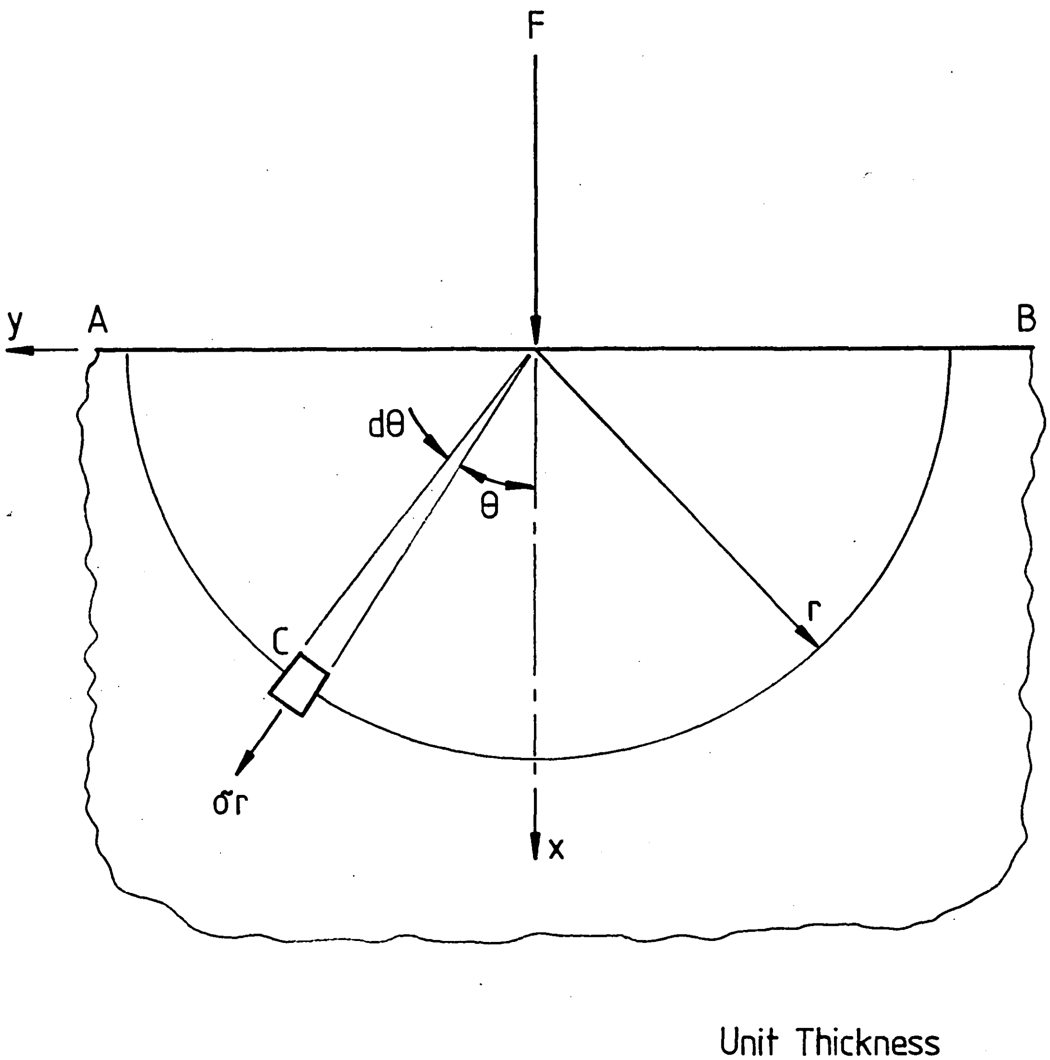

FIG 4.1 : CONCENTRATED LOADING OF A STRAIGHT BOUNDARY

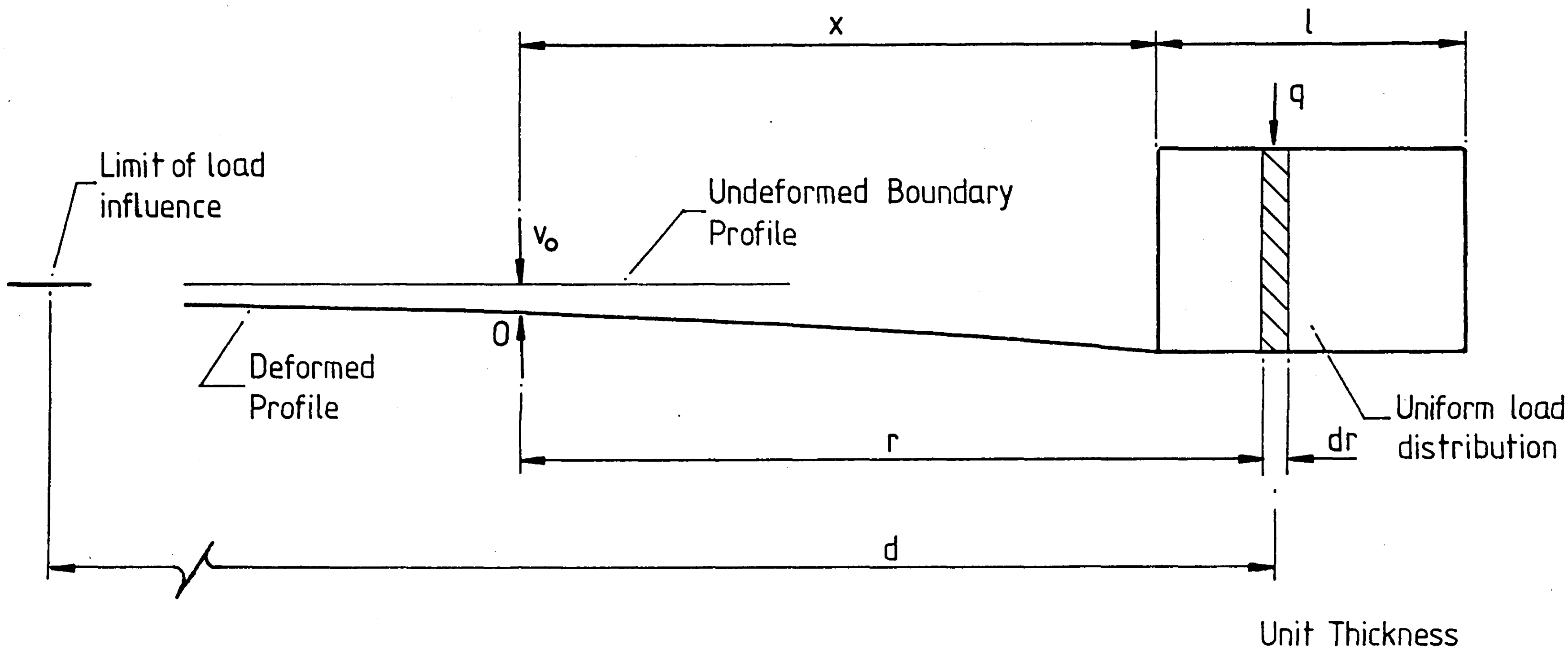

FIG 4.2 : UNIFORM LOADING OF A STRAIGHT BOUNDARY

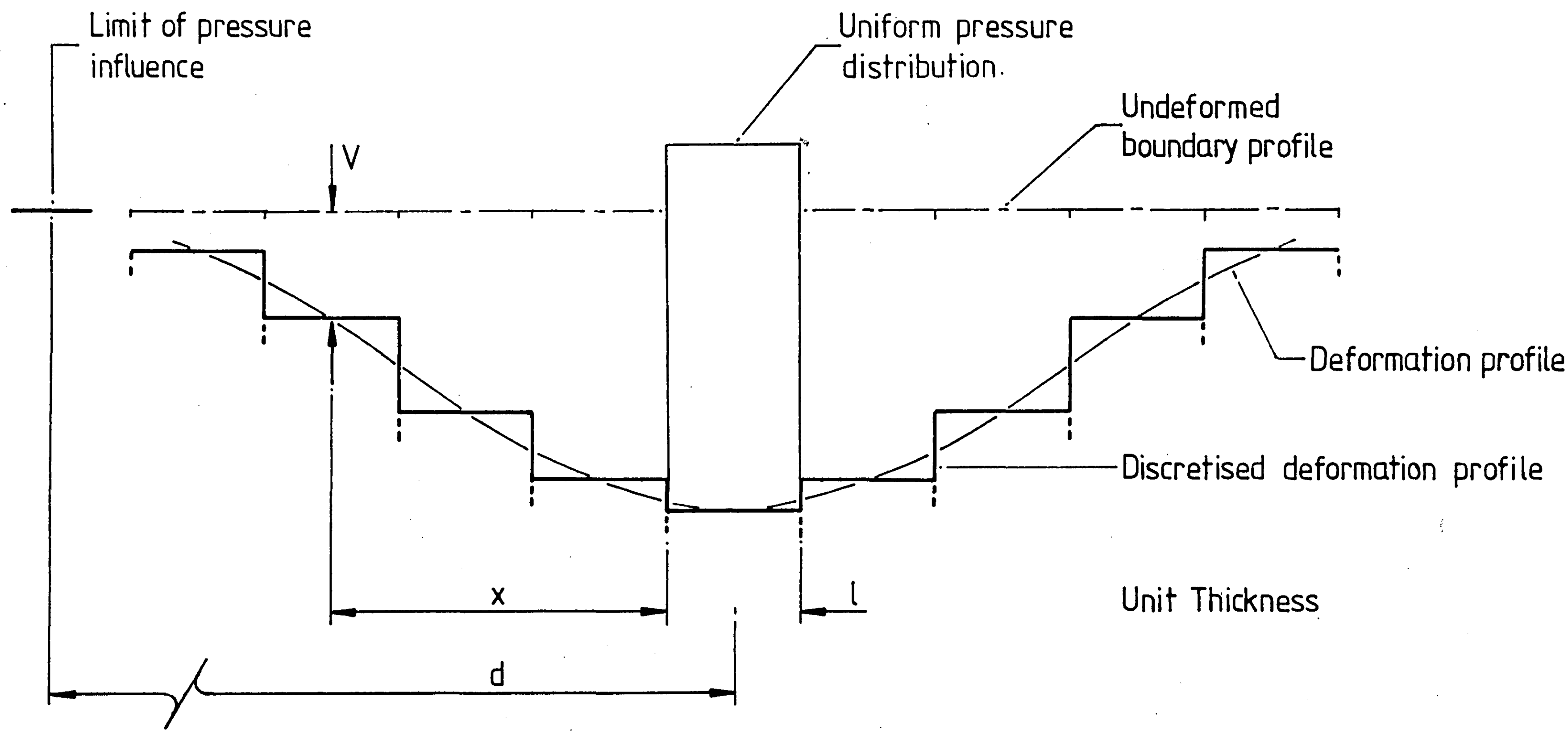

FIG 4.3 : UNIFORM PRESSURIZING OF AN ELEMENT ALONG A DISCRETIZED STRAIGHT BOUNDARY

CHAPTER 5

STRUCTURE OF THE COMPUTER PROGRAMS

5.1 Introduction

For each deformation mode under investigation, computer programs have been formulated to evaluate:

(a) Influence constant values.

(b) Pressure distributions and separating forces.

Based on readings and measurements relating to a single experimental test, program 'a' equates the applied and calculated separating forces to determine the value of the influence constant which satisfies the specific indenting or rolling conditions.

Determining influence constant values from a series of experimental tests in which specific parameters vary allows the formulation of relationships, applicable over the range of the variables. Insertion of the empirical relationships into program 'b' allows the determination of pressure distributions and separating loads for any deformation condition within the designated ranges by adopting similar measurement procedures.

The computer programs formulated to evaluate the influence constant values have been adapted from the pressure distribution programs 'b'.The necessary modifications have been discussed in section 5.6.

The analyses have been carried out on an IBM 4341 mainframe computer using the IBMBASIC computer language. This enables ready translation to most languages used by inexpensive 'desktop' micro-computers.

5.2 Pressure Distribution Program for Analysing the Static Indentation of Flat Strip Specimens

5.2.1 Basic Structure of the Program

The principal operations within the pressure distribution program for the static indentation of flat strip specimens have been listed below:

(i) Input mechanical and geometric parameters of the indentor and strip specimen.

(ii) Read nodal data relating to the measurements along the arc of contact at a single section across the strip width and establish the optimum circular arc passing through the points.

(iii) Compensate for the elastic recovery of the strip material along the arc of contact following load relaxation.

(iv) Compare the rigid and deformed indentor profiles along the arc of contact so determining the extent of elastic deformation under loading.

(v) Discretise the deviation between the rigid and deformed indentor arcs.

(vi) Estimate the influence constant by interpolation of empirical functions.

(vii) Estimate the pressure distribution impinging upon the elements along the arc of contact by augmented matrix solution methods applied to equations derived from solid body contact theory.

(viii) Repeat operations (ii) to (vii) for the remaining sections and calculate the separating force based on average pressure and contact arc length values.

The itemised operations are fully detailed in sections 5.2.3 to 5.2.8.

5.2.2 Underlying Assumptions and Simplifications Inherent in the Program

In formulating the pressure distribution program for the static indentation of flat strip specimens, a number of assumptions and simplifications were included, which are listed below:

(i) Values of Young's modulus of elasticity and Poisson's ratio for the indentor material were taken from BS Specifications.[52]

(ii) The elastic recovery in thickness of the strip material was considered constant along the arc of contract following load relaxation.

(iii) The stress within the strip material was considered independent of the thickness.

(iv) The deformation of the strip material was considered to be homogenous.

(v) The overall movement measured by the displacement transducers during loading was considered to be that produced by the rigid indentor profile produced at the centre of indentation.

(vi) Deflection of the indentor in the direction of load was considered to be negligible.

(vii) The profile of the elastically deformed indentor was considered to remain circular in section along the arc of contact during loading.

(viii) Deviations between the rigid and deformed indentor profiles were determined normal to the horizontal strip surface.

(ix) Displacement of the deformed indentor elements were considered to behave as do those along a straight boundary.

(x) Each deformed indentor element was considered subject to a uniform pressure distribution across its breadth (unit width).

(xi) The empirical functions used to evaluate the influence constant were related to the change in indentor radius.

(xii) The influence constant at a section was applied equally to all deformed indentor elements along the arc of contact.

5.2.3 Input of Mechanical and Geometric Parameters

In addition to the co-ordinates of nodal measurements along the contact arc at each section across the width of an indented flat specimen, operation of the computer program requires the input of the measured or estimated values for the following parameters. Methods of determination are indicated with each parameter.

(i) Undeformed radius of the indentor body : measured by micrometer (mm).

(ii) Young's modulus of elasticity of the indentor body material : established from British Standard Specifications[52] (MN mm^{-2}).

(iii) Poisson's ratio of the indentor body material : established from British Standard Specifications.

(iv) Width of the strip specimen : measured by micrometer (mm).

(v) Mean vertical displacement of the indentor and strip during loading : average change in position monitored by the displacement transducers (mm).

(vi) Mean recovered displacement of the indentor and strip following load relaxation : difference between (v) and the average position monitored by the displacement transducers following load relaxation (mm).

Each parameter was entered into the computer program in terms of the units as indicated within the brackets, above.

5.2.4 Determination of the Measured Indentation Radius

Operation of the computer program required evaluation of the radius of circular arc which exhibited the optimum correlation to the measured nodes at each section across the width of an indented flat specimen. This radius has been referred to as the Measured Indentation Radius, MIR, in the text.

Owing to measurement inaccuracies the nodal positions will not exactly lie on a circular arc. To establish the best circular arc through the points under consideration the following conditions were imposed:

(i) The circular arc always passes through the node at the indentation centre without error.

(ii) For all other nodes the measurement uncertainties were only considered in the vertical direction.

A least-squares curve-fitting routine was implemented to relate the vertical distances from each node to the corresponding points on a series of incrementing 'test-curves'.

The sum of the distances squared decreased as the optimum radius approached, and increased once it had passed. Refinement of the incremental step proceeded once the optimum radius had been passed. This routine was repeated until calculations over diminishing ranges converged to a solution of satisfactory precision.

To ensure that no erroneous measurements had corrupted the determined radius value, limits of $\pm 2\mu m$ were imposed on the accepted arc. Nodes outside the limits were disregarded and the radius re-evaluated using the acceptable points only. This procedure was repeated until all nodes during a cycle were within limits. Figure 5.1 depicts the configuration of a determined arc for a typical section, table 5.1 lists the format by which the analysis has been presented in the computer program for the same section. Giving an immediate assessment to the validity of a set of measurements by displaying the percentage of nodes accepted for the final radius evaluation.

5.2.5 Determination of the Deformed Indentor Radius

By assuming that the strip material recovers a constant radial distance along the arc of contact following load relaxation, it was considered that the deformed indentor radius, R, would be evaluated by a function of the form:

$$R = MIR + 0.1\ E_R \quad , \qquad (5.1)$$

TABLE 5.1 : PRESENTATION OF THE CURVE-FIT ANALYSIS FOR AN ARC ALONG A TYPICAL SECTION

% NODES ACCEPTABLE = 76

DEVIATION DATA FOR REJECTED NODE(S) :-

NODE	DEVIATION (MICRONS)
4	+2.2
11	+3.2
14	+3.0
16	-3.3

DEVIATION DATA FOR ACCEPTABLE NODE(S) :-

NODE	Y CO-ORD (EXP) (mm)	Y CO-ORD (CALC) (mm)	DIFFERENCE (MICRONS)
1	0.914	0.915	-1.0
2	0.706	0.704	+1.7
3	0.523	0.522	+0.6
5	0.242	0.241	+1.7
6	0.143	0.141	+1.7
7	0.067	0.067	-0.3
8	0.022	0.021	+1.3
9	0	0	0
10	0.023	0.021	+1.8
12	0.142	0.141	+0.9
13	0.242	0.241	+0.9
15	0.521	0.522	-1.2
17	0.914	0.915	-1.0

where E_R denotes the total recovered displacement of the indentor and strip following load relaxation.

Analysing the yield characteristics of the strip material by simple compression tests (see section 6.2) enabled the differences in true strain values between loaded and relaxed conditions to be compared. When applying the resulting empirical relationship to known relaxed strain values along typical contact arcs, it was found that the variations in elastic recovery were small (range of $0.075E_R$ - $0.125E_R$) with a mean of approximately $0.1E_R$.

5.2.6 Comparison between the Rigid and Deformed Indentor Profiles

The elastic deformations of the indentor body have been determined at each measured section across the width of the indented specimen. This has been achieved by superposition of the rigid indentor profile together with the deformed indentation radius along the arc of contact at each section.

It was considered that the maximum penetration of the rigid indentor profile from the original strip surface was equal to the mean vertical displacement of the indentor and strip during loading. By Pythagoras Theorem the positions on the horizontal strip surface through which the rigid indentor arc passed were determined. Positions A and B in figure 5.2 mark the limits of the elastic deformation zone and concur with the deformed indentor profile. Figure 5.2 schematically illustrates the configuration of the elastic deformation zone at a section showing the magnitude of the deviation between arcs varying between zero at the edges to a maximum at the centre.

Discretisation of the distance between A and B allows the deformation zone to be represented by a series of elements. The magnitude of each element corresponding to the deviation between the rigid and deformed circular arcs at the centre of each discretised region.

5.2.7 Determination of the Pressure Distribution

The active pressure distribution at the interface between the indentor and flat strip has been estimated at each measured section across the specimen width.

The displacement of each element within the elastic deformation zone was considered to be the result of a uniform pressure distribution acting over the surface and the effects of the pressure on the surrounding elements. The magnitude of the deviations have been predicted by solid body contact theory and expressed by equations 4.20 and 4.21. Interpolation of an influence constant C, from empirical relationships incorporated within the program enables the pressure distribution to be estimated by a standard matrix solution package applied to matrix equation 4.23.

5.2.8 Separating Load Estimation

Determination of the mean pressure along each arc of contact entailed averaging the values acting on the individual elements. Similarly the mean pressure and contact arc length across the indentation width were determined by averaging the sectional values. This enabled equation 4.25 to be used to give the indentor separating load.

5.3 Modifications to the Pressure Distribution Program for Analysing the Static Indentation of Inclined Strip Specimens

Analysis of the pressure distribution and separating loads developed at the interface between a vertically loaded indentor and an inclined strip specimen have been undertaken using a computer program of similar structure to that described in section 5.2.1. Minor alterations were necessary, mainly due to the non-alignment of the normal at the indentation centre and the direction of the applied load.

The underlying assumptions and simplifications within the computer model correspond to those listed in section 5.2.2, with minor modifications to (v) and (viii) and an addition (xiii) (the numerals in brackets correspond to the listing in section 5.2.2).

(v) The mean vertical movement measured by the displacement transducers during loading was considered to be that of the rigid indentor profile.

(viii) Deviations between the rigid and deformed indentor profiles were determined normal to the inclined strip surface.

(xiii) The magnitude of the applied load normal to the inclined surface was considered to be a component of the total applied load. Deformation of the strip specimen was attributed to the load normal to the inclined surface.

Operation of the pressure distribution model followed the sequence of operations described in sections 5.2.3 to 5.2.8 when related to the static indentation of flat strip specimens. A resumé of each section follows in which the requisite modifications are described:

Input of Mechanical and Geometric Parameters.

The nodal measurements at each section across the indented strip width and all parameters were required, in addition:

Angle of inclination of the strip specimen : measured by Angle Dekkor (radians).

Determination of the Measured Indentation Radius.

The nodal measurements at each section were established normal to the inclined surface by tilting the specimen through the angle of incline prior to commencement (see section 3.3). This allowed evaluation of the MIR by the previously described technique.

Determination of the Deformed Indentor Radius.

This remained unaltered when applied to the inclined specimen tests.

Comparison between the Rigid and Deformed Indentor Profiles.

The direction of movement monitored by the displacement transducers during loading was not collinear with the normal from the indentation centre. As a result geometric relationships were used to determine the distance between the undeformed inclined strip surface and the indentation centre, normal to the angle of inclination. This distance was considered the maximum penetration of the rigid indentor profile normal to the inclined surface. Determination of the positions on the inclined strip surface coincident with the rigid indentor arc and all other operations in the section proceeded as before.

Determination of the Pressure Distribution:

The form remained unaltered when applied to the inclined specimen tests.

Inclined Load Estimation:

The total separating load F_s, was determined by reconstituting the loads normal and perpendicular to the inclined strip surface which resulted in equation 4.25 becoming:

$$F_s = \frac{\bar{P} \times \overline{CL} \times W}{\cos \alpha} \tag{5.2}$$

5.4 Operational Difficulties using the Static Indentation Pressure Programs

Prior to formulating the pressure distribution model for analysing the interrupted-pass workpieces, considerations were given to the operational difficulties and weaknesses within the static indentation programs. The areas of concern are discussed along with the techniques adopted to improve the modelling process.

(i) Input of Measured Nodal Data

Due to the large number of nodal measurements required within an analysis the likelihood of entering erroneous data values proved to be high. By including a routine within the computer program which enabled the data at each individual node to be corrected, the process was made considerably more effective.

Initial analyses often entailed the repetition of calculation using the same nodal data. Blocks comprising the data for individual tests were stored in the computer memory or in separate files and merged with the pressure distribution programs when required, thus greatly reducing the time required for data input.

(ii) Sectional Evaluation of the Vertical and Recovered Displacements

The positional changes monitored by the displacement transducers were rarely identical following both load application and relaxation. This was primarily due to uneven loading of the specimen by the indentor. As a result compensatory factors were introduced to estimate the vertical and recovered displacements at each measured section. These assumed that the displacements along the indentor length between the transducers adhered to linear relationships.

(iii) Sectional Evaluation of the Measured Indentation Radius

The analyses of results from initial tests showed that a poor correlation existed between the nodal measurement positions and the optimum indentation arc, with an average of only 48 per cent nodal acceptance. This was attributed primarily to the consideration that the node at the indentation centre had no measurement uncertainties.

To improve correlation, the positioning of the nodes at the indentation centres were subject to alterations within the limits of the measurement uncertainties. These entailed maximum displacements of $\pm 2\mu m$ in the vertical and $\pm 20\mu m$ in the horizontal repositioning. Careful considerations of the polarity and magnitude of the rejected nodes presented in the curve-fit analysis at each section enabled the improved positioning of the central node.

Implementation of this technique improved acceptances to an average of 72 per cent for flat and 85 per cent for inclined specimen tests.

5.5 Modifications to the Pressure Distribution Program for Analysing the Interrupted Rolling Pass Workpieces

The basic structure of the programs previously developed were retained for this analysis. However, alterations were implemented due to consideration of the operational difficulties and assumptions associated with the previous programs, and the change of deformation mode. The detailed structure of the revised program is represented in the form of a flow chart, and presented along with the listing in Appendix II.

Alterations to the underlying assumptions and simplifications are detailed below (the numerals shown in brackets correspond to the listings in sections 5.2.2 and 5.3. All references to indentors should be reconsidered as rolls in the context of the present application):

(v) and (vi); not applicable to the present program.

(ii) The elastic recovery of the strip material was no longer considered constant along the arc of contact following load relaxation. Consequently, the deformed roll profile deviates from that of a circular arc.

(viii) Deviations between the rigid and deformed roll profiles were determined normal to the chord linking the extremities of the deformation zone.

The pressure distribution program follows the operational sequences described in sections 5.2.3 to 5.2.8. The sections which have undergone substantial modifications are discussed in the following sub-sections.

5.5.1 Input of the Mechanical and Geometric Parameters

The present program was formulated to have the option of inputting the measured nodal data in block or in single entry formats. The latter corresponds with the program documented in Appendix II.

For instances where the deformed surfaces have been inspected using a contact technique (such as with the Merlin 750M), compensatory calculations are introduced to minimise errors developed due to the contact configuration. Surface gradient is established at each node from which the discrepancies between the actual depth measurement (probing with a spherically ended stylus) and the theoretical measurement (probing with an infinitely sharp stylus) are determined.

Operation of the program requires the additional parameters:-

Initial strip thickness : Measured using a micrometer (mm)
Final strip thickness : Measured using a micrometer (mm)

The vertical and recovered displacements no longer apply.

5.5.2 Determination of the Measured Roll Radius

Evaluation of this variable in the present program does not employ the incremental least-squares curve-fitting technique previously used, since it was considered ineffective due to the arbitary positioning of the central node (assumed to have no measurement uncertainties) and the extensive time required to reach a satisfactory solution. Instead, a technique based on arc-chord theory was developed which similarly assumes that all measured points along a section are positioned on a circular arc.

Determination of the radius and central co-ordinates of a circular arc require knowledge of the relative positions of a minimum of three points along the arc. In the present analysis the relative positions of between 10 and 30 points were determined along the arc of contact at each section. This enabled the evaluation of each sectional radius and centre co-ordinates to proceed on a basis of averaging all specified nodal combinations.

An incremental routine was initiated to select each nodal combination. Within each combination, all constituent nodes were separated by a minimum of two measured points to avoid localised distortions along small arc lengths. A filtering system was used to detect and nullify all combinations whose radius appeared grossly inaccurate.

After ascertaining the average sectional radius and centre co-ordinate values, limits of $\pm 10\%$ were imposed on the mean and all combinations whose radius did not lie within the bounds of the limits were disregarded. All valid combinations were summed and averaged to determine the final sectional radius and centre co-ordinate values. The percentage of acceptable nodal combinations was presented to give an immediate assessment of the validity of the measurements.

5.3.3 Determination of the Differences Between the Rigid and Deformed Roll Profiles

In the present computer program a non-uniform elastic recovery of the strip material was considered. Empirical relationships were established by considering the differences between the axial lengths for loaded and relaxed conditions from uniaxial compression tests on samples of the strip material (detailed in section 6.2). This enabled the elastic recovery of the strip material to be estimated at any position along the measured profile.

Figure 5.3 shows the measured deformation profile along a typical section. To establish the positions at the ends of the rigid and deformed roll profiles, A and B, considerations were made regarding the elastic recovery of the strip material. Locating of points A and B proceeded by estimating the elastic recovery at each end of the measured arc, and angularly projecting these positions to coincide with the entry and exit planes, respectively.

Discretizing the chord linking A and B enabled the differences in the normal distances from each point to the rigid and measured profiles to be determined. By subtracting the normal component of the elastic recovery estimated at each point, the discretized deviations between the rigid and deformed roll profiles may be determined. Figure 5.4 schematically shows this procedure.

5.5.4 Determination of the Pressure Distributions and Separating Loads

Determination of the pressure distribution along each section proceeded unaltered. Similarly, the mean pressure and contact arc lengths were determined at each section across both deformed surfaces. Since it was considered that a constant separating load was developed between the workpiece and the rolls, a single value was determined from the sectional averages in accordance with equation 4.25.

Representative sections of the output from the computer program are presented in Appendix III. They relate to the analysis of a typical workpiece following an interrupted-pass rolling test.

5.6 Structure of the Influence Constant Evaluation Programs

The influence constant evaluation programs were developed by modifying the pressure distribution programs. Relating to each deformation mode, the requisite modifications were similar at a structural level with the detailed modelling of each operation remaining unaltered. The structure of the program relating to the interrupted-pass rolling tests is represented in the form of a flow chart, and presented along with the listing in Appendix II.

The structural similarities and differences are considered in conjunction with the listings in section 5.2.1.

Initial operations (i) to (v) remain applicable in the current program. The sequence and purpose of the remaining operations differ as follows:

(vi) Repeat operations (ii) to (v) for all remaining measured sections and determine the mean values of:

- deformed roll/indentor radius
- deformed and rigid contact arc lengths and angles
- discretized deviations between the rigid and deformed indentor/roll profiles.

(vii) Input experimentally determined applied load. Select the range and increment of the prospective influence constant and initiate the first value.

(viii) Estimate the pressure distribution and separating load using the averaged data in conjunction with the selected constant.

(ix) Repeat operation (viii) with the remaining influence constant values within the loop. Implement range refinement routines until the calculated load converges to the applied load.*

(x) Display the constant and related data appertaining to the optimum correlation conditions.

---

* Convergence of the calculated load depends upon the suitability of the range and increment of the influence constant.

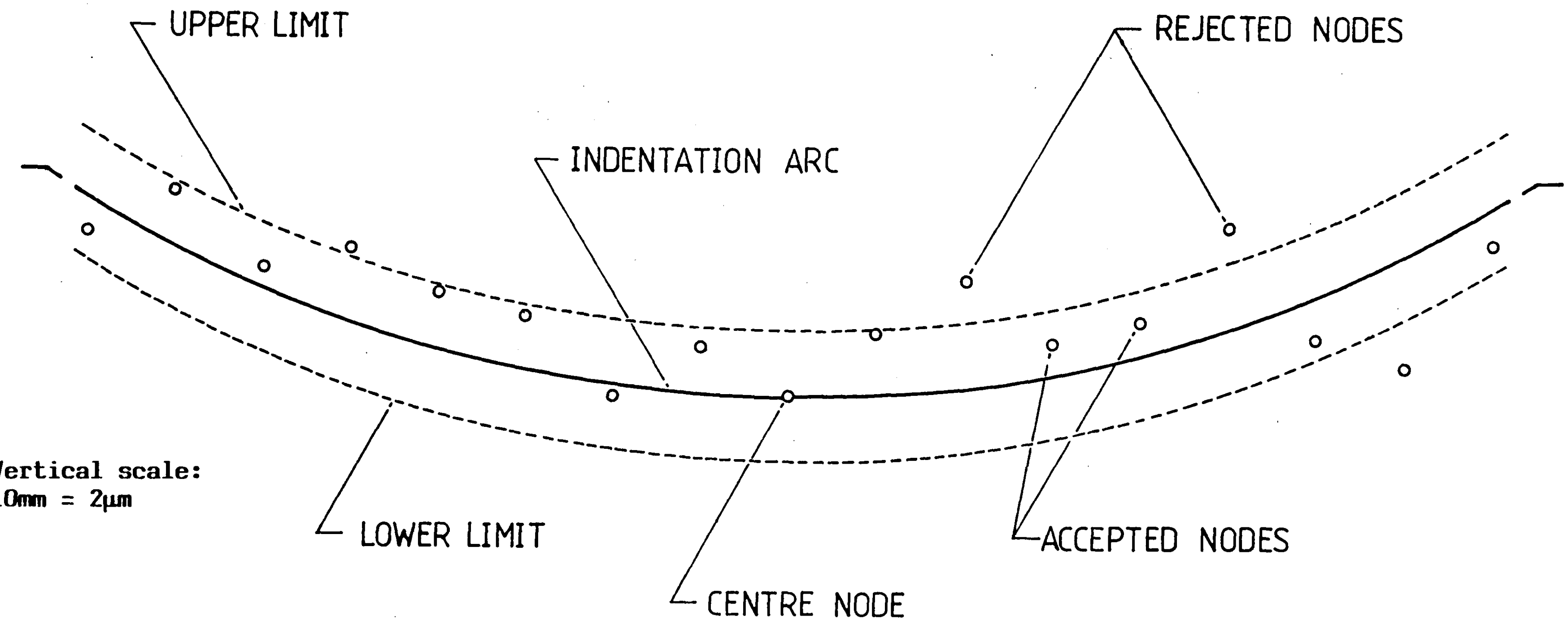

FIG 5.1 : SCHEMATIC REPRESENTATION OF THE CURVE FIT ANALYSIS FOR AN ARC ALONG A TYPICAL SECTION : STATIC INDENTATION TEST

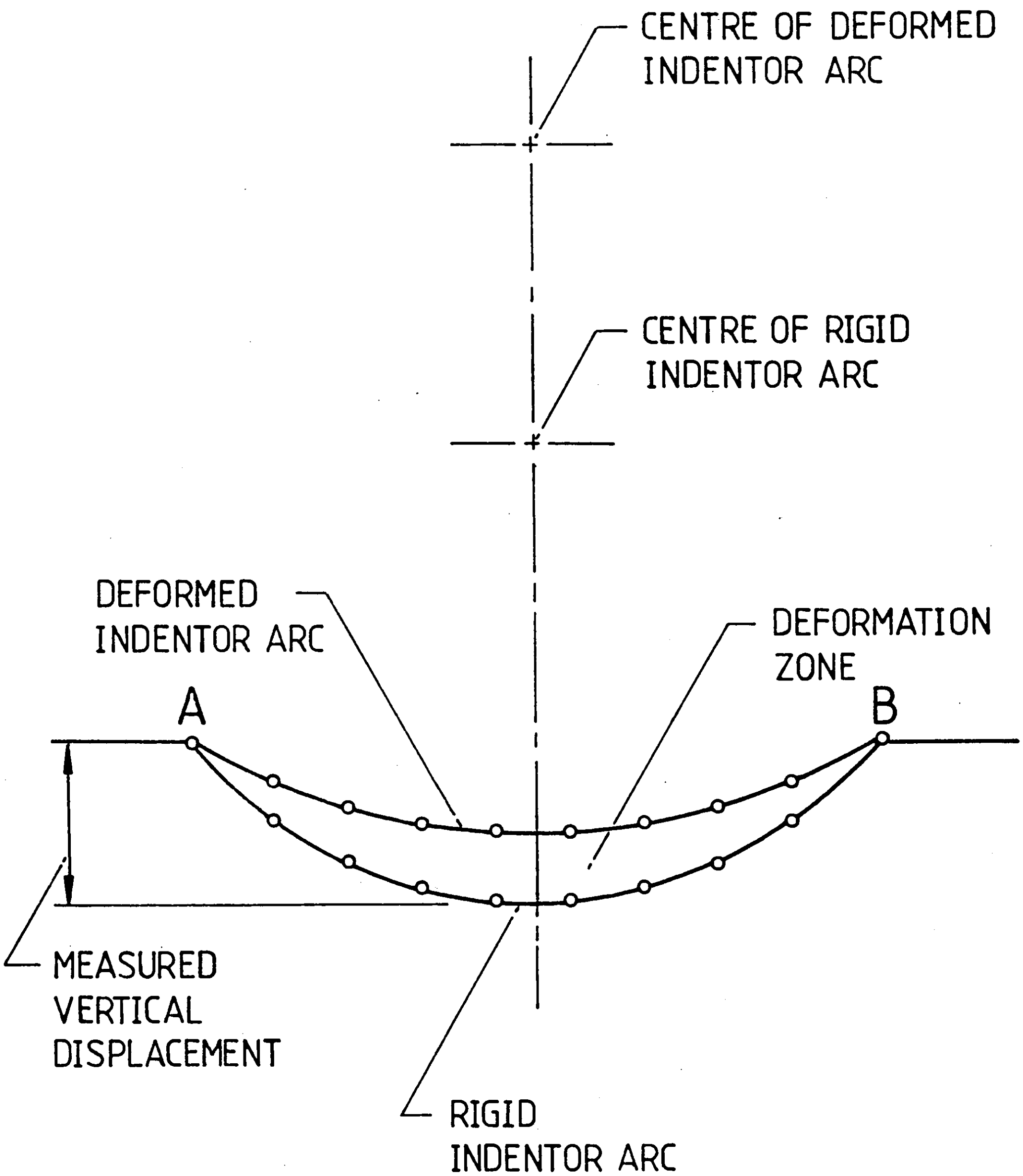

FIG 5.2 : SCHEMATIC REPRESENTATION OF THE RIGID AND DEFORMED INDENTATION ARC CONFIGURATIONS : FLAT STRIP SPECIMEN

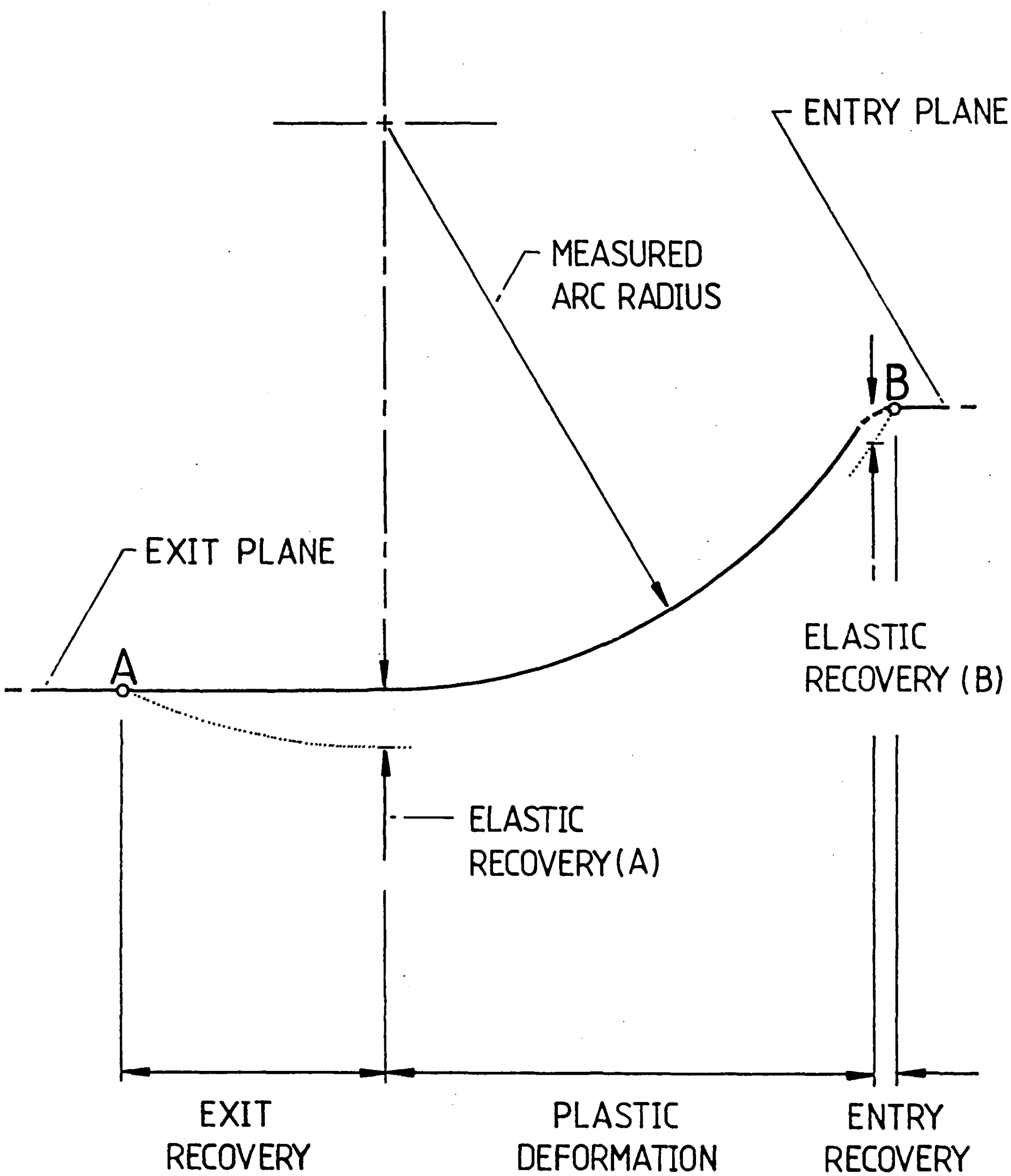

FIG 5.3 : SCHEMATIC REPRESENTATION OF THE MEASURED DEFORMATION PROFILE : INTERRUPTED-PASS WORKPIECE

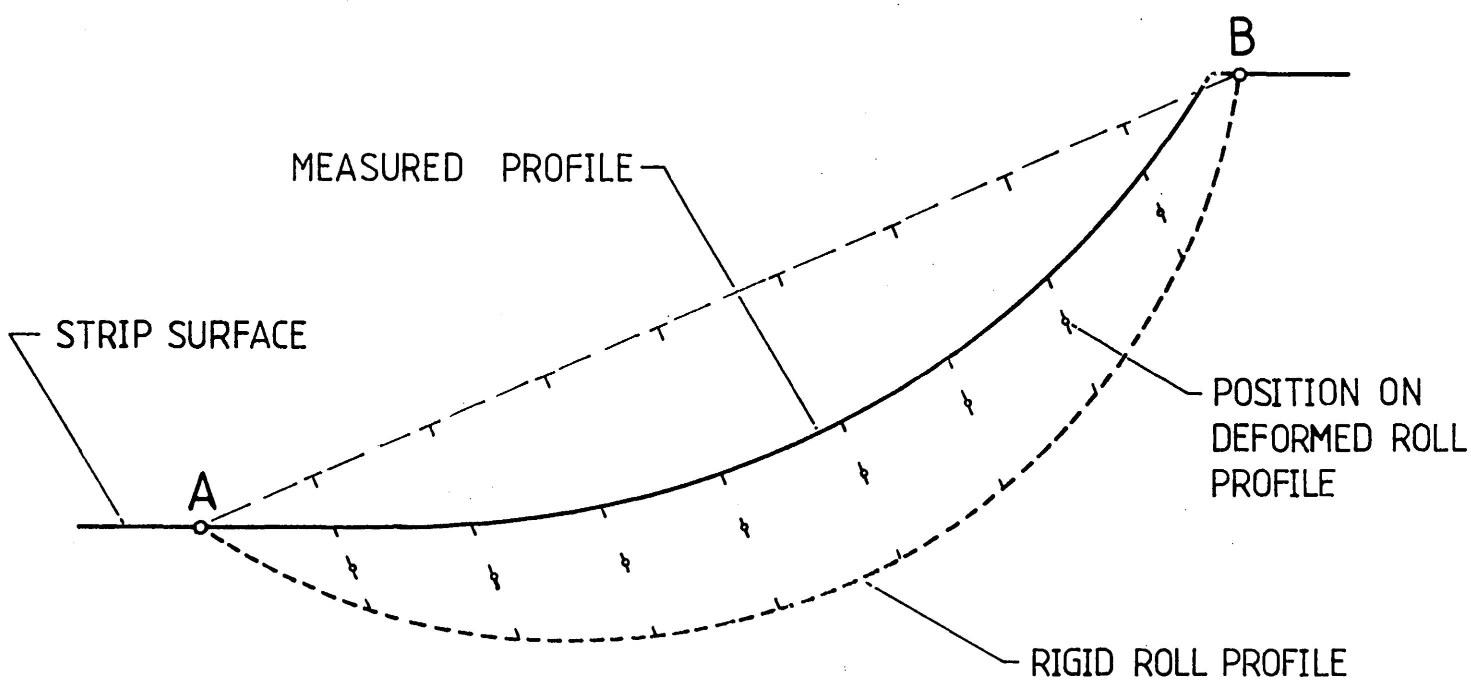

FIG 5.4 : SCHEMATIC REPRESENTATION OF THE CONFIGURATION OF THE MEASURED, DEFORMED AND RIGID ROLL PROFILES ALONG A TYPICAL SECTION : INTERRUPTED-PASS WORKPIECE

CHAPTER 6

EXPERIMENTAL RESULTS

6.1 Introduction

The experimental work was aimed at deforming strip workpieces in the following modes:

(i) quasi-static indentation of flat strip specimens;

(ii) quasi-static indentation of inclined strip specimens;

(iii) interrupted passes during cold rolling.

The profiles of the indentors or rolls imparted into the surfaces of the workpieces during the deformations were accurately measured at a number of sections. The extent of the elastic deformation of the indentor or roll along the arc of contact at each section was determined by 'fitting' the optimum circular arc passing through the measured data points, then compensating for the elastic recovery of the workpiece material. The displacements of the workpiece material within the plastic region is less predictable than during its elastic deformation. Consequently preliminary experimentations were conducted to ascertain the characteristics of the stress- strain behaviour of each workpiece material under plastic deformation conditions. By establishing the stress-strain behaviour at both the loaded and relaxed states at each deformation setting, semi-empirical relationships were developed to predict the extent of elastic recovery of the workpieces following load relaxations.

Under each deformation mode, the experimental data from each test was formulated to evaluate the influence constant required the calculated and applied loads when implementing solid body contact theory.[51] The influence constants from a series of correlated deformation tests were formulated as semi-empirical functions. Computer programs incorporating the influence constant functions were used to evaluate the sectional pressure distributions and the separating loads for the corresponding test configurations and may be used as a means of predicting these parameters for deformation conditions somewhat similar to those involved in the tests.

Detail of the experiments and preliminary analyses used in developing the influence constant functions for each deformation mode and examples of the predicted pressure distributions and comparisons between the measured and calculated separating loads are documented in this chapter.

6.2 Stress-Strain Characteristics of the Strip Materials

Although the technique developed in this investigation should provide results independent of the strip material (see section 1.4), the stress-strain characteristics of the strip materials were established for the record and in the process the relationship between the strains under loaded and relaxed states were also determined.

Initially, plane strain compression tests were carried out but were found to be non-repeatable due to the size and shape of the punch and test material. It was therefore decided to carry out relatively more controllable and accurate uniaxial compression tests on cylindrical specimens having an aspect ratio of unity, prepared from the strip material. The test results were then converted to those corresponding to plane strain conditions.

For each test, the contact surfaces between the specimens and the platens were lubricated with graphite in tallow in order to minimise frictional effects. Readings of loads and compressions were taken at close intervals throughout the tests. Knowing the initial length and diameter of each specimen, true stress and natural strain values were calculated assuming constant volume and ignoring the 'barrelling' effect.

Several compression tests were carried out for each strip material and the results are shown in figures 6.1, 6.2 and 6.3, which are assumed to take the form:

$$S = S_o + K_o \epsilon^n \tag{6.1}$$

Where S_o denotes the initial yield stress

K_o denotes the strain hardening constant

n denotes the strain hardening index

and ϵ denotes the natural strain

Using the experimental results, the above parameters were evaluated by 'curve-fitting' for each material, giving the relationships:

First batch of annealed En43A steel: Flat strip specimens:

$$S = 173 + 556\,\epsilon^{0.29} \tag{6.2}$$

Second batch of annealed En43A steel: Inclined strip specimens:

$$S = 173 + 571\,\epsilon^{0.31} \tag{6.3}$$

Annealed En2 steel: Interrupted-pass workpieces:

$$S = 173 + 627\,\epsilon^{0.28} \tag{6.4}$$

In addition to the method described, readings of the displacement following load relaxation were taken at each measurement interval. The relaxed strain value was calculated, enabling the difference between the strain values corresponding to the loaded and relaxed states to be determined.

A graphical representation of the results relating the relaxed strain to the change in strain between loaded and unloaded conditions, for the strip material of the interrupted-pass rolling tests is illustrated in figure 6.4. By curve fitting, the results closely adhere to the empirical relationship:

$$\Delta\varepsilon = 0.058\varepsilon_R^{1.257} + 0.012 \qquad (6.5)$$

Where $\Delta\varepsilon$ = Difference between natural strain and relaxed natural strain

ε_R = Relaxed natural strain

6.3 Experimental Results Relating to the Static Indentation of Flat Strip Specimen Tests

6.3.1 Scope of the Experimental Tests

The experimental work described in this section was carried out using the equipments previously described in section 2.1. Tests were carried out using both the 75mm Ø and 100mm Ø En9 steel strip specimens of 8.9mm thickness, 28.65mm length and the width varying between 30mm and 70mm.

Initial tests were undertaken to establish:

(i) The basic trends and characteristics associated with this mode of deformation.

(ii) An empirical relationship between the influence constant and the change in indentor radius.

In these tests both indentors were used to indent strip specimens of uniform width, 44.65mm at loads varying between 150kN and 400kN.

Secondary tests were later conducted using the 75mm Ø indentor to indent specimens of width varying between 30mm and 70mm, in increments of 10mm, whilst being subjected to a constant applied load of 300kN. The separating loads and pressure distributions were then predicted using the computer program encompassing the influence constant function formulated from the initial tests. The predicted and actual separating loads at the indentor and strip interface were then compared.

6.3.2 Profile Measurements showing the Effects of Data Refinement

For the strips indented during the initial tests, profile measurements were taken at three sections across the indentation width, at locations close to the edges and at the centre. Following evaluation of the profile radius along each section, a single value was determined for the strip based on the mean radius between the central and averaged edge profiles. The effects of the applied indentor load upon the averaged indentation radius for tests using both indentors are shown in figures 6.5 and 6.6.

In determining the indentation radius along each section, the data refinement technique described in section 5.2.4 was developed by considering the unsatisfactory correlation between points when using the 'original' and 'equalised' data. The 'original' data was comprised of the x and averaged z values at each node for all passes along a section. This data was directly transformed to the 'equalised' state. Since the curve-fitting routine ensures that the optimum curve passes through the central node, it was considered that by repositioning this point within its measurement uncertainties (both x and z axes) could improve the curve-fit. Two examples are illustrated in figure 6.7 in which the correlation between measured nodes and the optimum curve would improve by implementing this 'equalising' technique. Often, the corrective repositioning is aided by considering the direction of the deviations between the nodes and the optimum curve.

The positions of points evaluated using the three data processing techniques are included in figures 6.5 and 6.6. The curves adhere to the optimum curve-fit through the refined data points which approximate to hyperbolic functions of the forms when related to the applied load, L:

75mm Ø indentor:

$$\text{Measured Indentor Radius (mm)} = 37.15 + \frac{313.1}{L} \quad (6.6)$$

100mm Ø indentor:

$$\text{Measured Indentor Radius (mm)} = 49.92 + \frac{275.1}{L} \quad (6.7)$$

These functions are used in evaluating the influence constant functions.

6.3.3 Vertical Displacement and Elastic Recovery Characteristics

These parameters were directly measured during experimental operation. The effects of the applied indentor load upon the vertical displacement, V_D, of the indentor and the elastic recovery of the indentor E_R, and strip following load relaxation are shown in figures 6.8 and 6.9, respectively. Empirical relationships were established using a standard curve-fitting package on the mainframe computer. The vertical displacement relationships can be approximately described as power functions of the load, thus:

75mm Ø indentor

$$\text{Vertical displacement}, V_D \text{ (mm)} = L^{1.265} \quad , \qquad (6.8)$$

and 100mm Ø indentor

$$\text{Vertical displacement}, V_D \text{ (mm)} = L^{1.228} \quad . \qquad (6.9)$$

The elastic recovery relationships can be approximately described as hyperbolic functions of the load thus:

75mm Ø indentor

$$\text{Elastic recovery}, E_R \text{ (mm)} = \frac{L}{164.8 + 2.16\ (L)} \quad , (6.10)$$

and 100mm Ø indentor

$$\text{Elastic recovery}, E_R \text{ (mm)} = \frac{L}{162.7 + 2.52\ (L)} \quad . (6.11)$$

These functions are used in evaluating the influence constant functions.

6.3.4 Application of the Empirical Functions and the Determination of Associated Variables

The empirical relationships represented by equations 6.6 to 6.11 were used in conjunction with the geometric parameters and the material properties of the indentor and strip specimen to determine influence constant values within the designated loading range.

By equating the computed to the experimental load within the appropriate computer program, values of associated parameters were evaluated in addition to the influence constant. Over the range of the initial experimental tests the variation of these parameters with respect to the equated applied/calculated loads are graphically represented in figures 6.10 to 6.15.

6.3.5 Evaluation of Influence Constant Functions

Since the pressure distribution computer program gives both the pressure distribution and the separating load, the relationship incorporating the influence constant must be independent of these variables. Consequently, the influence constant is related to the change in indentor radius, ΔR which is defined as the arithmetic difference between the deformed and the rigid indentor radii.

By evaluating the corresponding influence constant and change in indentor radius at specific loads, a standard curve-fitting package was implemented to relate the points. Relationships were established and can be approximately described as linear functions of the change in indentor radius:

75mm Ø indentor:

$$\text{Influence constant}, C = 5 + 3.36\Delta R \qquad (6.12)$$

100mm Ø indentor:

$$\text{Influence constant}, C = 5 + 1.85\Delta R \qquad (6.13)$$

Both functions are graphically represented in figure 6.16.

6.3.6 Predictions of Pressure Distributions and Separating Loads

The effectiveness of the pressure distribution computer program incorporating the influence constant functions were assessed using data from the secondary experimental tests described in section 6.3.1. These provided an independent data-base from which the sectional pressure distributions and the total separating loads were predicted.

Across the width of each indented specimen, the profiles were measured at five equidistant sections, with three independent sets of measurements taken along each. The measured indentation radius for each section was determined using the averaged nodal measurements.

In running the computer program using solely the experimental data, pressure distributions were estimated along each section and combined to predict the distribution over the entire indentation. For a typical indentation, the extent of the elastic deformation of the indentor along a typical section is illustrated in figure 6.17(a), with the resulting pressure distribution shown in figure 6.17(b). The corresponding maximum and mean pressure values per section, across the strip width are illustrated in figure 6.18, with a three dimensional representation of the entire pressure regime active over the indented surface illustrated in figure 6.19.

The mean pressure acting on the indentation surface is used to evaluate the separating load. Table 6.1 tabulates

TABLE 6.1

VARIATIONS BETWEEN THE MEASURED AND PREDICTED SEPARATING LOADS : INDENTATION OF FLAT SPECIMENS

(static indentation of flat strip specimens - uniform loading, varying strip widths)

Strip Width mm	Applied Load kN	Predicted Load kN	Percentage Difference
30*	300	305.3	+1.7
40	300	248.9	-17.0
50	300	281.1	-6.3
60	300	324.8	+8.3
70	300	300.8	+0.3

* The displacement and pressure profiles depicted in figures 6.17, 6.18 and 6.19 correspond to this strip.

the differences between the actual and predicted separating loads corresponding to the secondary experimental tests.

To check the extent of elastic deformation of the indentor during loading a three-dimensional finite-element analysis was implemented, details of which are given in Appendix IV.

6.4 Experimental Results Relating to the Static Indentation of Inclined Strip Specimen Tests

6.4.1 Scope of the Experimental Tests

The pressure distributions and separating loads developed during the quasi-static indentation of inclined strip specimens by cylindrical indentors are predicted. The experimental tests were carried out using the equipments and in accordance with the procedures detailed in section 2.1.

The greater part of the experimental work involved using the 75mm diameter indentor to deform strips of width W, varying between 30mm and 60mm, in 10mm increments, with each deformed surface set at an angle α, of 5°, 10° and 15° to the horizontal. The strip lengths l, and maximum thicknesses t, remained constant throughout the experiments. Most combinations of the strip width and inclination angle were subjected to loads of 200kN, 300kN and 400kN. However, all combinations which included a strip width of 40mm were subjected to tests in which a range of loads varying between 200kN and 450kN were applied in 50kN increments.

The remaining experimental work involved the use of the 100mm indentor to deform each combination of strip width and angle whilst subjected to an applied load of 400kN.

6.4.2 Profile Measurements and the Sectional Variation in the Deformed Indentor Radius across an Indented Width

At insets of 1mm from each edge, profile measurements were established at five equally spaced sections across the width of each indentation, using equipments and in accordance with the procedures described in section 3.3.1. The deformed indentor radius is determined at each section by applying the refined data curve-fitting technique discussed in section 6.3.2, and then corrected to allow for the elastic recovery of the strip material following load relaxation. A single deformed indentor radius, DIR, is established for each indentation which approximates to that of the mean across the indentation width.

Values corresponding to the measured and deformed indentor radius at sections across the width of a typical indentation are listed in table 6.2. A graphical representation of the sectional variations across the indentation width is shown in figure 6.20.

6.4.3 The Relationship between the Deformed Indentor Radius and the Applied Load

Averaged deformed indentor radius values were developed from experimental results for each strip indented during

TABLE 6.2

THE VARIATION OF THE MEASURED AND DEFORMED INDENTOR RADIUS ACROSS THE WIDTH OF A TYPICAL INCLINED INDENTATION

STRIP WIDTH = 40mm

ANGLE OF INCLINE = 10°

RIGID INDENTOR RADIUS = 37.5mm

APPLIED LOAD = 350kN

VERTICAL DISPLACEMENT = 1.378mm

ELASTIC RECOVERY = 0.708mm

SECTION	MEASURED INDENTATION RADIUS (mm)	PERCENTAGE OF NODES WITHIN LIMITS	DEFORMED INDENTATION RADIUS (mm)
1	39.84	82	39.91
2	41.87	64	41.95
3	42.06	64	42.13
4	41.67	76	41.74
5	39.80	70	39.87

MEAN DEFORMED INDENTOR RADIUS = 41.82mm

the experimental tests. Figures 6.21 to 6.23 show the effects of the applied load, L, upon the deformed indentor radius, DIR, for each combination of strip width and angle, when deformed by the 75mm diameter indentor. Initial inspection of the curves suggested that the angle of incline had minimal effect upon the DIR against L relationships. Consequently the curves were combined to form the composite relationships depicted in figure 6.24. A working empirical relationship was formulated for each curve using a standard curve-fitting package. The curves can be approximately described as hyperbolic functions of the load thus:

$$\text{Deformed indentor radius DIR, (mm)} = A + \frac{B}{L} \qquad (6.14)$$

The values of A and B are also shown in figure 6.24 in tabulated form.

Values of the deformed indentor radius ascertained from the tests involving the 100mm diameter indentor, are tabulated in table 6.3.

6.4.4 Vertical Displacement and Elastic Recovery Characteristics

These parameters were measured during the experimental operation and were directly related to the prevailing loading conditions.

For the strips deformed by the 75mm diameter indentor, working empirical relationships were formulated between each parameter and the loading conditions for all combinations of strip width and angle of incline. Each

TABLE 6.3

DEFORMED INDENTOR RADIUS VALUES : 50mm RADIUS

INDENTOR INDENTING INCLINED SPECIMENS

APPLIED INDENTOR LOAD = 400kN

INCLINATION ANGLE (°) \ STRIP WIDTH (mm)	30	40	50	60
5	54.73	55.74	57.02	59.32
10	54.19	55.74	56.66	58.95
15	54.36	55.03	55.95	58.99

Radius values in mm

relationship was formulated using a standard curve-fitting package.

The function relating the vertical displacement of the indentor V_D, to the applied load L, was found to approximate to a hyperbolic of the form:

$$V_D = \frac{L}{A + B.L} \quad , \qquad (6.15)$$

where A and B are constants. The values of A and B relating to each strip configuration are listed in table 6.4. Figure 6.25 shows representative curves of the effects of applied load upon the vertical displacement of the indentor.

The variation in the elastic recovery of the strip thickness and indentor material E_R, with respect to the applied load L, were found to approximate to linear relationships of the form:

$$E_R = A.L \quad , \qquad (6.16)$$

where A is a constant. The values of A for each strip configuration are listed in table 6.5. Figure 6.26 shows representative curves of the effects of applied load upon the elastic recovery of the indentor and strip material.

From the experimental tests in which the 100mm diameter indentor was used, similar relationships were developed but on a limited scale.

6.4.5 Determination of the Influence Constant Functions

The working empirical relationships developed in sections 6.4.3 and 6.4.4 were used in association with geometric

TABLE 6.4

WORKING EXPERIMENTAL RELATIONSHIPS FOR PREDICTING THE VERTICAL DISPLACEMENT OF THE INDENTOR DURING LOADING : 37.5mm RADIUS INDENTOR INDENTING INCLINED SPECIMENS

Functional format : $V_D = \dfrac{L}{A + B.L}$

Where V_D = Vertical displacement of indentor (mm)

L = Applied load (kN)

A, B = Constants

Constant values:

Strip Width (mm)	Inclination Angle(°)	A	B
30	5	401.3	-0.51
	10	276.7	-0.27
	15	215.0	-0.16
40	5	727.2	-0.97
	10	362.4	-0.31
	15	240.4	-0.13
50	5	705.1	-0.81
	10	373.5	-0.23
	15	253.1	-0.02
60	5	603.9	-0.32
	10	419.3	-0.18
	15	290.1	-0.04

TABLE 6.5

WORKING EMPIRICAL RELATIONSHIPS FOR PREDICTING THE ELASTIC RECOVERY OF THE INDENTOR AND STRIP FOLLOWING LOAD RELAXATION : 37.5mm RADIUS INDENTOR INDENTING INCLINED SPECIMENS

Functional format : $E_R = A.L$

Where E_R = Elastic recovery of indentor and strip (mm)

L = Applied load (kN)

A = Constant

Constant values:

Strip Width (mm)	Inclination Angle (°)	A ($\times 10^3$)
30	5	1.34
	10	2.36
	15	3.45
40	5	1.32
	10	1.98
	15	3.04
50	5	1.33
	10	2.08
	15	2.97
60	5	1.25
	10	1.84
	15	3.10

parameters and material properties of the 75mm diameter indentor and specimens to evaluate influence constant values over extended loading ranges.

The influence constant evaluation computer program equates the calculated load to the effective component of the applied load active normal to the inclined surface by a converging iterative routine. The resulting influence constant value which satisfies the loading conditions is recorded. From the analysis of a typical strip configuration subject to various loading conditions over an extended load range, the applied and effective loads along with the resulting influence constants are listed in table 6.6. Due to large fluctuations in the influence constant values, a logarithmic transformation was used, and reversed in the pressure distribution program.

Functions relating the natural logarithmic values of the influence constants ln(C), to the change in the deformed indentor radius ΔR, for each strip configuration, were formulated using a standard curve-fitting package. Each relationship was found to approximate to a hyperbolic function of the form:

$$\ln(C) = D + \frac{\Delta R}{A + B(\Delta R)} , \qquad (6.17)$$

where A, B and D are constants. Calculated values of these constants are tabulated along with the respective curves in figures 6.27, 6.28 and 6.29.

TABLE 6.6

THEORETICAL VARIATION OF THE INFLUENCE CONSTANT OVER AN EXTENDED LOADING RANGE DURING DEFORMATION OF A TYPICAL INCLINED STRIP CONFIGURATION

STRIP WIDTH = 40mm

ANGLE OF INCLINE = 10°

INDENTOR RADIUS = 37.5mm

APPLIED LOAD (kN)	EFFECTIVE LOAD (kN)	INFLUENCE CONSTANT	NAT. LOG OF INFLUENCE CONSTANT
50	49.2	9635	9.17
100	98.5	1005	6.91
150	147.7	364.3	5.9
200	197.0	210.2	5.35
250	246.2	152.2	5.03
300	295.5	125.9	4.84
350	344.7	113.7	4.73
400	394.0	109.5	4.7
450	433.2	111.3	4.71
500	492.5	118.9	4.78
600	590.9	158.5	5.07
700	689.4	278.3	5.63

6.4.6 Pressure Distribution and Separating Load Predictions

The effectiveness of the pressure distribution computer program incorporating the influence constant functions was assessed by computing the calculated values with the original experimental data.

Pressure distributions were determined at each measured section, then combined to predict the pressure distribution over the entire indentation. The extent of the elastic deformation of the indentor along each section and the resulting pressure distribution were similar in profile to those depicted in figures 6.17(a) and (b) which pertain to the indentation of flat specimens. Similarly, the variation of the maximum and mean pressure across each indentation were found to be similar to the profiles illustrated in figure 6.18. A three-dimensional representation of the pressure regime acting over the indented surface of a typical inclined specimen is shown in figure 6.30.

Separating loads were determined based upon the mean pressure and the affected area of each indentation. Table 6.7 lists the differences between the actual and predicted separating loads corresponding to all the experimental tests. Predictions of separating loads from tests which involved the 100mm diameter indentor are made based on limited experimental relationships.

To confirm, or otherwise, the extent of the elastic deformation of the indentors during loading, a three-dimensional finite-element analysis was implemented using

TABLE 6.7

VARIATIONS BETWEEN THE MEASURED AND PREDICTED

SEPARATING LOADS : INDENTATION OF INCLINED SPECIMENS

75mm Ø Indentor

ANGLE OF INCLINE /°	STRIP WIDTH /mm	APPLIED LOAD /kN	PREDICTED LOAD /kN	PERCENTAGE DIFFERENCE
5	30	200	214.4	+ 7.2
		300	357.6	+19.2
		400	422.0	+ 5.5
	40	200	170.6	-14.7
		250	249.8	- 0.1
		300	293.1	- 2.3
		350	417.6	+19.3
		400	569.6	+42.4
		450	567.5	+26.1
	50	200	178.4	-10.8
		300	278.4	- 7.2
		400	403.2	+ 0.8
	60	200	210.2	+ 5.1
		300	303.3	+ 1.0
		400	401.6	+ 0.4
10	30	200	180.0	-10.0
		300	283.8	- 5.4
		400	326.0	-18.5
	40	200	199.4	- 0.3
		250	251.8	+ 0.7
		300	315.9	+ 5.3
		350	356.3	+ 1.8
		400	428.0	+ 7.0
		450	486.0	+ 8.0
	50	200	181.0	- 9.5
		300	272.7	- 9.1
		400	410.8	+ 2.7
	60	200	197.0	- 1.5
		300	293.1	- 2.3
		400	356.8	-10.8

TABLE 6.7 (cont)

ANGLE OF INCLINE /°	STRIP WIDTH /mm	APPLIED LOAD /kN	PREDICTED LOAD /kN	PERCENTAGE DIFFERENCE
15	30	200	201.6	+ 0.8
		300	315.9	+ 5.3
		400	432.4	+ 8.1
	40	200	194.0	- 3.0
		250	232.5	- 7.0
		300	276.6	- 7.8
		350	323.1	- 7.7
		400	335.2	-16.2
		450	434.3	- 3.5
	50	200	190.8	- 4.6
		300	290.4	- 3.2
		400	382.4	- 4.4
	60	200	218.6	+ 9.3
		300	284.7	- 5.1
		400	389.2	- 2.7

100mm Ø Indentor

ANGLE OF INCLINE /°	STRIP WIDTH /mm	APPLIED LOAD /kN	PREDICTED LOAD /kN	PERCENTAGE DIFFERENCE
5	30	400	416.0	+ 4.0
	40	400	389.2	- 2.7
	50	400	411.6	+ 2.9
	60	400	400.0	0
10	30	400	395.2	- 1.2
	40	400	422.4	+ 5.6
	50	400	402.4	+ 0.6
	60	400	419.6	+ 4.9
15	30	400	399.6	- 0.1
	40	400	416.4	- 4.1
	50	400	417.2	- 4.3
	60	400	414.0	+ 3.5

the indentor configuration and the predicted pressure distribution. Details are given in Appendix IV.

6.5 Experimental Results relating to the Interrupted-Pass Rolling Tests

6.5.1 Scope of the Experimental Work

The experimental tests were carried out using the Farmer-Norton two-high laboratory reversing rolling mill fitted with the monitoring devices and instrumentations detailed in section 2.2. Strips of annealed En2 steel (initial thickness 11.7 $\pm$ 0.1mm widths varying between 40mm and 100mm in 20mm increments) were subjected to a series of interrupted passes without lubrication. The thickness of each strip was reduced nominally by 10%, 15% or 20% during five successive interrupted passes. Tests, involving 10% reductions, were repeated for each strip configuration under lubricated rolling conditions, using Evco BRHP rolling oil prior to deformation.

During each test, the load acting upon the upper roll was determined by interpreting the load/time traces. Measurements of the reduced thickness and the surface hardness were established following the removal of the workpiece from the roll bite. The repeatability of the system was established by the deformation of strips of similar configuration during successive 20% reductions.

6.5.2 <u>Profile Measurement : A Comparison between Measuring Systems</u>

The roll profiles imparted into the upper and lower workpiece surfaces when each rolling pass was terminated, were determined by accurate measurements along five equally spaced sections across the width of each deformed region. Along each section, the deformed roll radius was determined by applying the arc-chord data-correlation technique to each combination of nodal positions, then correcting for the elastic recovery of the strip material. The values corresponding to the measured profile radius and the deformed roll radius along each section across the width of each deformed surface of a typically reduced workpiece are listed in table 6.8. A graphical representation of the sectional variations in the deformed roll radius is shown in figure 6.31.

The acquisition of the Merlin 750M Metrology System gave a choice of precision measuring systems capable of determining the nodal locations along the arcs of contact. An experimental investigation was undertaken in which this system, along with the SIP Universal Measuring Machine were used to measure the same profiles imparted into the surfaces of a typical workpiece. Details of the deformed roll radius values evaluated from the series of measurements at each section are given in table 6.9. The merits and demerits of each system, and the preference for using the Merlin 750M system are discussed in section 7.3.

TABLE 6.8

VARIATION OF THE MEASURED AND DEFORMED ROLL RADIUS ACROSS THE WIDTHS OF A TYPICAL INTERRUPTED-PASS WORKPIECE

STRIP WIDTH = 40.81mm
INITIAL THICKNESS = 9.39mm
FINAL THICKNESS = 8.22mm
RIGID ROLL RADIUS = 127mm

SECTION	MEASURED PROFILE RADIUS (mm)	PERCENTAGE OF NODAL COMBINATIONS ACCEPTED	DEFORMED ROLL RADIUS (mm)
1	146.7	94	146.8
2	164	59	164.1
3	168.2	93	168.3
4	154.1	85	154.2
5	147.4	96	147.5
6	136.0	80	136.1
7	152.3	85	132.3
8	163.6	75	163.7
9	147.1	52	147.2
10	137.6	91	137.7

$$\text{Mean Deformed Roll Radius} = \frac{1 + 5 + 6 + 10 + 2(2 + 3 + 4 + 7 + 8 + 9)}{16}$$

$$= 154.2\text{mm}$$

Sections 1-5 : Locations on the upper surface

Sections 6-10 : Locations on the lower surface

TABLE 6.9

COMPARISON OF THE DEFORMED ROLL RADIUS VALUES EVALUATED USING THE SIP AND MERLIN 750M MEASURING SYSTEMS

GEOMETRIC DETAILS
Roll Radius = 127mm
Strip Width = 61.1mm
Initial Thickness = 5.7mm
Final Thickness = 4.56mm

SECTION NUMBER	DRR (using the SIP) (mm)	DRR (using the Merlin 750M) (mm)
1	165.8 (31)*	143.8 (43)
2	205.2 (20)	146.4 (74)
3	161.4 (61)	161.3 (52)
4	176.5 (28)	145.1 (70)
5	155.7 (63)	131.7 (65)
6	190.9 (60)	193.6 (88)
7	188.9 (98)	192.6 (96)
8	190.6 (98)	192.3 (96)
9	192.9 (80)	192.4 (97)
10	193.6 (85)	190.9 (82)

Note : Sections 1 to 5 correspond to locations across the upper strip surface.

Sections 6 to 10 correspond to locations across the lower strip surface.

* The numbers listed in brackets refer to the percentage of node combinations accepted for the final evaluation of each value.

6.5.3 Preliminary Analyses of the Applied Load and the Variation in Surface Hardness Following Workpiece Reduction

For both dry and lubricated rolling conditions, measurement of the strip widths before and after each partial reduction showed that the deformation process approximated to plane strain conditions. Under these conditions, and providing that all other parameters remain constant, the load per unit width should remain constant for a given reduction.

Considering the experimentally determined results from each test, the measured load per unit width L/W, was related to the actual percentage reduction $\frac{\Delta H}{H}$ in workpiece thickness and plotted in graphical form in figure 6.32. The effects of the lubricant upon this relationship appeared minimal even though the frictional conditions within the roll-bite would be altered during such tests. Consequently, points corresponding to the experimental tests under lubricated conditions are included in figure 6.32.

A standard curve-fitting package was used to formulate a working empirical function from which a refined load value could be determined to correspond to the configuration of each rolled workpiece. The relationship can be approximately described as a hyperbolic function of the percentage reduction, thus:

$$\text{Load per unit width, L/W (kN mm}^{-1}) = \frac{\Delta H/H}{A + B(\Delta H/H)} \quad (6.18)$$

The values of A and B are indicated on figure 6.32. The applied loads used in formulating the influence constant functions were determined by equation 6.18.

By subjecting each workpiece to a series of interrupted reductions, the effects of strain hardening upon the strip material became apparent. The variation in surface hardness (VPN) with the cumulative reductions in strip thickness is graphically illustrated in figure 6.33 for the nominal 20% reduction tests.

6.5.4 Determination of the Influence Constant Functions

By considering the geometric configuration of the rolls and workpiece and the elastic material properties of the rolls associated with each reduction, an influence constant was computed by substituting the calculated load to the corresponding value determined by equation 6.18. A deformed roll radius was evaluated to represent the average profile imparted into both sides of the deformed strip at the termination of the pass. This corresponded to an average of the sectional values in which the edge sections were disproportionately weighted by a 1:2 ratio. Consideration of the variations in deformed roll radius across a typical rolled workpiece, depicted in figure 6.31 clearly shows the need for such a weighting system in the determination of a representative mean.

For the tests at each nominal reduction and lubricating condition, influence constants C were formulated as empirical functions with respect to the average change in the roll radius, ΔR. Figures 6.34 to 6.37 graphically show the data points at each nominal reduction and lubrication condition. The curves representing the optimum correlation between the data points are indicated, along with their corresponding functions formulated using a standard curve-fitting package.

6.5.5 Pressure Distribution and Separating Load Predictions

The effectiveness of the pressure distribution computer program incorporating the influence constant functions was assessed by predicting the pressure values and separating loads using the original experimental data corresponding to each reduction.

Following the initial evaluation of the average deformed roll radius and the influence constant from the appropriate function, the pressure distribution corresponding to each measured section was predicted. For a typical section, the extent of the elastic displacement of the roll along the arc of contact is depicted in discretised form in figure 6.38(a). The predicted pressure distribution responsible for the displacements is shown in figure 6.38(b). Elements 1 and 10, correspond to positions at the ends of the contact arc and have no effective displacement. Since these elements are subjected to the influence of the displacements of the intermediate elements along the contact arc, a restraining pressure in the opposite direction is required to maintain equilibrium conditions. Figures 6.39 to 6.55 show the predicted pressure distributions appertaining to tests representative of each reduction configuration. The restraining pressures at the arc ends are omitted.

Based on the mean pressure value acting over the upper and lower deformation zones, separating loads were determined for each test configuration. The mean sectional pressure values were weighted in a similar manner to the deformed roll radius values (discussed in sub-section 6.5.4) to determine a representative average. Appertaining to each test, the discrepancies between the predicted and measured separating loads are listed in table 6.10.

TABLE 6.10

VARIATIONS BETWEEN THE MEASURED AND PREDICTED SEPARATING LOADS : INTERRUPTED-PASS ROLLING TESTS

(i) Dry Rolling Conditions

NOMINAL REDUCTION /%	NOMINAL STRIP WIDTH /mm	REDUCTION NUMBER	APPLIED LOAD /kN	PREDICTED LOAD /kN	PERCENTAGE DIFFERENCE
10	100	1	434	582	+34.1
		2	607	711	+17.1
		3	525	609	+15.9
		4	579	513	-11.4
		5	670	532	-20.6
10	80	1	389	430	+10.7
		2	491	555	+13.0
		3	474	438	- 7.7
		4	506	434	-14.3
		5	562	425	-24.3
10	60	1	316	370	+17.2
		2	368	376	+ 2.1
		3	370	339	- 8.3
		4	388	339	-12.5
		5	418	324	-22.4
10	40	1	214	234	+ 9.2
		2	247	224	- 9.4
		3	255	203	-20.5
		4	271	208	-23.1
		5	285	186	-34.7
15	100	1	775	923	+19.1
		2	684	936	+36.8
		3	863	-	-
		4	797	561	-29.6
		5	804	927	+15.3
15	80	1	633	945	+49.4
		2	558	752	+34.8
		3	699	657	- 6.0
		4	697	627	- 9.9
		5	668	539	-19.3

TABLE 6.10 (cont)

NOMINAL REDUCTION /%	NOMINAL STRIP WIDTH /mm	REDUCTION NUMBER	APPLIED LOAD /kN	PREDICTED LOAD /kN	PERCENTAGE DIFFERENCE
15	80	1	449	643	+43.3
		2	386	546	+41.6
		3	506	518	+ 2.3
		4	491	455	- 7.3
		5	469	432	- 7.9
15	40	1	323	293	- 9.4
		2	301	326	+ 8.3
		3	348	304	-12.6
		4	332	257	-22.7
		5	299	243	-18.8
20	100(a)	1	754	1496	+98.4
		2	986	-	-
		3	1054	992	- 5.9
		4	976	961	- 1.6
		5	825	737	-10.7
20	100(b)	1	672	1528	+127.5
		2	946	-	-
		3	969	1030	+ 6.3
		4	892	975	+ 9.3
		5	825	910	+10.3
20	80	1	566	1283	+126.8
		2	839	-	-
		3	800	756	- 5.5
		4	778	786	+1.0
		5	754	748	- 0.8
20	60	1	451	817	+81.1
		2	652	367	-43.8
		3	688	558	-18.8
		4	582	516	-11.3
		5	581	586	+ 0.9
20	40	1	238	543	+128.2
		2	393	514	+30.9
		3	409	410	+ 0.2
		4	335	265	-20.8
		5	362	347	- 4.2

(ii) <u>Lubricated Rolling Conditions</u>

NOMINAL REDUCTION /%	NOMINAL STRIP WIDTH /mm	REDUCTION NUMBER	APPLIED LOAD /kN	PREDICTED LOAD /kN	PERCENTAGE DIFFERENCE
10	100	1	520	601	+15.6
		2	588	605	+ 3.0
		3	584	558	- 4.5
		4	613	538	-12.3
		5	642	467	-27.2
10	80	1	420	446	+ 6.3
		2	480	466	- 2.9
		3	471	429	- 8.9
		4	509	418	-17.8
		5	537	418	-22.1
10	60	1	350	367	+ 4.9
		2	373	337	- 9.8
		3	373	328	-12.1
		4	391	308	-21.1
		5	407	296	-27.3
10	40	1	285	231	-18.9
		2	291	243	-16.5
		3	288	220	-23.6
		4	301	201	-33.3
		5	326	193	-40.8

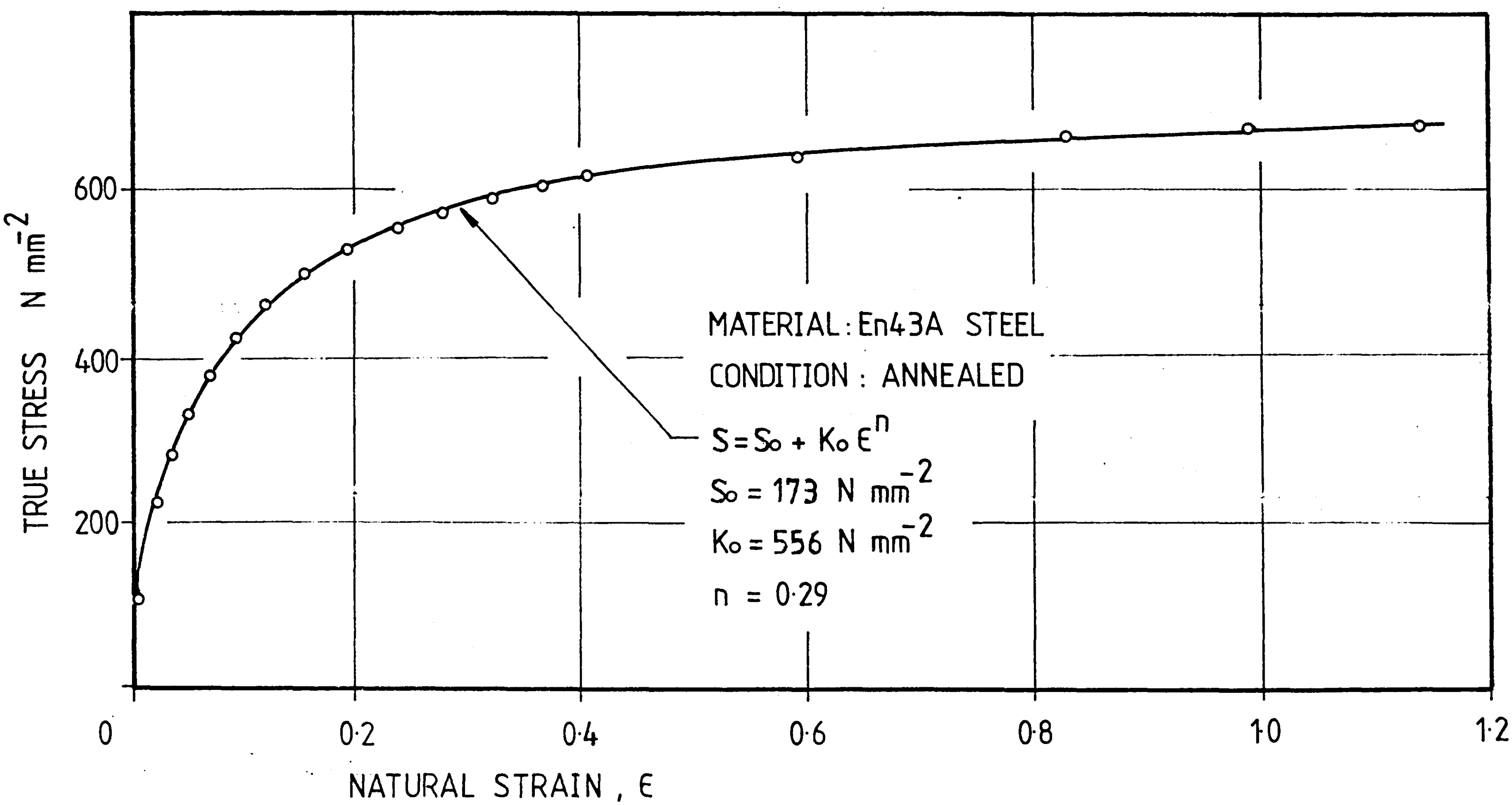

FIG 6.1 : STRESS-STRAIN BEHAVIOUR OF ANNEALED En43A STEEL (FIRST BATCH) UNDER PLANE STRAIN CONDITIONS

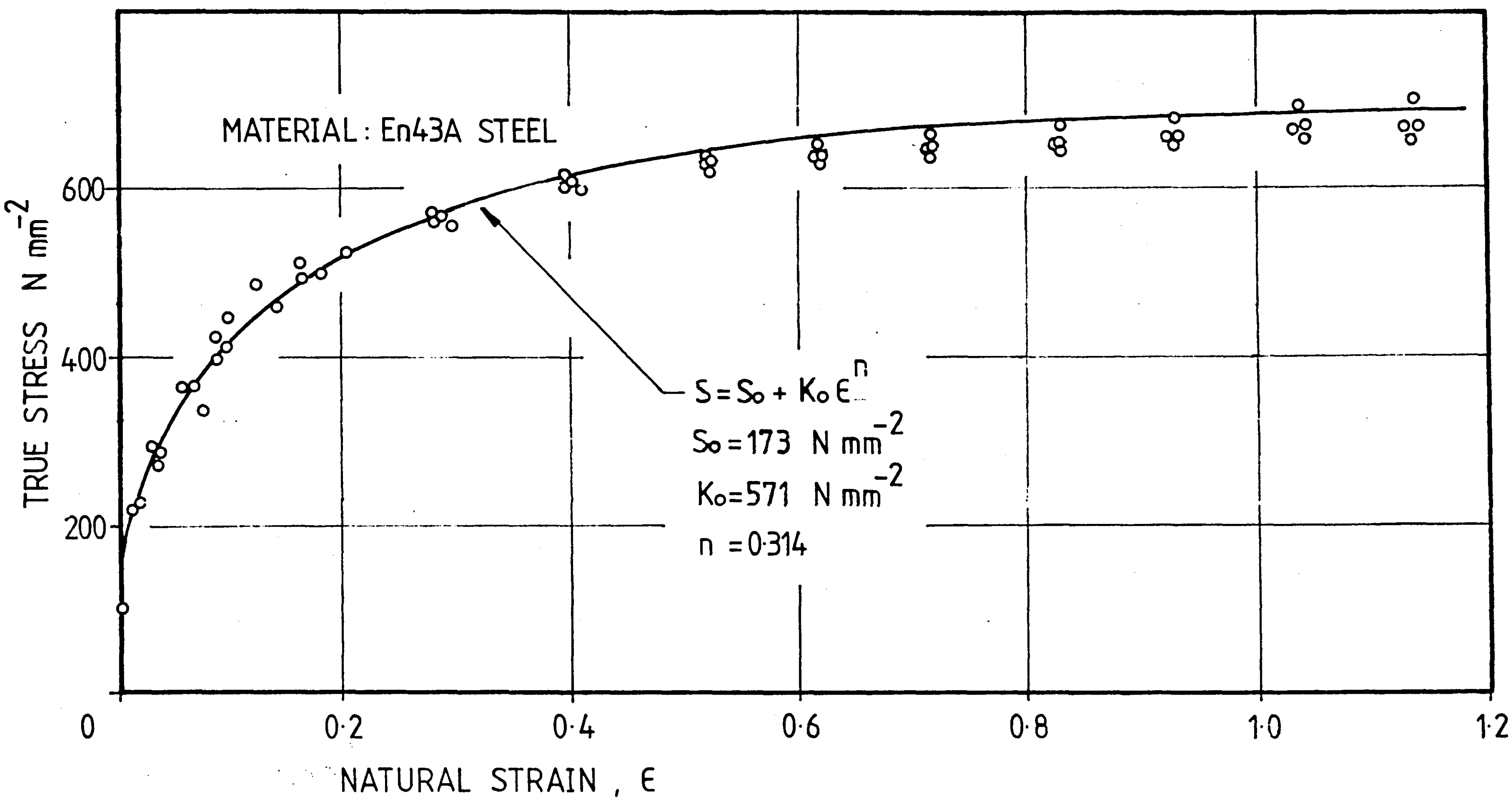

FIG 6.2 : STRESS-STRAIN BEHAVIOUR OF ANNEALED En43A STEEL (SECOND BATCH) UNDER PLANE STRAIN CONDITIONS

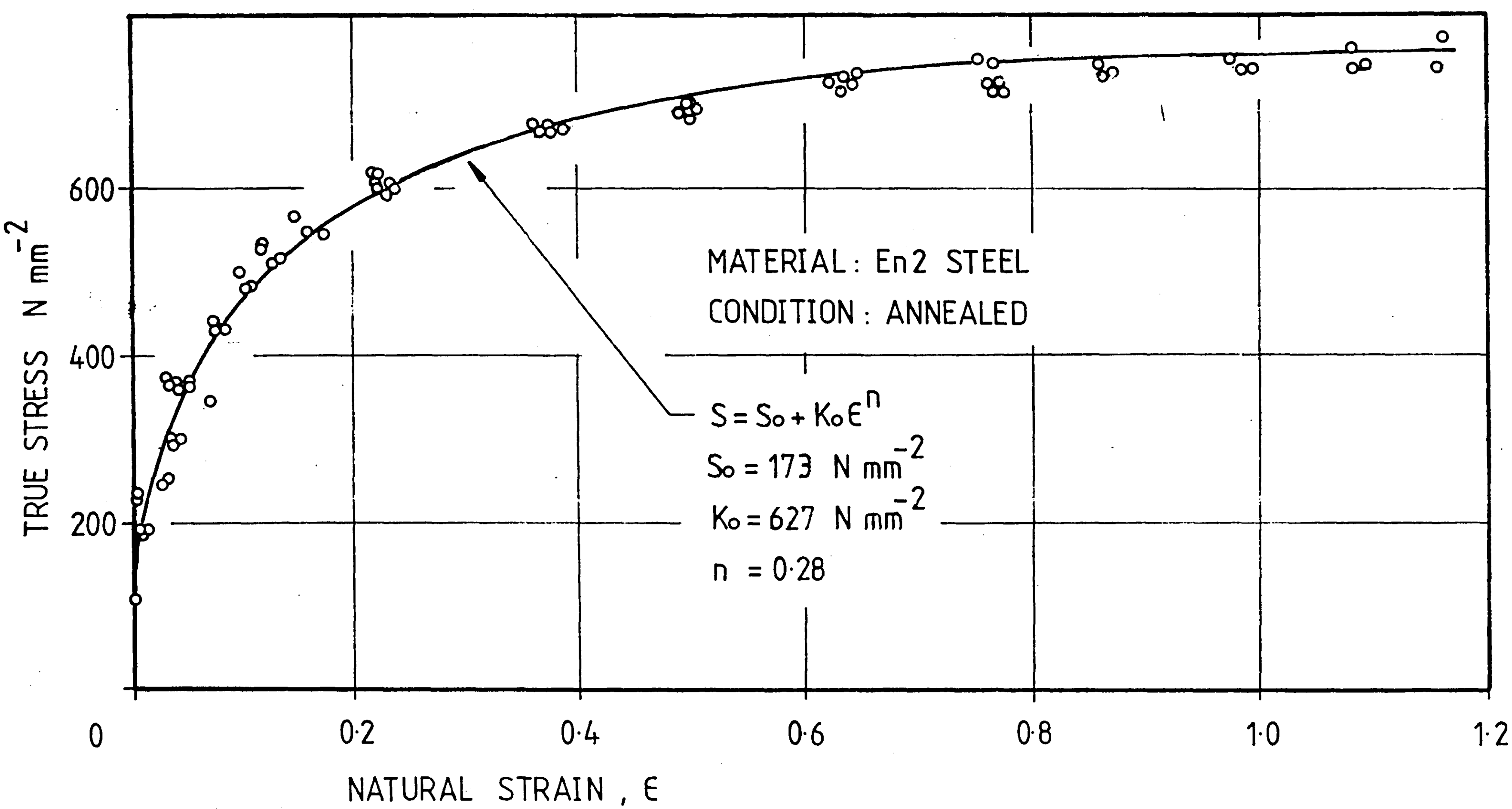

FIG 6.3 : STRESS-STRAIN BEHAVIOUR OF ANNEALED En2 STEEL UNDER PLANE STRAIN CONDITIONS

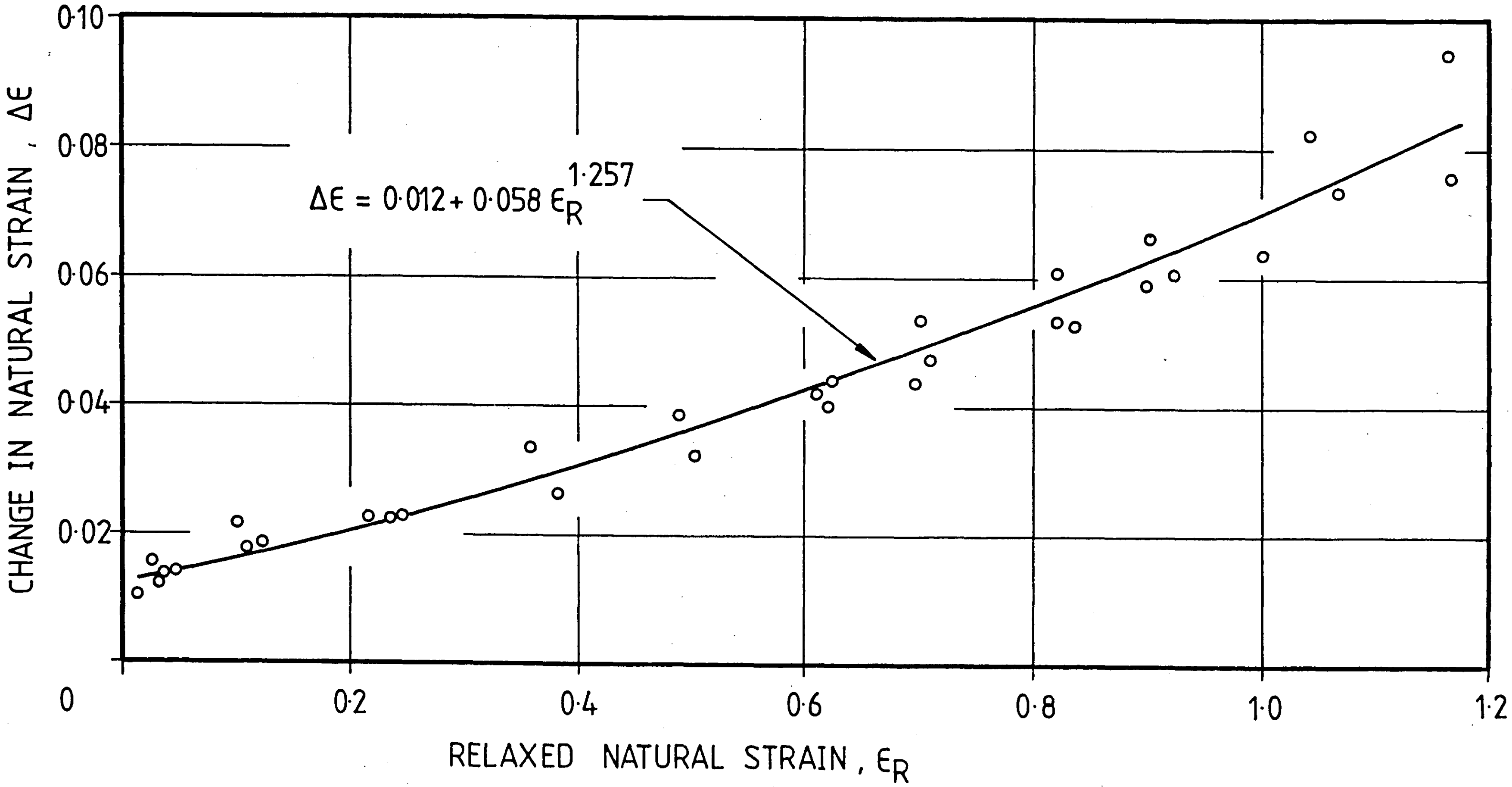

FIG 6.4 : VARIATION OF THE CHANGE IN NATURAL STRAIN AGAINST THE RELAXED NATURAL STRAIN : En2 STEEL INTERRUPTED-PASS WORKPIECES

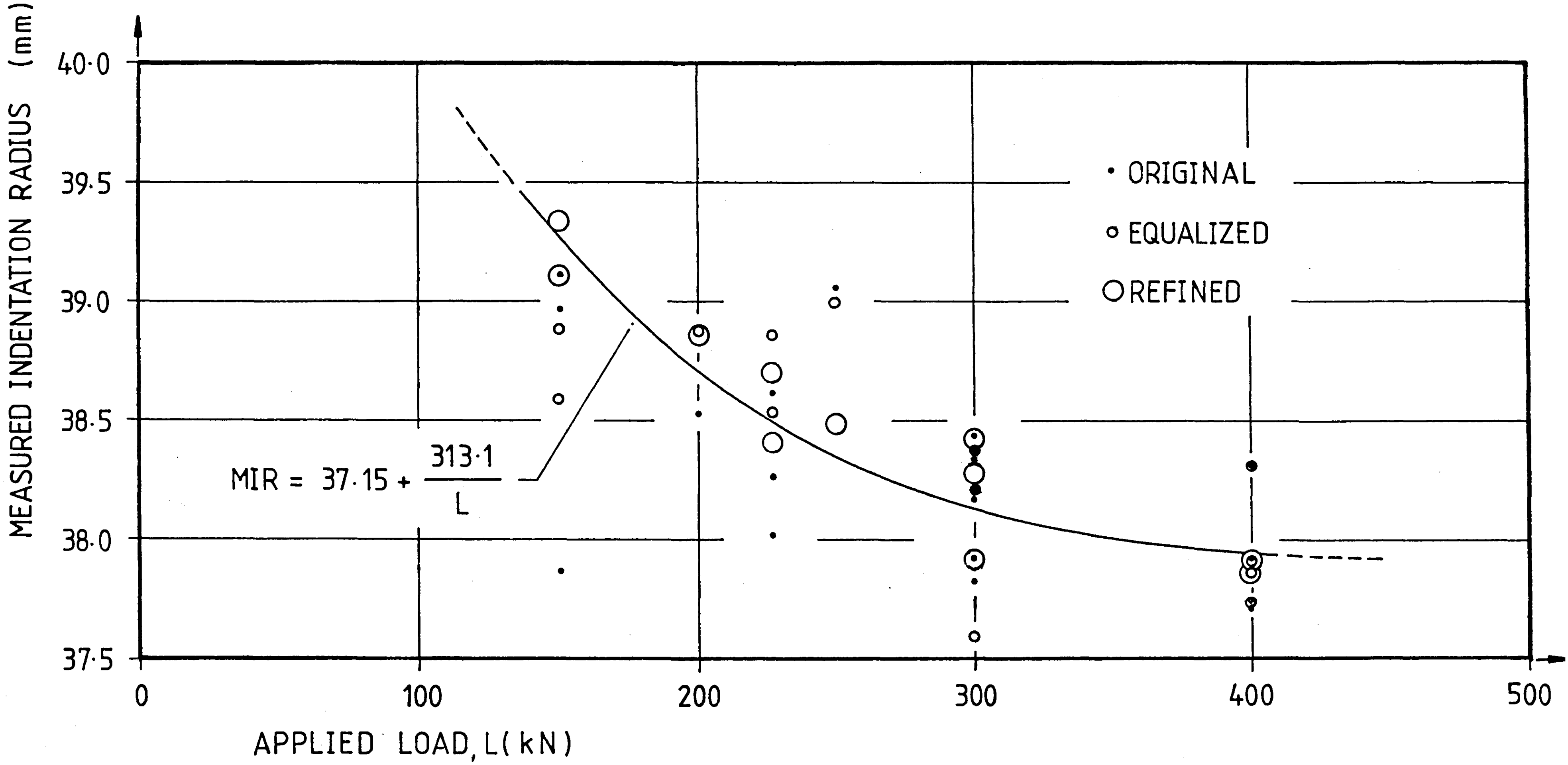

FIG 6.5 : EFFECTS OF APPLIED LOAD ON THE MEASURED INDENTATION RADIUS : 37.5mm RADIUS INDENTOR INDENTING FLAT SPECIMENS

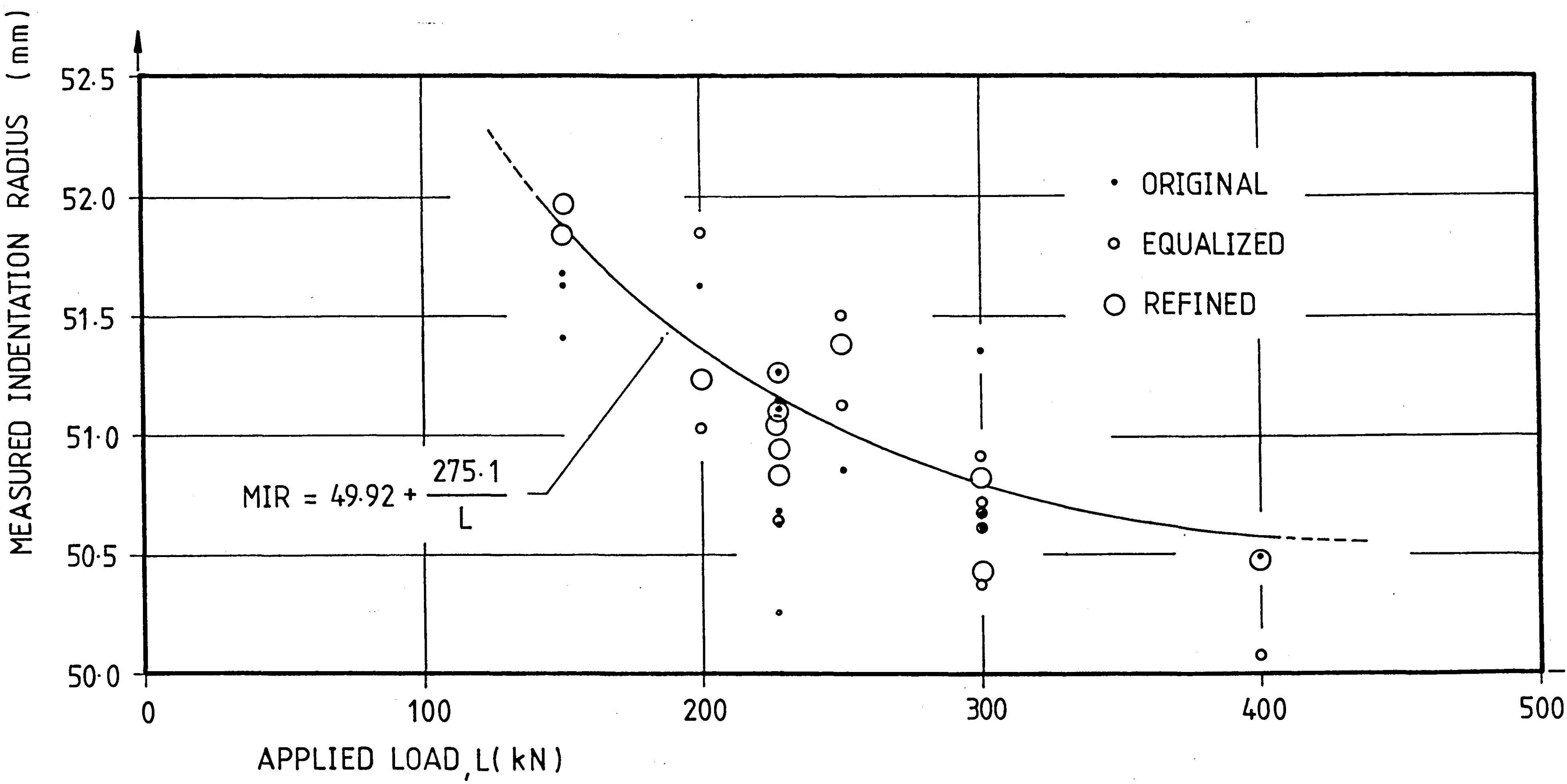

FIG 6.6 : EFFECTS OF APPLIED LOAD ON THE MEASURED INDENTATION RADIUS : 50mm RADIUS INDENTOR INDENTING FLAT SPECIMENS

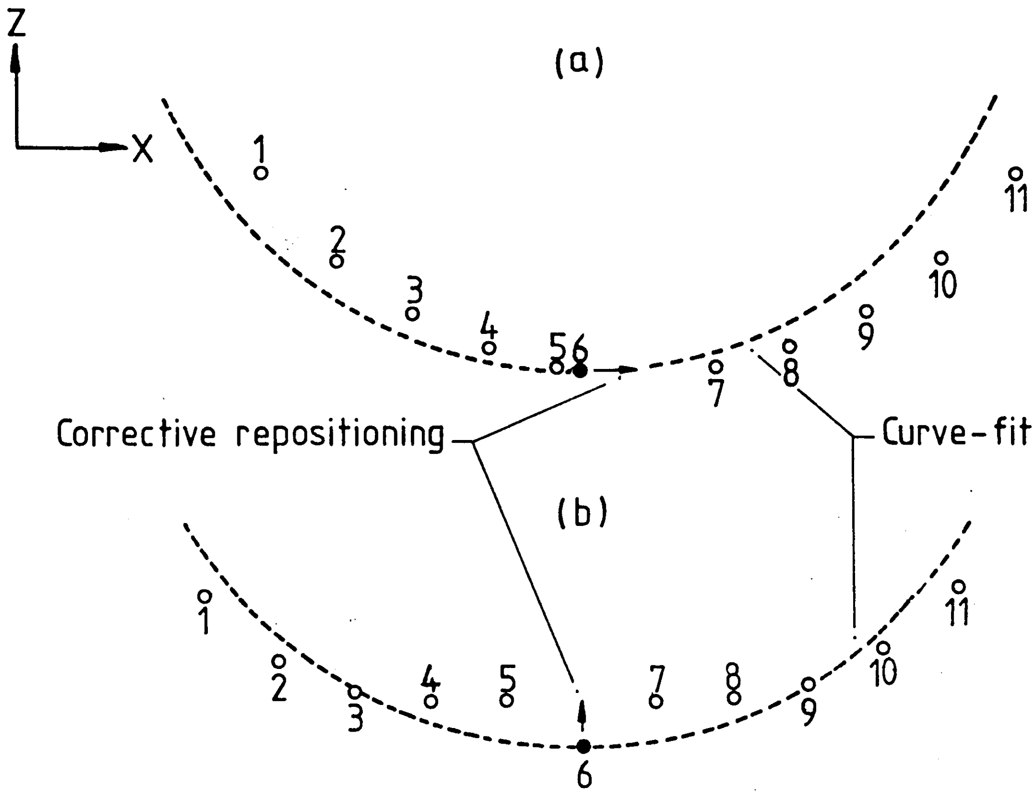

6 ● Fixed centre node

	node	polarity of deviation
(a)	1	+
	⋮	+ + +
	5	+
	7	−
	⋮	− − −
	11	−
(b)	1	−
	⋮	− − +
	5	+
	7	+
	⋮	+ − −
	11	−

FIG 6.7 : SCHEMATIC REPRESENTATION OF 'EQUALISED' DATA FITS

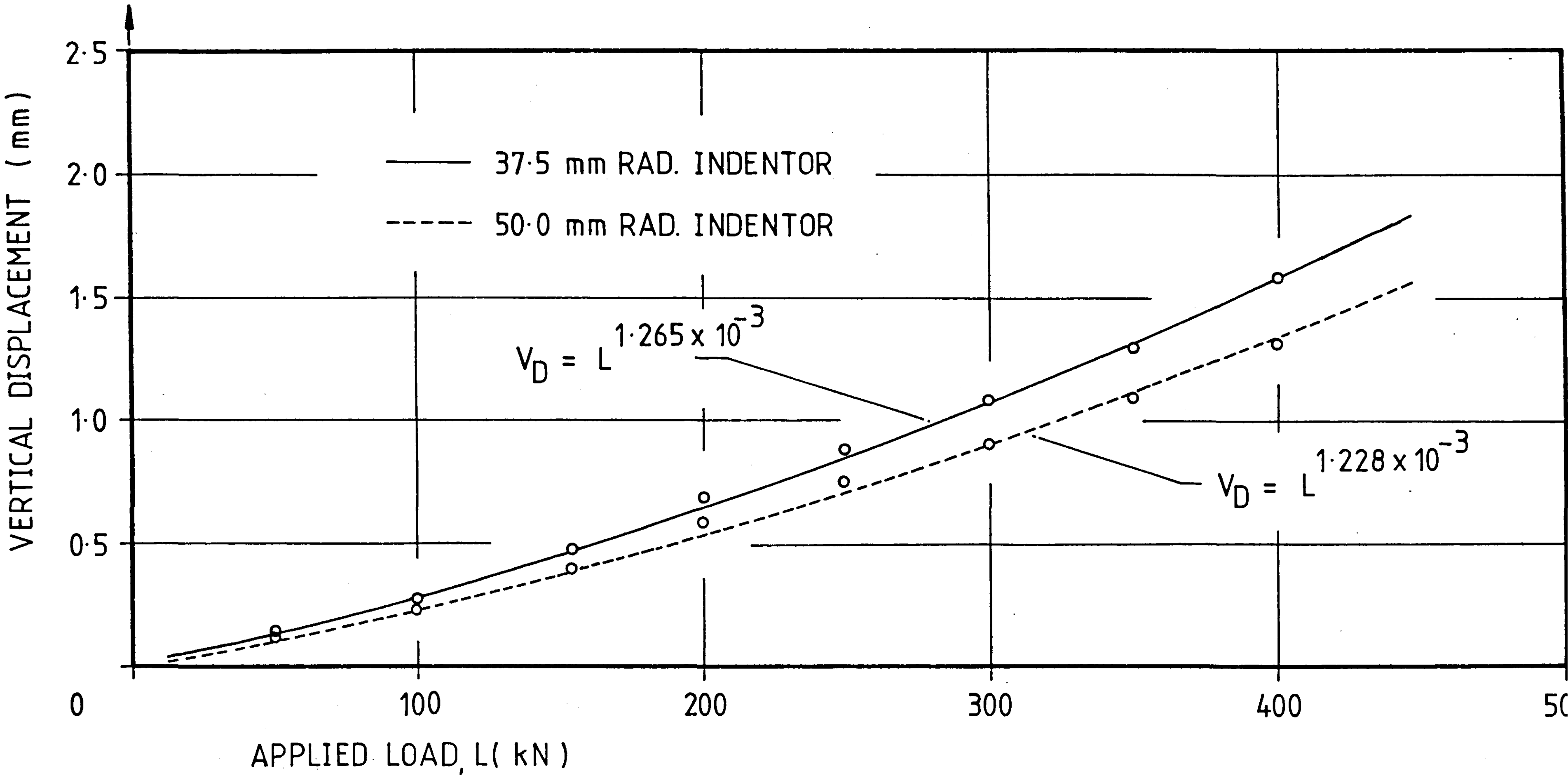

FIG 6.8 : EFFECTS OF APPLIED LOAD ON THE VERTICAL DISPLACEMENT OF THE INDENTORS : INDENTATION OF FLAT SPECIMENS

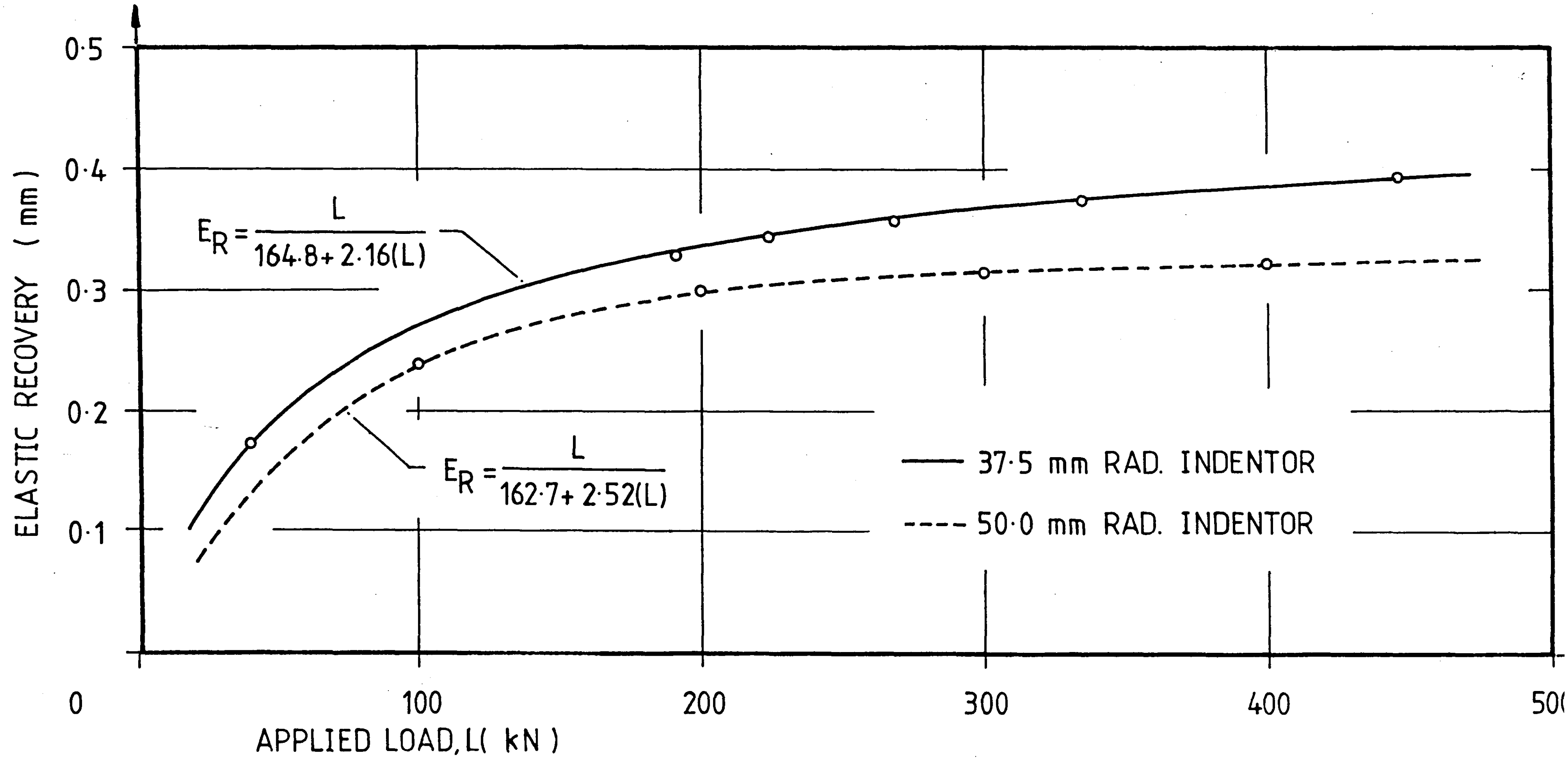

FIG 6.9 : EFFECTS OF APPLIED LOAD ON THE ELASTIC RECOVERY OF THE INDENTOR AND STRIP FOLLOWING LOAD RELAXATION : INDENTATION OF FLAT SPECIMENS

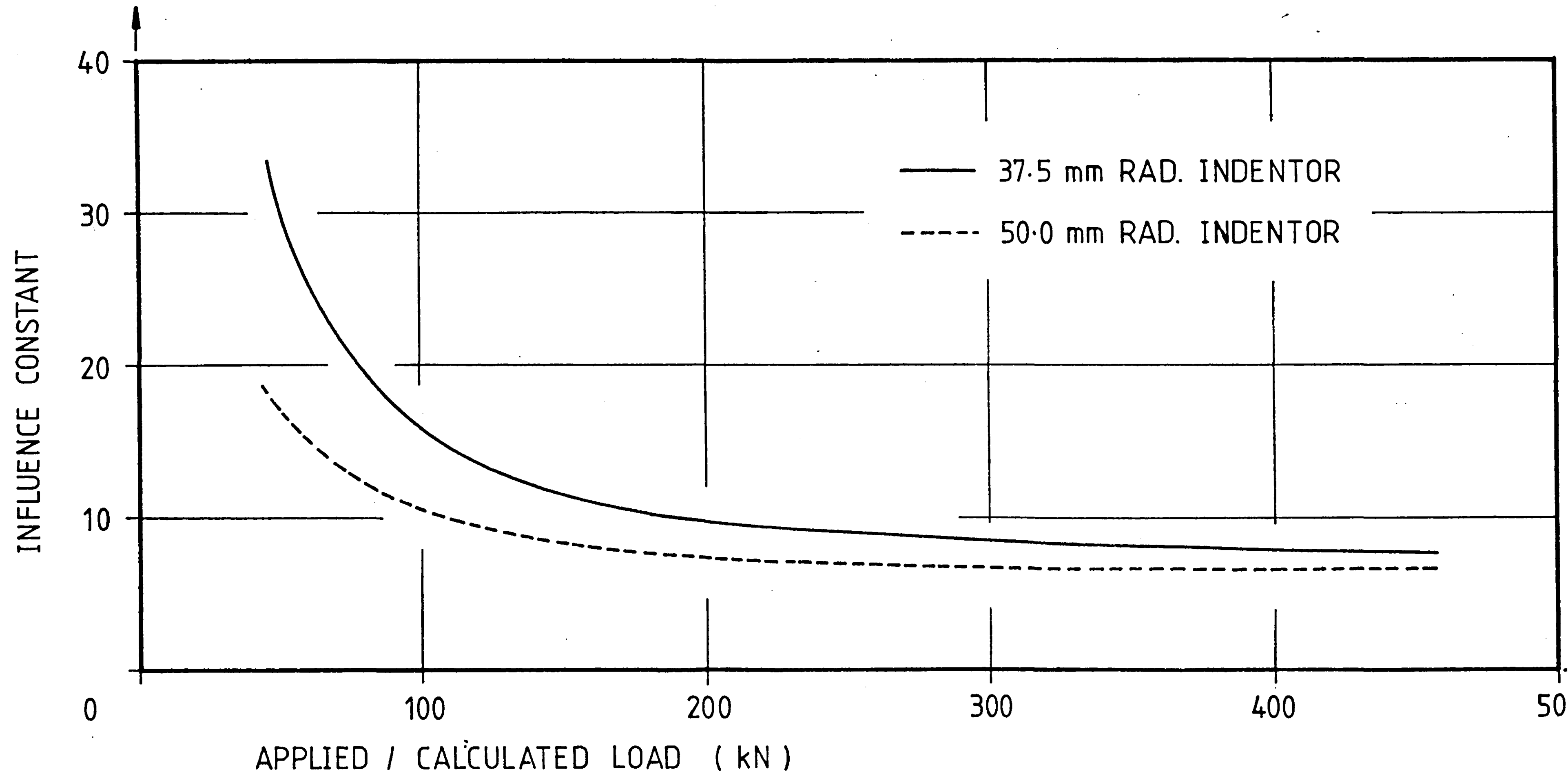

FIG 6.10 : THEORETICAL EFFECTS OF LOAD ON THE INFLUENCE CONSTANT : INDENTATION OF FLAT SPECIMENS

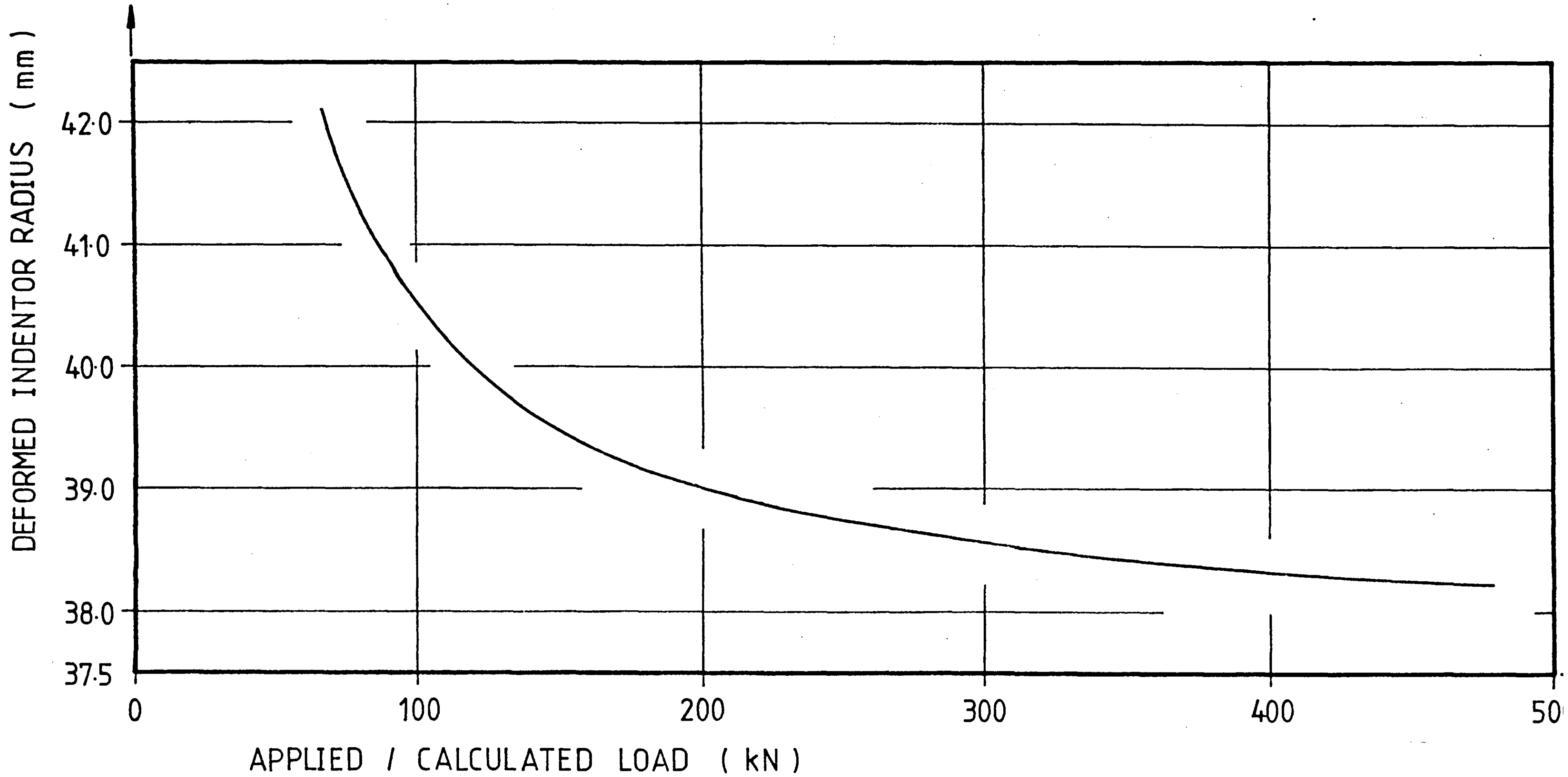

FIG 6.11 : THEORETICAL EFFECTS OF THE LOAD ON THE DEFORMED INDENTOR RADIUS : 37.5mm RADIUS INDENTOR INDENTING FLAT SPECIMENS

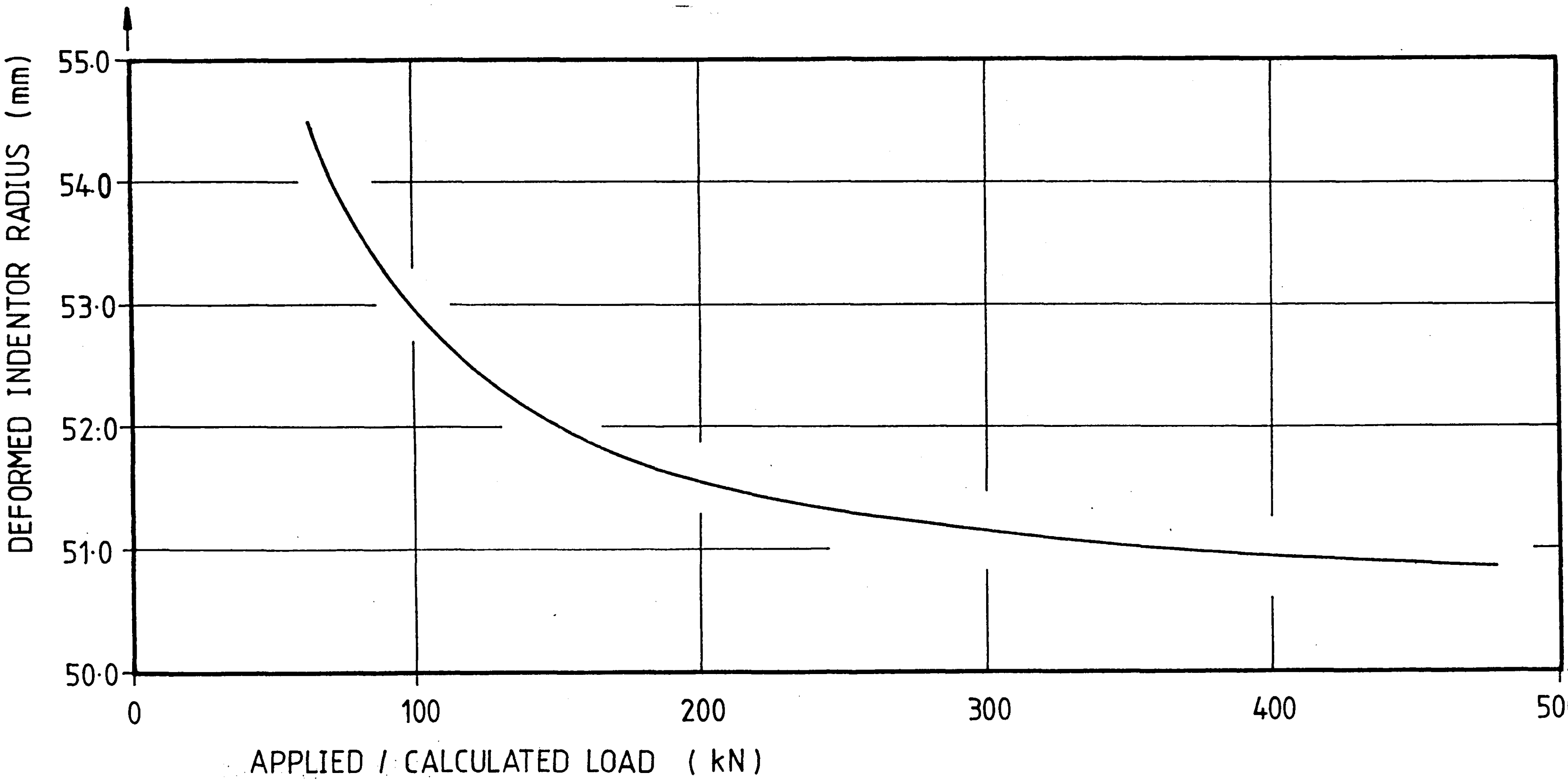

FIG 6.12 : THEORETICAL EFFECTS OF THE LOAD ON THE DEFORMED INDENTOR RADIUS : 50mm RADIUS INDENTOR INDENTING FLAT SPECIMENS

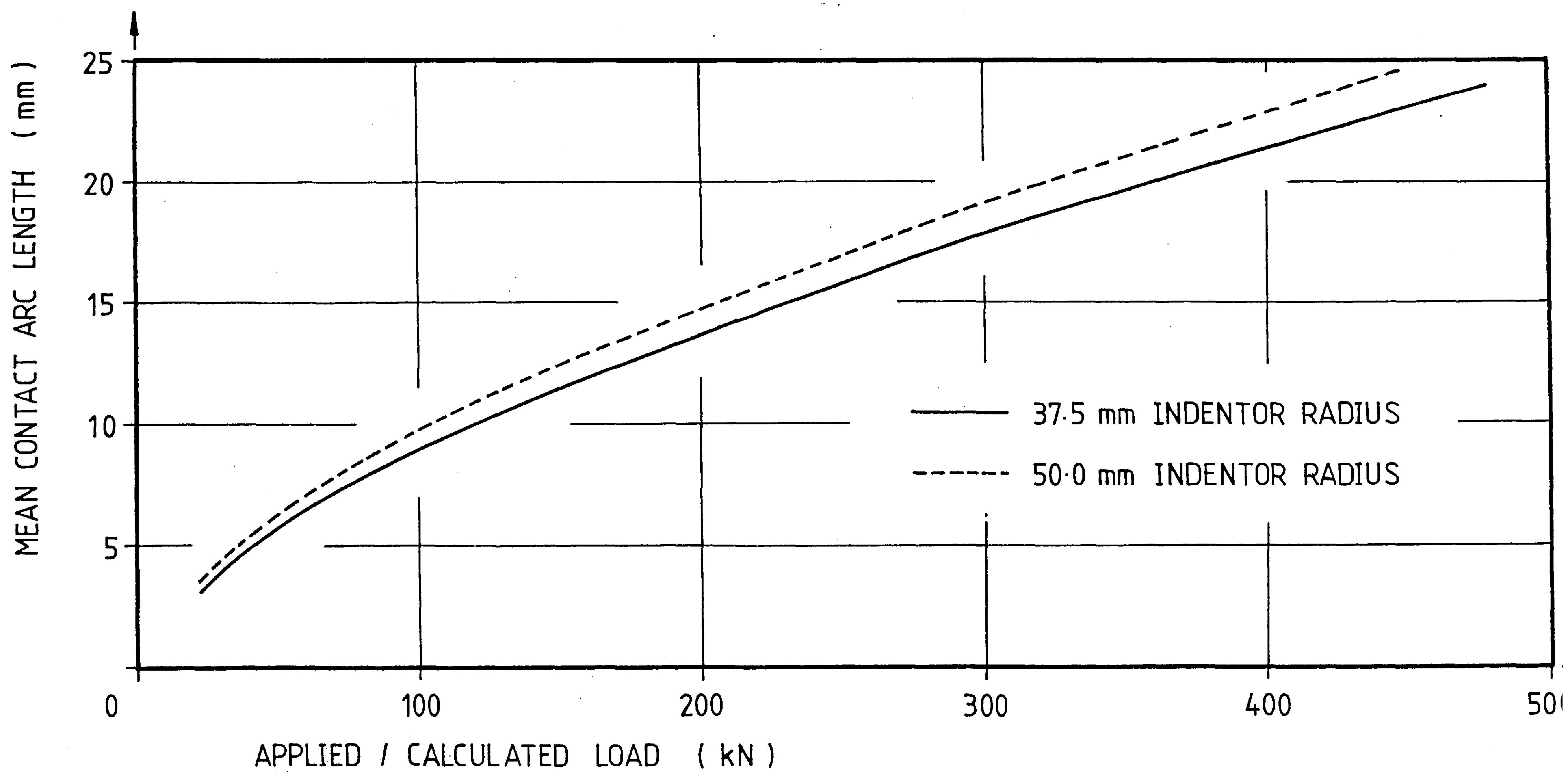

FIG 6.13 : THEORETICAL EFFECTS OF LOAD ON THE MEAN CONTACT ARC LENGTH : INDENTATION OF FLAT SPECIMENS

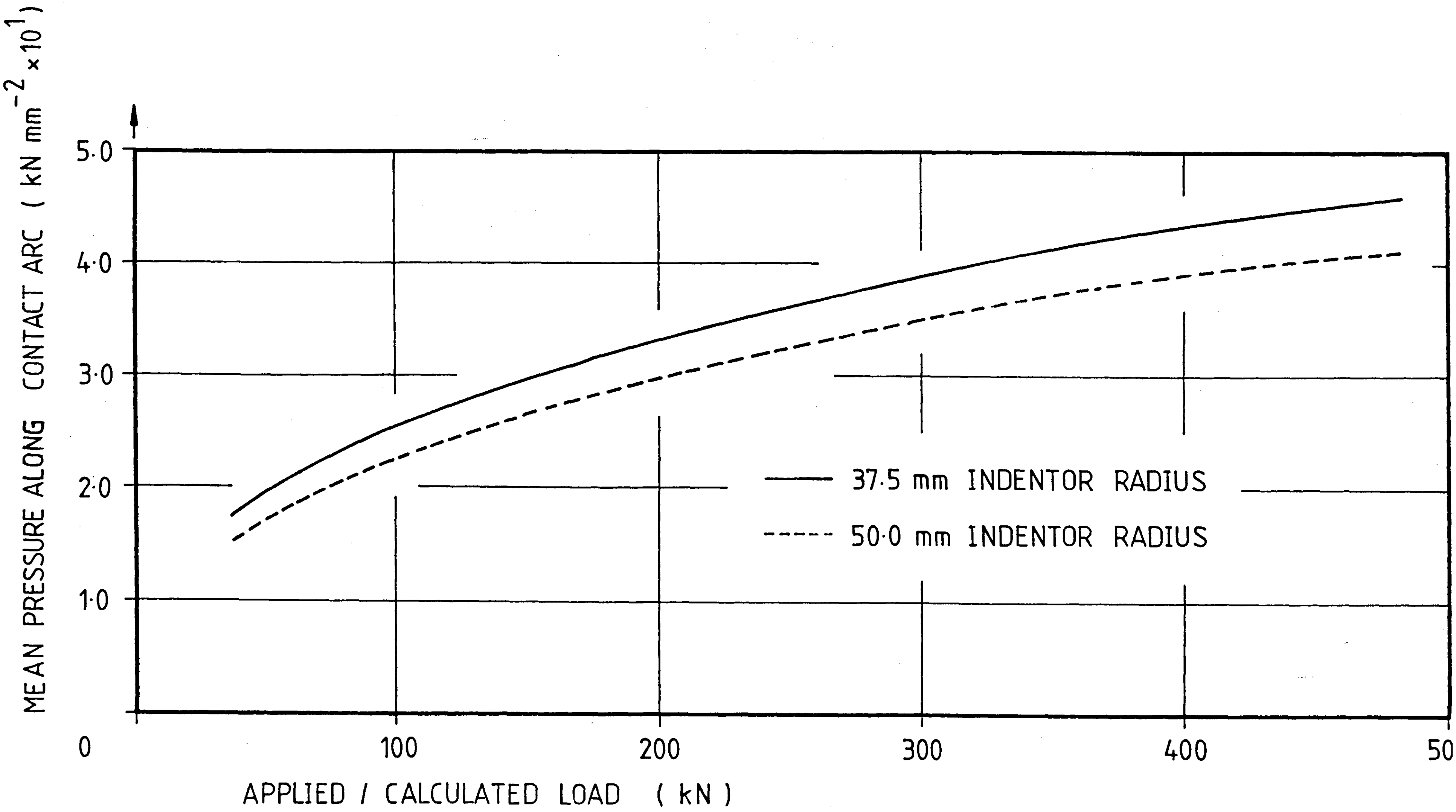

FIG 6.14 : THEORETICAL EFFECTS OF LOAD ON THE MEAN PRESSURE ALONG THE CONTACT ARC : INDENTATION OF FLAT SPECIMENS

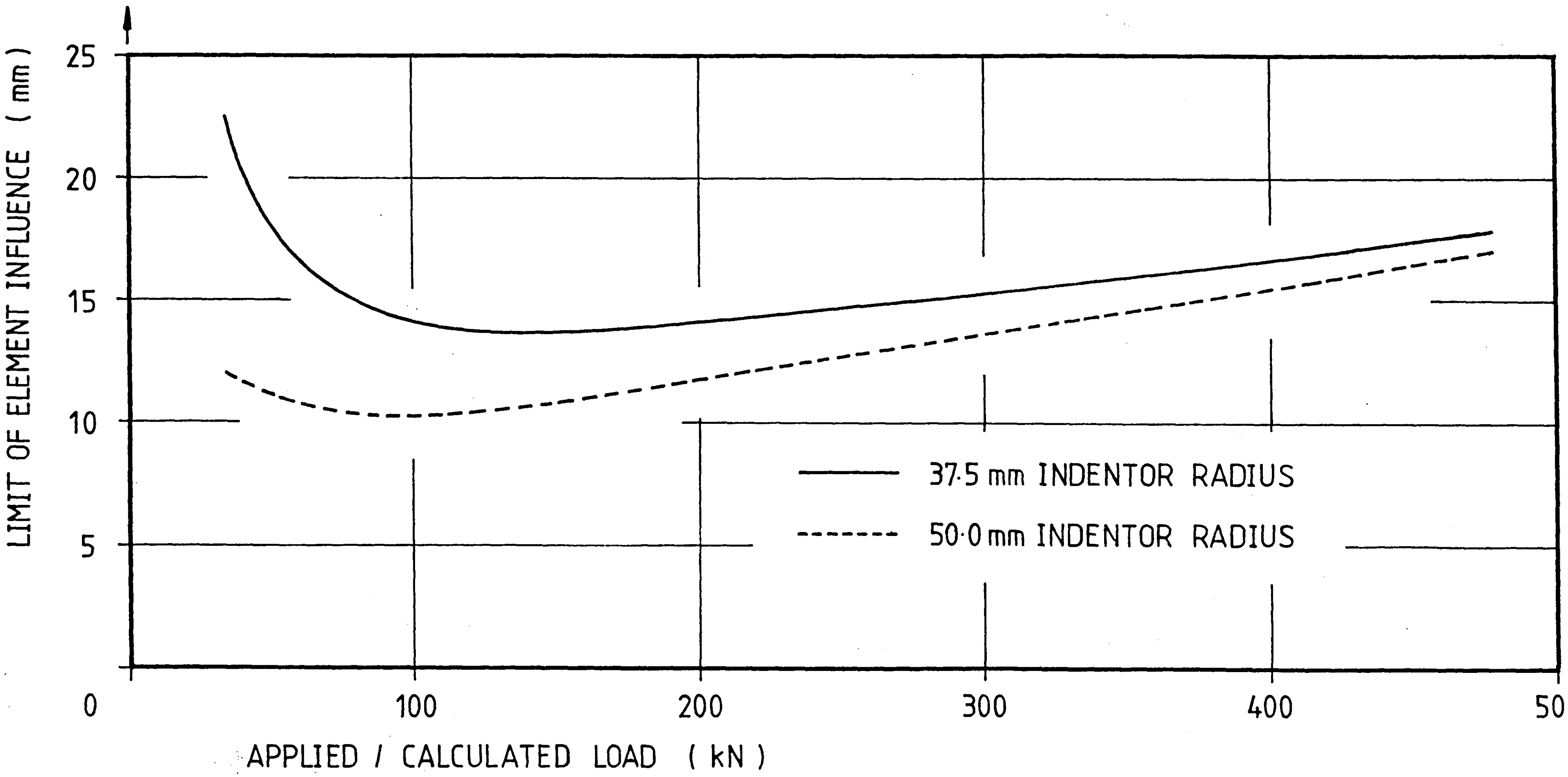

FIG 6.15 : THEORETICAL EFFECTS OF LOAD ON THE LIMIT OF ELEMENT INFLUENCE : INDENTATION OF FLAT SPECIMENS

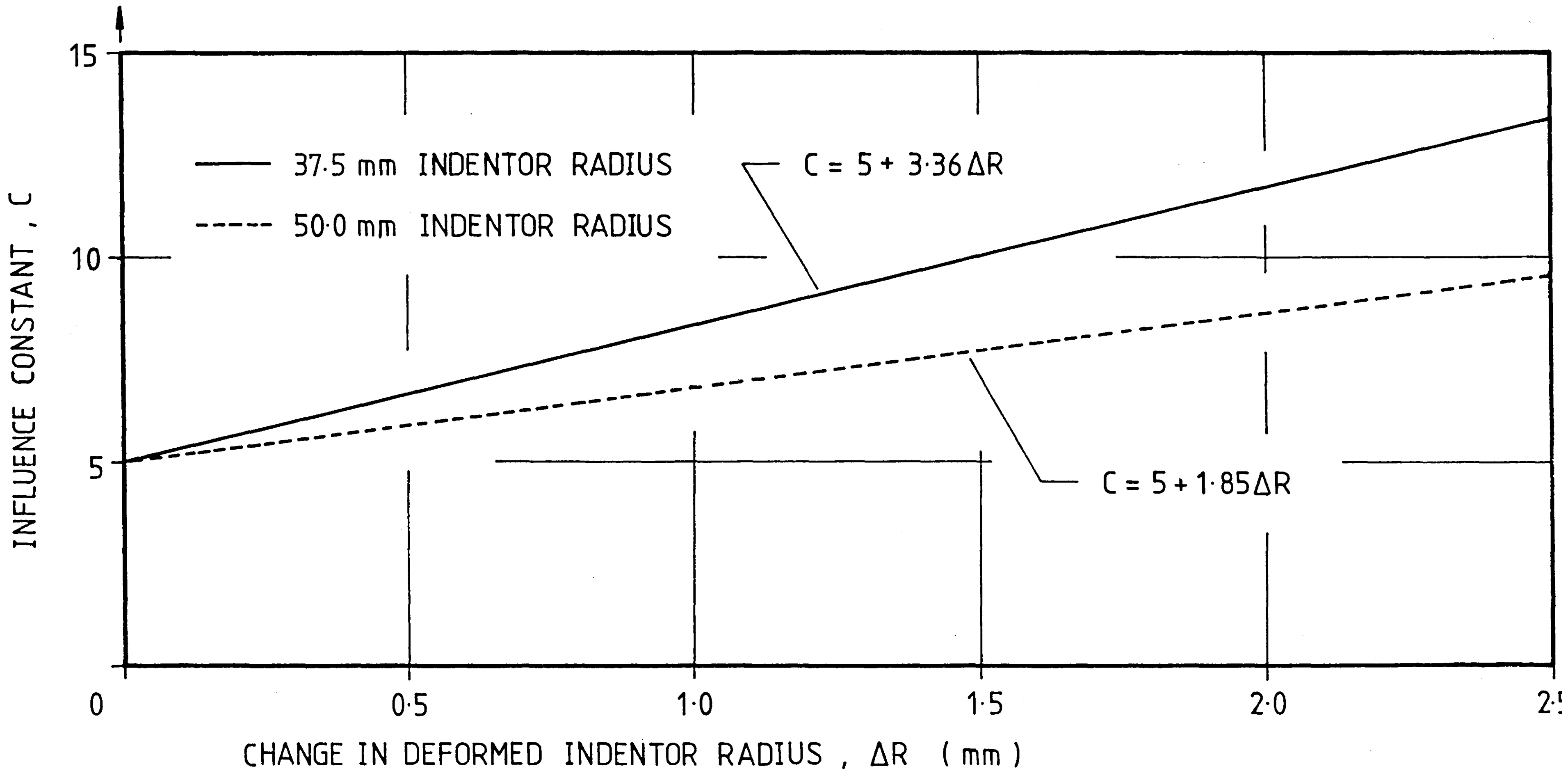

FIG 6.16 : INFLUENCE CONSTANT FUNCTIONS : INDENTATION OF FLAT SPECIMENS

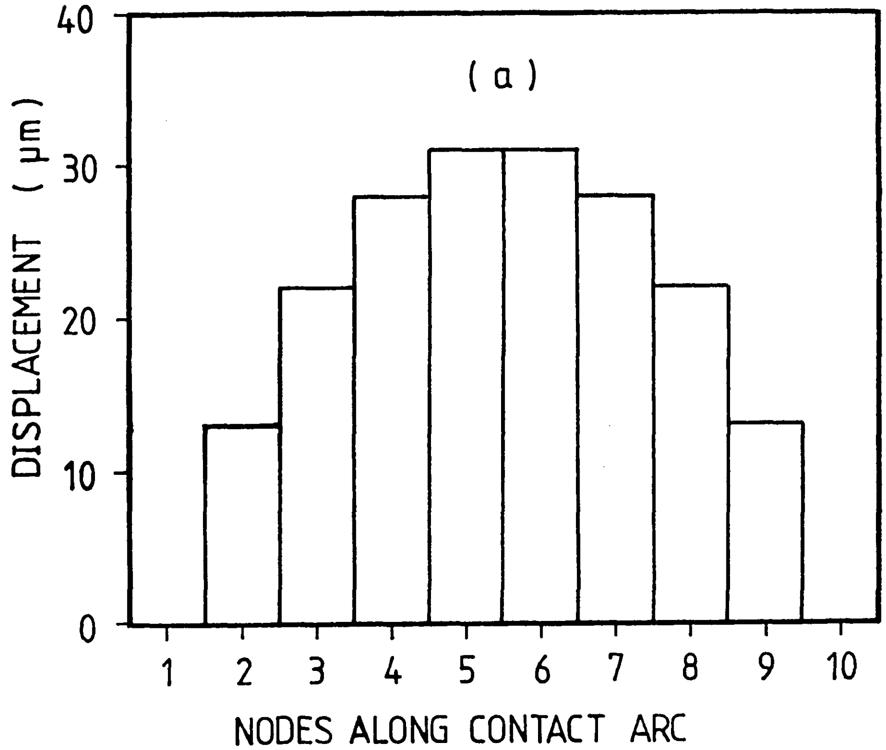

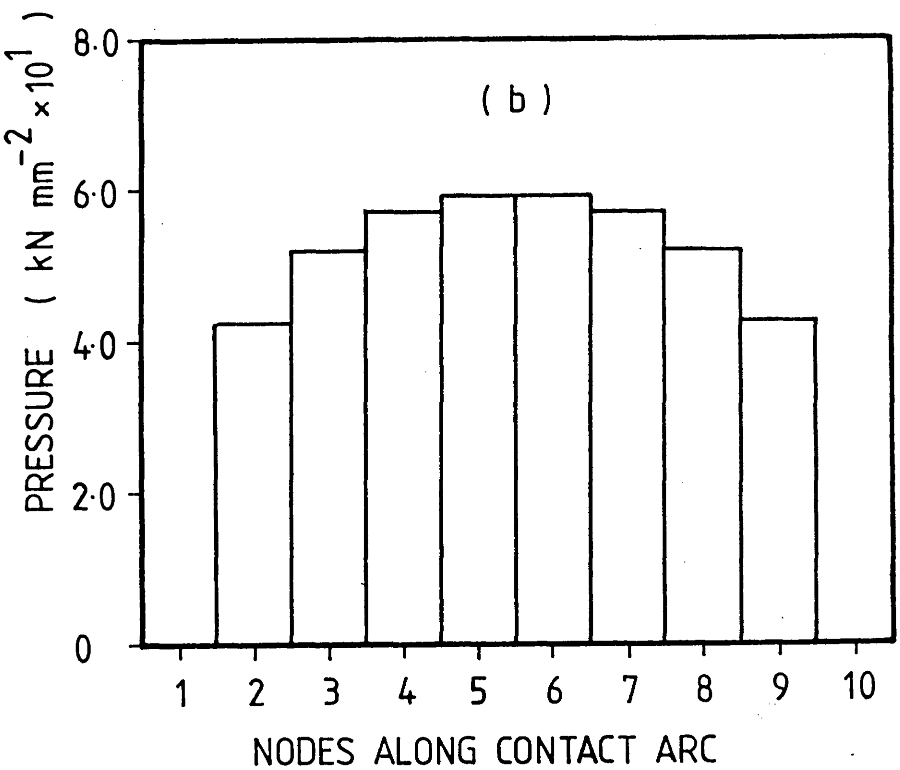

FIG 6.17 : DISCRETISED DEVIATIONS (a) AND PREDICTED PRESSURE DISTRIBUTION (b) ALONG A TYPICAL CONTACT ARC : INDENTATION OF FLAT SPECIMENS

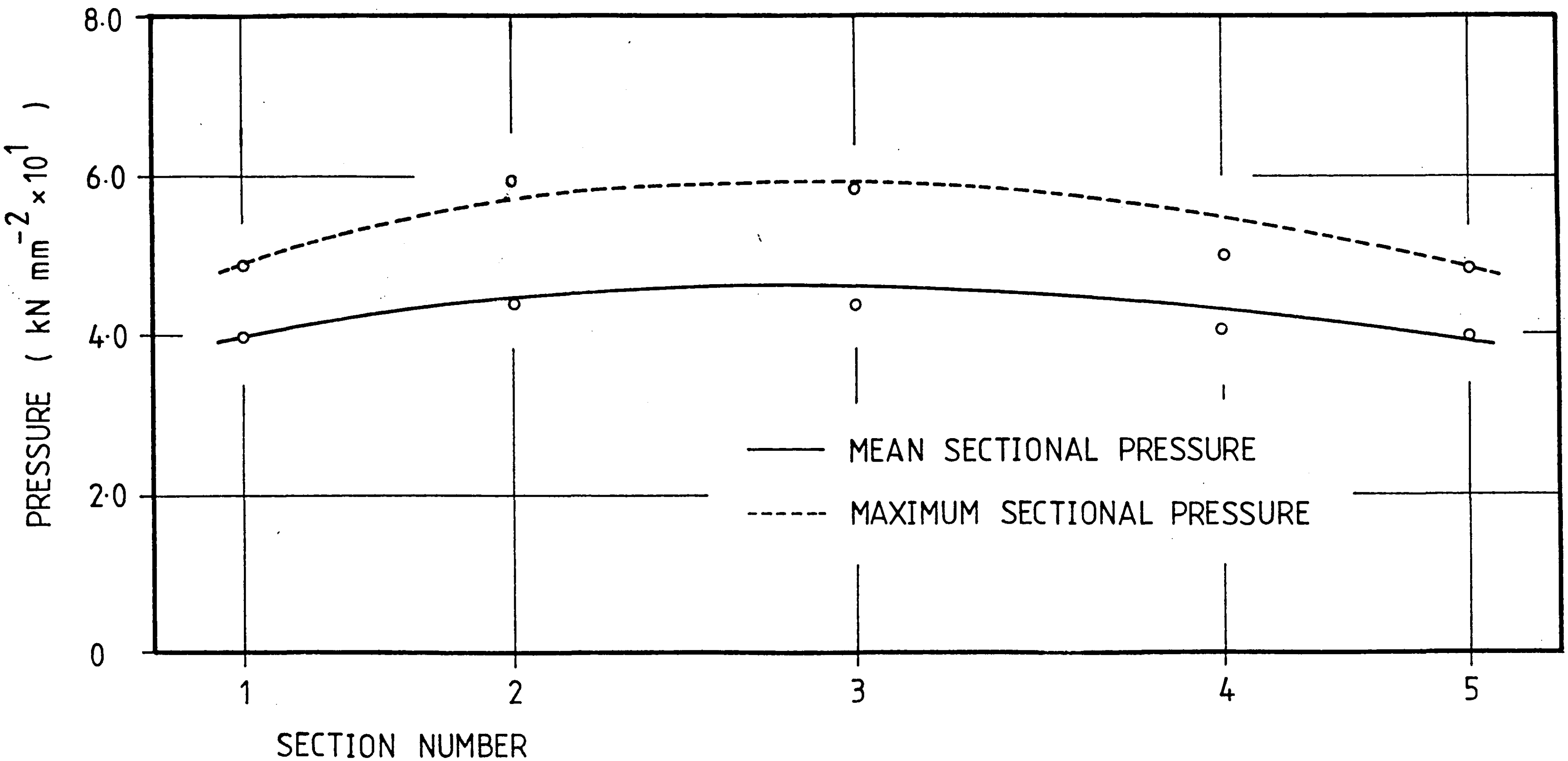

FIG 6.18 : VARIATIONS IN THE MAXIMUM AND MEAN PRESSURE ACROSS THE WIDTH OF A TYPICAL INDENTED FLAT SPECIMEN

SPECIMEN DETAILS.

Strip width = 30 mm

Mean contact arc length = 24·4 mm

(neither drawn to scale)

Applied load = 300 kN

PRESSURE DISTRIBUTION.

Vertical scale :

1mm = 20 N mm^{-2}

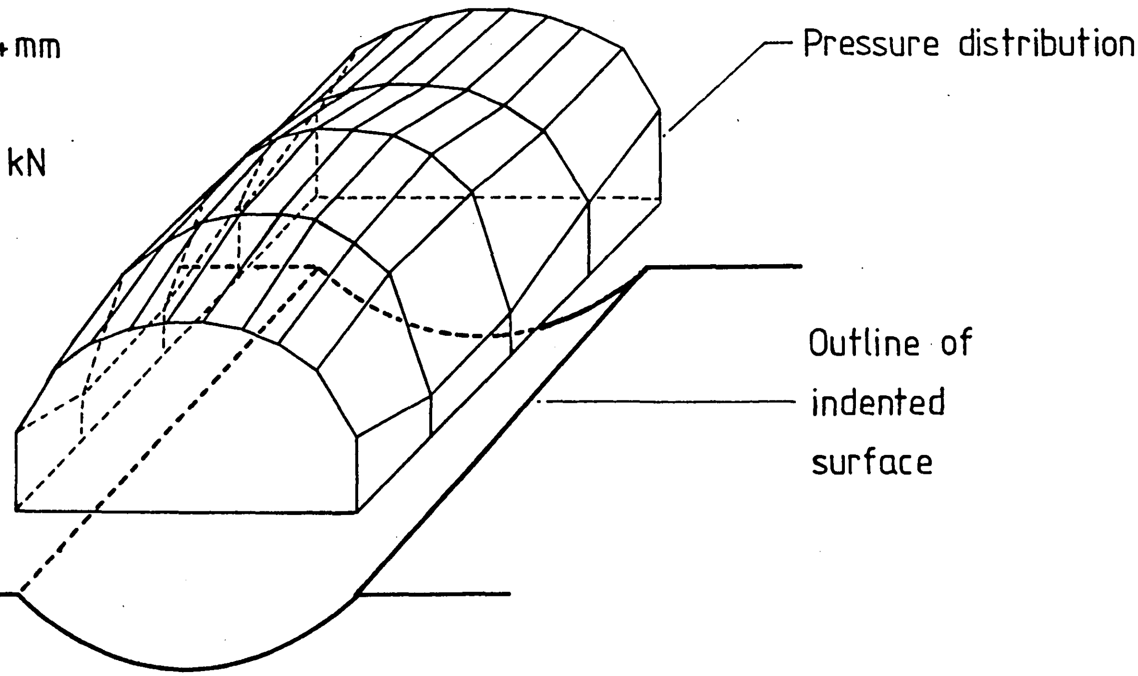

FIG 19 : THREE-DIMENSIONAL REPRESENTATION OF A TYPICAL PRESSURE REGIME : INDENTATION OF FLAT SPECIMENS

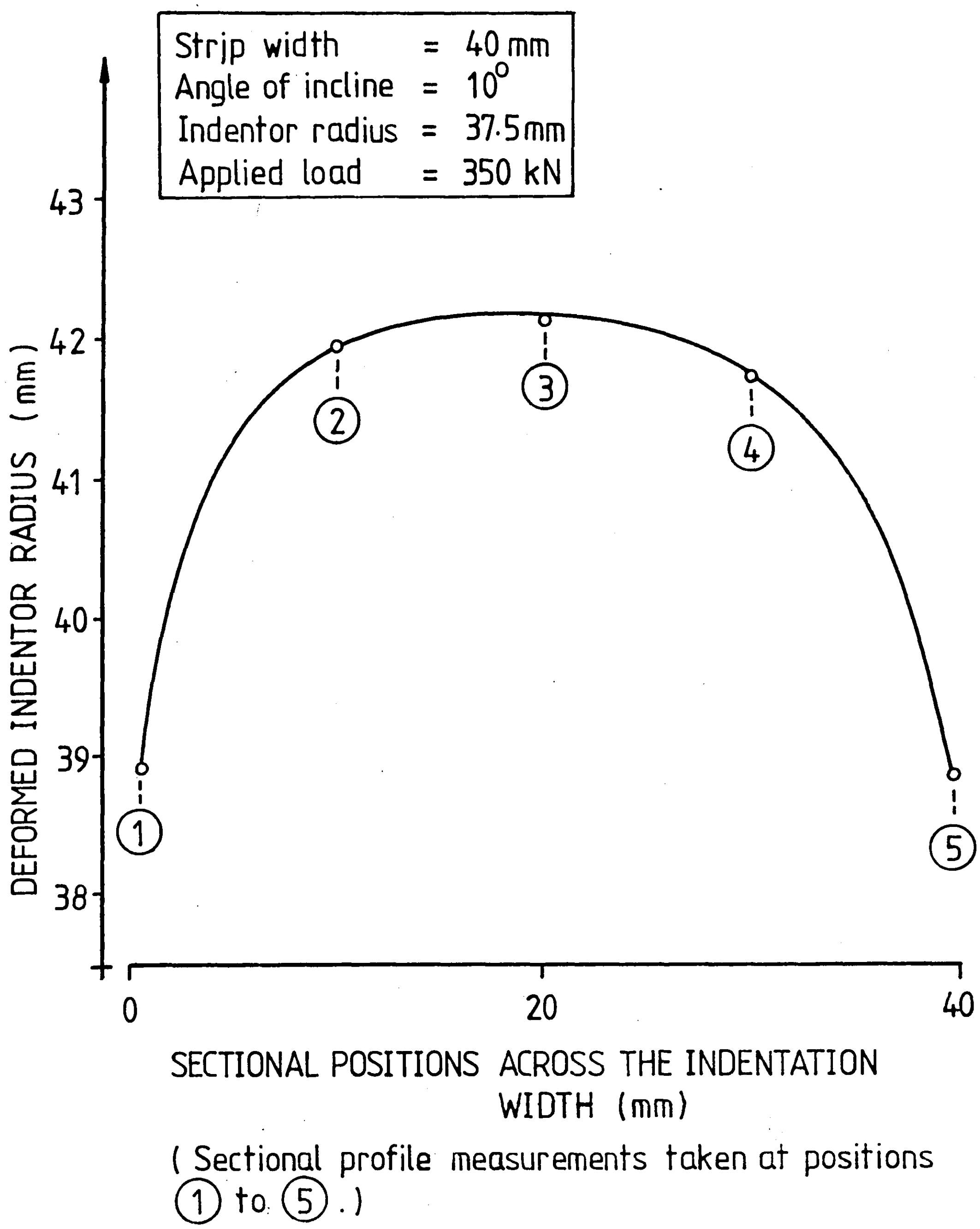

FIG 6.20 : VARIATION OF THE DEFORMED INDENTOR RADIUS ACROSS THE WIDTH OF A TYPICAL INCLINED INDENTATION

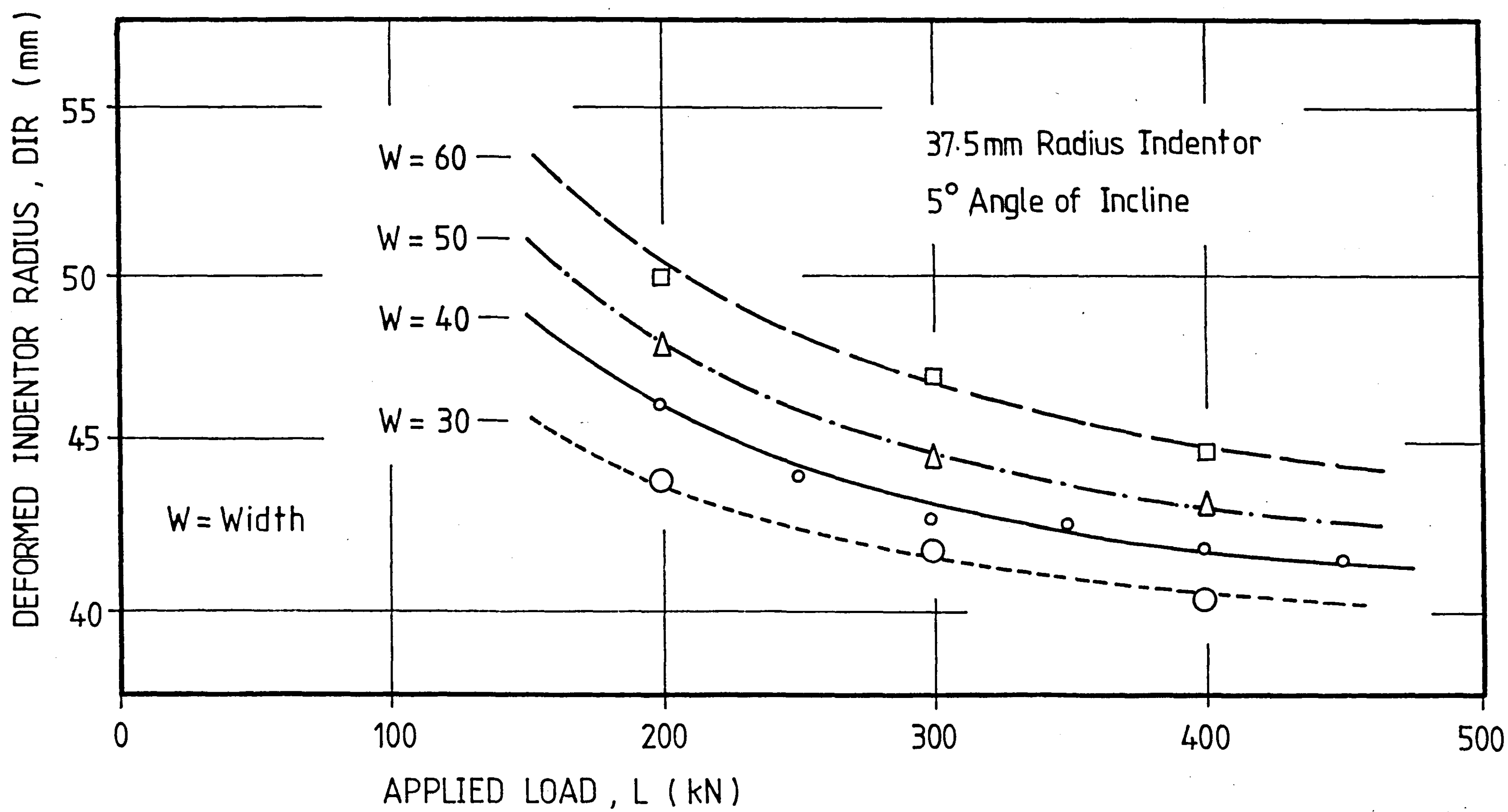

FIG 6.21 : EFFECTS OF APPLIED LOAD ON THE DEFORMED INDENTOR RADIUS : 37.5mm RADIUS INDENTOR INDENTING SPECIMENS WITH A 5° INCLINATION ANGLE

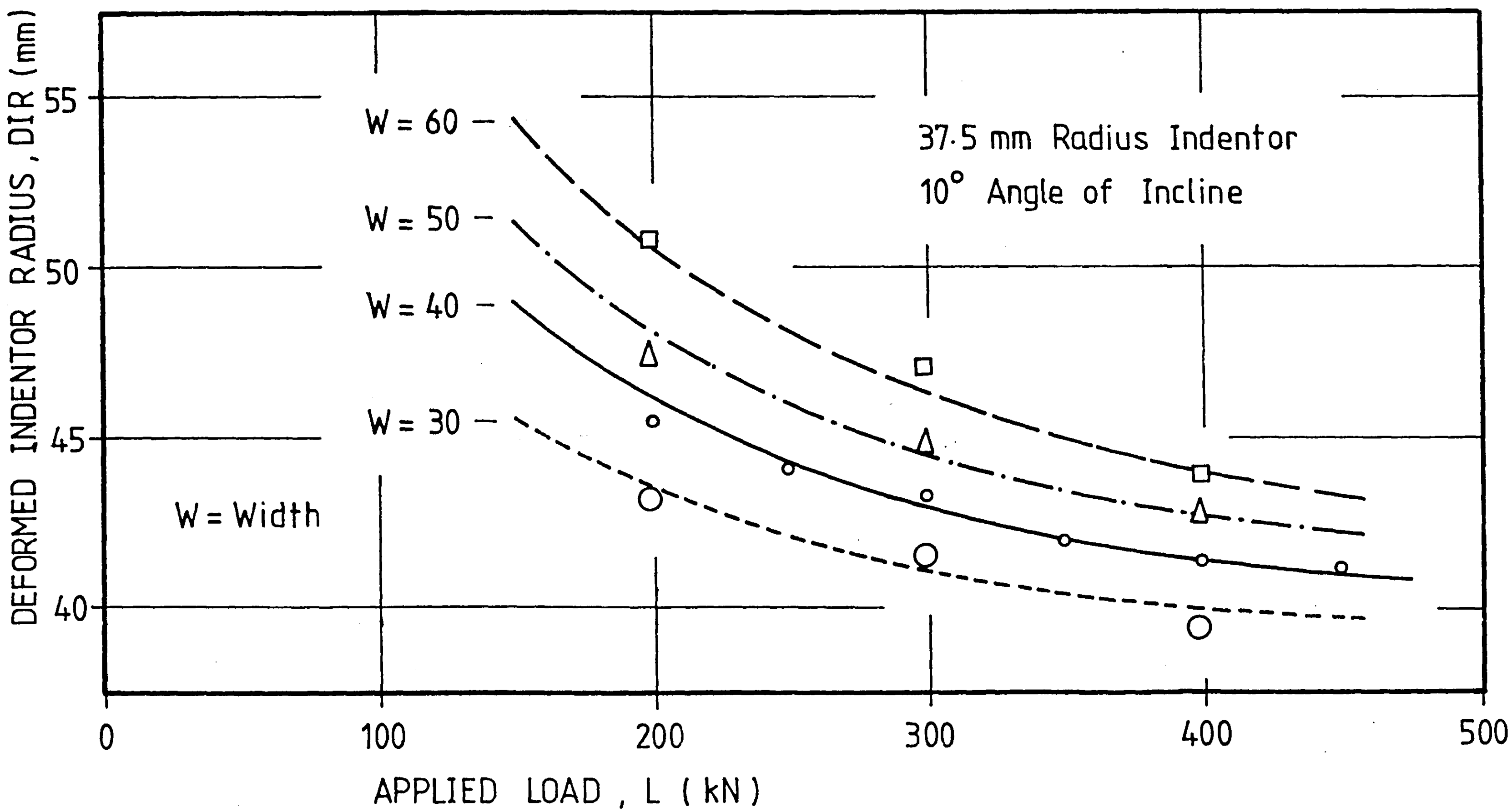

FIG 6.22 : EFFECTS OF APPLIED LOAD ON THE DEFORMED INDENTOR RADIUS : 37.5 mm RADIUS INDENTOR INDENTING SPECIMENS WITH A 10° INCLINATION ANGLE

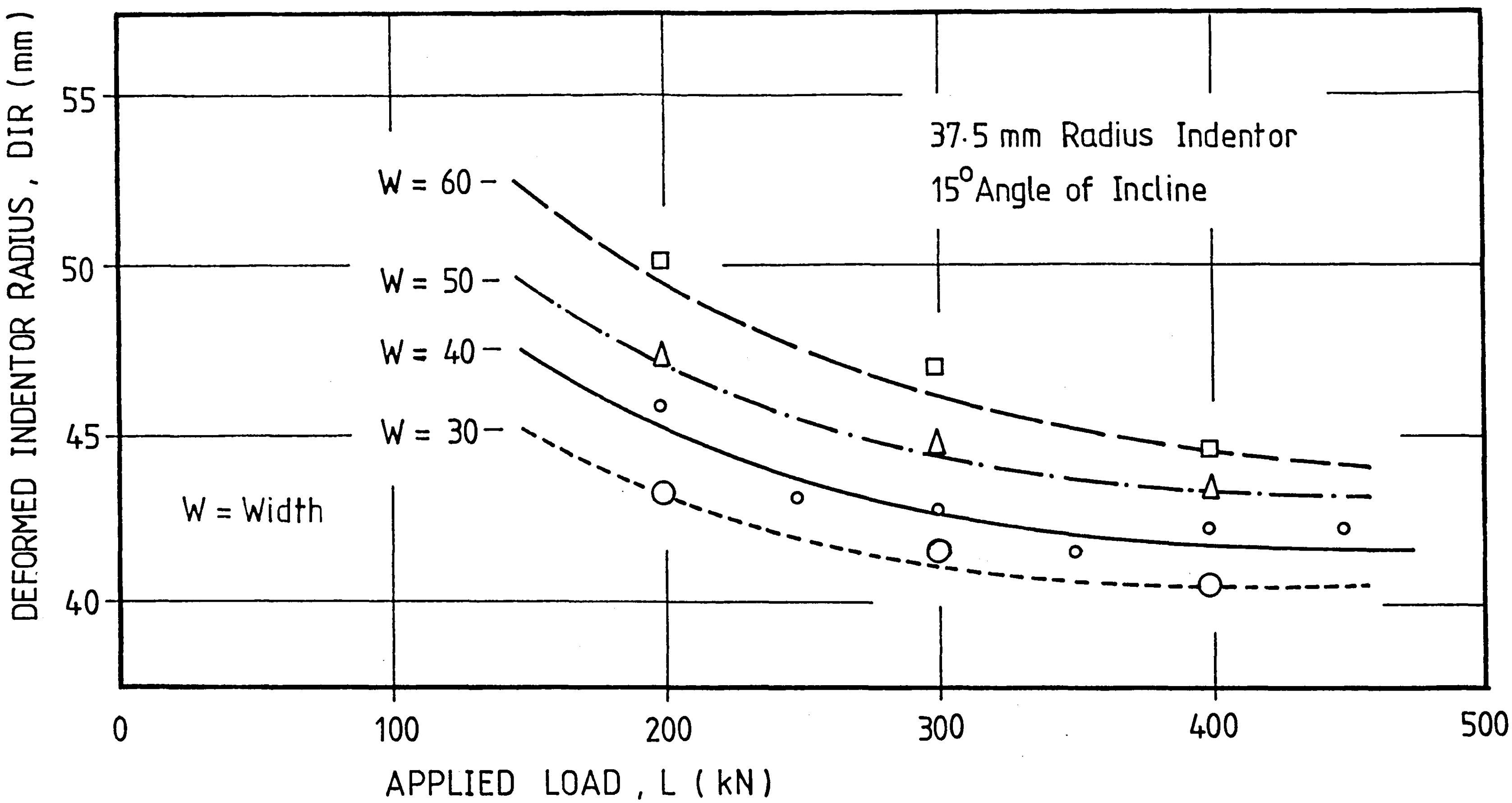

FIG 6.23 : EFFECTS OF APPLIED LOAD ON THE DEFORMED INDENTOR RADIUS : 37.5mm radius indentor indenting specimens with a 15° INCLINATION ANGLE

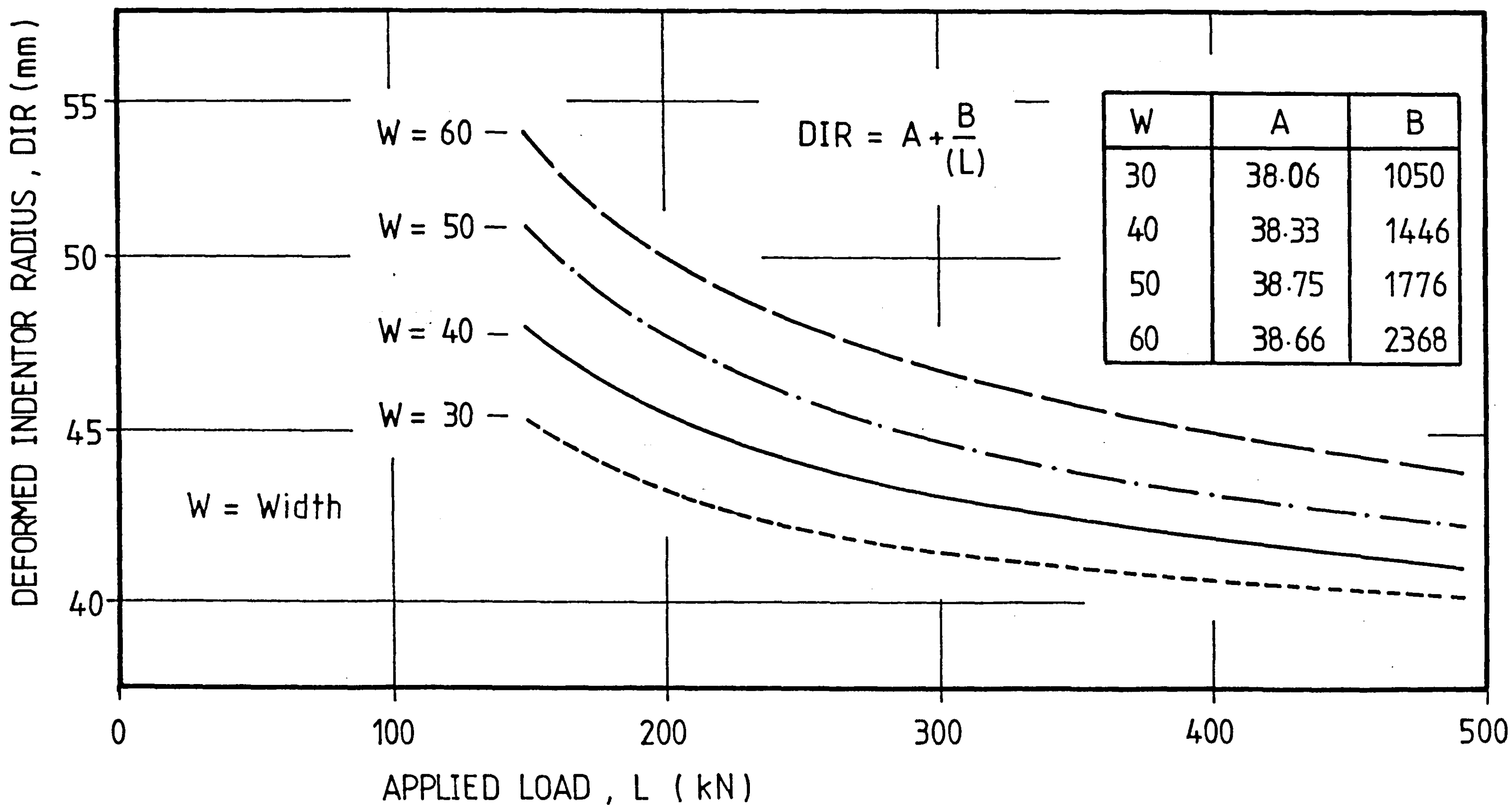

W	A	B
30	38·06	1050
40	38·33	1446
50	38·75	1776
60	38·66	2368

$$DIR = A + \frac{B}{(L)}$$

FIG 6.24 : COMPOSITE RELATIONSHIPS BETWEEN THE APPLIED LOAD AND DEFORMED INDENTOR RADIUS : INDENTATION OF INCLINED SPECIMENS

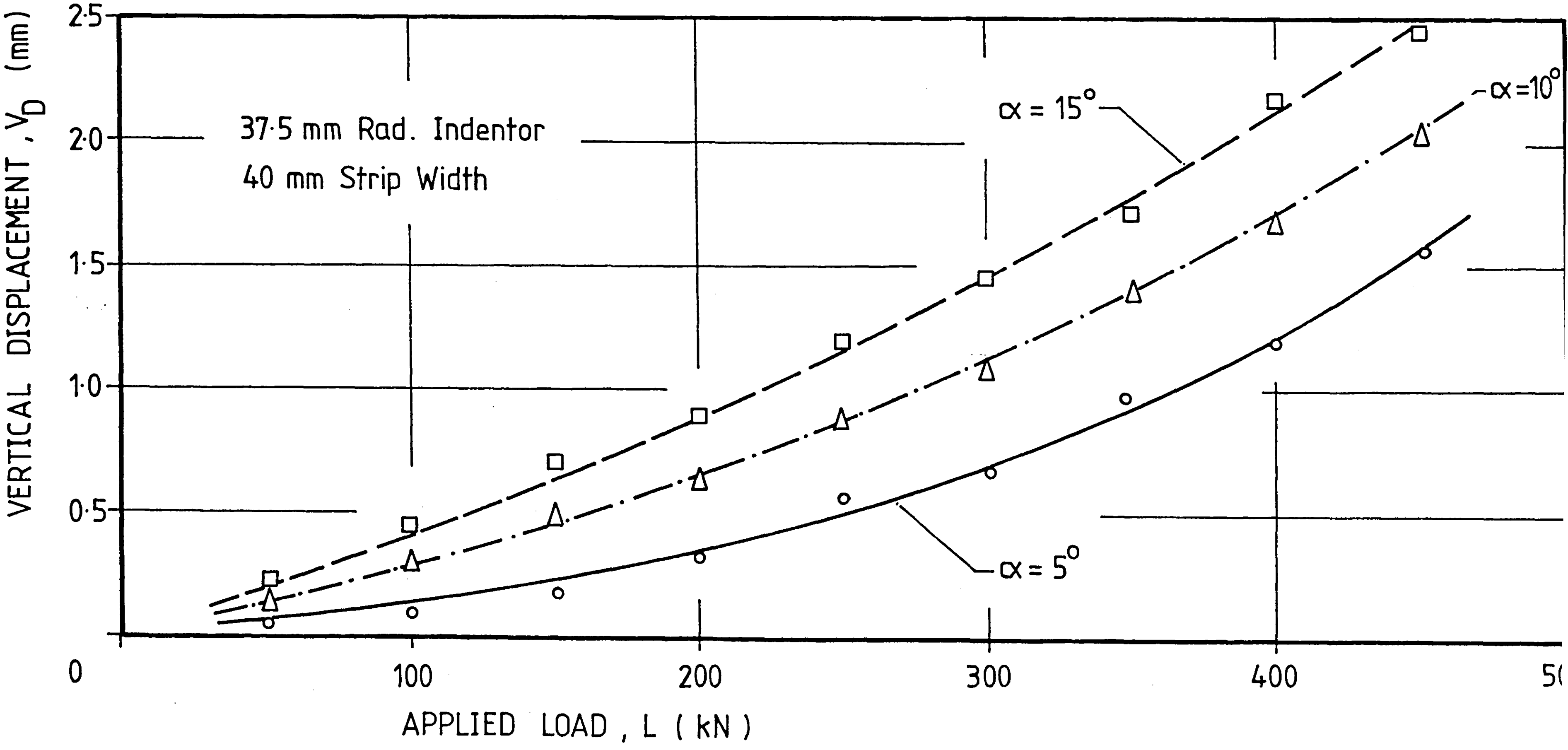

FIG 6.25 : EFFECTS OF APPLIED LOAD ON THE VERTICAL DISPLACEMENT OF THE INDENTOR : 37.5mm RADIUS INDENTOR INDENTING 40mm WIDE INCLINED SPECIMENS

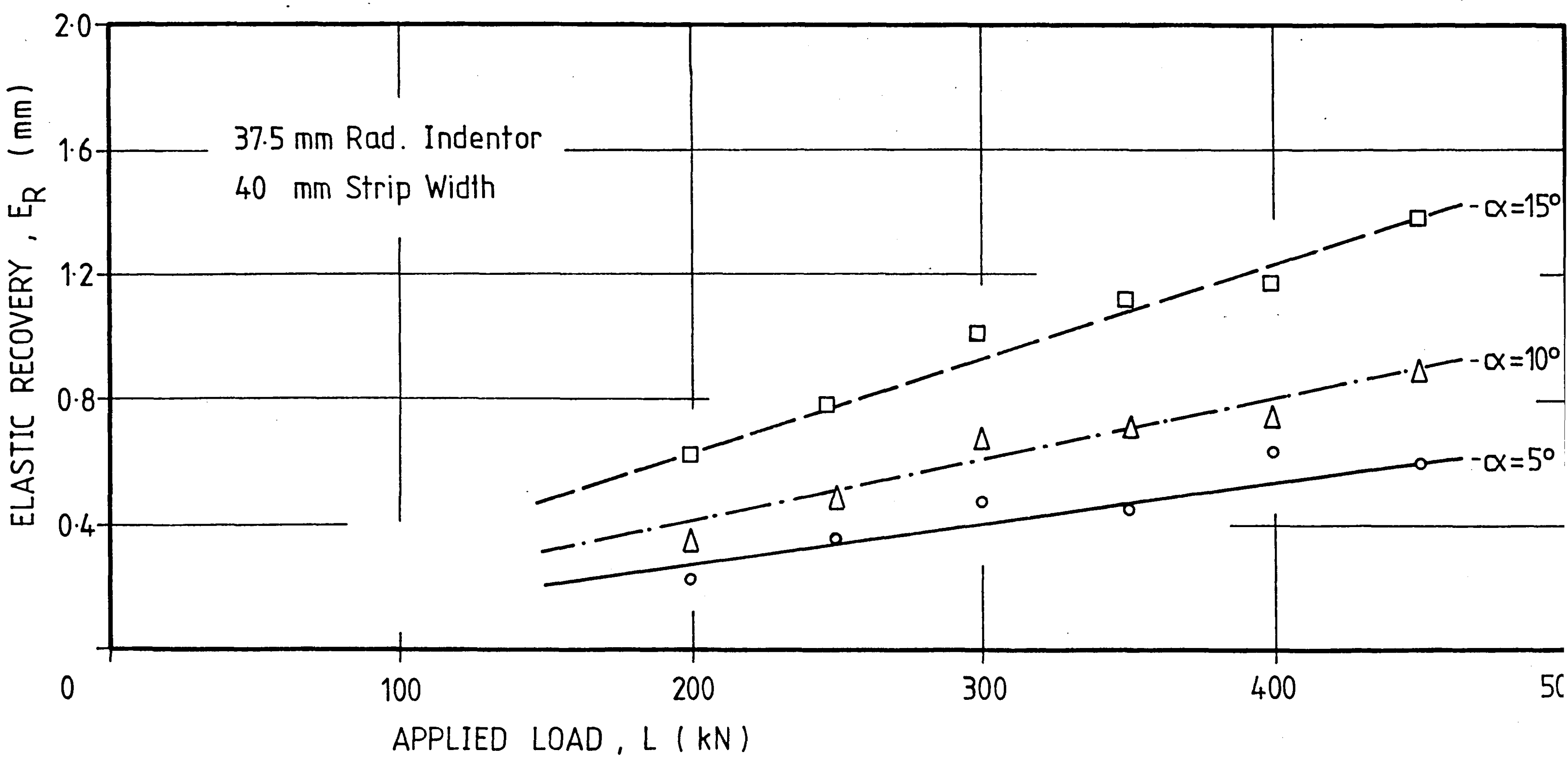

FIG 6.26 : EFFECTS OF APPLIED LOAD ON THE ELASTIC RECOVERY OF THE INDENTOR AND STRIP FOLLOWING LOAD RELAXATION : 37.5mm RADIUS INDENTOR INDENTING 40mm WIDE INCLINED SPECIMENS

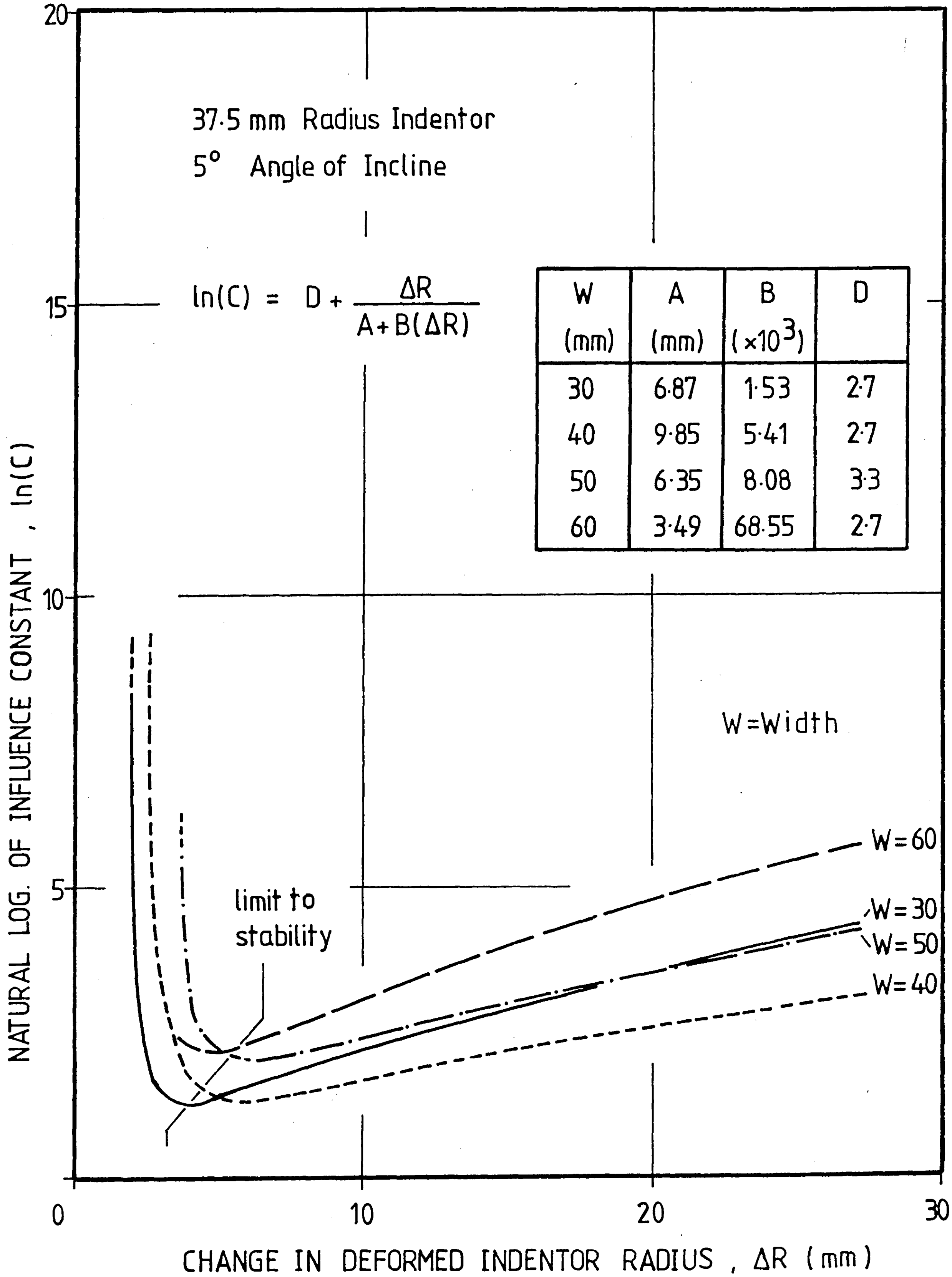

W (mm)	A (mm)	B ($\times 10^3$)	D
30	6·87	1·53	2·7
40	9·85	5·41	2·7
50	6·35	8·08	3·3
60	3·49	68·55	2·7

FIG 6.27 : INFLUENCE CONSTANT FUNCTIONS : 37.5mm RADIUS INDENTOR INDENTING SPECIMENS WITH A 5° INCLINATION ANGLE

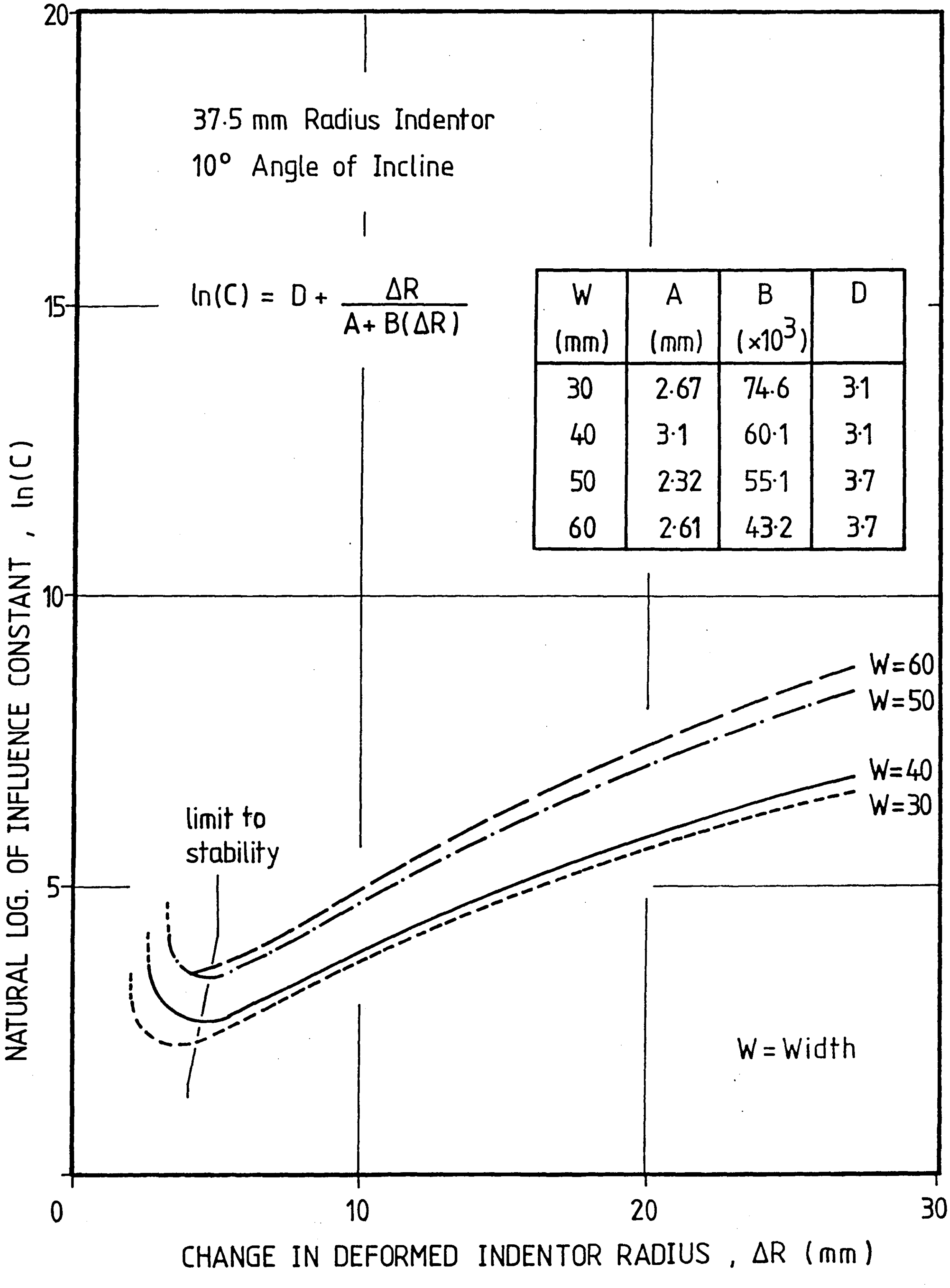

FIG 6.28 : INFLUENCE CONSTANT FUNCTIONS : 37.5mm RADIUS INDENTOR INDENTING SPECIMENS WITH A 10° INCLINATION ANGLE

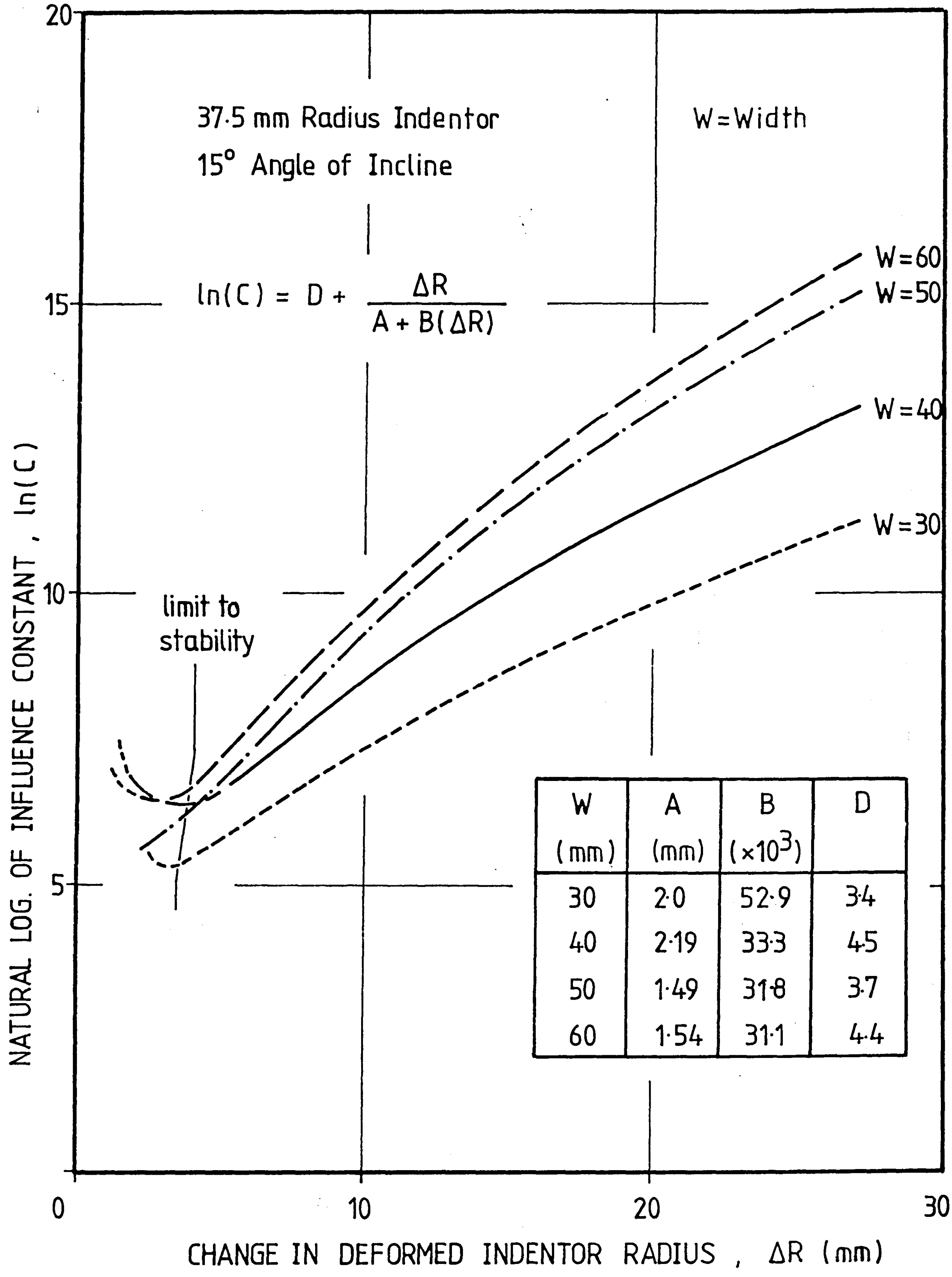

FIG 6.29 : INFLUENCE CONSTANT FUNCTIONS : 37.5mm RADIUS INDENTOR INDENTING SPECIMENS WITH A 15° INCLINATION ANGLE

SPECIMEN DETAILS.

Strip width	= 40 mm
Angle of incline	= 10°
Mean contact arc length	= 20·2mm
Applied load	= 350 kN

PRESSURE DISTRIBUTION.

Vertical scale :
1mm = 10 N mm^{-2}

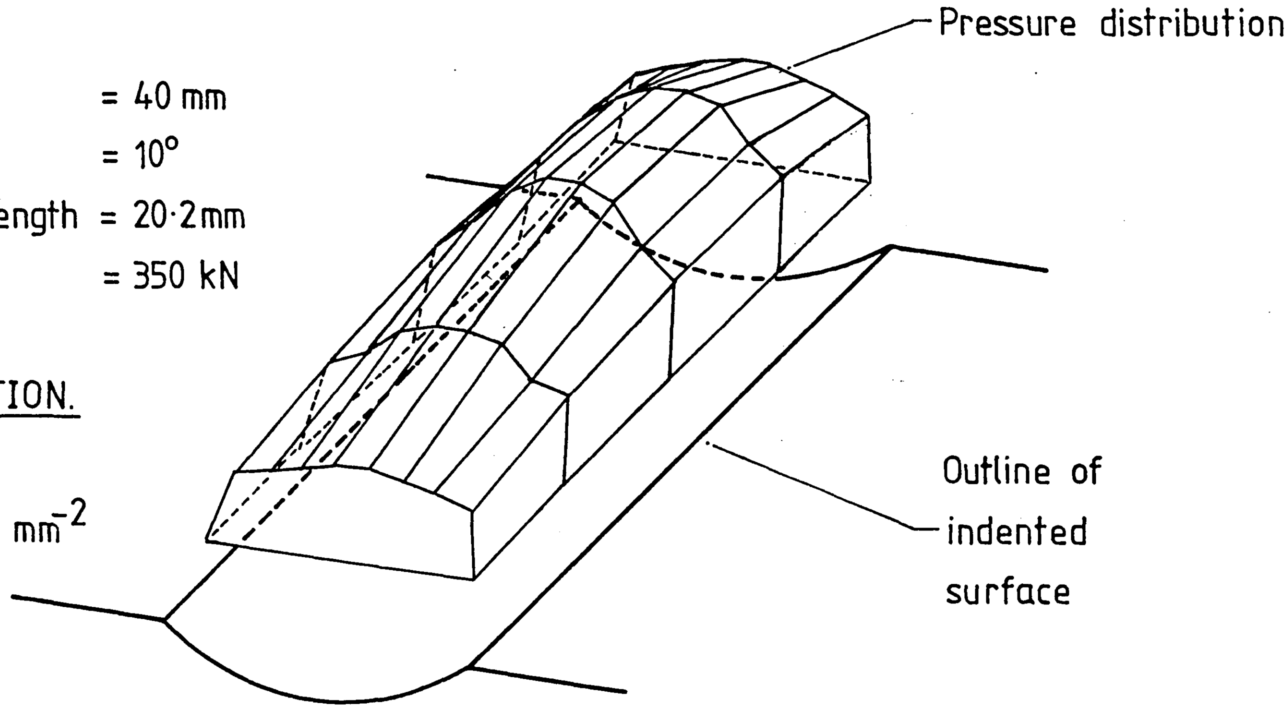

FIG 6.30 : THREE-DIMENSIONAL REPRESENTATION OF A TYPICAL PRESSURE REGIME : INDENTATION OF INCLINED SPECIMENS

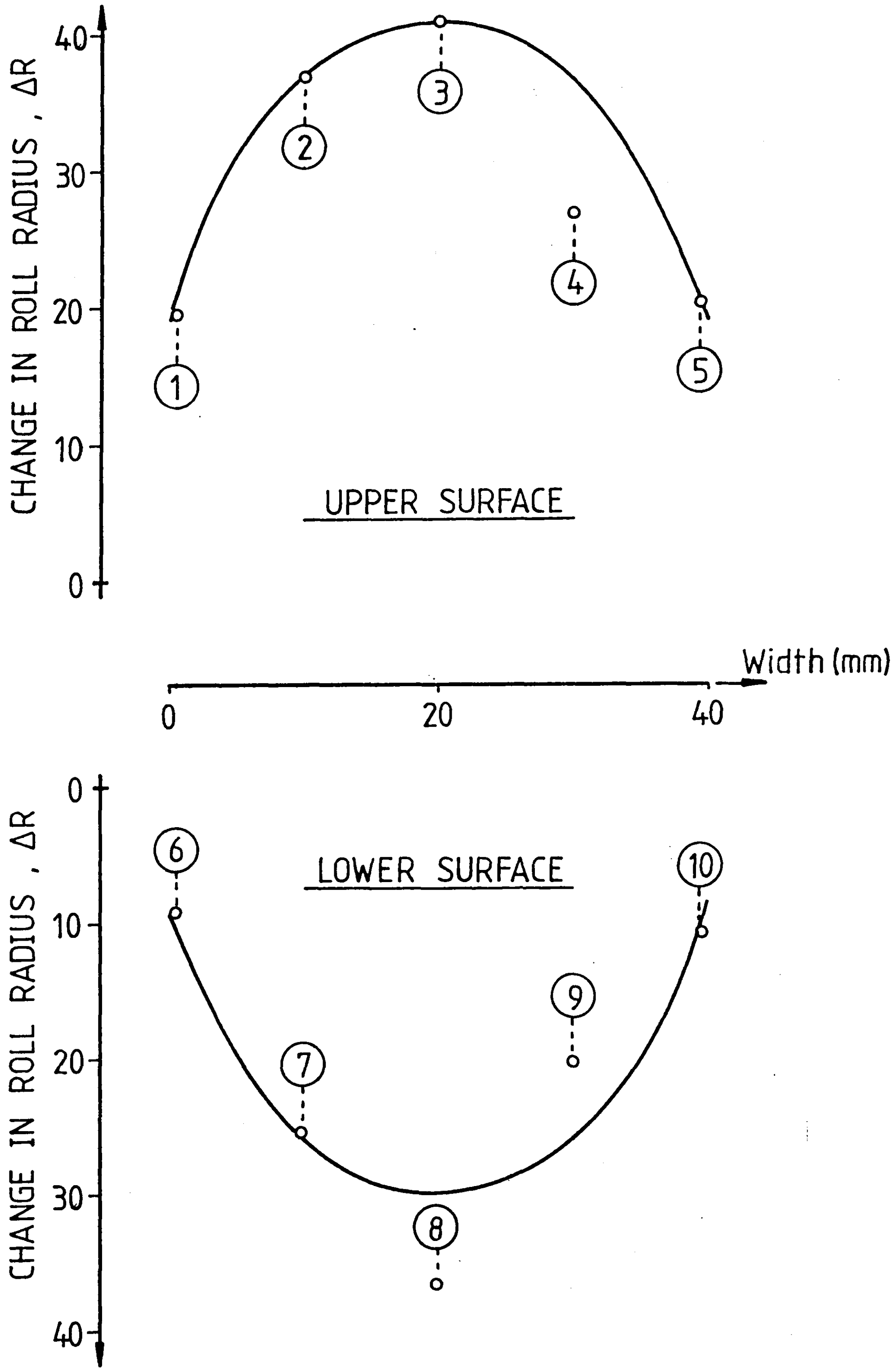

FIG 6.31 : VARIATIONS IN THE 'CHANGE IN ROLL RADIUS' ACROSS THE WIDTHS OF A TYPICAL INTERRUPTED-PASS WORKPIECE

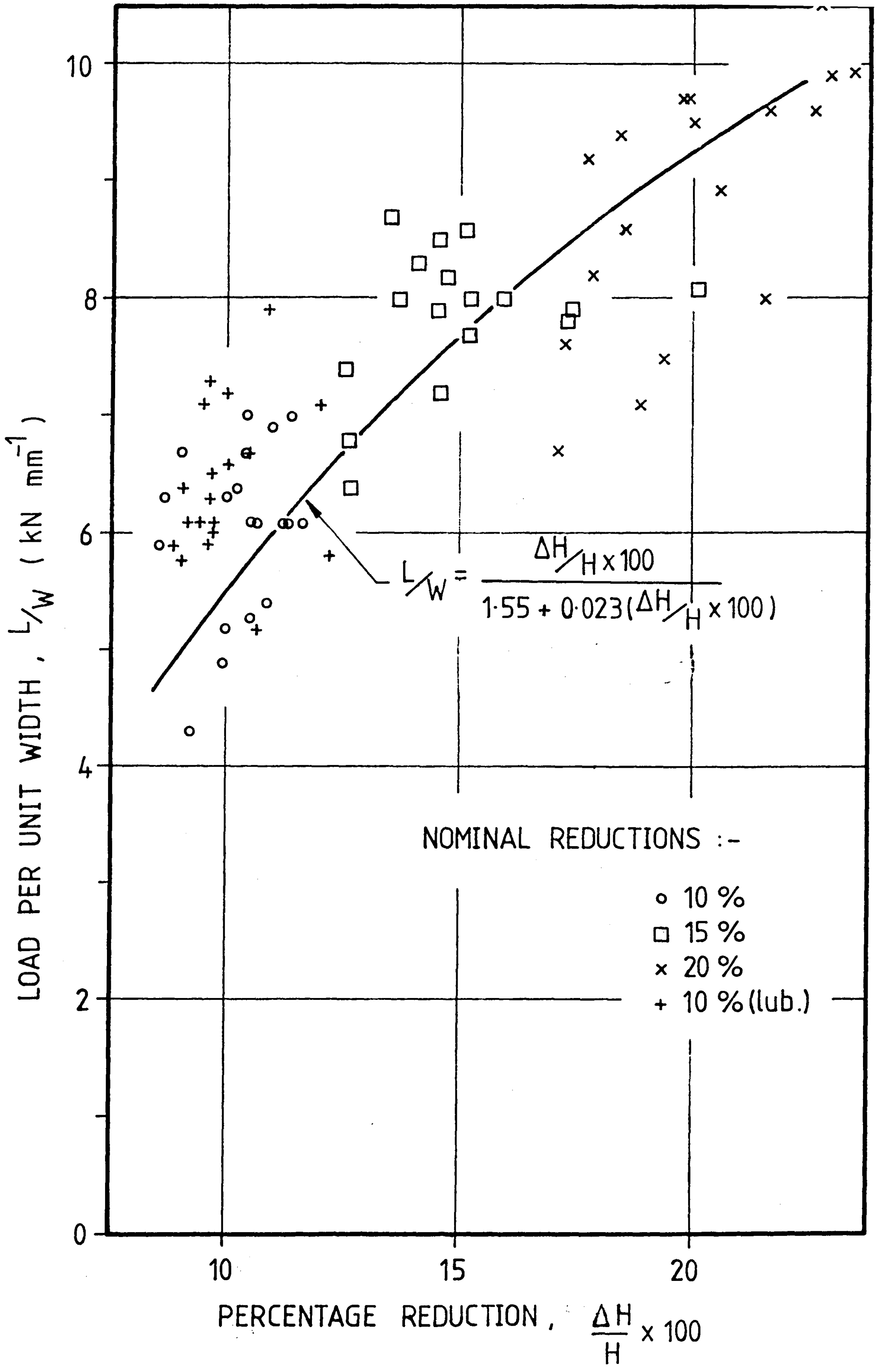

FIG 6.32 : EFFECTS OF THE PERCENTAGE REDUCTION IN STRIP THICKNESS ON THE LOAD PER UNIT WIDTH : INTERRUPTED-PASS ROLLING TESTS

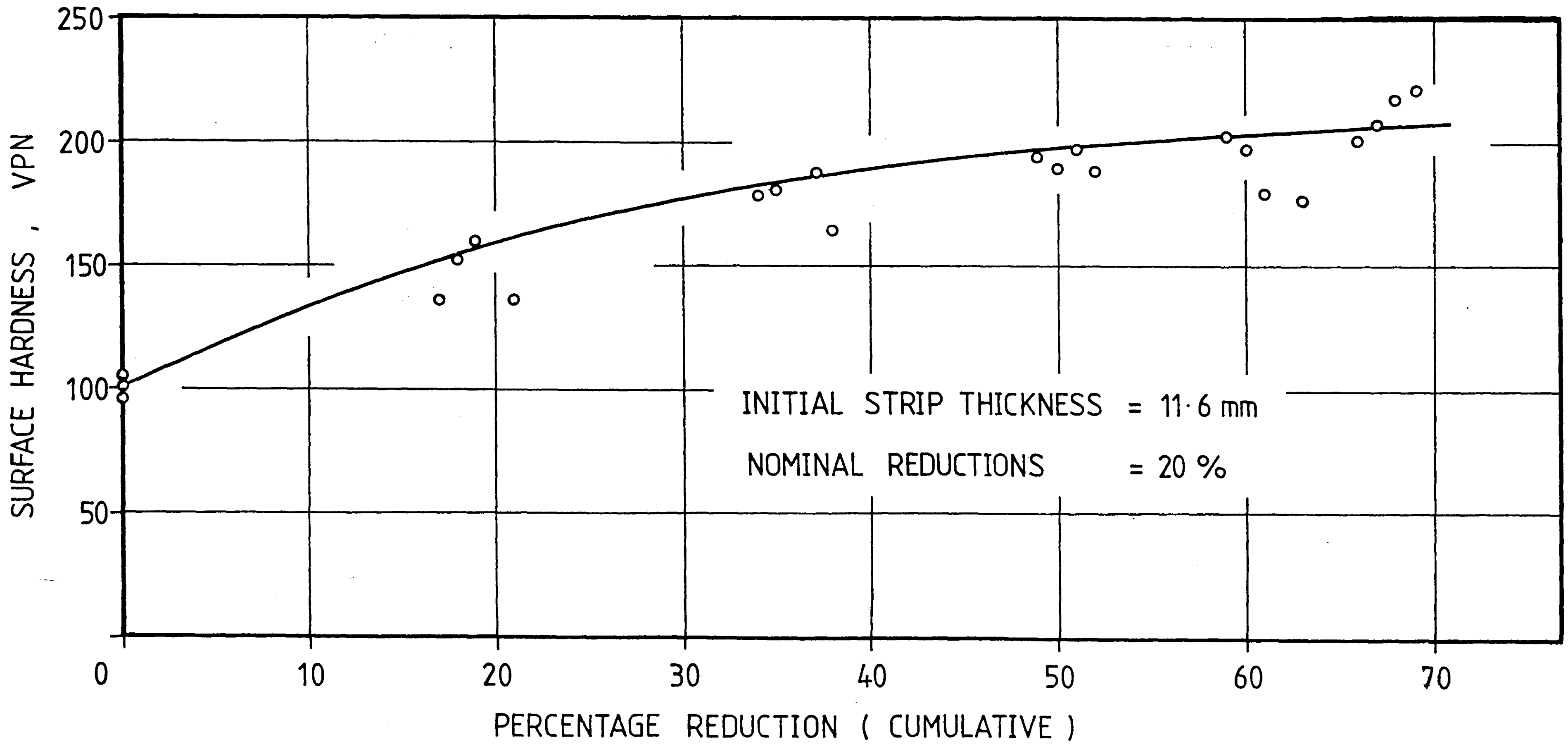

FIG 6.33 : EFFECTS OF THE PERCENTAGE REDUCTION IN STRIP THICKNESS (CUMULATIVE) ON THE SURFACE HARDNESS : INTERRUPTED PASS ROLLING TESTS

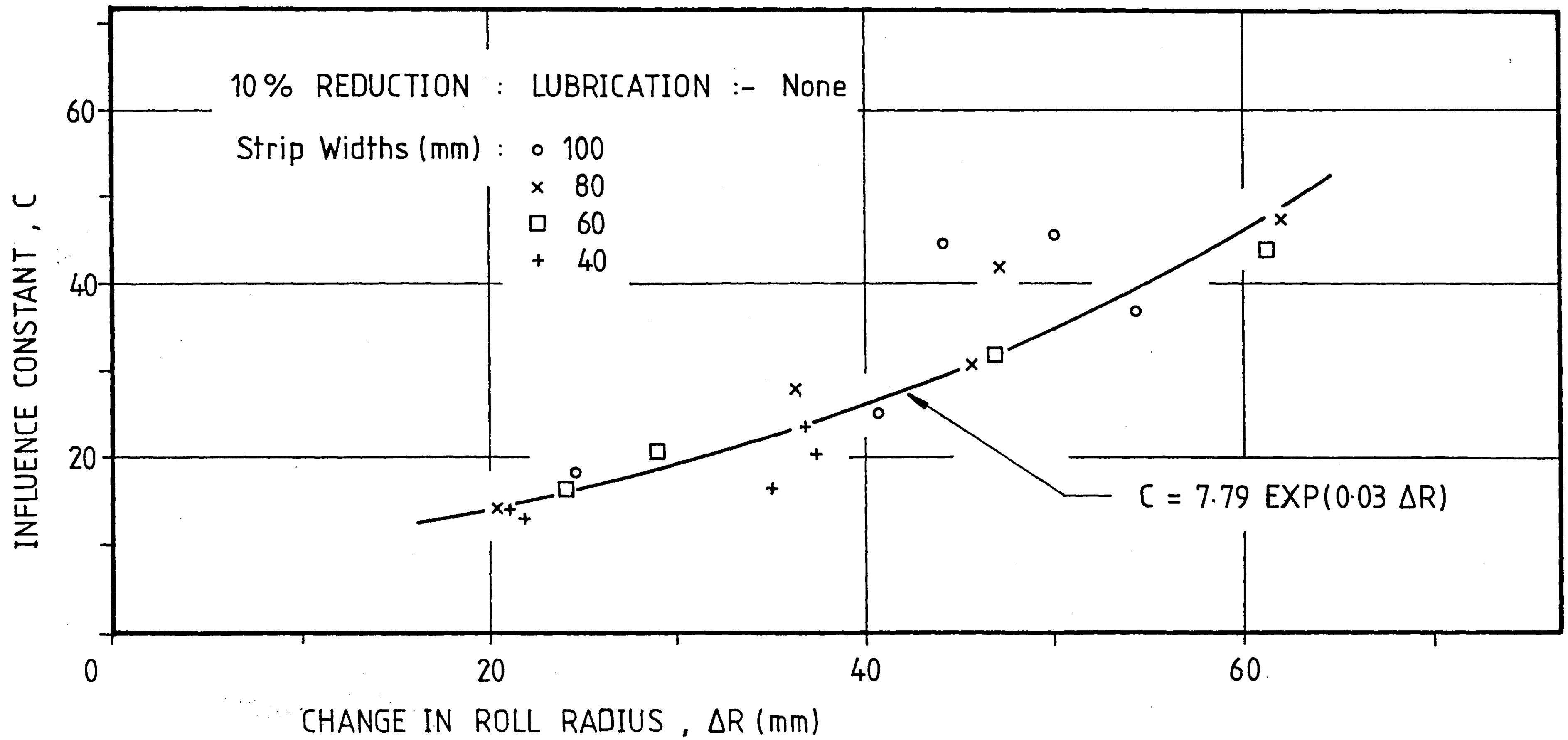

FIG 6.34 : INFLUENCE CONSTANT FUNCTIONS : INTERRUPTED-PASS ROLLING TESTS, 10% NOMINAL REDUCTIONS - DRY ROLLING CONDITIONS

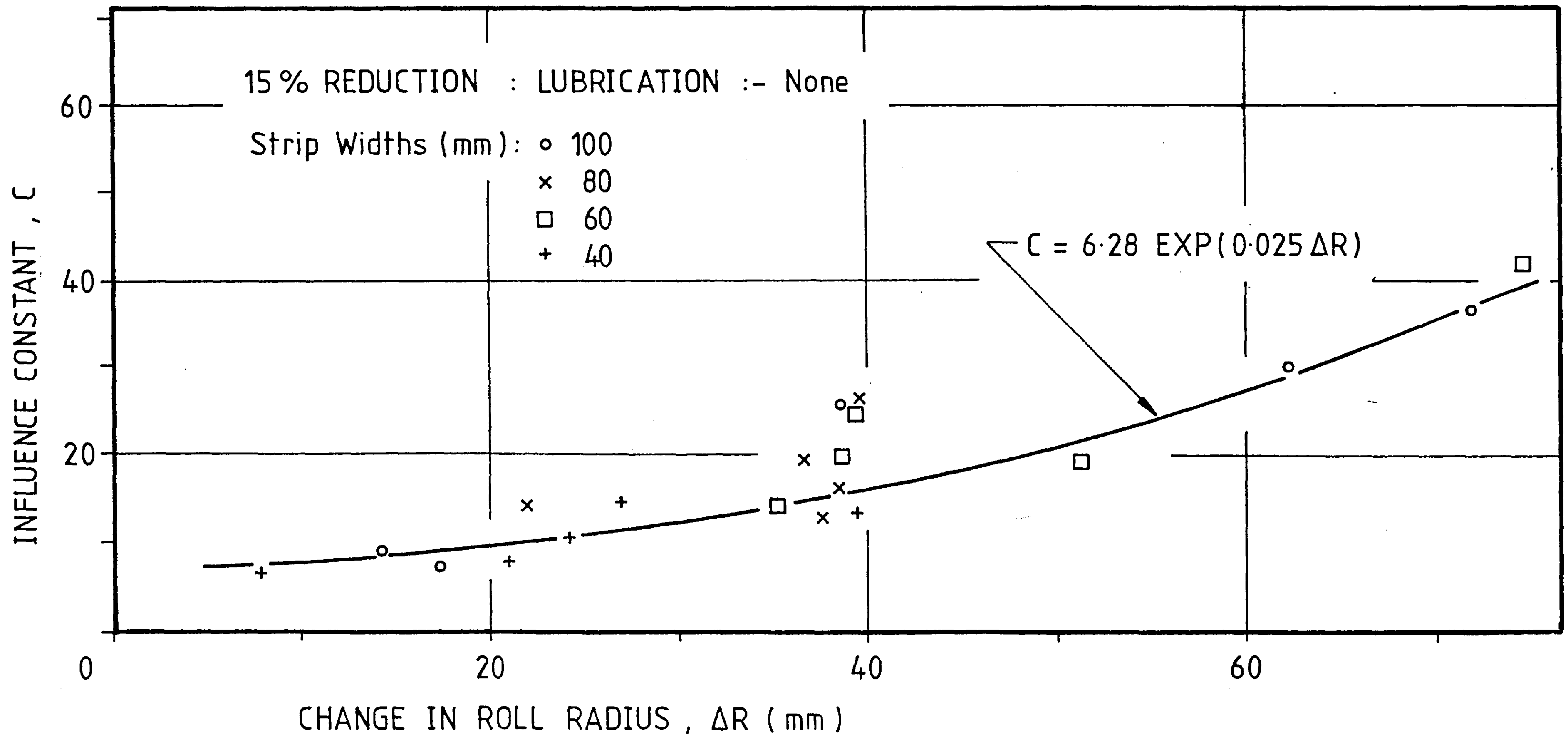

FIG 6.35 : INFLUENCE CONSTANT FUNCTIONS : INTERRUPTED-PASS ROLLING TESTS, 15% NOMINAL REDUCTIONS - DRY ROLLING CONDITIONS

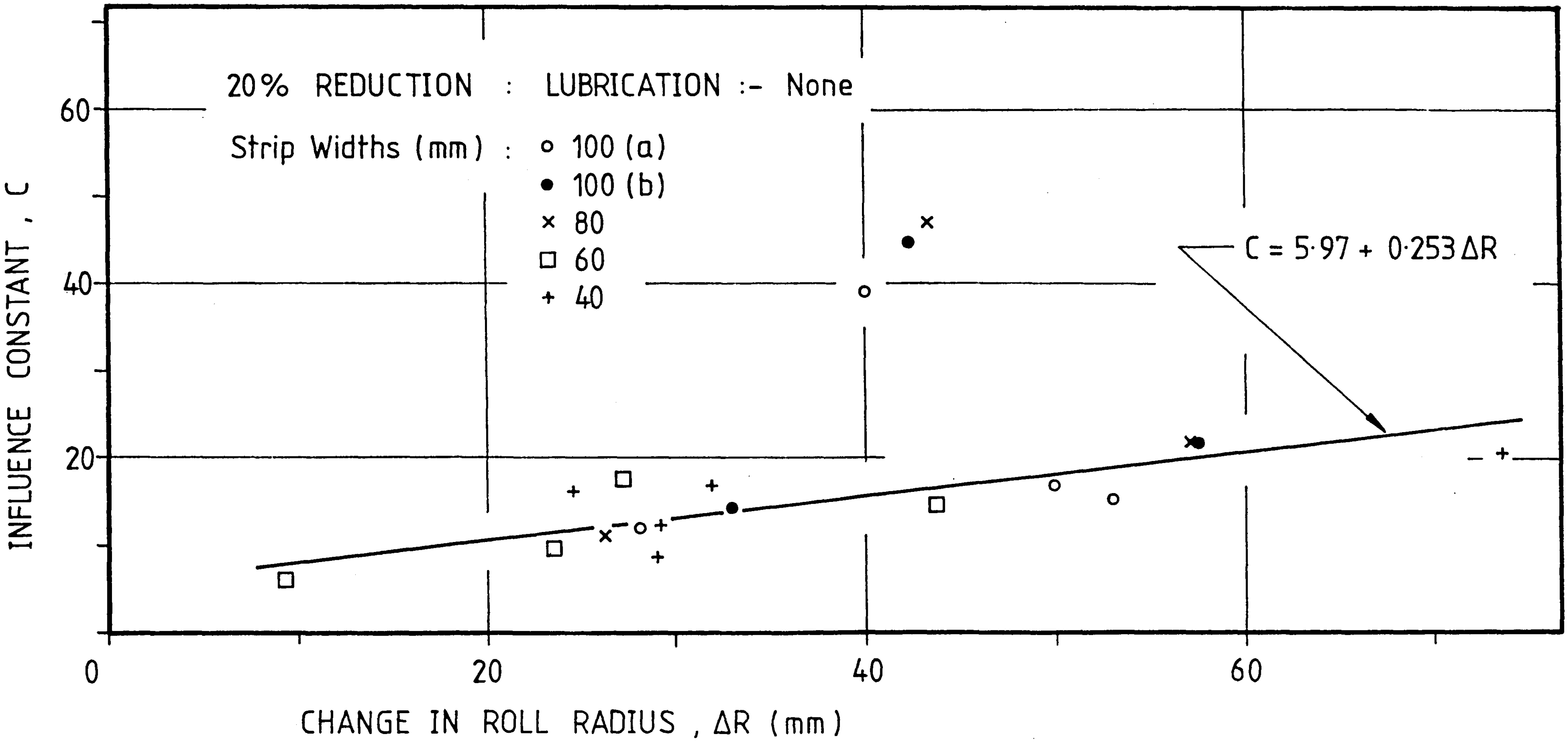

FIG 6.36 : INFLUENCE CONSTANT FUNCTIONS : INTERRUPTED PASS ROLLING TESTS, 20% NOMINAL REDUCTIONS - DRY ROLLING CONDITIONS

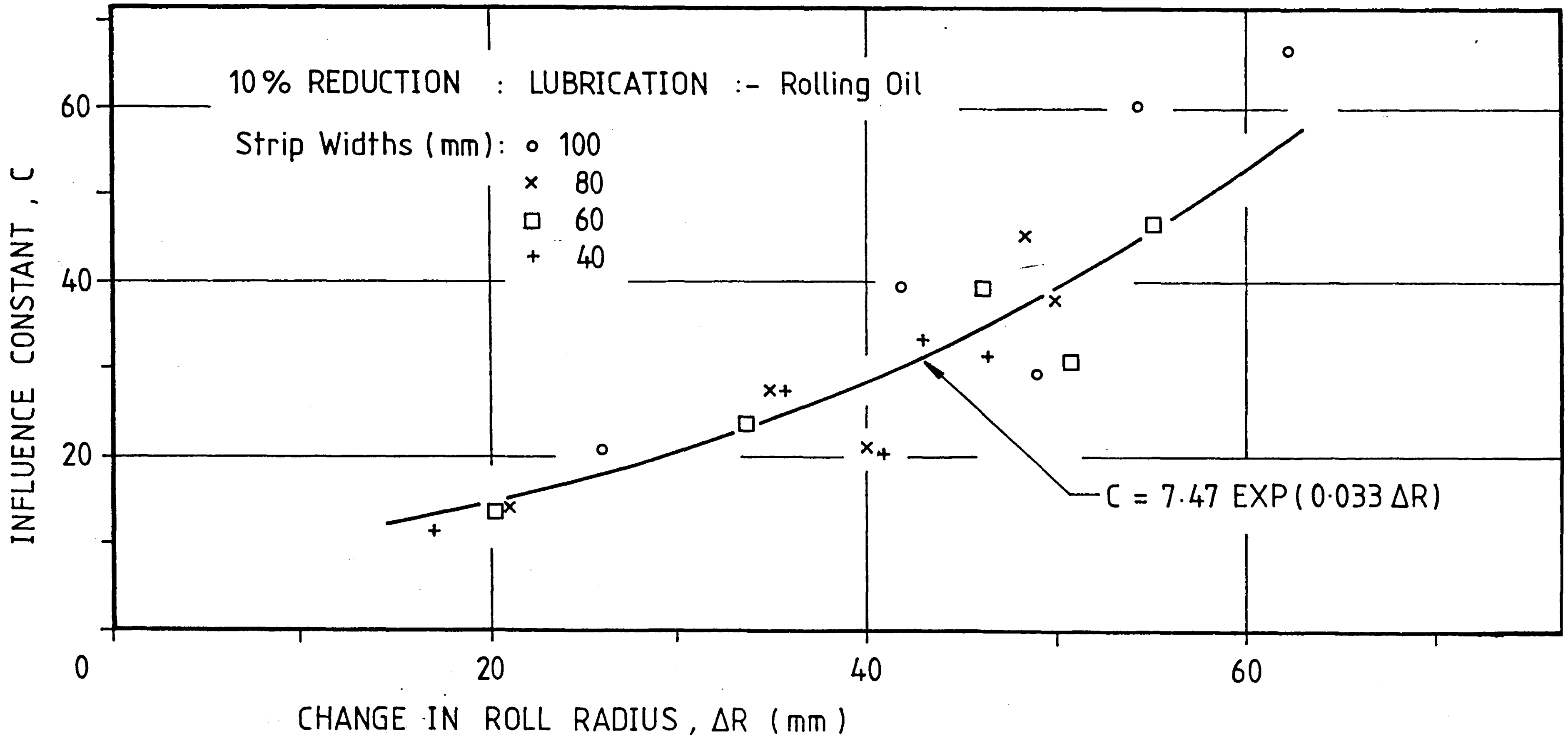

FIG 6.37 : INFLUENCE CONSTANT FUNCTIONS : INTERRUPTED-PASS ROLLING TESTS, 10% NOMINAL REDUCTIONS - LUBRICATED (ROLLING OIL)

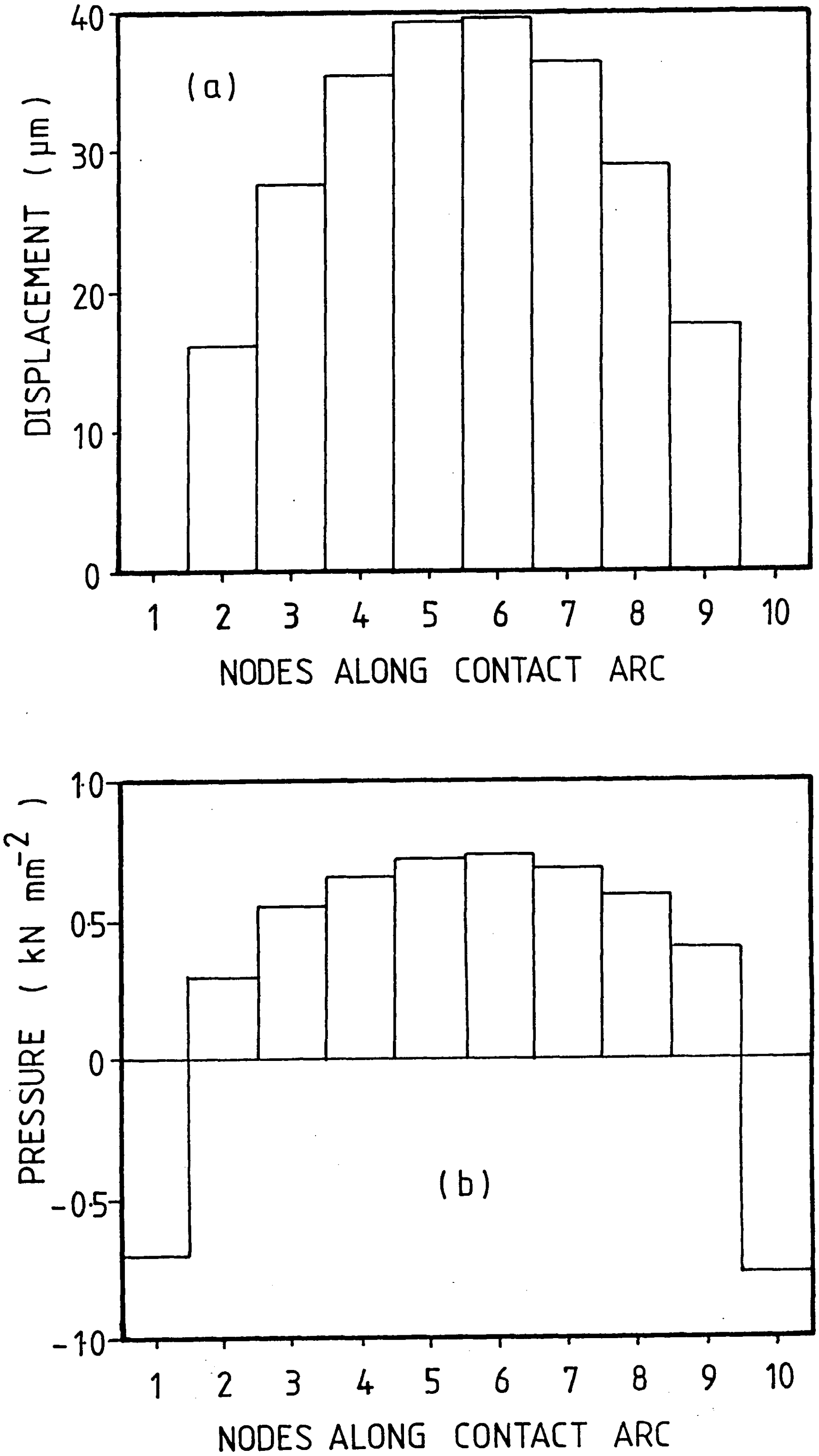

FIG 6.38 : DISCRETISED DEVIATIONS (a) AND PREDICTED PRESSURE DISTRIBUTION (b) ALONG A TYPICAL CONTACT ARC : INTERRUPTED-PASS ROLLING TESTS

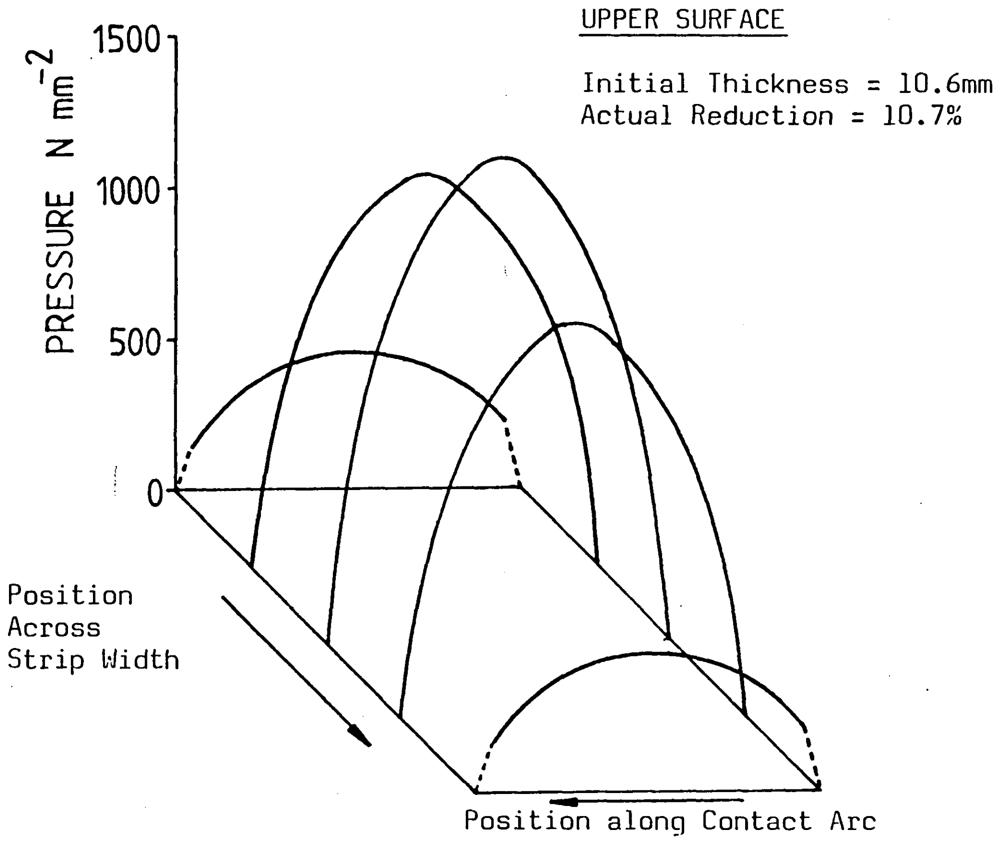

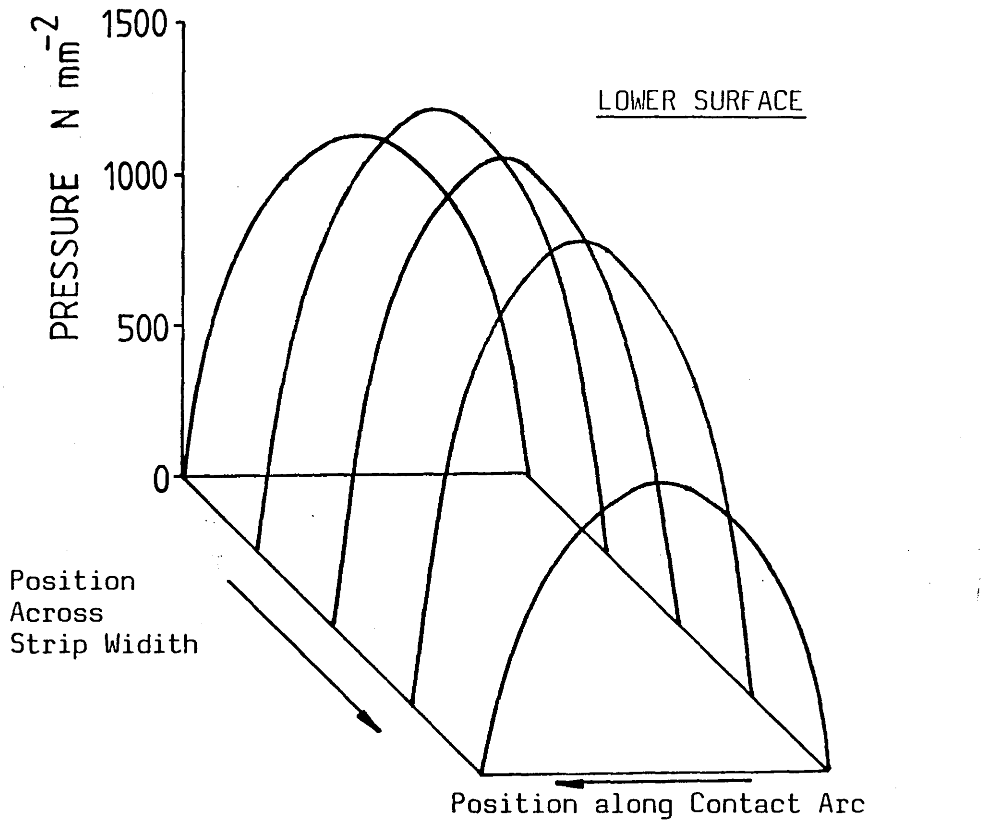

FIG 6.39 : PREDICTED PRESSURE PROFILES : 10% NOMINAL REDUCTION, 100mm STRIP WIDTH, DRY ROLLING CONDITIONS

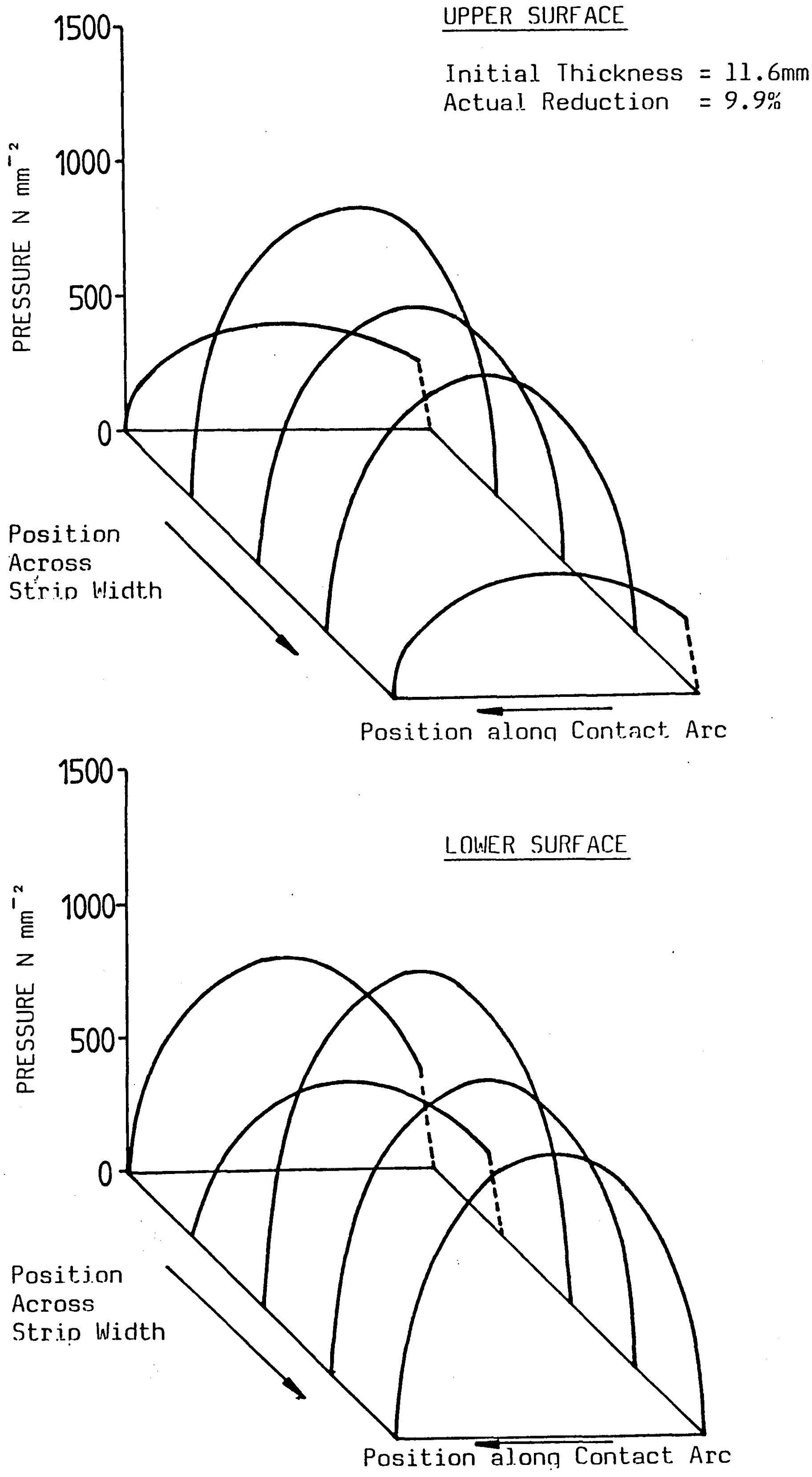

FIG 6.40 : PREDICTED PRESSURE PROFILES : 10% NOMINAL REDUCTION 80mm STRIP WIDTH, DRY ROLLING CONDITIONS

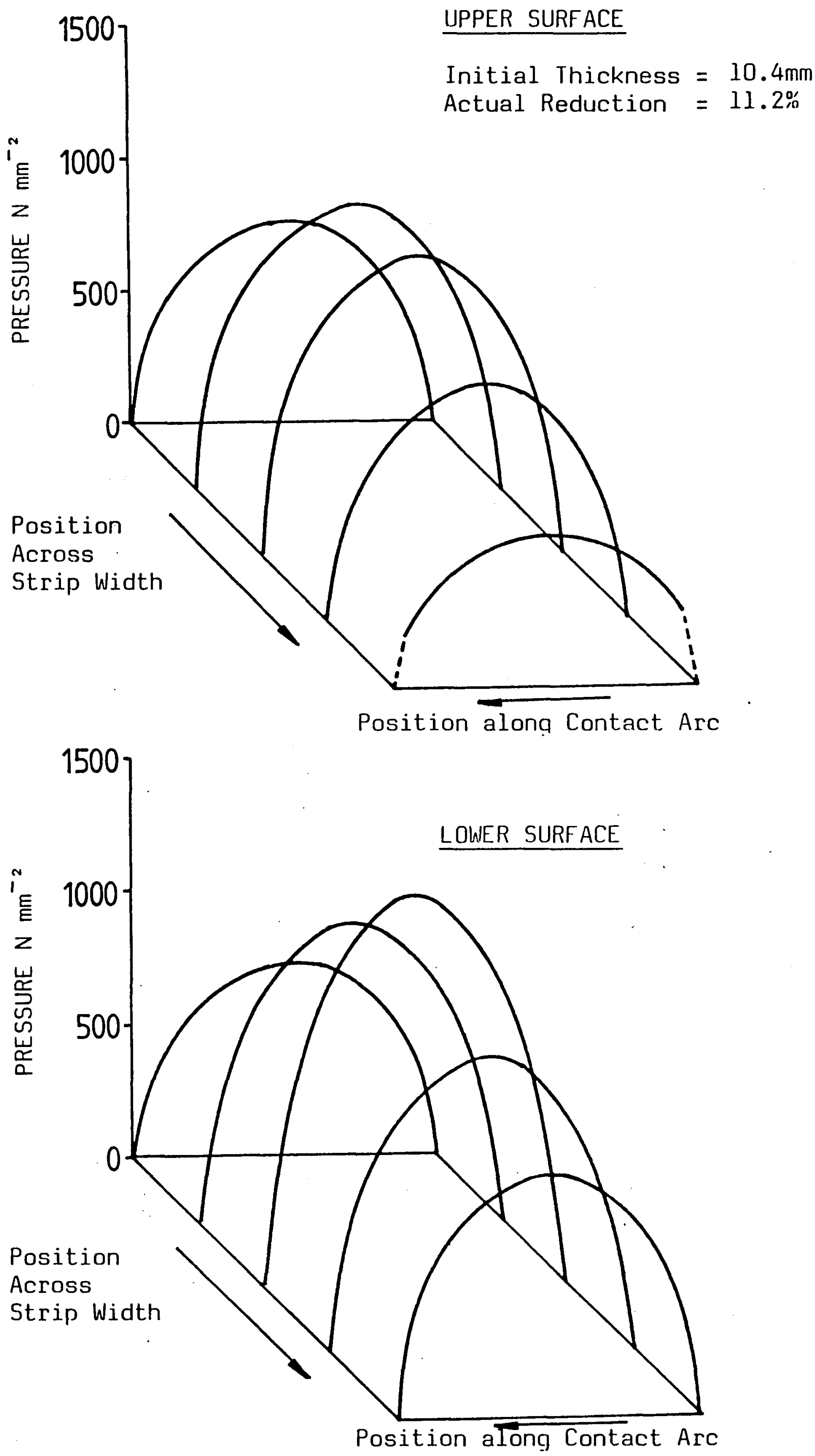

FIG 6.41 : PREDICTED PRESSURE PROFILES : 10% NOMINAL REDUCTION 60mm STRIP WIDTH, DRY ROLLING CONDITIONS

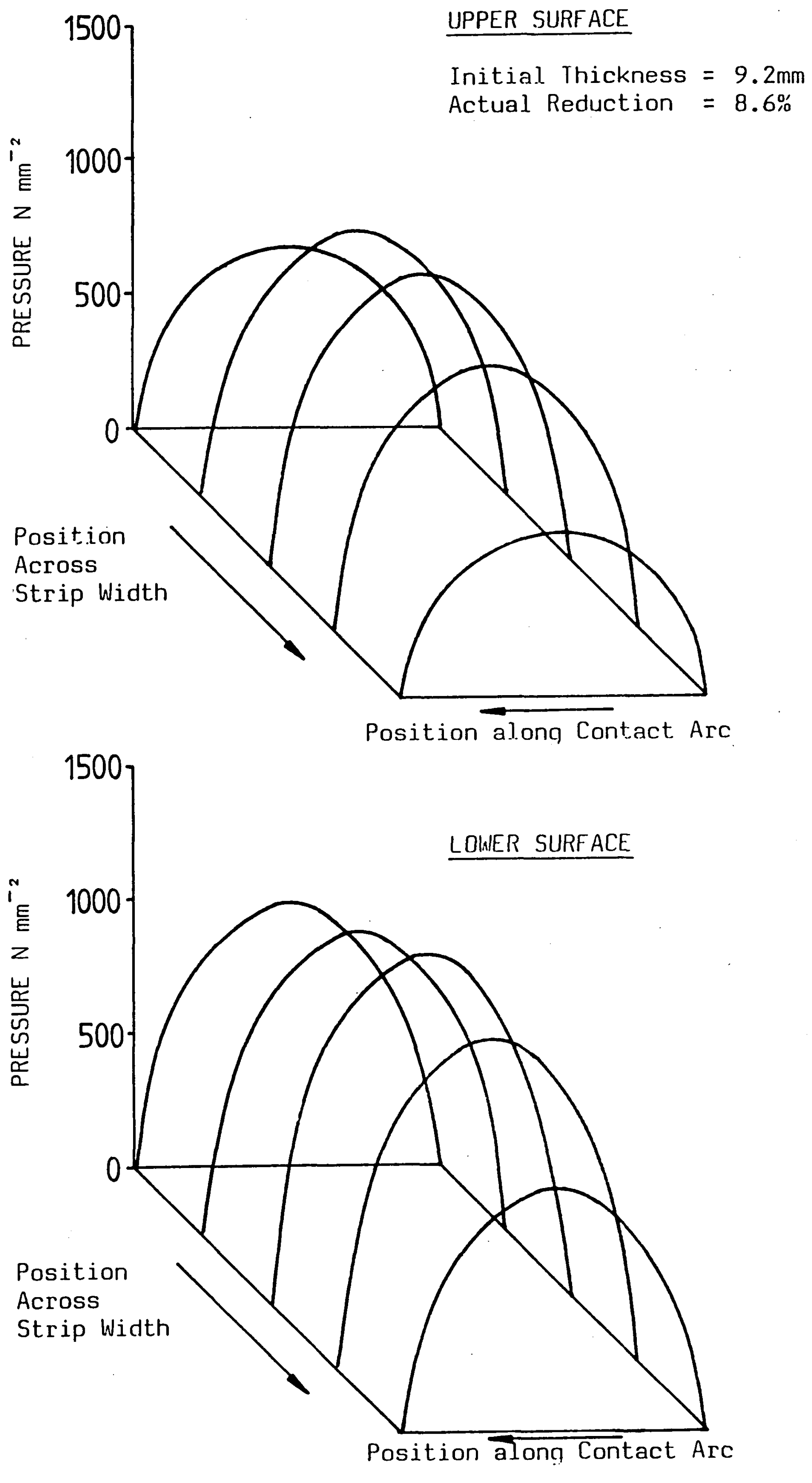

FIG 6.42 : PREDICTED PRESSURE PROFILES : 10% NOMINAL REDUCTION 40mm STRIP WIDTH, DRY ROLLING CONDITIONS

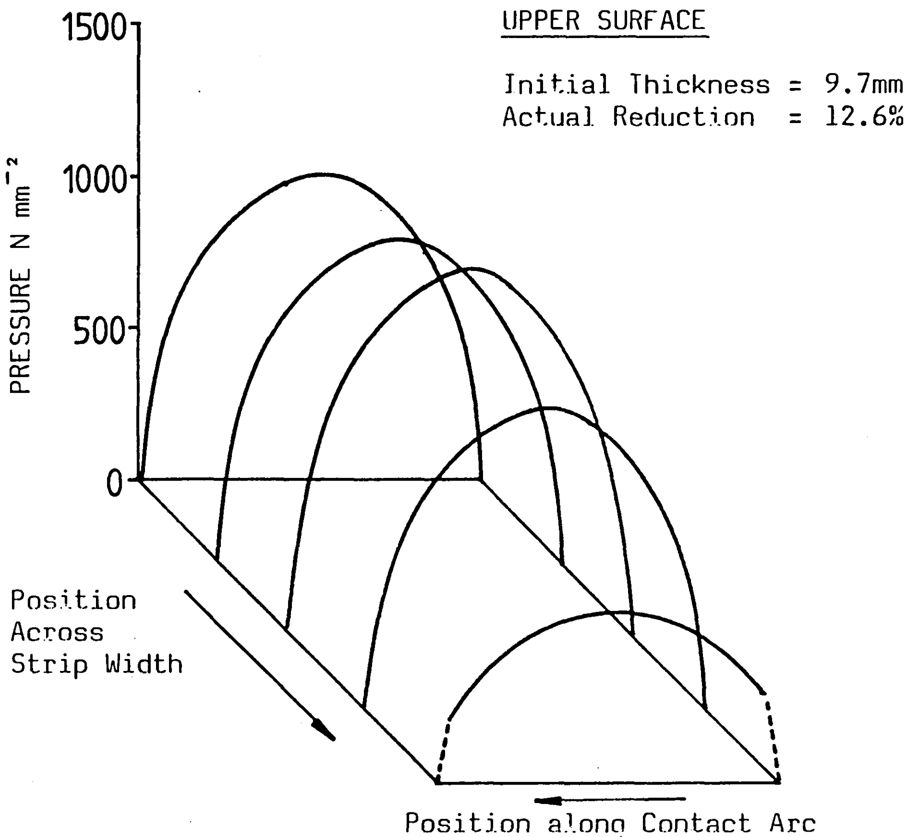

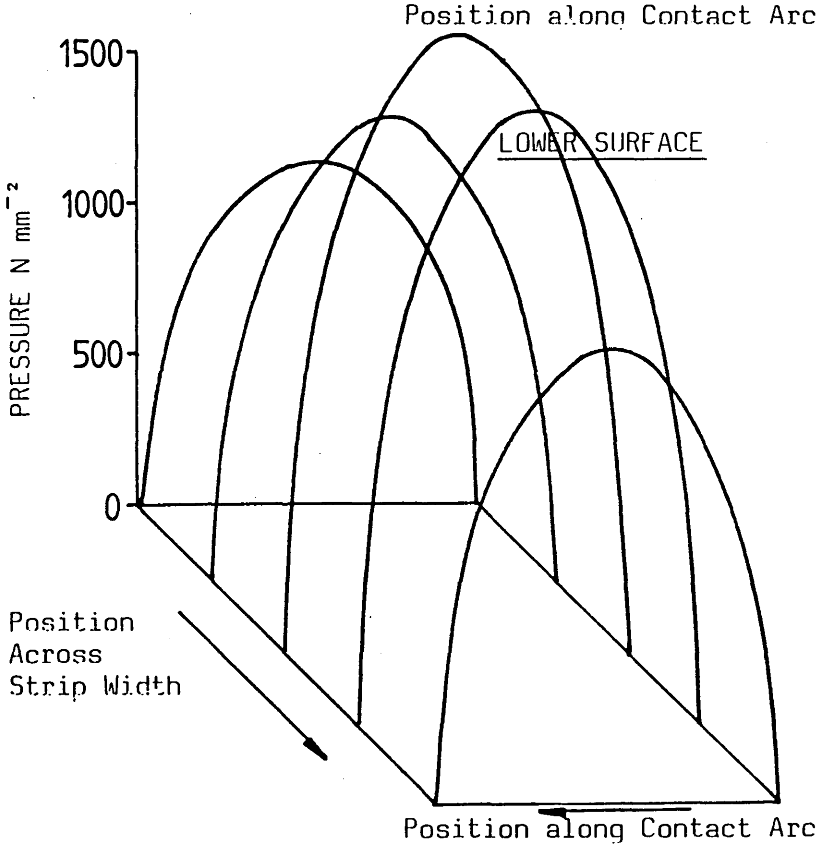

FIG 6.43 : PREDICTED PRESSURE PROFILES : 15% NOMINAL REDUCTION 100mm STRIP WIDTH, DRY ROLLING CONDITIONS

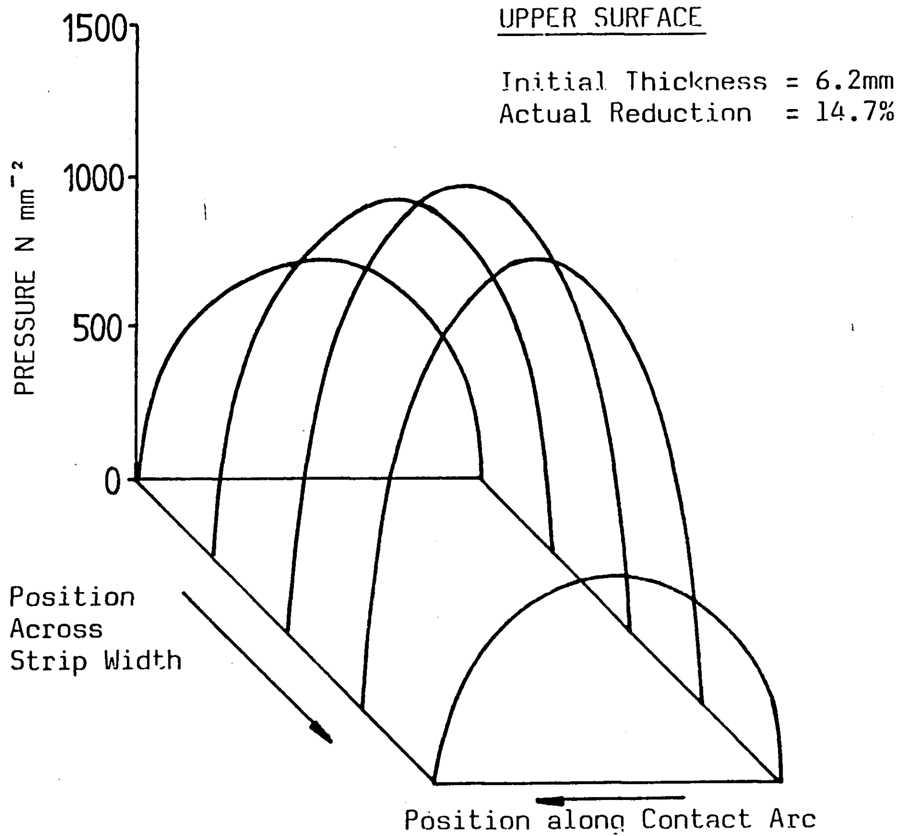

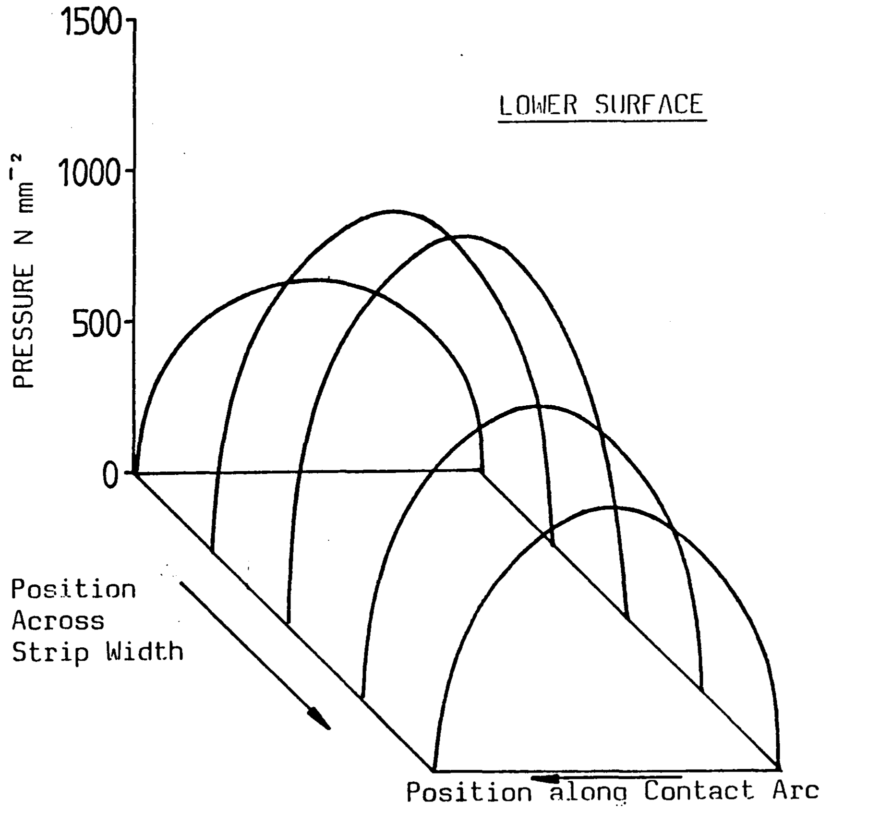

FIG 6.44 : PREDICTED PRESSURE PROFILES : 15% NOMINAL REDUCTION 80mm STRIP WIDTH, DRY ROLLING CONDITIONS

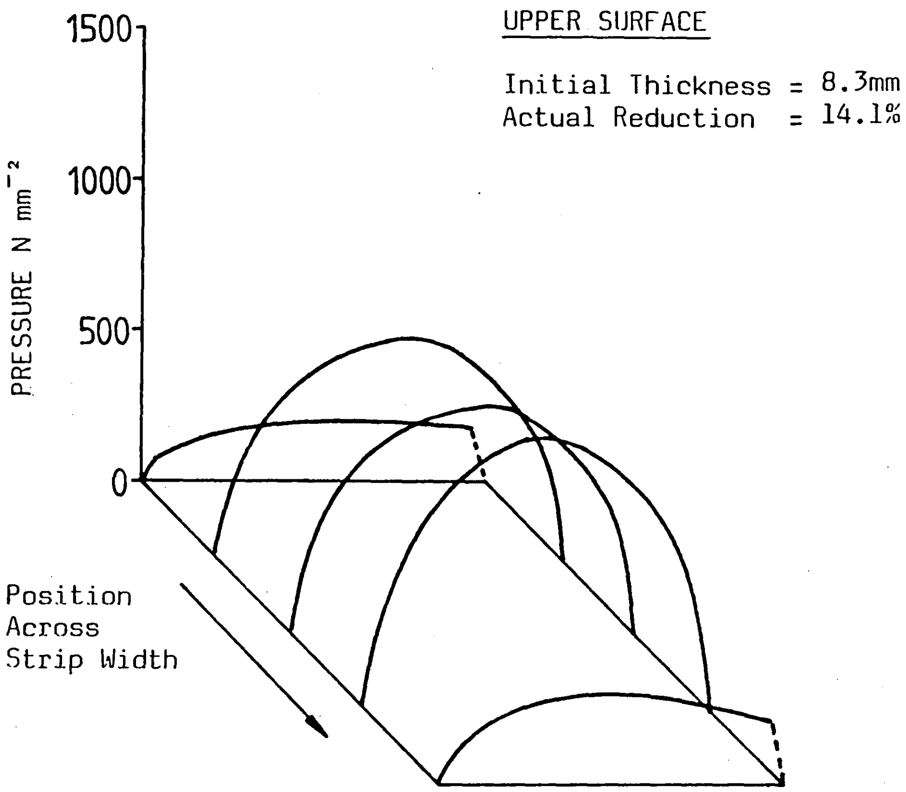

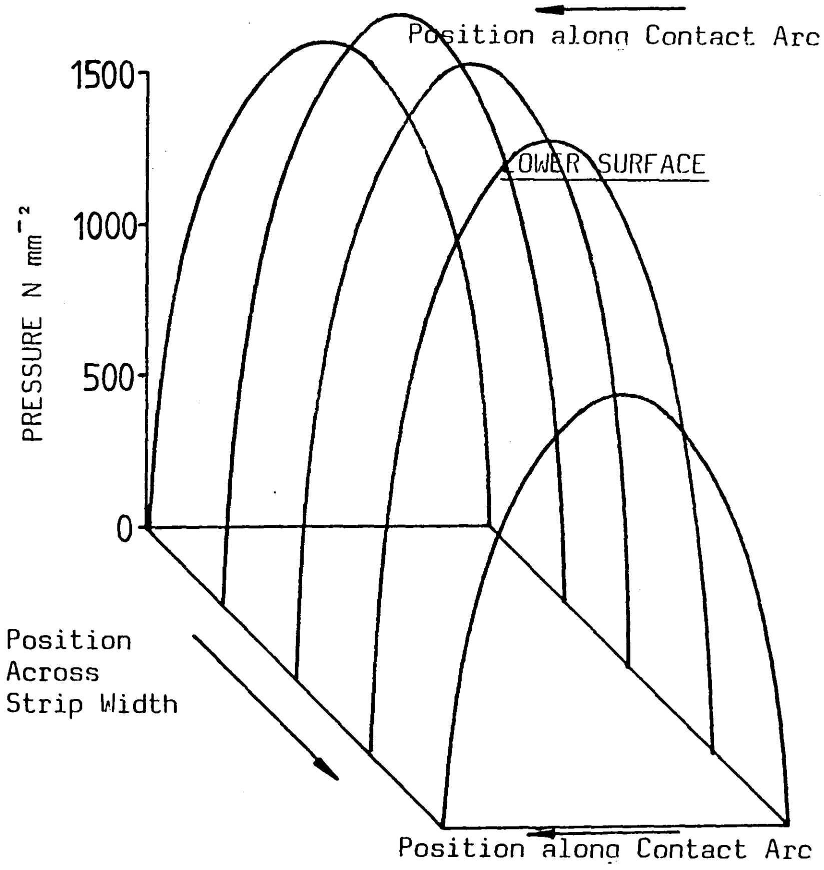

FIG 6.45 : PREDICTED PRESSURE PROFILES : 15% NOMINAL REDUCTION 60mm STRIP WIDTH, DRY ROLLING CONDITIONS

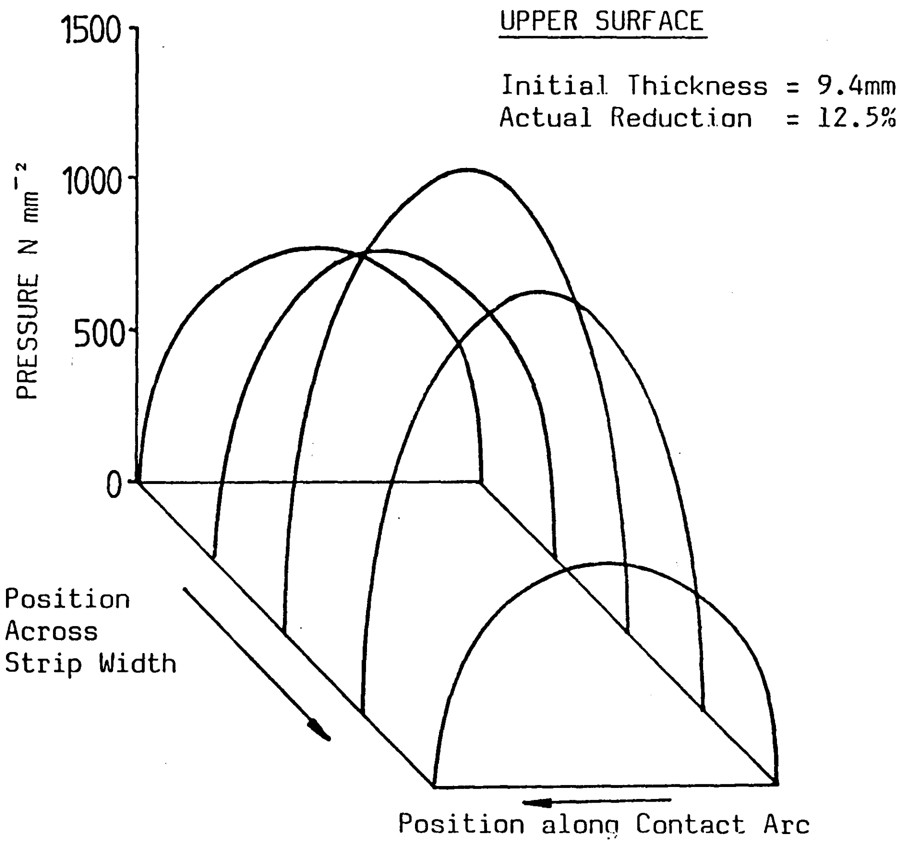

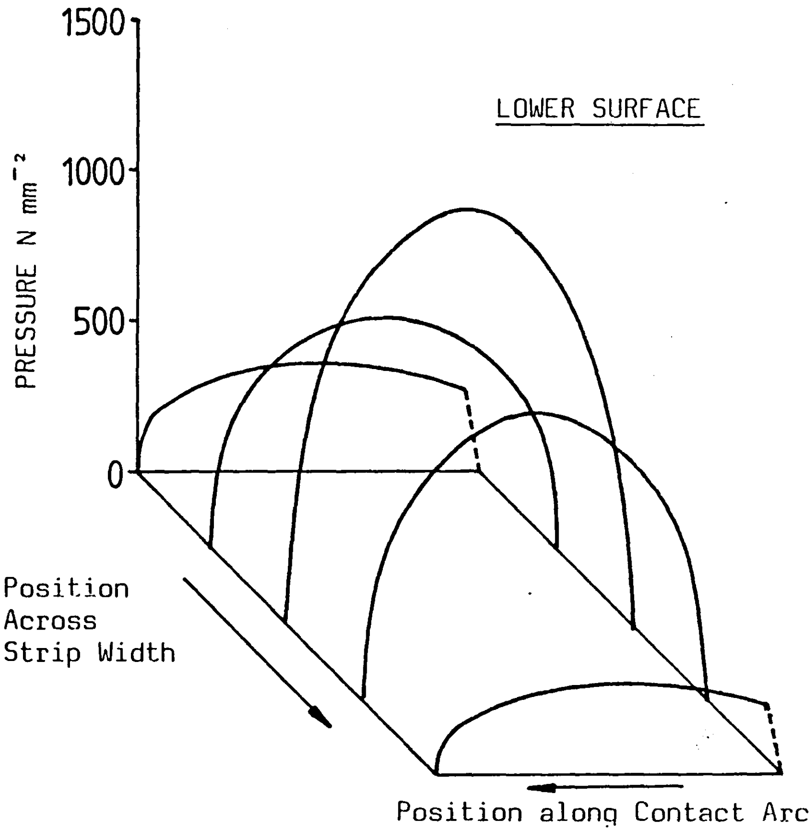

FIG 6.46 : PREDICTED PRESSURE PROFILES : 15% NOMINAL REDUCTION 40mm STRIP WIDTH, DRY ROLLING CONDITIONS

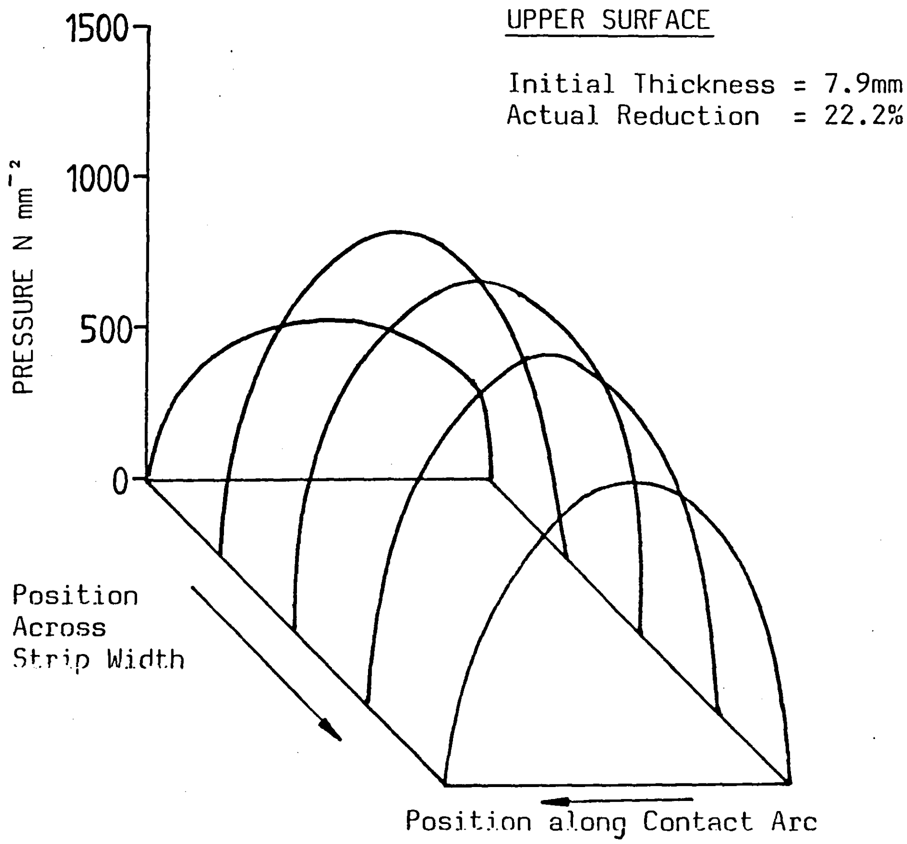

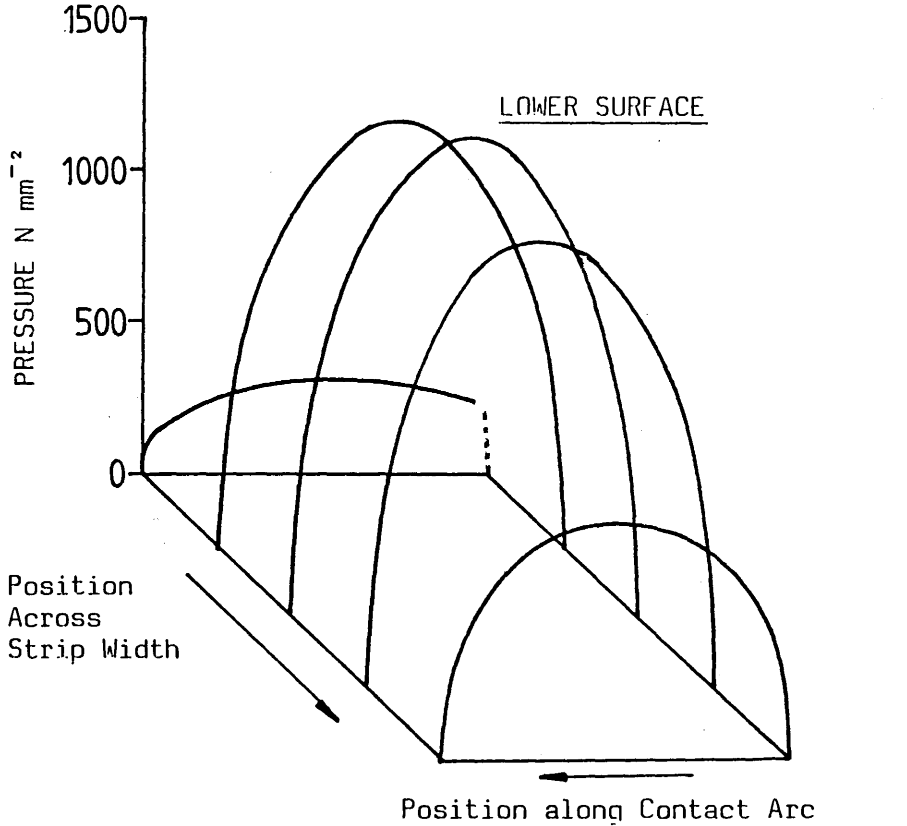

FIG 6.47 : PREDICTED PRESSURE PROFILES : 20% NOMINAL REDUCTION 100mm STRIP WIDTH, DRY ROLLING CONDITIONS (a)

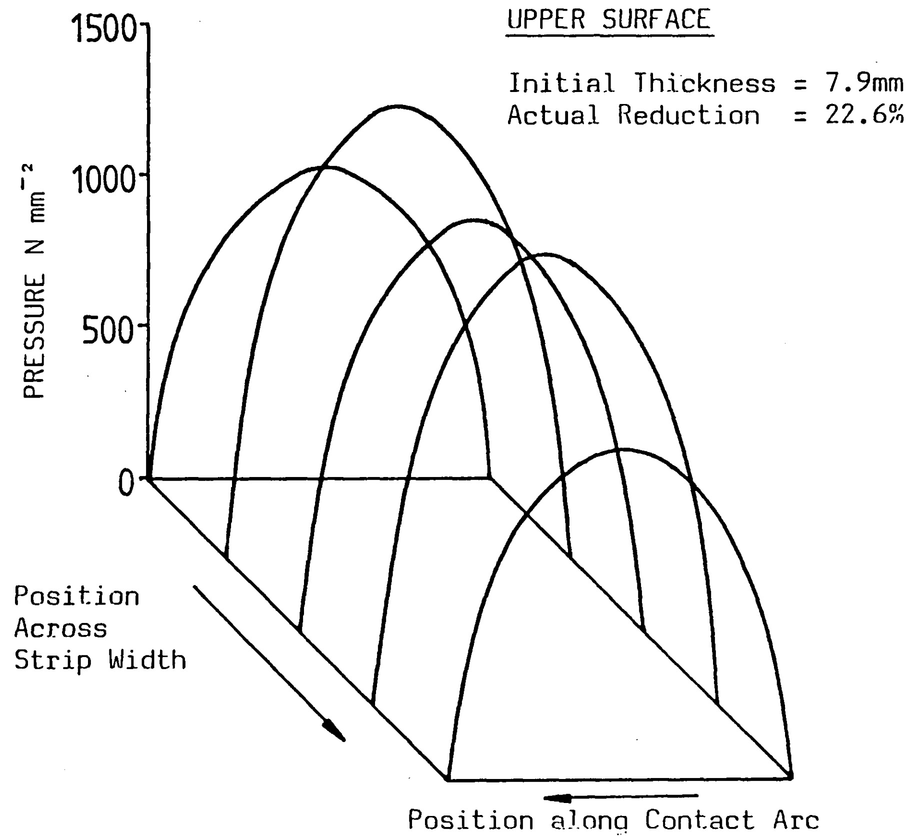

FIG 6.48 : PREDICTED PRESSURE PROFILES : 20% NOMINAL REDUCTION 100mm STRIP WIDTH, DRY ROLLING CONDITIONS (b)

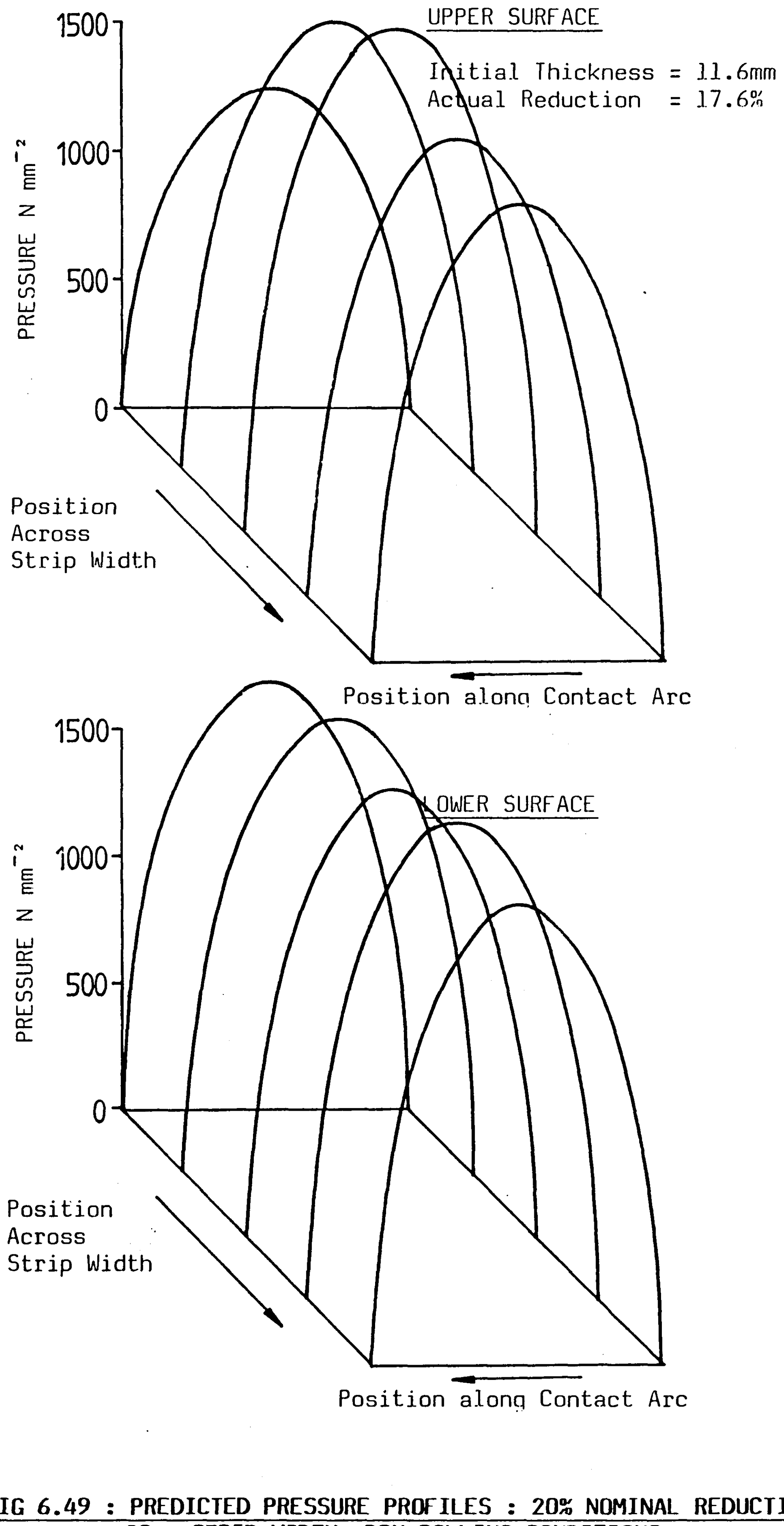

FIG 6.49 : PREDICTED PRESSURE PROFILES : 20% NOMINAL REDUCTION 80mm STRIP WIDTH, DRY ROLLING CONDITIONS

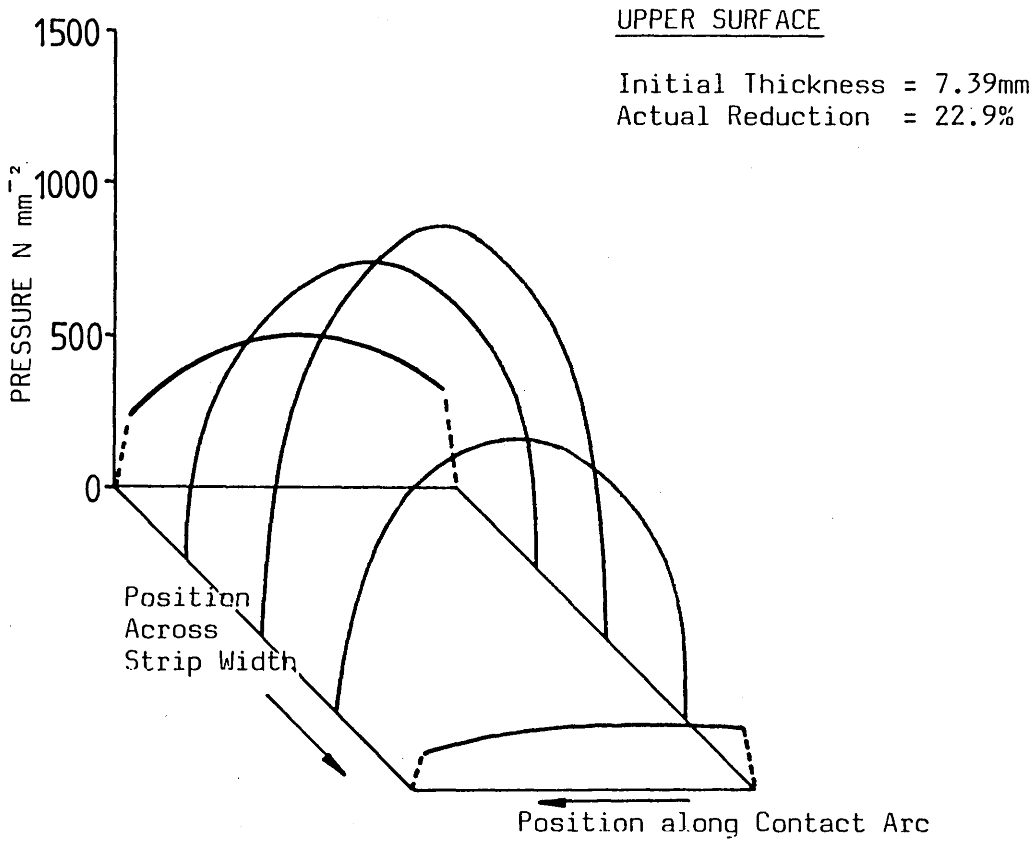

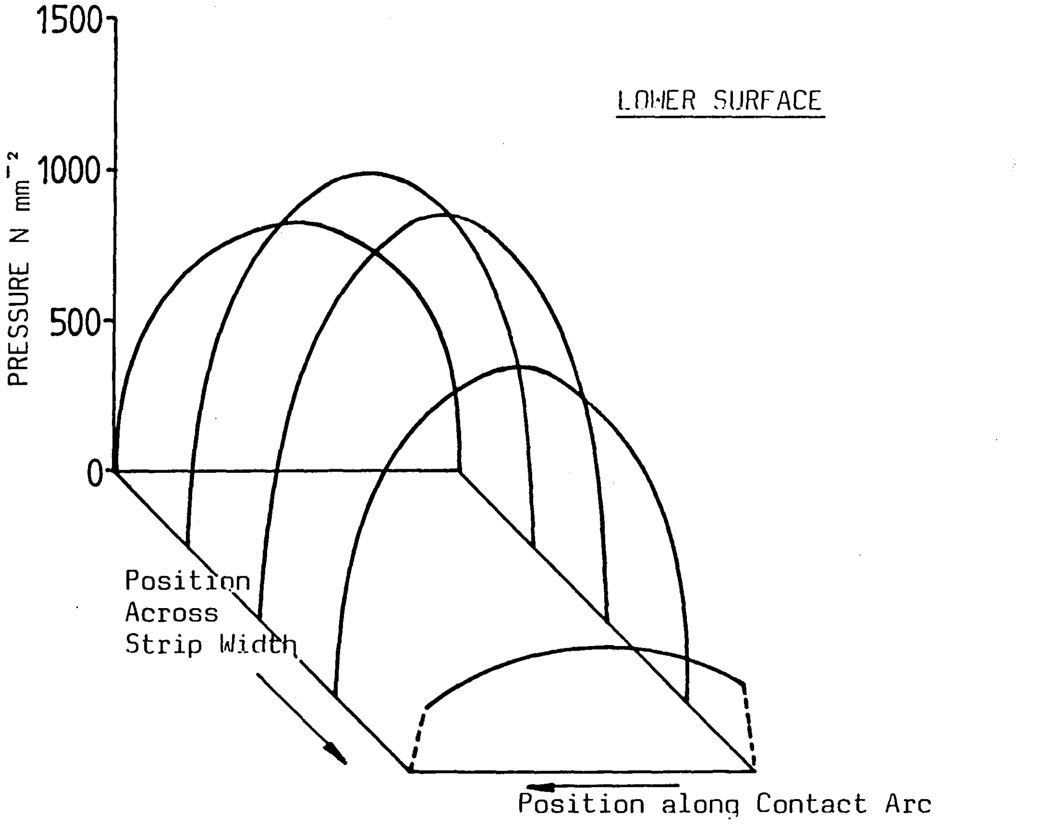

FIG 6.50 : PREDICTED PRESSURE PROFILES : 20% NOMINAL REDUCTION 60mm STRIP WIDTH, DRY ROLLING CONDITIONS

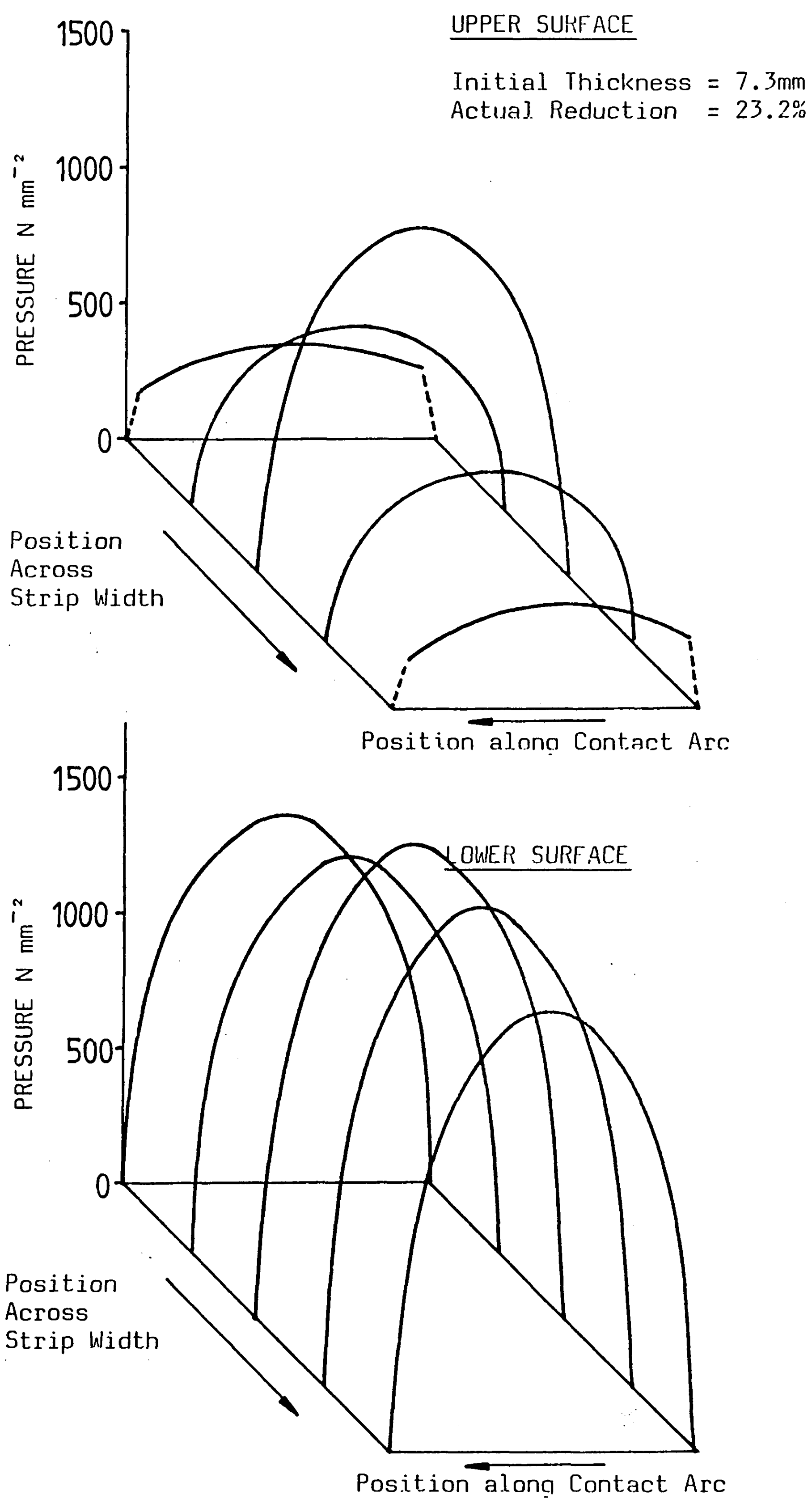

FIG 6.51 : PREDICTED PRESSURE PROFILES : 20% NOMINAL REDUCTION 40mm STRIP WIDTH, DRY ROLLING CONDITIONS

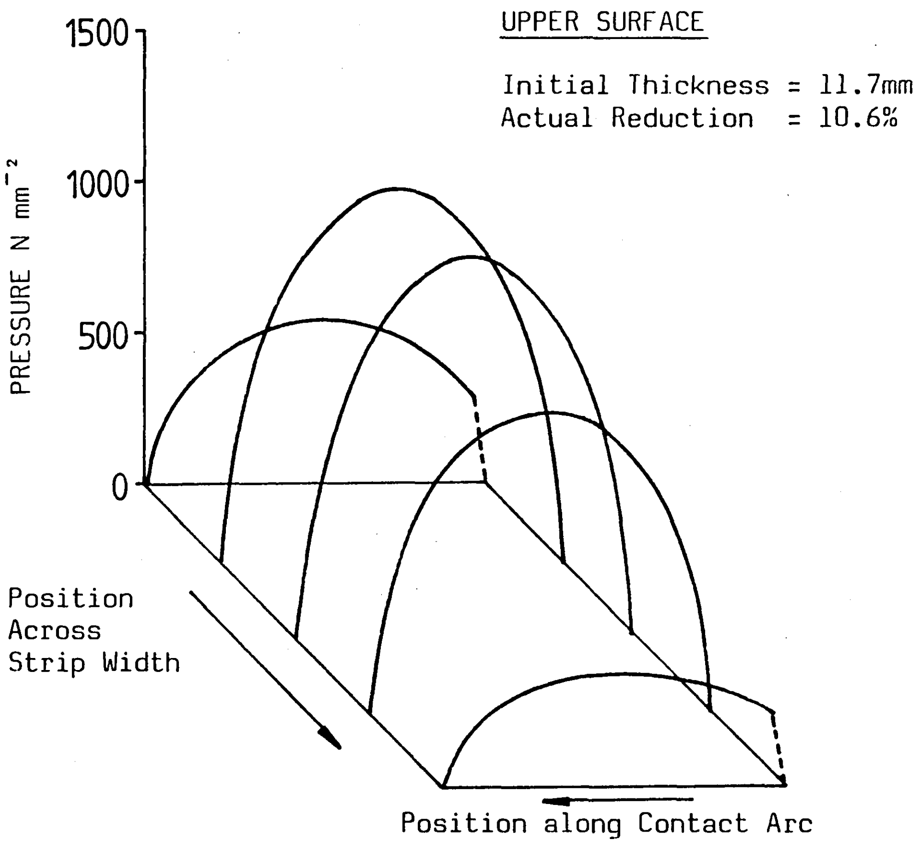

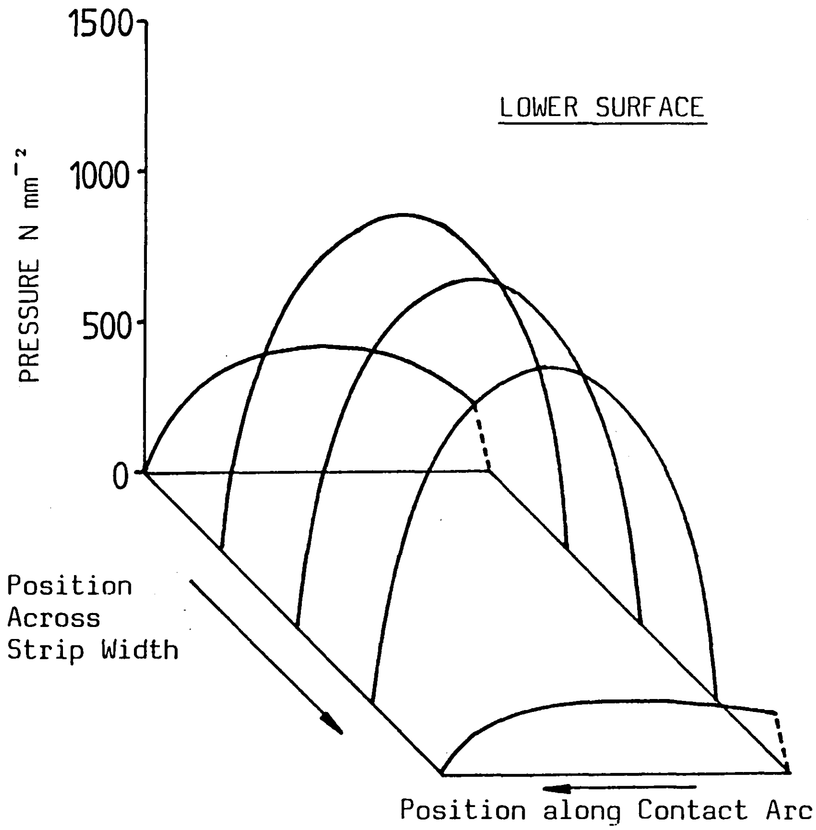

FIG 6.52 : PREDICTED PRESSURE PROFILES : 10% NOMINAL REDUCTION 100mm STRIP WIDTH, LUBRICATED ROLLING CONDITIONS

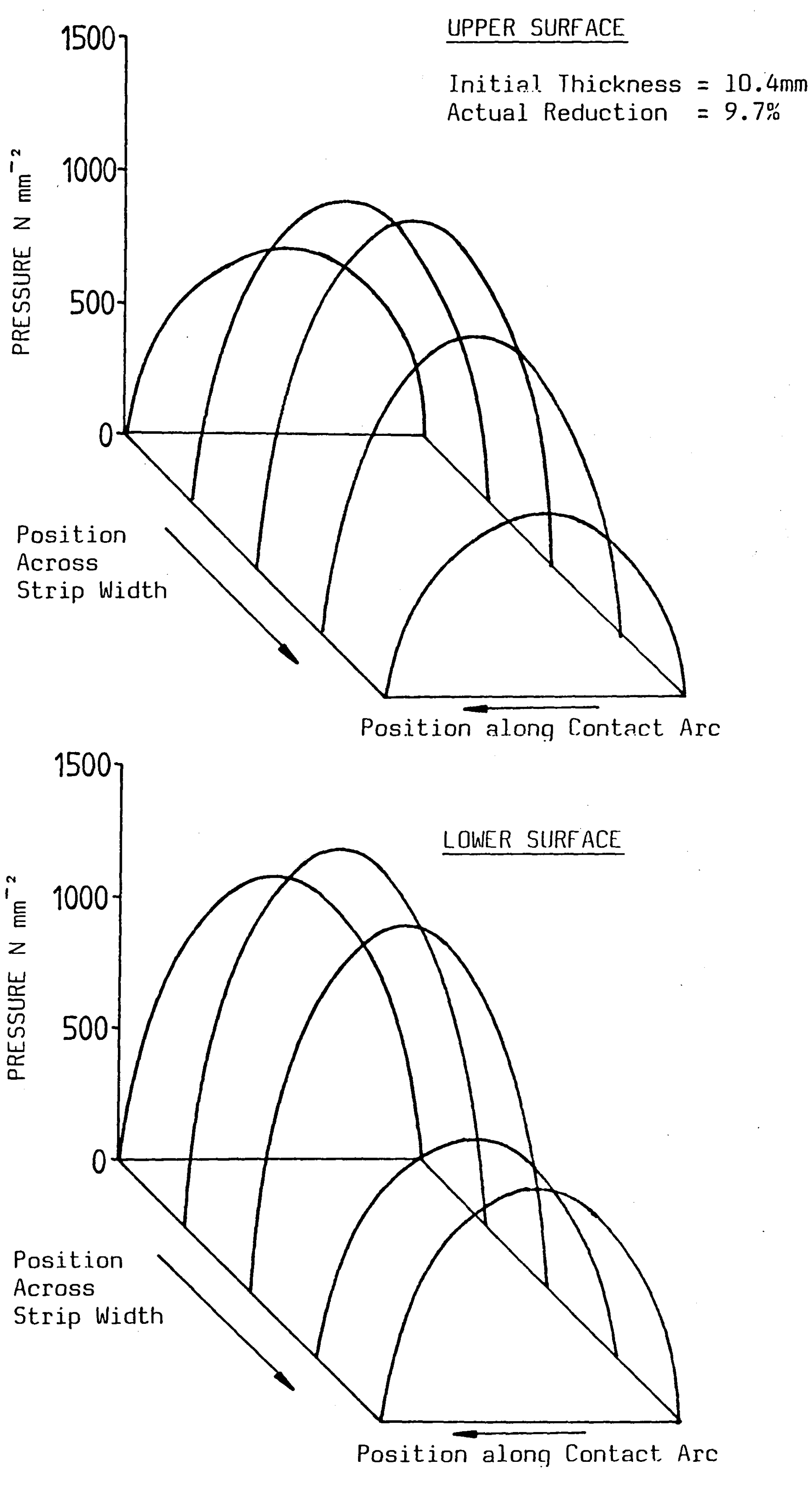

FIG 6.53 : PREDICTED PRESSURE PROFILES : 10% NOMINAL REDUCTION 80mm STRIP WIDTH, LUBRICATED ROLLING CONDITIONS

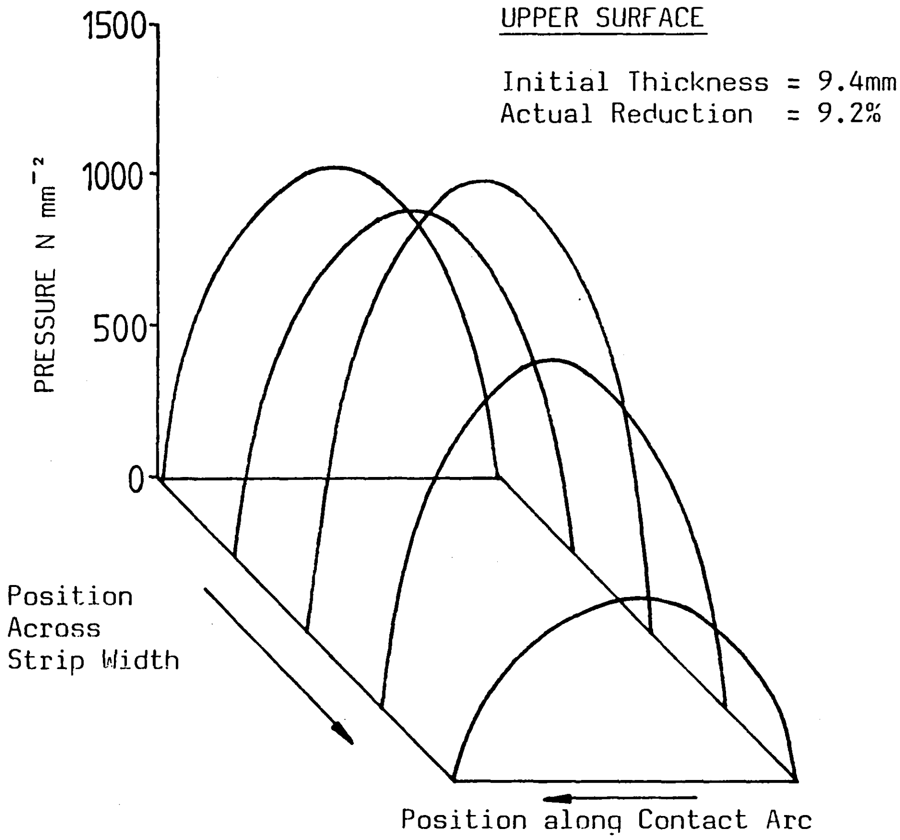

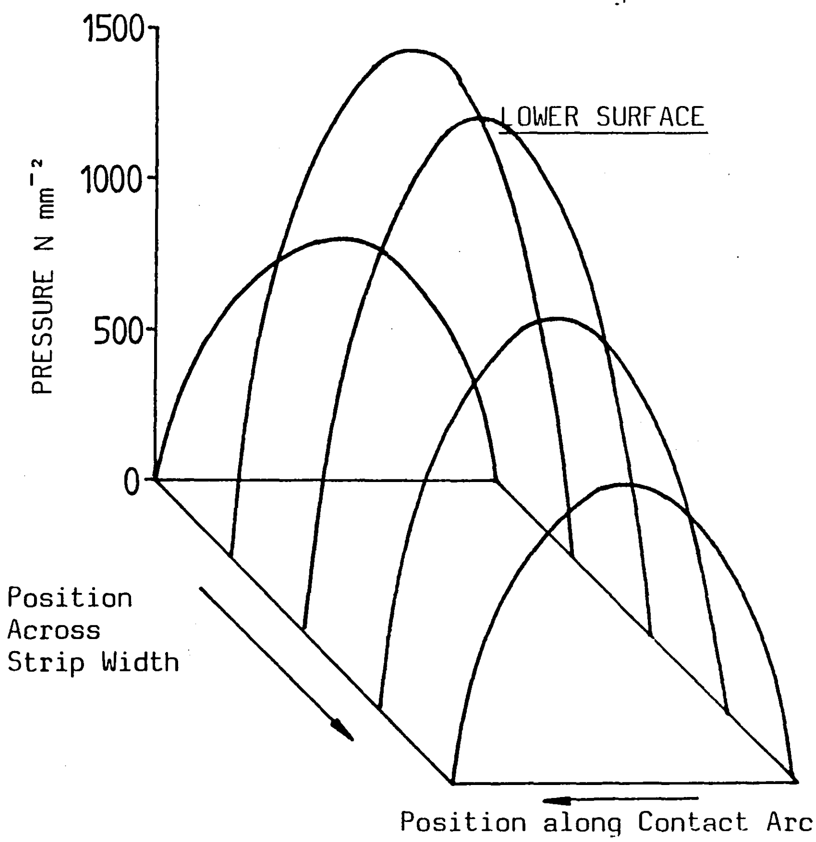

FIG 6.54 : PREDICTED PRESSURE PROFILES : 10% NOMINAL REDUCTION 60mm STRIP WIDTH, LUBRICATED ROLLING CONDITIONS

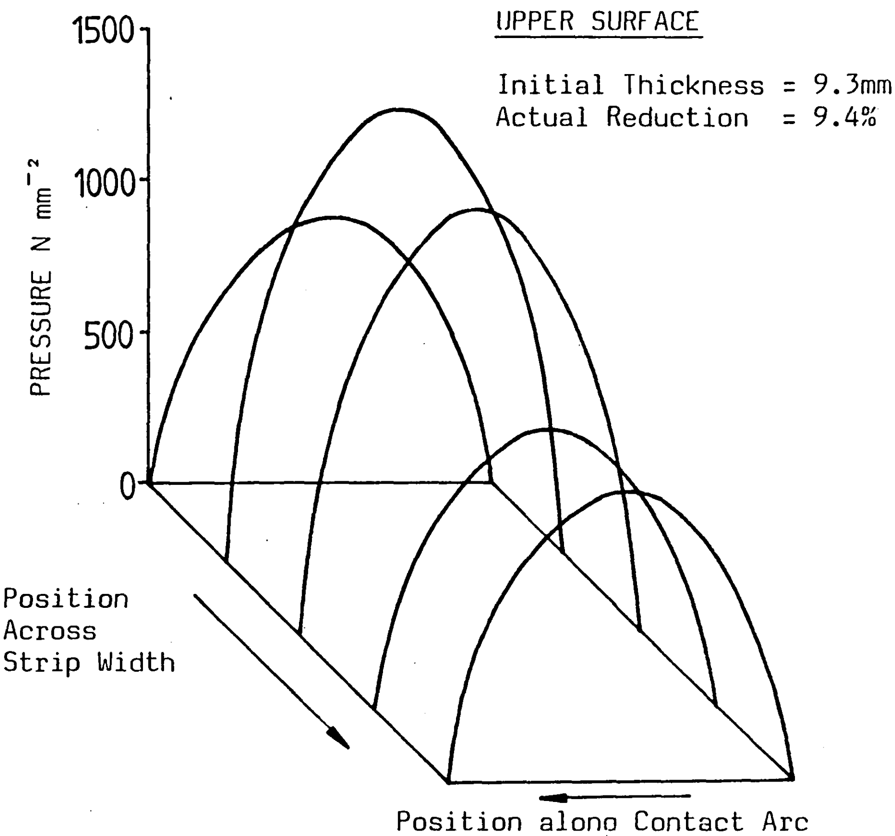

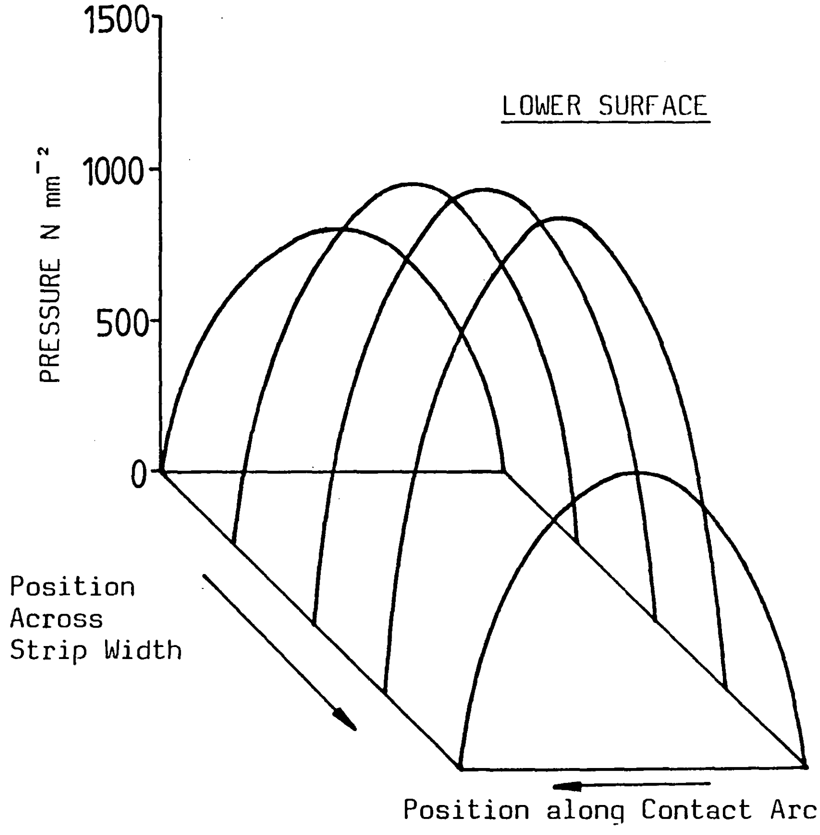

FIG 6.55 : PREDICTED PRESSURE PROFILES : 10% NOMINAL REDUCTION 40mm STRIP WIDTH, LUBRICATED ROLLING CONDITIONS

CHAPTER 7

DISCUSSIONS

7.1 Introduction

The principal objective of the present work was to develop a non-destructive technique to predict the pressure distributions and roll separating loads generated during the cold rolling process. With this objective in mind, a rigorous test programme was undertaken in which the proposed technique was developed by initially considering the quasi-static indentation of flat and inclined strip specimens, then the deformation of strip workpieces resulting from interrupted rolling passes.

The technique involved measurement of the extent of the elastic deformation of the indentor or roll along the interface with the deforming workpiece. Under each deformation mode, the basic shape of the indentor or roll was imparted into the workpiece surface. By accurate measurement of the imparted profiles along the contact arcs at different sections across the width of each workpiece, and by making allowances for the elastic recovery of the strip material, the shape of the deformed tool was established. To determine the pressure distributions responsible for the sectional deviations between the rigid and deformed tool profiles, analysis based on solid body contact theory was implemented. The analysis required the predetermination of a parameter termed the influence constant. Values of the constant quantified the magnitude and effective range of the influence that each discretised deviation (element) had upon the displacement of its neighbouring elements.

Influence constant values were determined appertaining to a series of correlated test configurations. Empirical relationships were established to estimate the appropriate influence constant value when considering indentations or reductions of the same or similar configurations. Computer programs were formulated for deformation made to evaluate influence constants. The influence constant relationships were incorporated in a second computer program to predict the pressure distributions and separating loads.

To assess the effectiveness of the technique it has been possible to compare the predicted pressure profiles with those determined experimentally with pressure transducers as reported in references [46 and 47]. Similarly it has been possible to compare the predicted separating loads with those experimentally measured.

Significant features of the technique applied to each deformation mode are discussed in this chapter.

7.2 The Experimentations

The purpose of the experimental tests was to establish a data-base for the development of the techniques for predicting the pressure distributions and separating loads for each of the deformation modes considered. The experimentations relating to the deformation modes are discussed.

7.2.1 The Static Indentation Tests

The quasi-static indentation of flat and inclined specimens were carried out using the equipment and procedures detailed in section 2.1.

During the experimentations, considerations were given to the effects of bending and the deterioration of the indentor surfaces. By the application of standard bending equations to the most severe loading conditions, small deviations along the length of the indentor were established. These were considered to have some effect on the transverse profiles imparted into the strip specimens, and compensatory factors could be included for the vertical and recovered displacements.

7.2.2 The Interrupted-Pass Rolling Tests

The interrupted-pass rolling tests were carried out using the equipment and procedures detailed in section 2.2

Difficulties arose during the tests in accurately predicting the reduced strip thickness when using the somewhat insensitive strip thickness indicator, and the distortion of the workpiece following multiple reductions. An investigation of the workpiece shape following a succession of interrupted rolling passes is detailed in Appendix V. Profiles depicted in this section clearly show the 'edge drop' phenomenon, and a 'bowing' of the material across the strip width. The latter was attributed to the absence of forward and back tensions during rolling.

During the experiments the roll separating loads were determined by interpreting a load/time trace using a calibrated conversion factor. Consideration of the sample load/time trace, shown in figure 2.9 (p.34) clearly identifies the three distinct regions during a test. From right to left, these represent the forward, interrupted and reversed stages of the rolling sequence. The rolling load was evaluated corresponding to the average value during the forward rolling stage. A small secondary deformation resulted when reversing the pass to remove the workpiece. This was not deemed significant when considering the overall distortion of the workpiece profile and that it should not effect the imparted 'roll profiles' at the termination of each pass.

7.3 The Profile Measurement Systems and Operational Procedures

The effectiveness of the present work depended on the precision with which the nodal measurements along each sectional profile could be obtained. Initial consideration of the performances would suggest that this requirement was satisfied using both measurement systems. However, each system had certain advantageous and disadvantageous aspects of its operation, which are discussed as follows.

7.3.1 Advantages and Disadvantages of Profile Measurement Using the SIP Universal Measuring Machine

This instrument has the considerable advantage of optically inspecting the workpiece surfaces, so avoiding the systematic errors developed by physical contact between the machine and workpiece.

Each directional setting was determined to a resolution of 1μm, and the combined measurement uncertainties of settings in the X and Z directions (see figures 3.1 and

3.2) were estimated at $\pm 2.8\mu m$ (at a 95% confidence level), confirming that the instrument was suitable for making precise and repeatable point measurements.

The accuracy of each nodal measurement was dependent on the operator. The measuring process was slow (often taking several hours to inspect a single indentation) and required high levels of concentration to be maintained throughout, otherwise a loss of accuracy could result. The positioning of the locating and micrometer microscopes led to considerable discomfort during long measurement sessions.

In focussing the locating microscope, there was a tendency to focus at any pronounced feature on the surface image. Since the relative positioning of these features was unlikely to coincide for successive settings, a loss of accuracy resulted.

7.3.2 Advantages and Disadvantages of Profile Measurement using the Merlin 750M

Operation of this machine considerably reduced the dependency on the operator by implementation of computerised control for the inspection routines. Flexibilities within the part-program (used to control the measurement routine) enabled the number of sections, the scan length and the increments to be adjusted to suit the configuration and the required accuracy of each inspection (see figure 3.3). By computerising the inspection routine, the time required to inspect both sides of an interrupted-pass workpiece was reduced to approximately 30 minutes.

Each directional setting was determined to a resolution of 1μm, and the measurement uncertainties in the Z direction of 1μm. This confirmed that the system was very suitable for establishing precise and repeatable point measurements.

During operation the workpiece surface was probed by a spherical ended stylus. Consequently some minor error could arise in the Z direction due to the contact configurations. These errors were compensated in the influence constant and pressure distribution computer programs.

By including the additional effects of contact errors in the measurement uncertainties associated with the Merlin 750M, it can be considered that there is little difference between the proven performances of both inspection systems. However, the effective performance of the SIP does depend upon the ability of the operator.

Consideration of inspection times suggested that the Merlin 750M was much better suited for the inspection of workpieces of similar configurations in reasonably sized batches.

Operation of the systems were successfully implemented by following the procedures listed in chapter 3.

7.4 The Analysis

Numerous attempts have been made to accurately predict the pressure distributions developed during the cold rolling process. From a generalised assessment of the various solution techniques (detailed in section 4.1) it was considered that the only reliable method of determining such pressure distributions was through direct measurement using pressure transducers. However, the practical implementation of such techniques would be prohibitively expensive.

For companies with limited R and D budgets, the most favourable method of determining the pressure distributions appears to be analytical, featuring empirically derived functions. Although not completely accurate it was considered that this form of solution could be optimised by developing the functions to relate to specific mill stands and rolling schedules. In the current investigation such a method was adopted based on the theory of solid body contact, see Timoshenko and Goodier[51] (fully presented in section 4.2).

In implementing this analysis there were initially two unknown variables, the pressure distribution and influence constant. Evaluation of the latter proceeded from tests relating to specific deformation conditions and configurations. The individual values were correlated to form functions and incorporated in the analysis to enable the prediction of pressure activities under the same or similar processing conditions as those of the tests under consideration.

Within the analysis certain assumptions were unavoidable. However, since the same analysis was used to evaluate each influence constant as those needed to predict the pressure distributions, loss of accuracy due to the assumptions will be compensated within the influence constant values.

The scope of the analysis is limited because it can only be applied to situations where the magnitudes of discretised deviations are known. In the current investigation the deviations between the rigid and deformed roll/indentor profiles can be determined along each measured arc of contact. However, regions of the roll/indentor surface external to the contact interface which may be subject to deviations in the opposite direction will not be considered.

The analysis was incorporated in the computer programs which have been fully discussed in chapter 5.

7.5 The Experimental Results

7.5.1 Stress-Strain Characteristics of the Strip Materials

The stress-strain behaviours of the workpiece materials were successfully determined by the technique in which cylindrical samples of each material were subjected to uniaxial compression tests, and the result converted to those pertaining to plane strain conditions (multiply stress by $\sqrt{3}/2$, deformation during the rolling process approximates to plane strain conditions). The stress-strain curves for each material are shown in figures 6.1, 6.2 and 6.3, displaying the expected characteristics. Careful examination of the curves relating to the characteristics of the annealed En43A steels (different batches used for the flat and inclined strip static indentation tests) reveal slight discrepancies. These are attributed to the steels originating from different batches and consequently having minor variations in composition and to the experimental uncertainties associated with the measurement technique.

Extension of the test procedure to enable the development of relationships between the differences in strain values for loaded and relaxed states, and the reduced strain proved worthwhile. It provided an improved representation of the elastic behaviour of the workpiece material following load relaxation. The high correlation between the data points in figure 6.4 is encouraging when considering the relative crudeness of this empirical technique.

7.5.2 The Indentation of Flat Specimen Test Results

In developing the influence constant functions relating to these tests, the initial point of interest was the effectiveness with which the imparted indentor profiles were determined. Figures 6.5 and 6.6 show the relationships between the averaged indentation radius and the applied load corresponding to each test. Examination of the figures shows that there is a notable improvement in correlation between the 'refined' data points. However, the functions representing the optimum correlation can only approximate an indentation radius value for a given load, since the correlation between points is poor. In the context of the overall analysis this lack of correlation must be considered as being a significant source of uncertainty. The trends shown by the curves suggest that at small loads there is a large indentor radius imparted into the workpiece surface. Explanation of this phenomenon may be aided by considering the length of the arc of contact, which will be short under such loading conditions. Applying zero load the arc of contact between indentor and workpiece will be infinitely short and represent a point on the workpiece surface of infinite radius. Evaluation of these variables under such loading conditions would prove pointless.

The functions relating the vertical displacement and elastic recovery to the applied loads were approximated by the hyperbolic equations 6.6 and 6.7. Although only approximate, the correlation between experimental points and the optimum curves were highly satisfactory.

Incorporation of these empirical relationships within the influence constant evaluation program enabled the determination of the influence constant and associated variables pertaining to each loading condition. Figures 6.10 to 6.15 graphically represented these variables with respect to the calculated and applied loads. Examination of the curves reveal the expected trends, with those figures relating to the indentor radius and influence constant variables becoming unstable at small loads.

The actual influence constant functions (in which this variable was related to the change in indentor radius) were found to be linear relationships. The applicability of these functions within the pressure distribution were investigated, using independently derived experimental data.

In determining the pressure distributions along each section, discretised deviations between the rigid and deformed indentor arcs were subjected to the solid body contact analysis, developed in chapter 4. Figures 6.17(a) and (b) show representative forms of the deviations along a typical section, and the predicted pressure distribution. Both profiles are symmetrical about the indentation centre but do not follow the same shape since the pressure is not directly proportional to the displacement of each element. Variations between the maximum and mean sectional pressure values across the width of a typical indentation is shown in figure 6.18. Examination of the curves reveals insignificant relative difference between the values at each section. The curves show that a greater pressure was developed at the centre of the indentation width than at the edges. A three-dimensional representation of a typical predicted pressure distribution is shown in figure 6.19. The general profile corresponds to those determined experimentally for rolling conditions.[46, 47 et al]

From these tests separating loads were predicted and compared with the measured values in table 6.1. These show discrepancies between 0.3% and 17% (average 6.7%). Thus, correlation was considered to be good for this initial application of the technique.

7.5.3 The Indentation of Inclined Specimen Test Results

Formulation of the influence constant functions and subsequent predictions of pressure distributions and separating loads proceeded using the same basic techniques as developed for the analysis of flat specimens. Consequently there is some repetition of the salient features associated with the operations during the development.

Considering the experimental relationships in which the average indentation radius, vertical displacement and elastic recovery values were related to the applied loads (figures 6.21 to 6.23, 6.25 and 6.26, respectively), the trends displayed by the curves correspond to those established during the flat specimen analysis.

Incorporation of these empirical relationships within the influence constant evaluation program enabled the influence constant values pertaining to each loading condition to be determined. The influence constant values determined from the program were found to fluctuate greatly in magnitude but follow similar trends. To develop more comprehensive relationships, natural logarithmic values were used to formulate the functions, and were reversed in the pressure distribution program. Figures 6.27 to 6.29 show the functions in which the influence constant values are related to the average change in indentor radius. Examination of the curves reveals a region of high instability corresponding to small changes in indentor radius. However, the meaningfulness of the relationships must be questioned when considering that the distance over which an element extends its influence corresponds to the product of the influence constant and element width. The magnitude of the influence constant values determined from the relationships would present unrealistic influence distances.

Sectional pressure distributions were predicted exhibiting features similar to those developed during the flat specimen analysis. Figure 6.30 shows a three-dimensional representation of a typical predicted pressure distribution.

Relating to each test, the separating loads predicted using the computer program were compared with the measured values and tabulated in table 6.7. Discrepancies of up to 20% are recorded corresponding to conditions within the stable regions of the influence constant functions. With an average discrepancy of approximately 5%, the correlation between applied and calculated loads was considered good.

7.5.4 The Interrupted-Pass Rolling Test Results

Prediction of the pressure distributions and separating loads generated during the cold rolling of steel strip were determined by adapting the technique to consider the roll profiles imparted to the workpiece surface when terminating a rolling pass.

Profile measurements were established along the arcs of contact at ten sections across the width of each workpiece (five across both upper and lower surfaces) following each interrupted pass. For the purposes of this initial investigation the number of measured profiles was considered adequate, however, for a practical application more sections may be inspected for a greater assurance of accuracy. Variations in the deformed roll radius across the widths of a typical workpiece are shown in figure 6.31. Consideration of these profiles illustrates the necessity of introducing a weighting system in the determination of a representative mean, in which the edge sectional values are given a lesser influence on the average.

During the tests, the workpieces were deformed with an absence of forward and backward tensions, consequently the strips were subject to bending in the longitudinal direction. Additionally, as each strip was subjected to successive reductions, the transverse surface profiles became non-linear as documented in Appendix V. Both were detrimental to the successful measurement of the imparted profiles, with the former being most significant. The effect of bending along the length of the workpiece caused significant differences between the radius values determined across the upper and lower surfaces which led to the prediction of non-symmetrical pressure distributions. These are considered later in the discussion.

In determining the influence constant functions a relationship between the load per unit width and the percentage reduction in strip thickness was formulated and is graphically represented in figure 6.32. This was validated by considering plane strain rolling conditions and produced a smooth relationship which reduced the effects of inhomogenities within the workpiece material and experimental uncertainties associated with the measurement of each test.

An assessment of the surface hardness of the workpiece material following successive tests was made and is illustrated in figure 6.33. The curve has a similar shape to that of the stress-strain curve of the workpiece material. The increase in surface hardness should not affect the predictions since the analysis is independent of this variable.

Incorporation of the load per unit width relationship in the influence constant evaluation program enabled values of the constant to be determined for each test. As the functions were related to the average change in roll radius, the positioning on the curves in figures 6.34 to 6.37 depended on the extent of curvature along the workpiece length.

Prediction of the sectional pressure distributions proceeded by incorporating the influence constant functions within the appropriate computer program, then by considering the deviations between the rigid and deformed roll profiles along each arc of contact. Figures 6.38(a) and (b) show representative forms of the deviations along a typical section and the resulting pressure distribution. The elements at the extremities of the arc have no displacement. However, the influence of the intermediate elements will tend to displace these points, and in order to maintain equilibrium conditions restraining pressures in the opposite direction are required, and are predicted by the program. This constitutes internal tensile stresses enhancing the effect of fatigue loading which manifests itself in practical rolling situations by the development of spalls within the rolls.[53, 54]

Provided that the same number of discretised elements along the arcs of contact are used in both the influence constant and pressure distribution programs, the technique should work. In the current investigation both programs were operated with ten elements. To determine the effects on the pressure profiles of an increased number of elements, computations were carried out with twenty and fifty elements (maximum pressure along a typical section remaining constant). The corresponding pressure profiles are illustrated in figure 7.1, showing insignificant differences for the different number of elements. The estimate of the mean sectional pressure will tend to converge to the true value with an increasing number of elements.

Consideration of the sectional pressure distributions across the widths of each workpiece enabled the total pressure activities to be established. Representative pressure profiles relating to each deformation configuration are shown in figures 6.39 to 6.55. Examination of these figures reveals that the pressure activities on both upper and lower surfaces adhere to similar trends:

(i) Each pressure profile is non-symmetrical, with the greatest pressure developed towards the entry side.

(ii) The magnitudes of the pressure profiles tend to reduce towards the edges of the workpiece.

Both these features are present when considering the measured pressure distribution profiles, particularly those reported in reference (46). In certain cases the neutral point (and the peak of the pressure profile) shifts significantly towards either the entry or exit points due to the combination of front and back tensions.[57] The predicted profile of the pressure distribution using this technique may differ from the actual ones since the maximum pressure evaluated by the computer program is restricted to between the centre and entry points.

The magnitudes of the maximum predicted pressures are high compared to the mean (often in the ratio of approximately three to one). This is due to the restraining pressures being included within the average. Consequently, the distributions presented in figures 6.39 to 6.55 give qualitative rather than quantitative predictions.

Examination of the profiles such as in figure 6.40 reveal discrepancies from the general trends. These can be attributed to anomalous measurements along the respective arcs of contact. Examination of the profiles such as in figure 6.51 clearly show the effects of longitudinal bending, in which the profiles corresponding to the upper and lower surfaces differ considerably.

From each test, roll separating loads were predicted based on the mean sectional pressure values and compared with the measured loads (listed in table 6.10). Consideration of the listed percentage differences reveals variations up to 130%. However, these were established from workpieces which had been subject to severe longitudinal curvature. Most percentage differences were included within $\pm$20% limits of the measured values.

7.6 Practical Applicability of the Technique

Considerations of the results determined from the interrupted-pass rolling tests suggest that the technique developed is suitable for qualitatively predicting the pressure distributions (perhaps only with additional refinement) and determining the roll separating loads to generally acceptable levels of accuracy. To put these achievements in perspective, consideration of the practical applicability of such a technique is discussed.

Implementation of such a technique would depend upon the availability of:

(i) A mill stand, or test mill equipped with suitable rolls of the required dimensions and devices for monitoring the separating loads developed during the individual interrupted-pass tests, (tests using the workpiece materials and passes of the proposed rolling schedule).

(ii) A suitable measuring system capable of providing measurements along the arcs of contact of the imparted roll profiles with high precision and repeatability (possible limitations were with regard to the size of the workpiece and the difficulties associated with measuring very small reductions in thickness).

Having fulfilled these requirements, the technique can be applied by formulating the influence constant and pressure distribution computer programs relating to a specific mill stand. By undertaking interrupted-pass rolling tests relating to a specified strip material and configuration, influence constants can be determined, formulated as functions and incorporated within the pressure distribution program. These functions would be valid in the prediction of pressure distributions and roll separating loads for process conditions the same or similar to those developed during the tests.

Having formulated the computer program relating to a specific mill stand, the only requirements for operation under different rolling conditions (different material, strip configuration or schedule) would be a further series of tests to determine the appropriate influence constant functions.

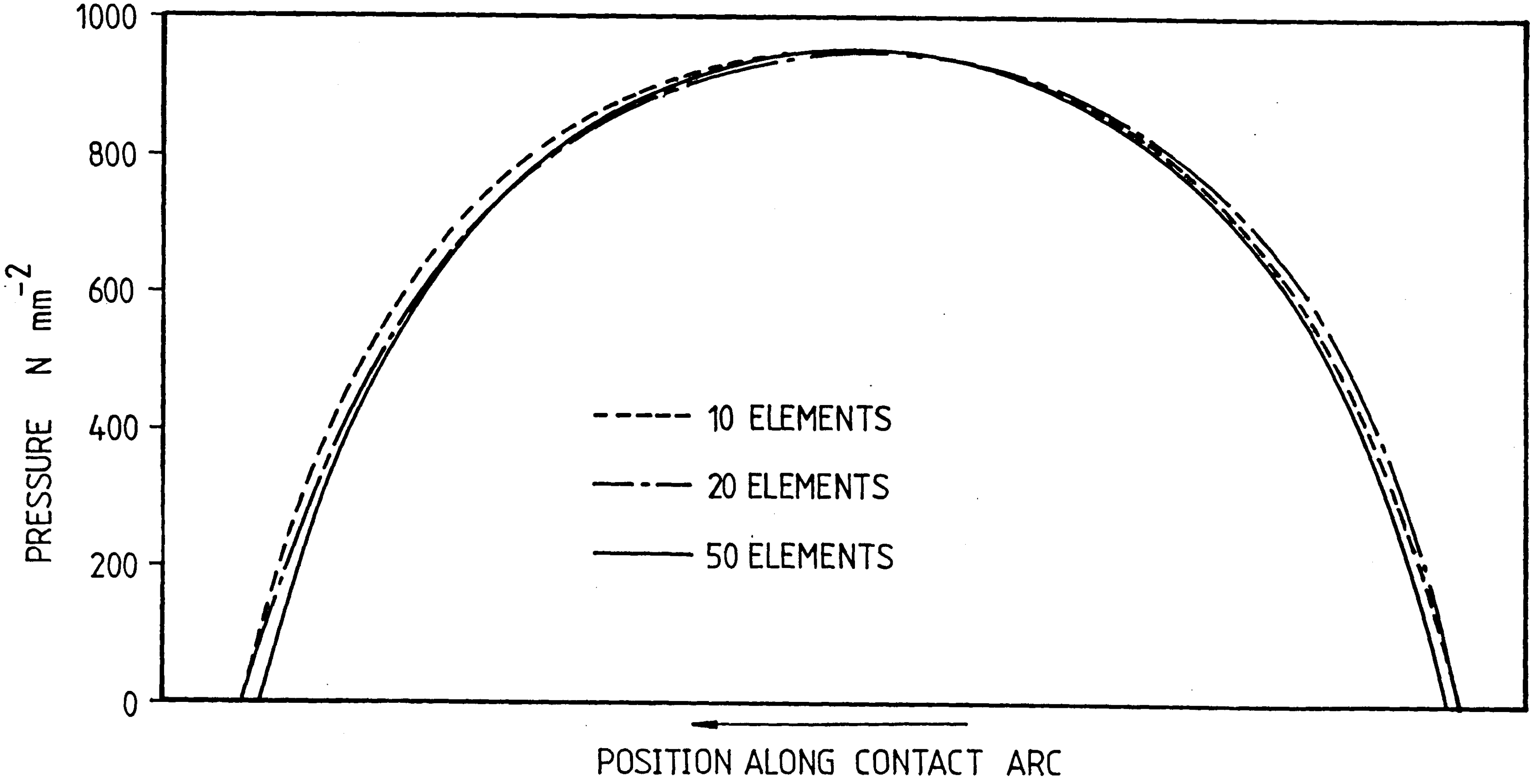

FIG 7.1 : EFFECTS ON THE PREDICTED PRESSURE PROFILES OF VARYING THE NUMBER OF DISCRETISED ELEMENTS ALONG A TYPICAL CONTACT ARC

CHAPTER 8

CONCLUSIONS AND SUGGESTIONS FOR FUTURE WORK

8.1 Pressure Distributions and Separating Loads

In the present study, the weaknesses of the current methods used to predict the pressure distributions and roll separating loads generated during the cold rolling process has been reviewed and an alternative technique has been developed by which these parameters can be determined from the measurement of the profile along the arc of contact.

Initial investigations were undertaken relating to the quasi-static indentation of flat and inclined strip specimens. The technique was established for these deformation modes before relating it to the cold rolling process in the form of interrupted pass rolling tests. Based on the outcome of the experimental work relating to each deformation mode, the following conclusions were reached.

(a) Quasi-Static Indentation of Flat and Inclined Specimens

(i) The forms of the predicted pressure profiles (schematically represented in figures 6.19 and 6.30) show that the maximum pressure is developed at the mid-point of the arc of contact and across the width of the indentation.

(ii) Correlation between the predicted and measured indentor separating loads were within $\pm 20\%$.

(b) Interrupted-Pass Rolling Tests

By analysing the technique and results pertaining to these tests (representative of the conditions present during the cold rolling of strips) the following conclusions were drawn:

(i) The forms of the predicted pressure profiles (schematically represented in figures 6.39 to 6.55) appeared similar to those determined experimentally using pressure transducers, and reported in references (46 and 47).

(ii) By implementing this technique the maximum sectional pressure values are found to lie between the centre and entry points along each measured arc of contact regardless of the prevailing rolling conditions.

(iii) At the ends of each measured arc of contact the technique predicted restraining forces which would develop tensile stresses within the rolls thus enhancing the effects of fatigue loading.

(iv) Implementation of this technique is dependent on the restriction of longitudinal curvature of the workpiece during the interrupted-pass rolling tests.

(v) Correlation between the predicted and measured roll separating loads varied up to 130% (workpieces exhibiting excessive longitudinal bending), but was within ±20% for most test conditions.

8.2 Practical Applications

In the current investigation the technique has been implemented to predict the pressure distribution profiles and roll separating loads relating to the interrupted-pass rolling tests during the deformation of a single material, using a two-high laboratory mill. Similar implementations of the technique should be possible relating to commercial strip production, provided that:

(i) An appropriate test mill is available for carrying out the interrupted-pass rolling tests.

(ii) An appropriate measurement system be available/accessible for measuring the imparted profiles.

In applying the technique a minimum of information is required regarding the rolls and workpiece configurations, with the influence constant values being determined independently of the material properties of the workpiece. If the test mill is not equipped with a suitable load measuring device, then an influence distance of about twice the length of the arc of contact should be assumed for an approximate solution. The technique will then permit determination of the pressure distribution and roll separating force.

8.3 Scope for Further Work

In its present form, the technique is only capable of estimating the pressure distributions and separating loads generated during the cold rolling process. This is mainly due to the assumption that the arcs of contact between the rolls and workpiece remain circular during rolling, in accordance with reference (2). However, further useful work can be undertaken with regard to the analysis and experimental confirmation of the technique.

(a) Analysis

The technique could be enhanced by the investigation of the following:

(i) Consideration of the elastic deformation (tensile) of the roll surfaces external to the contact regions. This could be attempted theoretically by imposing the predicted (or measured) pressure distributions on a suitable finite element model of the rolls.

(ii) The general modelling of the rolls using the finite element analysis. This could formulate a valid comparison between the deviation along the arcs of contact for both methods of analysis.

(b) Experimental

Increased validation of the technique could be achieved by the investigation of the following:

(i) Implementation of the technique using the same experimental equipment, but with different workpiece materials and configurations. These tests could establish the effectiveness of the same pressure distribution computer program incorporating different influence constant functions.

(ii) Implementation of the technique using different sized rolls and mill-stand configurations.

(iii) Implementation of the technique using tests in which the workpiece is kept flat during operation by the limited application of forward and back tensions, or by constraint using a fixture attached to the mill.

REFERENCES

1 von KARMAN, T, 'On the Theory of Rolling', Zeitschrift fur Angwandte Mathematik und Mechanik, 1925, Vol 5, p 139.

2 HITCHCOCK, J H, 'Elastic Deformation of Rolls During Cold Rolling', ASME report of special Research Committee on Roll Neck Bearings, June 1935, pp 33-41.

3 NADAI, A, 'The Forces Required for Rolling Steel Strip Under Tension', J App Mech, 1939, p A54, ASME.

4 OROWAN, E, 'The Calculation of Roll Pressure in Hot and Cold Flat Rolling', Proc Inst Mech Eng, 1943, Vol 150, pp 140-168.

5 FORD, H, 'Researches into the Deformation of Metals by Cold Rolling', Proc Inst Mech Eng, 1948, Vol 159, pp 115-143.

6 BLAND, D R and FORD, H, 'The Calculation of Roll Force and Torque in Cold Strip Rolling with Tensions', Proc Inst Mech Eng, 1948, Vol 159, pp 144-153.

7 HESSENBERG, W C F and SIMS, R B, 'The Effect of Tension on Torque and Roll Force in Cold Strip Rolling', J Iron Steel Inst, 1951, Vol 168, pp 155-164.

8 FORD, H, ELLIS, F and BLAND, D R, 'Cold Rolling with Strip Tension Part I - A New Approximate Method of Calculation and a Comparison with Other Methods', J Iron Steel Inst, 1951, Vol 168, pp 57-72.

9 FORD, H, and ELLIS, F, 'Cold Rolling with Strip Tension Part II - Comparison of Calculated and Experimental Results', J Iron Steel Inst, 1952, Vol 171, pp 239-245.

10 BLAND, D R, and FORD, H, 'Cold Rolling with Strip Tension Part III - An Approximate Treatment of the Elastic Compression of the Strip in Cold Rolling', J Iron Steel Inst, 1952, Vol 171, pp 245-249.

11 BLAND, D R, and SIMS, R B, 'A Note on the Theory of Rolling with Tensions', Proc Inst Mech Eng, 1953, Vol 167, pp 371-374.

12 SIMS, R B, 'Calculation of Roll Force and Torque in Cold-Rolling by Graphical and Experimental Methods', J Iron Steel Inst, 1954, Vol 178, pp 19-34.

13 LIANIS, G and FORD, H, 'A Graphical Solution of the Cold Rolling Problem, When Tensions are Applied to the Strip', J Inst Met, 1955-56, Vol 84, pp 299-305.

14 ALEXANDER, J M, 'A Slip-Line Field for the Hot Rolling Process', Proc Inst Mech Eng, 1955, Vol 169, p 1021.

15 FIRBANK, T C and LANCASTER, P R, 'Note : On Some Aspects of the Cold Rolling Problem', Int J Mech Sci, 1966, Vol 8, pp 653-656.

16 CRANE, F A A and ALEXANDER, J M, 'Slip-Line Fields and Deformation in Hot Rolling of Strip', J Inst Metals, 1968, Vol 96, pp 289-300.

17 COLLINS, I F, 'Slip-Line Field Solutions for Compression and Rolling with Slipping Friction', Int J Mech Sci, 1969, Vol 11, pp 971-978.

18 DENTON, B K and CRANE, F A A, 'Roll Load and Torque in the Hot Rolling of Steel Strip', J Iron Steel Inst, 1972, pp 606-617.

19 SANSOME, D H, 'Predicting Rolling Behaviour', Met Tech, 1975, Vol 2, pp 139-142.

20 ALEXANDER, J M, 'On the Theory of Rolling', Proc R Soc London, 1972, Vol A326, pp 535-563.

21 TAMANO, T and YANAGIMOTO, S, 'Finite Element Analysis of Steady Metal Flow Problems', Trans JSME, 1969, Vol 41, p 1130.

22 RAO, S S and KUMAR, A, 'Finite Element Analysis of Cold Strip Rolling', Int J Mach Tool Des Res, 1977, Vol 17, pp 159-168.

23 DAWSON, P R and THOMPSON, E G, 'Finite Element Analysis of Elasto-Visco-Plastic Flow by the Initial Stress-Rate Method', Int J Num Meth Engng, 1978, Vol 12, pp 47-57.

24 ATREYA, A and LENARD, J G, 'A Study of Cold Strip Rolling', J Eng Mat Tech, 1979, Vol 101, pp 129-134.

25 KEY, S W, KRIEG, R D and BATHE k-J, 'On the Application of the Finite Element Method to Metal Forming Processes - Part I', Comp Meth Appl Mech Engng, 1979, Vol 17/18, pp 597-608.

26 VENTER, R D and ADB-RABBO, A, 'Modelling of the Rolling Process II : Evaluation of the Stress Distribution in the Rolled Material', Int J Mech Sci, 1980, Vol 22, pp 93-98.

27 SHIMA, S et al, 'Rigid-Plastic Finite Element Analysis of Strip Rolling', Proc 4th Int Conf Prod Eng, Tokyo, 1980, p 89.

28 MORI, K, OSAKADA, K and ODA, T, 'Simulation of Plane-Strain by the Rigid-Plastic Finite Element Method', Int J Mech Sci, 1982, Vol 24, pp 519-527.

29 OSAKADA, K, NAKANO, J and MORI, K, 'Finite Element Method for Rigid-Plastic Analysis of Metal Forming - Formulation for Finite Deformation', Int J Mech-Sci, 1982, Vol 24, pp 459-468.

30 NIKAIDO, N et al, 'FEM Simulation of Non-steady Deformation in Edge Rolling', J Jpn Soc Tech Plast, 1985, Vol 24, pp 486-492.

31 PIETRŻYK, M, 'Flat Rolling Process-Mathematical Models', Zesz Nauk AGH, Metal Odlew, 1983, Vol 97, p 97.

32 DAWSON, P R, 'A Model for the Hot or Warm Forming of Metals with Special Use of Deformation Mechanism Maps', Int J Mech Sci, 1984, Vol 26, pp 227-244.

33 MORI, K and OSAKADA, K, 'Simulation of Three-Dimensional Deformation in Rolling by the Finite-Element Method', Int J Mech Sci, 1984, Vol 26, pp 515-525.

34 KIEFER, B V, 'Three-Dimensional Finite Element Prediction of Material Flow and Strain Distributions in Rolled Rectangular Billets', Adv Tech Plasticity [Proc Conf], 1984, Vol 2, Tokyo.

35 YARITA, I et al, 'Stress and Deformation Analysis of Metal Rolling Process', Adv Tech Plasticity [Proc Conf], 1984, Vol 2, Tokyo.

36 ZIENKIEWICZ, O C, JAIN, P C and ONATE, E, 'Flow of Solids During Flow and Extrusion : Some Aspects of Numerical Solutions', Int J Solids Structures, 1978, Vol 14, pp 15-38.

37 BHARGAVA, V, HAHN, G T and RUBIN, C A, 'An Elastic-Plastic Finite Element Model of Rolling Contact, Part I : Analysis of Single Contacts', J Appl Mech, 1985, Vol 52(i), pp 75-82.

38 BHARGAVA, V, HAHN, G T and RUBIN, C A, 'An Elastic-Plastic Finite Element Model of Rolling Contact, Part 2 : Analysis of Repeated Contacts', J Appl Mech, 1985, Vol 52(i), pp 75-82.

39 LIU, C et al, 'Elastic-Plastic Finite-Element Modelling of Cold Rolling of Strip', Int J Mech Sci, 1985, Vol 27(7/8), pp 531-541.

40 SIEBEL, E and LEUG, W, 1933 Mitteilungen aus dem Kaiser Wilhelm Institut fur Eisenforschung, Dusseldorf, Vol 53, p 1.

41 MacGREGOR, C W and COFFIN, L F, 'The Distribution of Strains in the Rolling Process', J Appl Mech, 1943, Vol 10, pp A13-A20.

42 MacGREGOR, C W and PALME, R B, 'Contact Stresses in the Rolling of Metals - I', J Appl Mech, 1948, Vol 70, p 297.

43 SMITH, C C et al, 'Pressure Distribution Between Stock and Rolls in Hot and Cold Flat Rolling', J Iron Steel Inst, 1952, Vol 170, pp 347-359.

44 OHASHI, Y et al, 'A Photoelastic Analysis of the Stress Distribution in Roller-Dies for Strip Rolling', Int J Mech Sci, 1964, Vol 6, p 461.

45 KHYYAT, F A and LANCASTER, P R, 'A Photoelastic Examination of the Stresses in the Rolls During Rolling', J Strain Anal, 1969, Vol 4(4), pp 245-260.

46 MATSUURA, Y and MOTOMURA, M, 'Pressure Distribution over the Arc of Contact in Cold Strip Rolling of Steel', Waseda Univ Report of Castings Research Lab, 1968, No 18.

47 AL-SALEHI, F A R, FIRBANK, T C and LANCASTER, P R, 'An Experimental Determination of the Roll Pressure Distributions in Cold Rolling', Int J Mech Sci, 1973, Vol 15, pp 693-710.

48 KOBASA, D and SCHULTZ, R A, 'Experimental Determination of the Length of the Arc of Contact in Cold Rolling', Iron Steel Eng, April 1968, pp 97-102.

49 THOMPSON, P F and BROWN, J H, 'A Study of Deformation During Cold Rolling using Visioplasticity', Int J Mech Sci, 1982, Vol 24(9), pp 559-576.

50 THEOCARIS et al, 'Roll-Pressure Distribution and Coefficient of Friction in Hot Rolling by Caustics', Int J Mech Sci, 1983, Vol 25(11), pp 833-844.

51 TIMOSHENKO, S P and GOODIER, J N, 'Theory of Elasticity', Second Edition, 1951, pp 85-97, McGraw-Hill.

52 WOOLMAN, J and MOTTRAM, R A, 'The Mechanical and Physical Properties of the British Standard En Steels', 1964, Pergamon Press.

53 GUR'EV, A V et al, 'Causes of Certain Defects in Cold Rolling Rolls', Stal in Eng, 1963, May, pp 379-381.

54 SCHRODER, K H, 'Heavy Spalls Originating in the Cores of High Chromium Rolls', Met Plant Tech, 1986(2), pp 62-66.

55 PAFEC 75, Theory and Results Manual.

56 PAFEC 75, Data Preparation Manual.

57 LARKE, E C, 'The Rolling of Strip Sheet and Plate', Second Edition, 1963, pp 245-260, Chapman and Hall.

APPENDIX I

A STUDY OF THE MEASUREMENT UNCERTAINTIES IN THE PROFILE INSPECTION EQUIPMENTS

A study has been carried out to assess the precision of the SIP Universal Measuring Machine and the Ferranti Merlin 750M when measuring the positions at typical points along deformed arc profiles.

The precision of the measuring systems was determined by taking a number of repeated measurements at a point, or series of points, and calculating the resulting uncertainties to a 95% confidence level. Statistical analysis shows that the confidence level of a:

(i) Sample mean $= \bar{x} \pm \frac{ts}{\sqrt{n}}$

and (ii) Single measurement $= x \pm ts$

where $\bar{x}$ = sample mean

x = single measurement

t = constant from student's distribution

s = standard deviation $(n - 1)$

n = sample size

A study of the measurement precision exhibited by the SIP Universal Measuring Machine entailed re-focussing the locating microscope (Z direction) and re-aligning the longitudinal carriage (X direction) at a single point on a typically deformed strip surface. The vertical settings of the locating microscope were recorded for 100 repeated readings. The calculated uncertainties of the settings are presented in table AI.1 and the frequency distribution shown as a histogram in figure AI.1.

TABLE AI.1 : MEASUREMENT UNCERTAINTIES OF THE PROFILE INSPECTION EQUIPMENTS

Uncertainties determined to 95% confidence levels
Sample size, n = 100
Student's constant, t = 1.984

	POINT NUMBER	SAMPLE MEAN $\bar{x}$ (mm)	SAMPLE RANGE (μm)	STANDARD DEVIATION S(n - 1) (μm)	UNCERTAINTY OF SAMPLE MEAN (μm)	UNCERTAINTY OF SINGLE SETTING (μm)
SIP UNIVERSAL MEASURING MACHINE	-	.8528	8	1.43	±0.3	±2.8
MERLIN 750M x ORDINATE	1	0.0107	5	1.14	±0.2	±2.3
	2	0.5143	18	3.32	±0.7	±6.6
	3	1.0205	20	3.4	±0.7	±6.8
	4*	1.519	21	3.09	±0.6	±6.1
	5	2.013	16	3.68	±0.7	±7.3
MERLIN 750M z ORDINATE	1	-0.0016	2	0.48	±0.1	±1.0
	2	-0.056	2	0.54	±0.1	±1.1
	3	-0.1079	3	0.61	±0.1	±1.2
	4*	-0.1568	2	0.45	±0.1	±0.9
	5	-0.2037	3	0.47	±0.1	±0.9

* Frequency distributions of the settings in x and z are shown in figures AI.2 and AI.3

A study of the measurement precision shown by the Ferranti Merlin 750M was undertaken by programming the machine to repeat and record positional settings in the X and Z directions at five points along a typically deformed arc. The x and z settings at each point were determined for 100 repeated readings, the resulting uncertainties are presented in table AI.1. Frequency distributions of the x and z settings at a representative point are shown as histograms in figures AI.2 and AI.3, respectively.

The measurement uncertainties associated with a single setting indicate that both instruments exhibit high measurement precision in the Z direction, whilst the positioning in the X direction appears to have minimal affect. The smaller uncertainties exhibited by the Merlin 750M should be considered in context with the systematic errors developed between the spherical stylus of the probe and the workpiece surface.

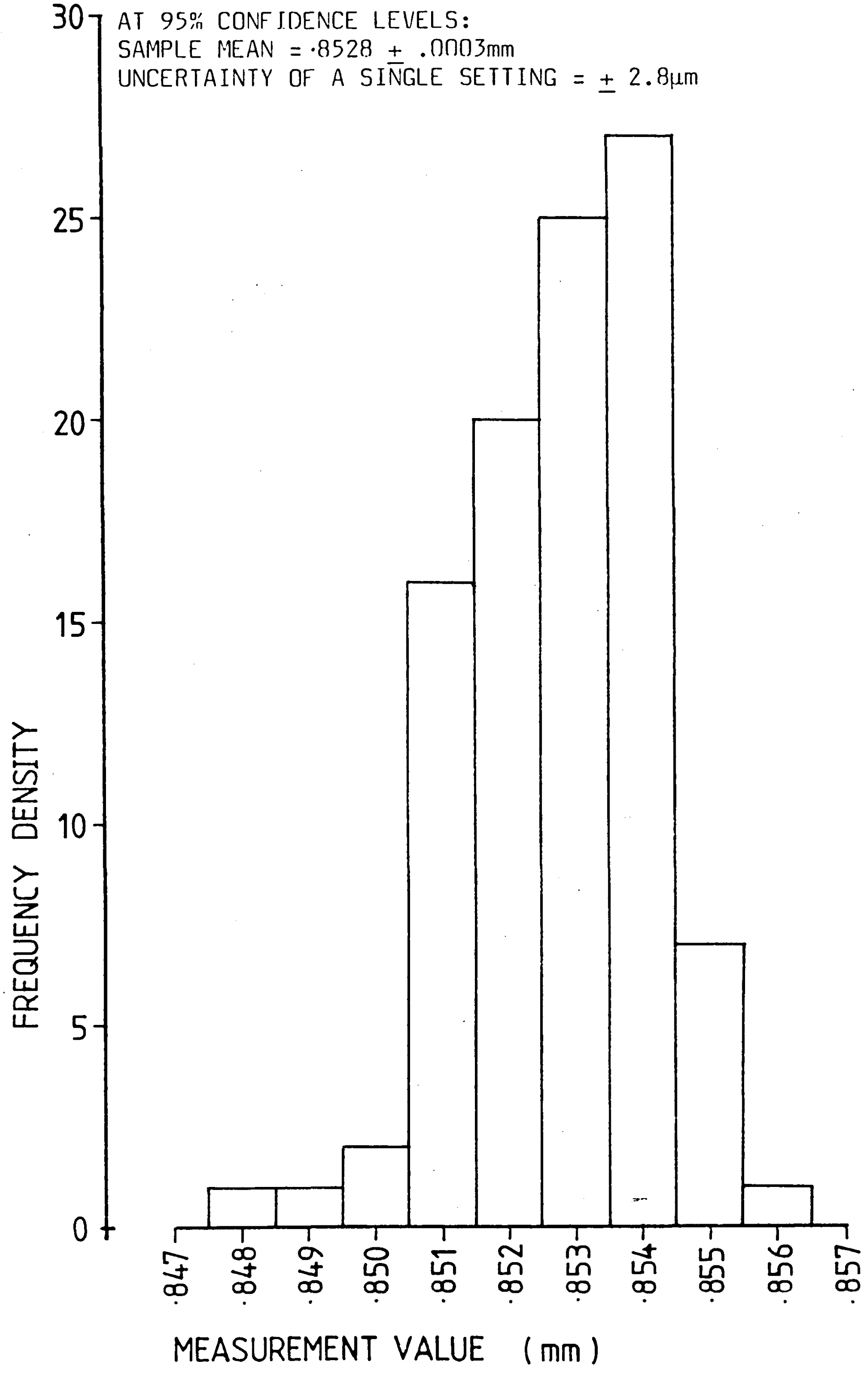

FIG AI.1 : A FREQUENCY DISTRIBUTION HISTOGRAM OF THE z SETTINGS FOR THE REPEATED MEASUREMENT OF A TYPICAL ARC NODE USING THE SIP

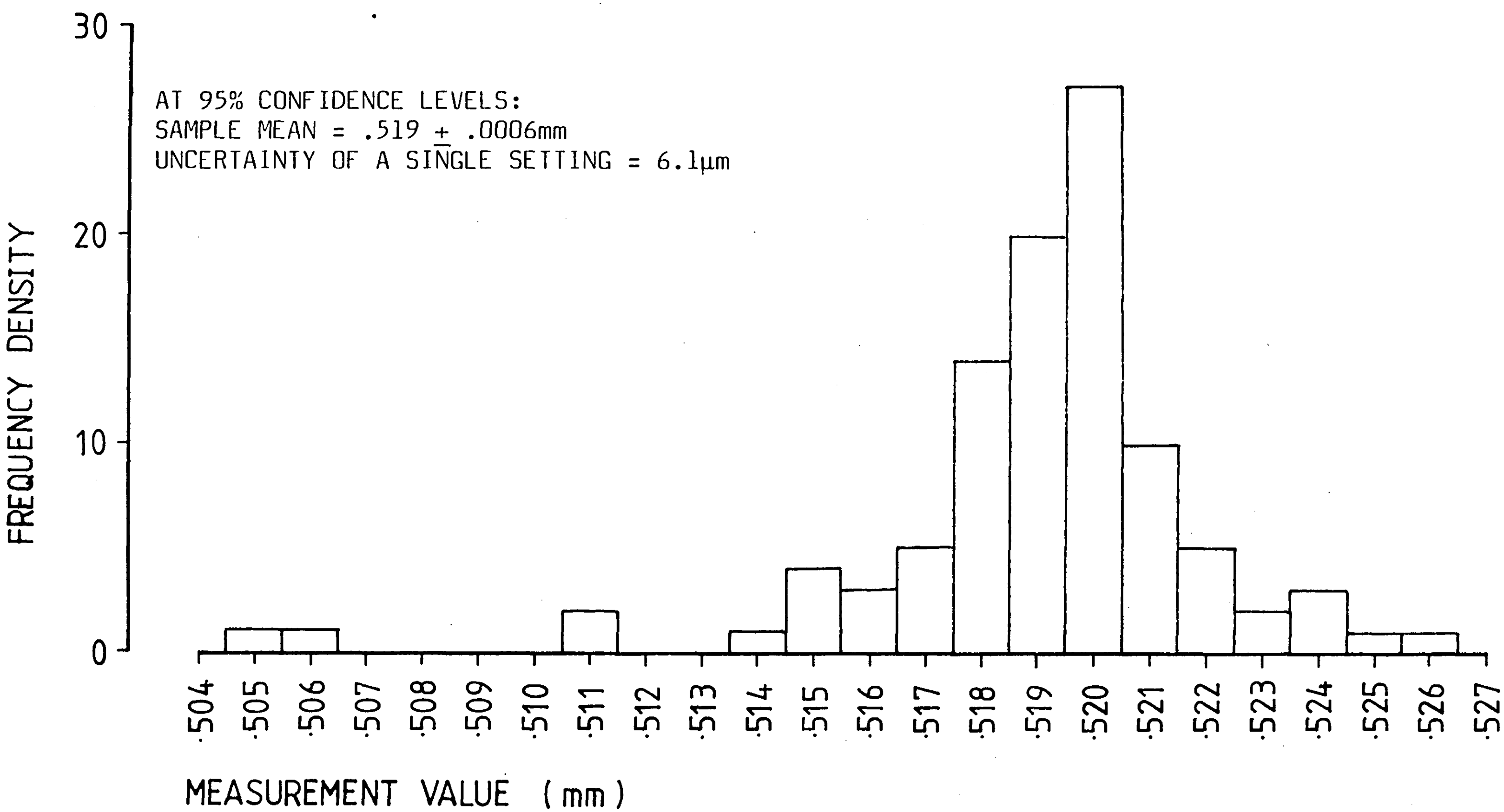

FIG AI.2 : A FREQUENCY DISTRIBUTION HISTOGRAM OF THE x SETTING FOR THE REPEATED MEASUREMENT OF A TYPICAL ARC NODE USING THE MERLIN 750M

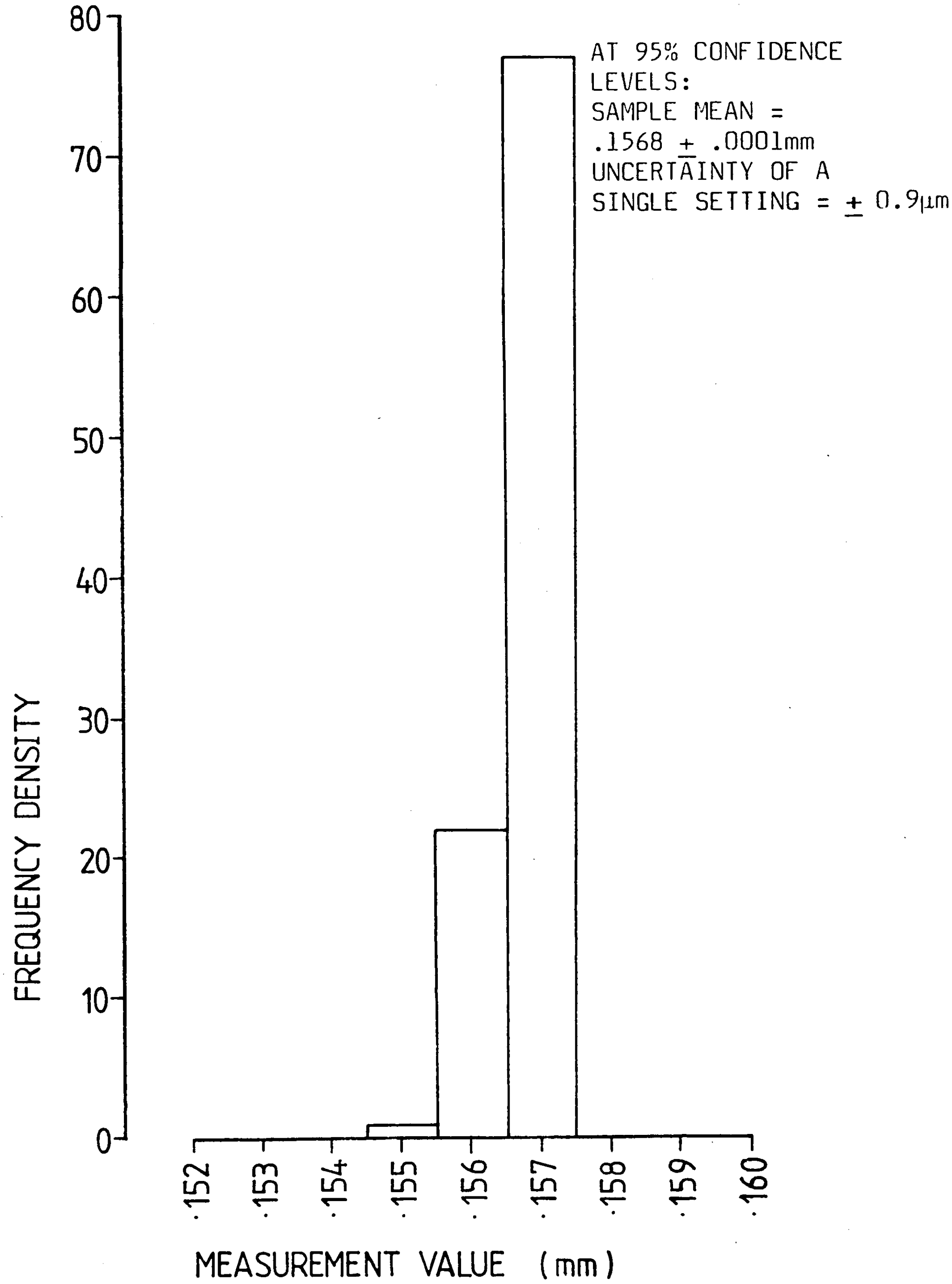

FIG AI.3 : A FREQUENCY DISTRIBUTION HISTOGRAM OF THE z SETTING FOR THE REPEATED MEASUREMENT OF A TYPICAL ARC NODE USING THE MERLIN 750M

APPENDIX II

FLOW CHARTS AND LISTINGS OF THE COMPUTER PROGRAMS RELATING TO THE INTERRUPTED-PASS ROLLING INVESTIGATIONS

(a) Pressure Distribution Program

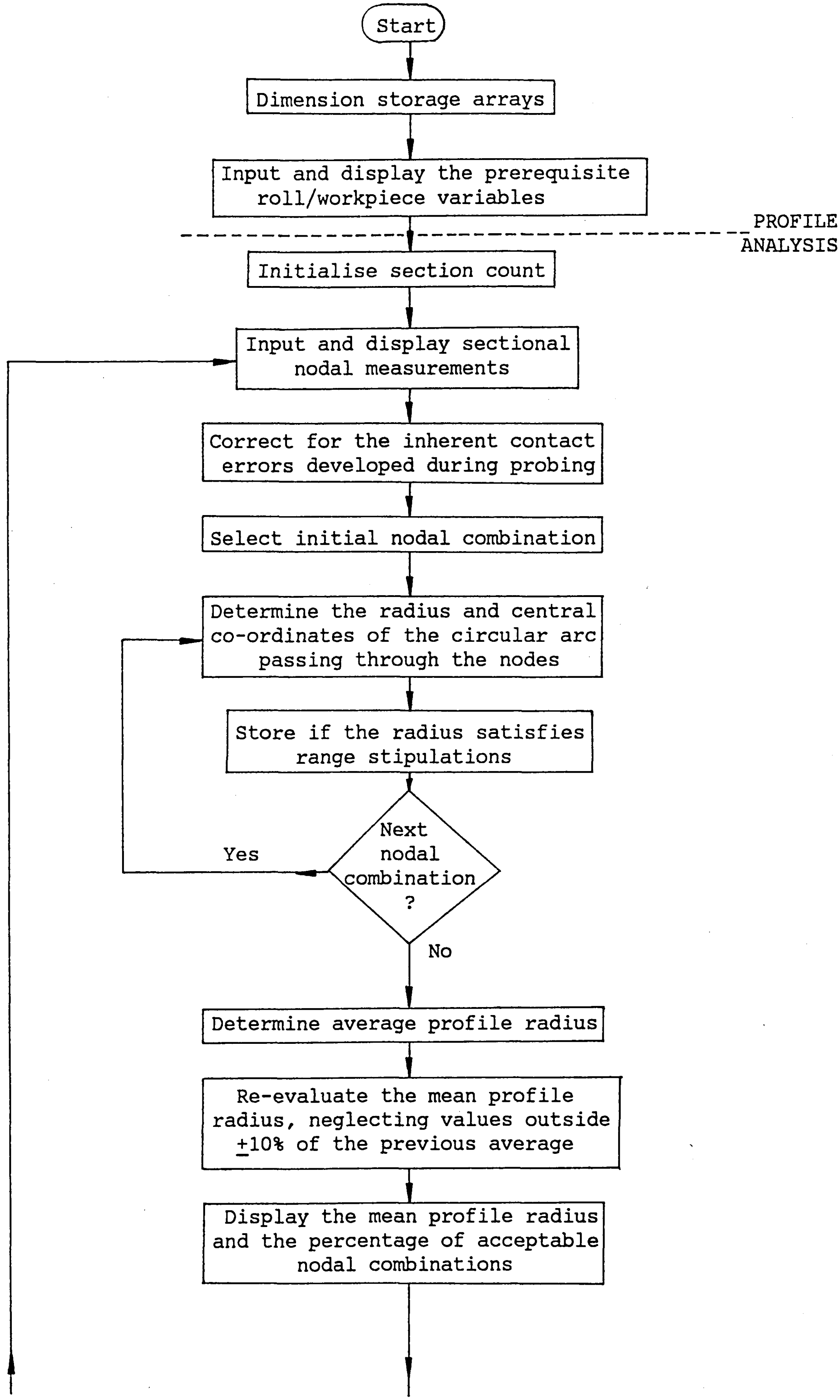
Start
Dimension storage arrays
Input and display the prerequisite roll/workpiece variables
PROFILE ANALYSIS
Initialise section count
Input and display sectional nodal measurements
Correct for the inherent contact errors developed during probing
Select initial nodal combination
Determine the radius and central co-ordinates of the circular arc passing through the nodes
Store if the radius satisfies range stipulations
Next nodal combination ?
Yes
No
Determine average profile radius
Re-evaluate the mean profile radius, neglecting values outside ±10% of the previous average
Display the mean profile radius and the percentage of acceptable nodal combinations

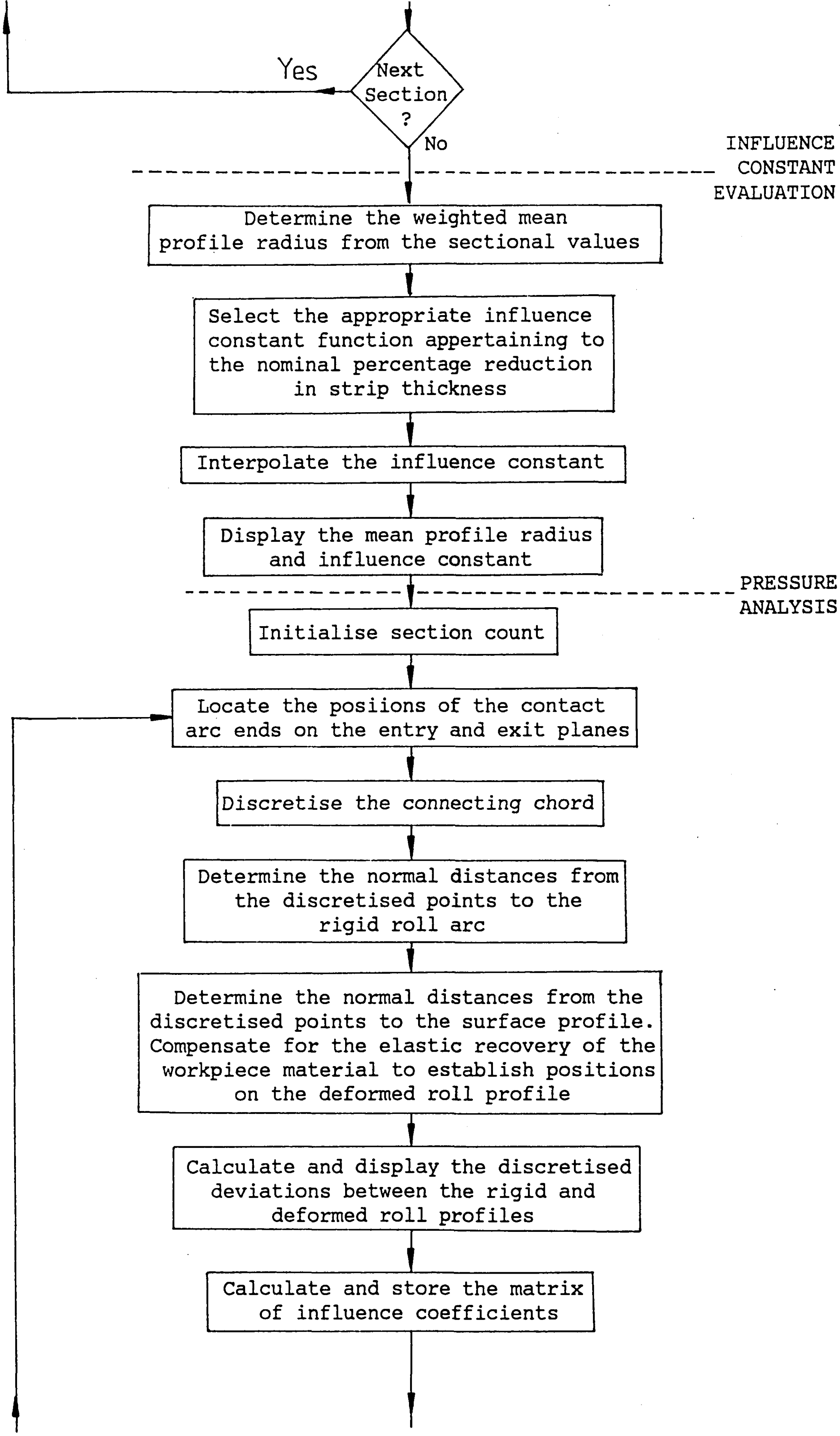
Yes
Next Section ?
No
INFLUENCE CONSTANT EVALUATION
Determine the weighted mean profile radius from the sectional values
Select the appropriate influence constant function appertaining to the nominal percentage reduction in strip thickness
Interpolate the influence constant
Display the mean profile radius and influence constant
PRESSURE ANALYSIS
Initialise section count
Locate the posiions of the contact arc ends on the entry and exit planes
Discretise the connecting chord
Determine the normal distances from the discretised points to the rigid roll arc
Determine the normal distances from the discretised points to the surface profile. Compensate for the elastic recovery of the workpiece material to establish positions on the deformed roll profile
Calculate and display the discretised deviations between the rigid and deformed roll profiles
Calculate and store the matrix of influence coefficients

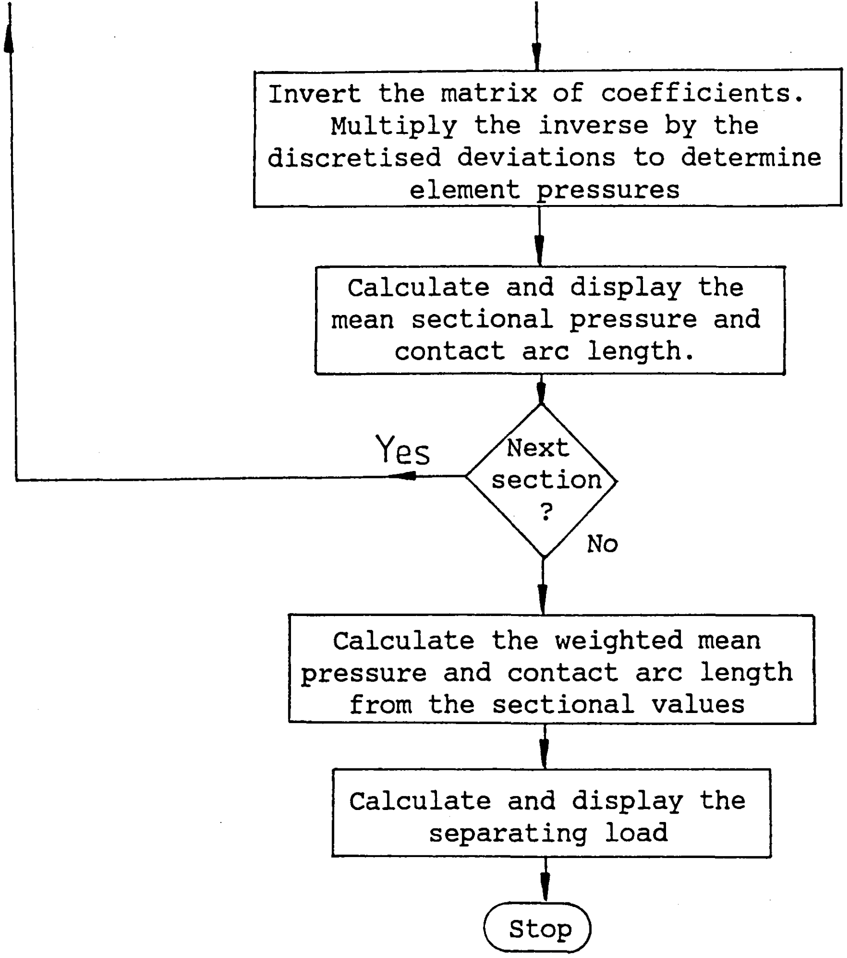
Invert the matrix of coefficients. Multiply the inverse by the discretised deviations to determine element pressures
Calculate and display the mean sectional pressure and contact arc length.
Yes
Next section ?
No
Calculate the weighted mean pressure and contact arc length from the sectional values
Calculate and display the separating load
Stop

```
100 REM  PRESSURE DISTRIBUTION AND SEPARATING LOAD EVALUATION -
110 REM                                 INTERRUPTED ROLLING CONDITIONS
120 REM
130 REM     THIS PROGRAM EVALUATES THE DYNAMIC PRESSURE DISTRIBUTIONS
140 REM  ACTIVE ALONG THE INTERFACES BETWEEN THE ROLLS AND DEFORMING
150 REM  STRIP WORKPIECE DURING COLD ROLLING .
160 REM     DETERMINATION OF THE SEPARATING LOAD PROCEEDS BASED UPON
170 REM  THE MEAN PRESSURE VALUE .
180 REM
190 REM  CURRENT VERSION BY S.R.BRADBURY  -  30/10/86
200 REM
210 REM  *** PROGRAM NOTATION ***
220 REM
230 REM     DETAILED BELOW ARE THE PRIMARY VARIABLES USED WITHIN THE
240 REM  PROGRAM . EACH IS DEFINED WITHIN THE SECTION IN WHICH IT FIRST
250 REM  APPEARS .
260 REM  NOTE : SYMBOLS PROCEEDED BY BRACKETS INDICATE ARRAYS .
270 REM
280 REM  INDENTOR/WORKPIECE PARAMETERS :-
290 REM     RR = RIGID ROLL RADIUS ; W = STRIP WIDTH ; H1 = INITIAL STRIP
300 REM     THICKNESS ; H2 = FINAL STRIP THICKNESS ; E = YOUNG'S MODULUS
310 REM     PO = POISSON'S RATIO
320 REM  PROFILE CONTROL :-
330 REM     NSC = NUMBER OF SECTIONS ; NPS = NUMBER OF PASSES PER SECTION
340 REM     ; NN = PN = NUMBER OF NODES PER SECTION
350 REM  SECTIONAL PROFILE ANALYSIS :-
360 REM     DATAX( ) = X-COORD OF MEASURED NODE ; DATAY( ) = Y-COORD ...(
370 REM     AS DATAX( ) )
380 REM    EACH NODAL COMBINATION :-
390 REM     DR( ) = RADIUS ; DCENTX( ) = X-COORD OF RADIUS CENTRE ;
400 REM     DCENTY( ) = Y-COORD ...( AS DCENTX( ) )
410 REM    SECTIONAL AVERAGE :-
420 REM     RMP( ) = RADIUS ; DX( ) = X-COORD OF RADIUS CENTRE ; DY( ) =
430 REM     Y-COORD ...( AS DX( ) )
440 REM  INFLUENCE CONSTANT EVALUATION :-
450 REM     RMPMEAN = MEAN RADIUS ; PRED = NOMINAL PERCENTAGE REDUCTION
```

```
460 REM     IN STRIP THICKNESS ; A = INFLUENCE CONSTANT
470 REM  PRESSURE ANALYSIS :-
480 REM   ARC DEVIATIONS AND ELASTIC RECOVERY COMPENSATION :-
490 REM    DELA = ELASTIC RECOVERY AT ONSET OF EXIT PLANE ; DELB =
500 REM    ELASTIC REC. AT ONSET OF ENTRY PLANE ; AX = X-COORD OF END
510 REM    OF CONTACT ARC - EXIT PLANE ; AY = Y-COORD ....( AS AX ) ; BX
520 REM    = X-COORD OF END OF CONTACT ARC - ENTRY PLANE ; BY =
530 REM    Y-COORD ...( AS BX ) ; RRX( ) = X-COORD OF DISCRETIZED NODE ON
540 REM    RIGID ARC ; RRY( ) = Y-COORD ....( AS RRX( ) ) ; DRR( ) =
550 REM    NORMAL DISTANCE FROM DATUM ; RDX( ) = X-COORD OF DISCRETIZED
560 REM    NODE ON DEFORMED ARC ; RDY( ) = Y-COORD ....( AS RDX( ) ) ;
570 REM    DDR( ) = NORMAL DISTANCE FROM DATUM ; B( ) = V( ) =
580 REM    DISCRETIZED DEVIATIONS BETWEEN RIGID AND DEFORMED ARCS
590 REM   EVALUATED PARAMETERS :-
600 REM    R = DEFORMED ROLL RADIUS ; AR = RIGID ROLL CONTACT ANGLE ;
610 REM    AD = DEFORMED ROLL CONTACT ANGLE ; CR = RIGID ROLL CONTACT
620 REM    LENGTH ; C = DEFORMED ROLL CONTACT LENGTH
630 REM   SECTIONAL PRESSURE EVALUATION :-
640 REM    S1 = ELEMENT BREADTH ; S2 = LIMIT OF ELEMENT INFLUENCE ;
650 REM    AA( , ) = INFLUENCE COEFFICIENT ; P( ) = ELEMENT PRESSURE
660 REM    MEANP( ) = SECTIONAL MEAN PRESSURE
670 REM   OVERALL AVERAGES :-
680 REM    A1 = MEAN CONTACT LENGTH ; A2 = MEAN PRESSURE ; LOAD =
690 REM    SEPARATING LOAD
700 REM
710 REM    THE FOLLOWING VARIABLES HAVE BEEN USED WITHIN THE ANALYSIS
720 REM  BUT HAVE NO LASTING SIGNIFICANCE AND ARE LISTED HERE FOR
730 REM  COMPLETENESS .
740 REM
750 REM  ITERATIVE COUNTS :-
760 REM    COUNT,COUNT2,COUNT3,COUNT4,COUNT5,CT,F,F1,G,H,I,J,L1,M,N,N1
770 REM    ,Q1,X,Y,Z
780 REM  PROFILE CONTROL AND EVALUATION :-
790 REM    SCT,PCT,ADSUM,ARSUM,BSUM( ),CSUM,CRSUM,RSUM,XSUM,YSUM,DAX,
800 REM    DAY,DRX,DBY,DCX,DCY,ANGAB,ANGBC,ANGAC,LA,LB,LC
810 REM  PRESSURE ANALYSIS :-
```

```
820 REM      B2,ANGAB,B3,D5,DATX( ),DATY( ),XDIST,YDIST,DCABX,DCABY,
830 REM      BD2,MH,DEL
840 REM
850 REM
860 PRINT TAB(20);"***********************************"
870 PRINT TAB(20);"*** PRESSURE EVALUATION PROGRAM ***"
880 PRINT TAB(20);"***********************************"
890 PRINT
900 PRINT
910 DIM DATAX(100),DATAY(100),DATX(100),DATY(100),V(100),P(100),AA(20,20)
920 DIM DR(1000),DCENTX(1000),DCENTY(1000),BSUM(10),B(20),RMP(100),DX(100)
930 DIM RRX(100),RRY(100),DRR(100),RDX(100),RDY(100),DDR(100),DY(100)
940 DIM CONTL(100),MEANP(100)
950 PRINT
960 PRINT TAB(14);"INPUT ROLL/STRIP DATA"
970 PRINT TAB(12);"*************************"
980 PRINT
990 PRINT TAB(4);"INPUT RIGID ROLL RADIUS (MM)"
1000 INPUT RR
1010 PRINT TAB(4);"INPUT STRIP CONTACT WIDTH (MM)"
1020 INPUT W
1030 PRINT TAB(4);"INPUT INITIAL STRIP THICKNESS (MM)"
1040 INPUT H1
1050 PRINT TAB(4);"INPUT FINAL STRIP THICKNESS (MM)"
1060 INPUT H2
1070 PRINT TAB(4);"INPUT YOUNG'S MODULUS OF ROLL MATERIAL (MN MM-2)"
1080 INPUT E
1090 PRINT TAB(4);"INPUT POISSON'S RATIO OF ROLL MATERIAL"
1100 INPUT PO
1110 PRINT TAB(4);"INPUT NUMBER OF SECTIONS ANALYSED"
1120 INPUT NSC
1130 PRINT TAB(4);"INPUT NUMBER OF PASSES PER SECTION"
1140 INPUT NPS
1150 PRINT TAB(4);"INPUT NUMBER OF NODES PER PASS"
1160 INPUT NN
1170 PRINT
1180 PRINT
1190 PRINT TAB(14);"SUMMARY OF ROLL/STRIP DIMENSIONS AND PROPERTIES"
```

```
1200 PRINT TAB(12);'****************************************************'
1210 PRINT
1220 PRINT USING 1230 : RR
1230 FORM '     UNDEFORMED ROLL RADIUS          =',POS39,PIC(ZZ£.£),POS48,&
  & 'MM',SKIP1
1240 PRINT USING 1250 : W
1250 FORM '     STRIP CONTACT WIDTH             =',POS39,PIC(ZZ£.££),POS48,&
  & 'MM',SKIP1
1260 PRINT USING 1270 : H1
1270 FORM '     INITIAL STRIP THICKNESS         =',POS40,PIC(Z£.££),POS48,&
  & 'MM',SKIP1
1280 PRINT USING 1290 : H2
1290 FORM '     FINAL STRIP THICKNESS           =',POS40,PIC(Z£.££),POS48,&
  & 'MM',SKIP1
1300 PRINT USING 1310: E*1000
1310 FORM X5,"YOUNG'S MODULUS                  =",POS39,PIC(Z££.£),POS48,&
  & 'KN MM-2',SKIP1
1320 PRINT USING 1330 : PO
1330 FORM "     POISSON'S RATIO                 =",POS41,PIC(£.£££),SKIP1
1340 PRINT
1350 PRINT
1360 PRINT TAB(15);"* * * * * * * * * * * * * * * *"
1370 PRINT
1380 PRINT TAB(14);'PROFILE ANALYSIS'
1390 PRINT TAB(12);'*********************'
1400 PRINT
1410 PRINT
1420 COUNT2 = 0
1430 SCT = 1 : PCT = 1 : PN = NN
1440 IF PCT < = NPS THEN GOTO 1460
1450 SCT = SCT + 1 : PCT = 1
1460 PRINT USING 1470 : SCT ; PCT
1470 FORM '  SECTION ',PIC(Z£),'  PASS ',PIC(Z£),SKIP1
1480 PRINT
1490 PRINT TAB(14);'INPUT MEASURED NODAL DATA'
1500 PRINT TAB(8);'( IN THE FORM X(N),Y(N) ON EACH LINE )'
```

```
1510 PRINT
1520 FOR I = 1 TO NN : PRINT 'NO.';I
1530 INPUT DATAX(I),DATAY(I) : NEXT I
1540 PRINT
1550 PRINT
1560 PRINT TAB(20);'MEASURED NODAL DATA'
1570 PRINT
1580 PRINT "    NODE       X CO-ORDINATE (MM)      Y CO-ORDINATE (MM)"
1590 PRINT
1600 FOR I = 1 TO NN
1610 PRINT USING 1620 : I, DATAX(I),DATAY(I)
1620 FORM POS5,PIC(Z£),POS15,PIC(Z£.£££),POS39,PIC(Z£.££££),SKIP1
1630 NEXT I
1640 PRINT
1650 PRINT 'DO YOU WISH TO ALTER THE DATA ? , 1 IF YES'
1660 INPUT Q1
1670 IF Q1 < > 1 THEN GOTO 1780
1680 PRINT
1690 PRINT 'INPUT NODE NUMBER'
1700 INPUT I
1710 PRINT 'INPUT REVISED DATA'
1720 INPUT DATAX(I),DATAY(I)
1730 GOTO 1550
1740 REM  COMPENSATE FOR PROBING ERRORS
1750 FOR I = 2 TO NN
1760 DATAY(I) = DATAY(I)-0.5*(1-COS((DATAY(I)-DATAY(I-1))/(DATAX(I)-&
  & DATAX(I-1))))
1770 NEXT I
1780 FOR I = NN TO 1 STEP -1 : DATAX(I) = DATAX(I) - DATAX(1)
1790 DATAY(I) = DATAY(I) - DATAY(1)
1800 NEXT I
1810 REM  RADIUS EVALUATION
1820 COUNT = 0 : RSUM = 0
1830 FOR X = 1 TO NN : FOR Y = X+3 TO NN : FOR Z = Y+3 TO NN
1840 DAX = DATAX(X) : DAY = DATAY(X) : DBX = DATAX(Y)
1850 DBY = DATAY(Y) : DCX = DATAX(Z) : DCY = DATAY(Z)
1860 ANGAB = ATN((DBY - DAY)/(DBX - DAX))
```

```
1870 ANGBC = ATN((DCY - DBY)/(DCX - DBX)) : ANGAC = ANGBC - ANGAB
1880 IF ANGAB > = ANGBC THEN GOTO 2000
1890 COUNT = COUNT + 1
1900 LA = SQR(((DCY - DBY)/2)**2 + ((DCX - DBX)/2)**2)
1910 LB = SQR(((DBY - DAY)/2)**2+((DBX - DAX)/2)**2) + LA/COS(ANGAC)
1920 LC = LB/SIN(ANGAC) - LA*TAN(ANGAC)
1930 DR(COUNT) = SQR( LC**2 + LA**2 )
1940 IF DR(COUNT) < 5*RR THEN GOTO 1960
1950 COUNT = COUNT - 1 : GOTO 2000
1960 DBCX = DCX - (( DCX - DBX )/2) : DBCY = DCY - (( DCY - DBY )/2)
1970 DCENTX(COUNT) = DBCX - LC*SIN(ANGBC)
1980 DCENTY(COUNT) = DBCY + LC*COS(ANGBC)
1990 RSUM = RSUM + DR(COUNT)
2000 NEXT Z : NEXT Y : NEXT X
2010 RSUM = RSUM / COUNT
2020 J = 0 : RSUMM = 0 : XSUMM = 0 : YSUMM = 0
2030 FOR I = 1 TO COUNT
2040 IF ABS(RSUM - DR(I))/RSUM > 0.1 THEN GOTO 2090
2050 J = J + 1
2060 DR(J) = DR(I) : RSUMM = RSUMM + DR(J)
2070 DCENTX(J) = DCENTX(I) : XSUMM = XSUMM + DCENTX(J)
2080 DCENTY(J) = DCENTY(I) : YSUMM = YSUMM + DCENTY(J)
2090 NEXT I
2100 RMP(COUNT2+1)=RSUMM/J:DX(COUNT2+1)=XSUMM/J:DY(COUNT2+1)=YSUMM/J
2110 PRINT
2120 PRINT USING 2130 : INT((J/COUNT)*100)
2130 FORM '   PERCENTAGE OF COMBINATIONS ACCEPTABLE =',POS45,PIC(ZZ£),&
   & SKIP1
2140 PRINT USING 2150 : (INT(RMP(COUNT2+1)*10))/10
2150 FORM '   PROFILE RADIUS                    =',POS45,PIC(ZZ£.£),&
   & ' MM',SKIP1
2160 PRINT
2170 COUNT2 = COUNT2 + 1 : PCT = PCT + 1
2180 IF COUNT2 < NSC*NPS THEN GOTO 1440
2190 COUNT4 = 4
2200 RMPSUM = RMP(1)+RMP((NSC*NPS)/2)+RMP((NSC*NPS)/2+1)+RMP(NSC*NPS)
2210 FOR I = 2 TO (NSC*NPS)/2-1
```

```
2220 RMPSUM = RMPSUM + 2*RMP(I) : COUNT4 = COUNT4 + 2 : NEXT I
2230 FOR I = (NSC*NPS)/2+2 TO NSC*NPS-1
2240 RMPSUM = RMPSUM + 2*RMP(I) : COUNT4 = COUNT4 + 2 : NEXT I
2250 RMPMEAN = RMPSUM/COUNT4
2260 PRED = 5*INT((2*(1-H2/H1)+0.05)*10)
2270 IF PRED > 11 THEN GOTO 2290
2280 A = 7.79*EXP(0.03*(RMPMEAN - RR)) : GOTO 2320
2290 IF PRED > 16 THEN GOTO 2310
2300 A = 6.28*EXP(0.025*(RMPMEAN - RR)) : GOTO 2320
2310 A = 5.97 + 0.253*(RMPMEAN - RR)
2320 PRINT
2330 PRINT USING 2340 : RMPMEAN
2340 FORM '   MEAN PROFILE RADIUS                    =',POS45,PIC(ZZ£.£),&
   & ' MM',SKIP1
2350 PRINT USING 2360 : A
2360 FORM '   INFLUENCE CONSTANT                     =',POS45,PIC(ZZ£.£),&
   & SKIP1
2370 PRINT ;'INF CONST =';A
2380 PRINT
2390 PRINT
2400 PRINT TAB(14);'PRESSURE ANALYSIS'
2410 PRINT TAB(12);'*********************'
2420 PRINT
2430 PRINT
2440 L1 = 0
2450 SCT = 1 : PCT = 1 : PN = NN
2460 IF PCT < = NPS THEN GOTO 2480
2470 SCT = SCT + 1 : PCT = 1
2480 PRINT USING 2490 : SCT ; PCT
2490 FORM '  SECTION ',PIC(Z£),'  PASS ',PIC(Z£),SKIP1
2500 PRINT
2510 CT = L1 + 1
2520 DELA = (H2-((EXP(-((0.058*(ABS(LOG(H2/H1)))**1.257)+0.012)))*H2))/2
2530 DELB = (H1-(EXP(-0.012)*H1))/2
2540 AY = DY(CT) - RMP(CT)
```

```
2550 AX = DX(CT) - SQR((RMP(CT)+DELA)**2 - RMP(CT)**2)
2560 BY = AY + (H1 - H2)/2
2570 BX = DX(CT) + SQR((RMP(CT)+DELB)**2 - (DY(CT)-BY)**2)
2580 B2 = SQR( (BX-AX)**2 + (BY-AY)**2 )/2
2590 ANGAB = ATN(( BY-AY)/(BX-AX))
2600 B3 = SQR( RR**2 - B2**2 )
2610 RX = AX + ( BX-AX )/2 - B3*SIN(ANGAB)
2620 RY = AY + ( BY - AY )/2 + B3*COS(ANGAB)
2630 H = 19 : D5 = (2*B2)/(H-1)
2640 DATX(1) = AX : DATY(1) = AY : DATX(19) = BX : DATY(19) = BY
2650 FOR I = 2 TO H-1 : DATX(I) = AX + (( BX-AX )/( H-1 ))*(I-1)
2660 DATY(I) = AY + (( BY-AY )/( H-1 ))*(I-1) : NEXT I
2670 RRX(1) = AX : RRY(1) = AY : RRX(19) = BX : RRY(19) = BY
2680 DRR(1) = 0 : DRR(19) = 0
2690 FOR I = 2 TO (H-1)/2
2700 XDIST = B2-D5*(I-1) : YDIST = SQR( RR**2 - XDIST**2 )
2710 RRX(I) = RX + YDIST*SIN(ANGAB) - XDIST*COS(ANGAB)
2720 RRY(I) = RY - YDIST*COS(ANGAB) - XDIST*SIN(ANGAB)
2730 DRR(I) = SQR((RRX(I)-DATX(I))**2 + (RRY(I)-DATY(I))**2) : NEXT I
2740 FOR I = ((H-1)/2)+1 TO H-1
2750 XDIST = D5*(I-1)-B2 : YDIST = SQR(RR**2 - XDIST**2 )
2760 RRX(I) = RX + YDIST*SIN(ANGAB) + XDIST*COS(ANGAB)
2770 RRY(I) = RY - YDIST*COS(ANGAB) + XDIST*SIN(ANGAB)
2780 DRR(I) = SQR((RRX(I)-DATX(I))**2 + (RRY(I) - DATY(I))**2) : NEXT I
2790 RDX(1) = AX : RDY(1) = AY : RDX(19) = BX : RDY(19) = BY
2800 DDR(1) = 0 : DDR(19) = 0
2810 BBX = SQR(RMP(CT)**2 - (RMP(CT) -((H1-H2)/2))**2) + DX(CT)
2820 FOR I = 2 TO H-1
2830 IF D5*(I-1) > (DX(CT)-AX)*COS(ANGAB) THEN GOTO 2880
2840 RDX(I)=AX+D5*(I-1)/COS(ANGAB)
2850 RDY(I) = DY(CT)-SQR((RMP(CT)+DELA)**2-(DX(CT)-RDX(I))**2)
2860 DDR(I) = SQR((RDX(I)-DATX(I))**2+(RDY(I)-DATY(I))**2)
2870 GOTO 3100
2880 IF D5*(I-1) > (2*B2)-((BX-BBX)*COS(ANGAB)) THEN GOTO 3020
2890 DCABX = DX(CT)+(RMP(CT)-TAN(ANGAB)*(DX(CT)-AX))*COS(ANGAB)*SIN(ANGAB)
2900 DCABY = DY(CT)-(RMP(CT)-TAN(ANGAB)*(DX(CT)-AX))*COS(ANGAB)*COS(ANGAB)
2910 BD2 = SQR((DCABX-AX)**2+(DCABY-AY)**2)
2920 IF D5*(I-1) > BD2 THEN GOTO 2960
```

```
2930 XDIST = BD2-D5*(I-1) : YDIST = SQR(RMP(CT)**2-XDIST**2)
2940 RDX(I) = DX(CT) + YDIST*SIN(ANGAB)-XDIST*COS(ANGAB)
2950 RDY(I) = DY(CT) - YDIST*COS(ANGAB)-XDIST*SIN(ANGAB) : GOTO 2990
2960 XDIST = D5*(I-1)-BD2 : YDIST = SQR(RMP(CT)**2 - XDIST**2)
2970 RDX(I) = DX(CT) + YDIST*SIN(ANGAB)+XDIST*COS(ANGAB)
2980 RDY(I) = DY(CT) - YDIST*COS(ANGAB) + XDIST*SIN(ANGAB)
2990 DDR(I) = SQR((RDX(I)-DATX(I))**2+(RDY(I)-DATY(I))**2)
3000 IF RDY(I) < DATY(I) THEN GOTO 3020
3010 DDR(I) = -1*DDR(I)
3020 HH = H1 - 2*(BY-RDY(I))
3030 DEL = (HH-((EXP(-((0.058*(ABS(LOG(HH/H1)))**1.257)+0.012)))*HH))/2
3040 DDR(I) = DDR(I) + DEL*COS((RDY(I)-AY)/(RDX(I)-AX))
3050 GOTO 3100
3060 RDX(I) = BX-(2*B2-D5*(I-1))/COS(ANGAB): RDY(I)=BY
3070 DDR(I) =-(2*B2-D5*(I-1))*TAN(ANGAB)
3080 DEL = (DELB*((2*B2-D5*(I-1))*TAN(ANGAB)))/(BX-BBX)
3090 DDR(I) = DDR(I)+DEL*COS(ANGAB)
3100 NEXT I
3110 FOR I = 1 TO K : V(I) = DRK(I)-DDR(I)
3120 NEXT I
3130 B(1) = 0 : B(10) = 0
3140 FOR I = 2 TO 9 : B(I) = V((I*2)-1) : NEXT I
3150 R = ((RMP(CT)+DELA)+SQR((BX-DX(CT))**2 + (BY-DY(CT))**2))/2
3160 AR = 2*ASIN(B2/RR) : AD = 2*ASIN(B2/R)
3170 CR = RR*AR : C = R*AD
3180 PRINT TAB(20);"CALCULATED ROLL DATA"
3190 PRINT
3200 PRINT USING 3210 : R
3210 FORM X4,'DEFORMED ROLL RADIUS              =',POS39,PIC(ZZ£.£££),X3,&
   & 'MM',SKIP1
3220 PRINT USING 3230 : AR
3230 FORM X4,'RIGID ROLL CONTACT ANGLE          =',POS39,PIC(ZZ£.£££),X3,&
   & 'RADS',SKIP1
3240 PRINT USING 3250 : AD
3250 FORM X4,'DEFORMED ROLL CONTACT ANGLE       =',POS39,PIC(ZZ£.£££),X3,&
   & 'RADS',SKIP1
3260 PRINT USING 3270 : CR
```

```
3270 FORM X4,'RIGID ROLL CONTACT LENGTH         =',POS39,PIC(ZZ£.£££),X3,&
   & 'MM',SKIP1
3280 PRINT USING 3290 : C
3290 FORM X4,'DEFORMED ROLL CONTACT LENGTH      =',POS39,PIC(ZZ£.£££),X3,&
   & 'MM',SKIP1
3300 PRINT
3310 PRINT
3320 PRINT TAB(11);"VERTICAL DEFORMATION OF ROLL ELEMENTS"
3330 PRINT
3340 PRINT "    ELEMENT NO.    DISPLACEMENT (MICRONS)"
3350 PRINT
3360 FOR I = 1 TO 10
3370 PRINT USING 3380 : I , B(I)*1000
3380 FORM POS10,PIC(Z£),POS27,PIC(ZZ£.£),SKIP1
3390 NEXT I
3400 PRINT
3410 S1 = C/10 : S2 = S1*A : M = 10 : N = 10
3420 FOR I = 1 TO N:FOR J = 1 TO M
3430 S9 = S1 * ABS( 2 * ABS ( I - J ) - 1 ) / 2
3440 IF I < > J THEN GOTO 3480
3450 AA(I,J) = ((S1-S9) * LOG (S2 / (S1-S9)) + S9 * LOG(S2 / S9))
3460 AA(I,J) = ( 2 * ( AA(I,J)) + ( 1 - PO ) * S1 ) / PI / E
3470 GOTO 3500
3480 AA(I,J) = ((S1+S9) * LOG (S2 / (S1+S9)) - S9 * LOG(S2 / S9))
3490 AA(I,J) = ( 2 * ( AA(I,J)) + ( 1 - PO ) * S1 ) / PI / E
3500 NEXT J:NEXT I
3510 N1 = 10:FOR F = 1 TO N1:U = AA(F,F):F1 = F+1
3520 REM CHECKING FOR SINGULARITY
3530 IF ABS(U) < 0.000001 THEN GOTO 3600
3540 REM DIVIDE THE ROW BY THE DIAGONAL ELEMENT
3550 FOR J = F1 TO N:AA(F,J) = AA(F,J)/U:NEXT J:B(F) = B(F)/U
3560 REM ELIMINATION BY SUBTRACTION
3570 FOR I = F1 TO N:U = AA(I,F):FOR J = F1 TO N:AA(I,J)=AA(I,J)-U*AA(F,J)
3580 NEXT J:B(I) = B(I)-U*B(F):NEXT I:NEXT F
3590 IF ABS(AA(N,N)) > 0.000001 THEN 3630
3600 PRINT 'SINGULARITY IN ROW ';F
3610 PRINT 'DETERMINANT = 0.0'
```

```
3620 GOTO 3950
3630 REM BACK SUBSTITUTION
3640 FOR L = 1 TO N1-1:F = N-L:F1 = F+1:FOR J = F1 TO N
3650 B(F) = B(F) -AA(F,J)*B(J):NEXT J:NEXT L: D = 1
3660 FOR I = 1 TO N:D = D*AA(I,I):NEXT I
3670 PRINT TAB(16);"ESTIMATED ELEMENT PRESSURES"
3680 PRINT
3690 PRINT '     ELEMENT NO.     PRESSURE ( N MM-2 )'
3700 PRINT
3710 FOR I = 1 TO N : P(I) = B(I)
3720 IF P(I) < 0 THEN GOTO 3760
3730 PRINT USING 3740 : I , P(I)*10**6
3740 FORM POS(10),PIC(Z£),POS26,PIC(ZZZ£.£),SKIP1
3750 GOTO 3780
3760 PRINT USING 3770 : I , P(I)*10**6
3770 FORM POS10,PIC(Z£),POS24,PIC(--ZZZ£.£),SKIP1
3780 NEXT I
3790 U = 0:FOR I = 1 TO N:U = U+P(I):NEXT I
3800 L1 = L1 + 1:MEANP(L1) = U/N:CONTL(L1) = C
3810 PRINT
3820 PRINT USING 3830 : MEANP(L1)*10**6
3830 FORM X4,'MEAN PRESSURE ACROSS SECTION  = ',PIC(ZZZ£.£),X3,&
   & 'N MM-2',SKIP1
3840 PRINT
3850 PRINT
3860 PRINT TAB(15);"* * * * * * * * * * * * * * * *"
3870 PRINT
3880 PRINT
3890 PCT = PCT + 1
3900 IF L1 < NSC*NPS THEN GOTO 2460
3910 U1 = 0 : SCT = 1 : PCT = 1
3920 PRINT
3930 PRINT TAB(17);'SUMMARY OF SECTIONAL DATA'
3940 PRINT TAB(15);'******************************'
3950 PRINT
3960 PRINT '     SECTION NO.     MEAN PRESSURE        CONTACT LENGTH'
```

```
3970 PRINT '                              ( N MM-2 )            ( MM )'
3980 PRINT
3990 FOR I = 1 TO L1 : U1 = U3 + CONTL(I)
4000 PRINT USING 4010 : SCT,PCT,MEANP(I)*10**6,CONTL(I)
4010 FORM POS5,PIC(Z£),' - ',PIC(Z£),POS24,PIC(ZZZ£.£),POS44,PIC(ZZ£.£)&
   & ,SKIP1
4020 PCT = PCT + 1 : IF PCT <= NPS THEN GOTO 4040
4030 SCT = SCT + 1 : PCT = 1
4040 NEXT I
4050 A1 = U1/L1
4060 COUNT5 = 4 : PMEAN = MEANP(1)+MEANP(L1/2)+MEANP(L1/2+1)+MEANP(L1)
4070 FOR I = 2 TO L1/2-1 : PMEAN = PMEAN + 2*MEANP(I)
4080 COUNT5 = COUNT5 + 2 : NEXT I
4090 FOR I = L1/2+2 TO L1-1 : PMEAN = PMEAN + 2*MEANP(I)
4100 COUNT5 = COUNT5 + 2 : NEXT I
4110 A2 = PMEAN/COUNT5
4120 PRINT
4130 PRINT USING 4140 : A2*10**6
4140 FORM X4,'MEAN PRESSURE ACROSS STRIP          = ',PIC(ZZZ£.£),X3,&
   & 'N MM-2',SKIP1
4150 PRINT USING 4160 : A1
4160 FORM X4,'MEAN CONTACT LENGTH ACROSS STRIP   = ',PIC(ZZ£.££),X3,'MM',&
   & SKIP1
4170 PRINT
4180 LOAD = (A1*A2*W*1000)
4190 PRINT
4200 PRINT TAB(15);"* * * * * * * * * * * * * * * *"
4210 PRINT TAB(15);" * * * * * * * * * * * * * * *"
4220 PRINT USING 4230 : LOAD
4230 FORM X14,'* *  ROLL FORCE =    ',POS33,PIC(ZZ£.£),' KN   * *',SKIP1
4240 PRINT TAB(15);" * * * * * * * * * * * * * * *"
4250 PRINT TAB(15);"* * * * * * * * * * * * * * * *"
4260 STOP
```

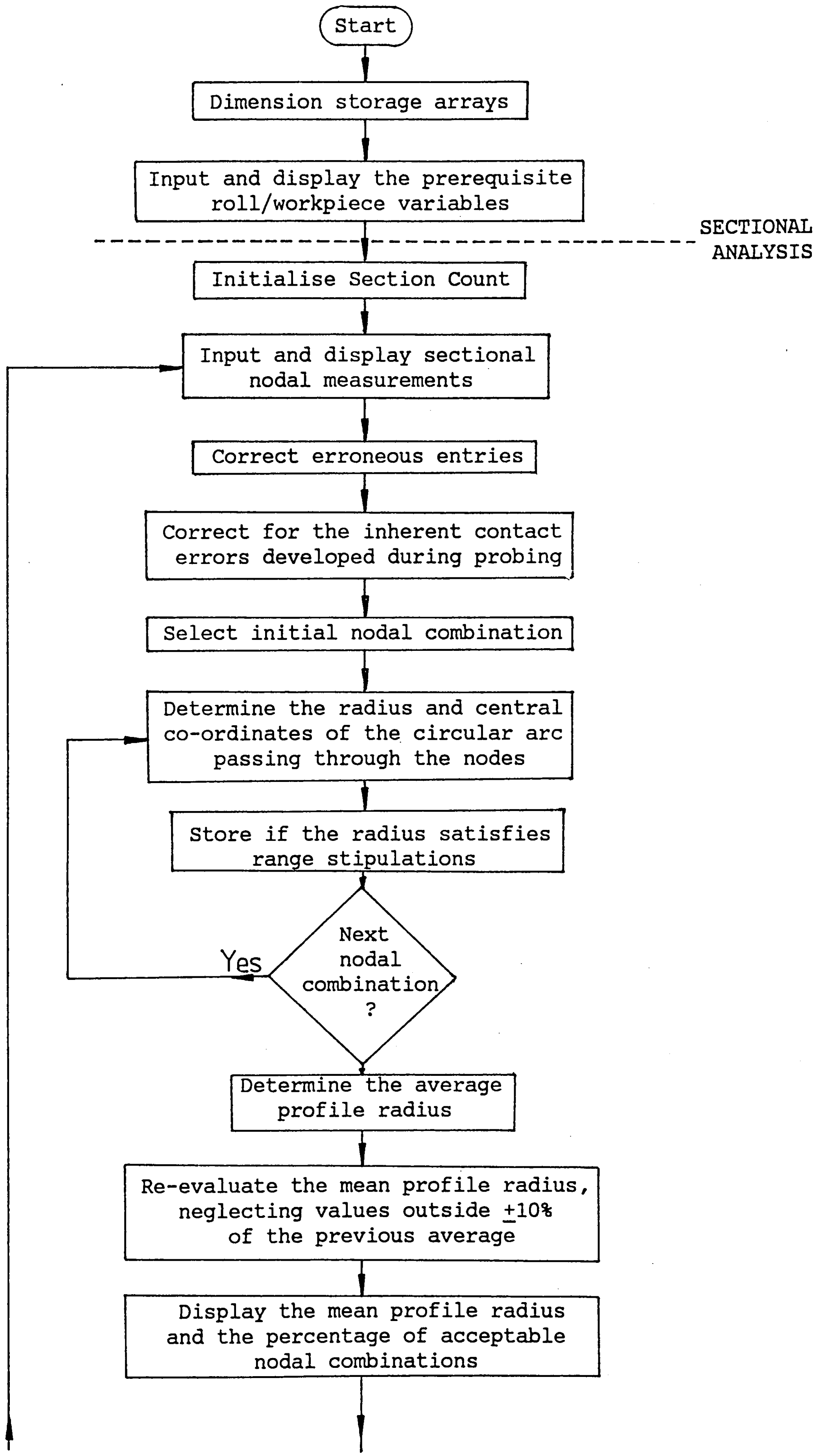
Start
Dimension storage arrays
Input and display the prerequisite roll/workpiece variables
SECTIONAL ANALYSIS
Initialise Section Count
Input and display sectional nodal measurements
Correct erroneous entries
Correct for the inherent contact errors developed during probing
Select initial nodal combination
Determine the radius and central co-ordinates of the circular arc passing through the nodes
Store if the radius satisfies range stipulations
Next nodal combination ?
Yes
Determine the average profile radius
Re-evaluate the mean profile radius, neglecting values outside ±10% of the previous average
Display the mean profile radius and the percentage of acceptable nodal combinations

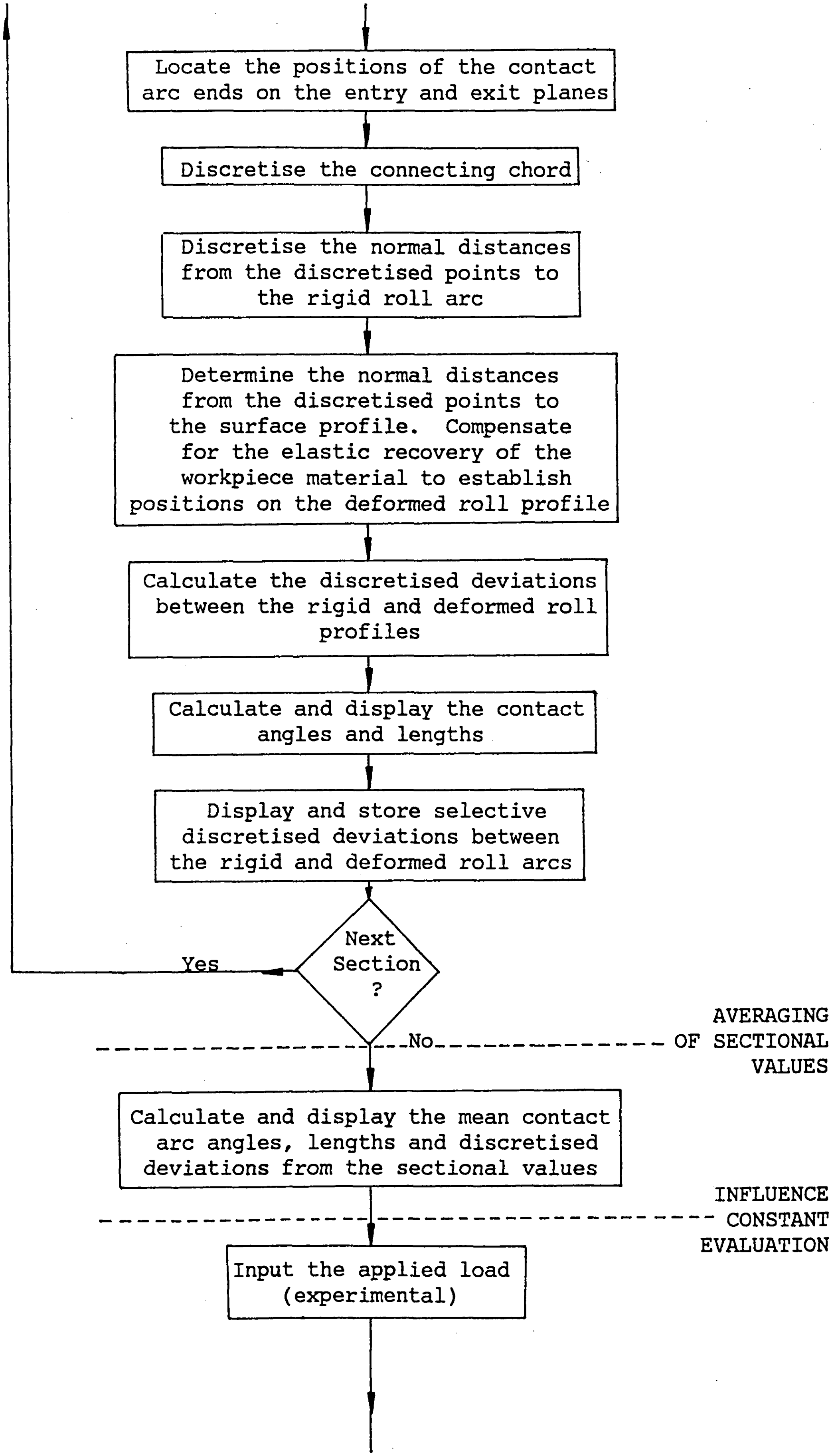
Locate the positions of the contact arc ends on the entry and exit planes
Discretise the connecting chord
Discretise the normal distances from the discretised points to the rigid roll arc
Determine the normal distances from the discretised points to the surface profile. Compensate for the elastic recovery of the workpiece material to establish positions on the deformed roll profile
Calculate the discretised deviations between the rigid and deformed roll profiles
Calculate and display the contact angles and lengths
Display and store selective discretised deviations between the rigid and deformed roll arcs
Next Section ?
Yes
No
AVERAGING OF SECTIONAL VALUES
Calculate and display the mean contact arc angles, lengths and discretised deviations from the sectional values
INFLUENCE CONSTANT EVALUATION
Input the applied load (experimental)

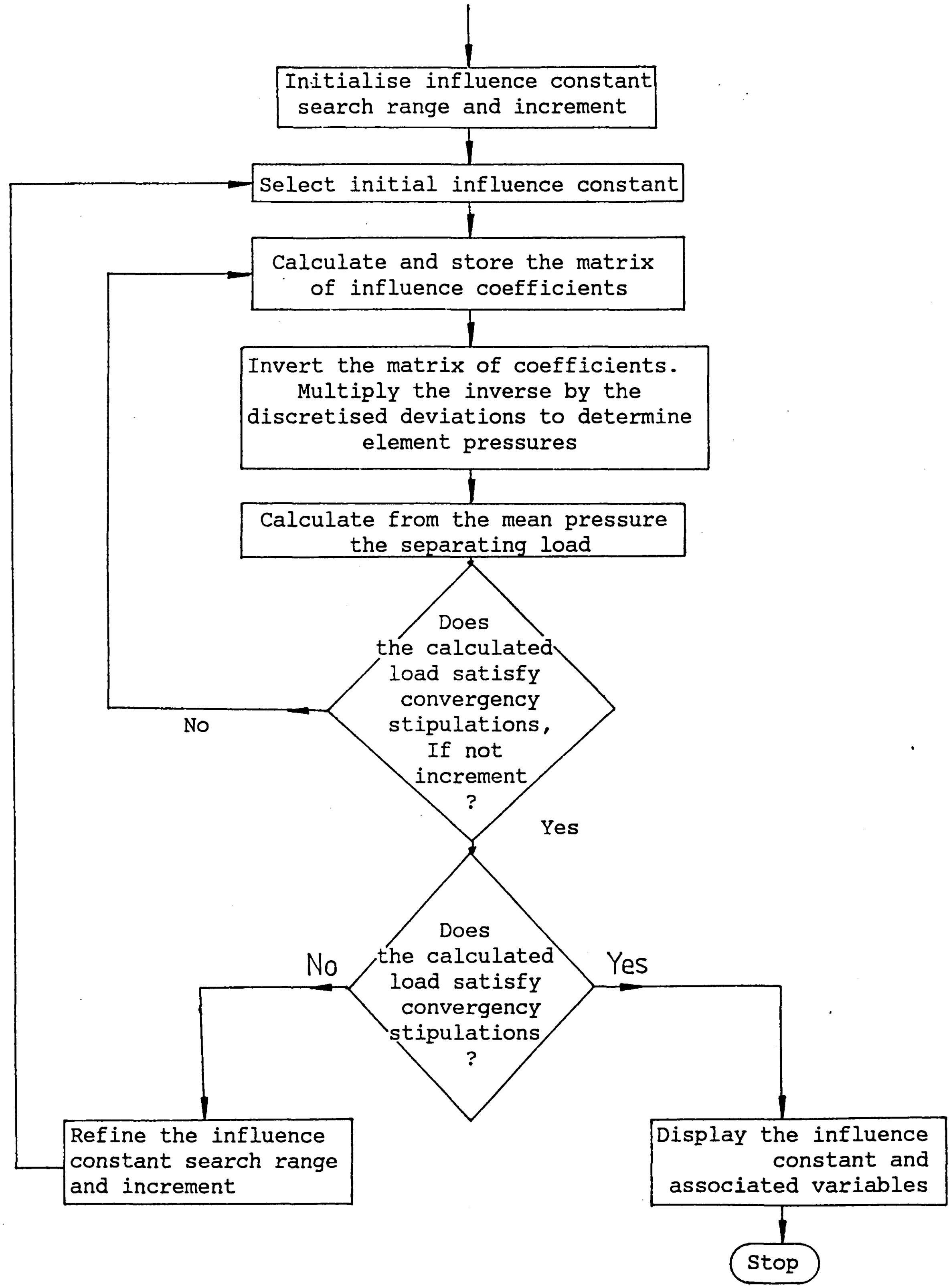
Initialise influence constant search range and increment
Select initial influence constant
Calculate and store the matrix of influence coefficients
Invert the matrix of coefficients. Multiply the inverse by the discretised deviations to determine element pressures
Calculate from the mean pressure the separating load
Does the calculated load satisfy convergency stipulations, If not increment ?
No
Yes
Does the calculated load satisfy convergency stipulations ?
No
Yes
Refine the influence constant search range and increment
Display the influence constant and associated variables
Stop

```
100  REM INFLUENCE CONSTANT EVALUATION  - INTERRUPTED ROLLING CONDITIONS
110  REM
120  REM    THIS PROGRAM EVALUATES THE INFLUENCE CONSTANT SUCH THAT THE
130  REM  CALCULATED ROLL LOAD EQUATES TO THE APPLIED ROLL LOAD .
140  REM    CALCULATIONS ARE BASED ON THE MEAN DISCRETIZED ELASTIC
150  REM  DISPLACEMENTS OF THE ROLL SURFACES ALONG THE CONTACT ARC
160  REM  LENGTHS AT SECTIONS ACROSS THE STRIP WIDTH .
170  REM
180  REM  CURRENT VERSION BY S.R.BRADBURY - 29/10/86
190  REM
200  REM *** PROGRAM NOTATION ***
210  REM
220  REM    DETAILED BELOW ARE THE PRIMARY VARIABLES USED WITHIN THE
230  REM   PROGRAM . EACH IS DESCRIBED WITHIN THE SECTION IN WHICH
235  REM   IT FIRST APPEARS .
240  REM   NOTE : SYMBOLS PROCEEDED BY BRACKETS INDICATE ARRAYS
250  REM
260  REM INDENTOR/WORKPIECE PARAMETERS :-
270  REM    RR = RIGID ROLL RADIUS ; W = STRIP WIDTH ; H1 = INITIAL STRIP
280  REM    THICKNESS ; H2 = FINAL STRIP THICKNESS ; E = YOUNG'S MODULUS
290  REM    PO = POISSON'S RATIO .
300  REM PROFILE ANALYSIS  :-
310  REM    NSC = NUMBER OF SECTIONS ; NPS = NUMBER OF PASSES PER SECTION
320  REM    NN = PN = NUMBER OF NODES PER SECTION ; DATAX( ) = X-COORD OF
330  REM     NODE ; DATAY( ) = Y COORD. OF  NODE .
340  REM RADIUS EVALUATION  :-
350  REM    FOR EACH NODAL COMBINATION :-
360  REM        DR( ) = RADIUS ; DCENTX( ) = X-COORD AT RADIUS CENTRE ;
370  REM        DCENTY( ) = Y-COORD AT RADIUS CENTRE .
380  REM    FOR SECTIONAL AVERAGE :-
390  REM       RMP = RADIUS ; DX = X-COORD AT RADIUS CENT. ; DY = Y-COORD
400  REM       AT RADIUS CENTRE .
410  REM ELASTIC RECOVERY COMPENSATION ;-
420  REM    DELA = ELASTIC REC. AT ONSET OF EXIT PLANE ; DELB = ELASTIC
430  REM    RECOVERY AT ONSET OF ENTRY PLANE ; AX = X-COORD AT END OF
440  REM    DEFORMED ARC - EXIT PLANE ; AY = Y-COORD ...(AS AX) ; BX =
```

```
450   REM    X-COORD AT END OF DEF. ARC - ENTRY PLANE ; BY = Y-COORD ...
460   REM    (AS BX) .
470   REM DEVIATIONS BETWEEN RIGID AND DEFORMED ARCS :-
480   REM    RRX( ) = X-COORD OF DISCRETIZED NODE ON RIGID ARC ; RRY( ) =
490   REM    Y-COORD ..(AS RRX( )) ; DRR( ) = NORMAL DISTANCE FROM DATUM ;
500   REM    RDX( ) = X-COORD OF DISCRETIZED NODE ON DEF. ARC ; RDY( ) =
510   REM    Y-COORD. .(AS RDX( )) ; DDR( ) = NORMAL DISTANCE FROM DATUM ;
520   REM    B( ) = V( ) = DISCRETIZED DEVIATIONS BETWEEN RIGID AND DEF.
530   REM    ARCS .
540   REM EVALUATED PARAMETERS :-
550   REM    R = DEF. ROLL RADIUS ; AR = RIGID ROLL CONTACT ANGLE ; AD =
560   REM    DEF. ROLL CONTACT ANGLE ; CR = RIGID ROLL CONTACT LENGTH ;
570   REM    C = DEFORMED ROLL CONTACT LENGTH
580   REM INFLUENCE CONSTANT EVALUATION :-
590   REM    Z6 = APPLIED LOAD ; AS = STARTING VALUE OF I.C. EST. ; AF =
600   REM    ENDING VALUE OF I.C. ESTIMATE ; AST = INITIAL INCREMENT ; A =
610   REM    INFLUENCE CONSTANT ; S1 = ELEMENT BREADTH ; S2 = LIMIT OF
620   REM    ELEMENT INFLUENCE ; AA( , ) = INFLUENCE COEFFICIENT ; P( ) =
630   REM    ELEMENT PRESSURE ; Q = MEAN CONT. PRESSURE ; W1 = CALCULATED
640   REM    LOAD
650   REM
660   REM    THE FOLLOWING VARIABLES HAVE BEEN USED IN THE ANALYSIS BUT
670   REM HAVE OF NO LASTING SIGNIFICANCE AND ARE LISTED FOR COMPLETENESS.
680   REM
690   REM ITERITIVE COUNTS :-
700   REM    CONT,COUNT2,COUNT3,F,F1,G,H,I,J,M,N,N1,Q1,X,Y,Z
710   REM SECTIONAL SUMMATIONS :-
720   REM    ADSUM,ARSUM,BSUM( ),CSUM,CRSUM,RSUM,XSUM,YSUM
730   REM RADIUS EVALUATION :-
740   REM    DAX,DAY,DBX,DBY,DCX,DCY,ANGAB,ANGBC,ANGAC,LA,LB,LC
750   REM DEVIATIONS BETWEEN RIGID AND DEFORMED ARCS :-
760   REM    B2,ANGAB,B3,D5,DATX( ),DATY( ),XDIST,YDIST
770   REM ELASTIC RECOVERY COMPENSATION ;-
780   REM    DCABX,DCABY,BD2,HH,DEL
790   REM INFLUENCE CONSTANT EVALUATION :-
```

```
800  REM    S9,U,D
810  REM
820 PRINT TAB(20);'***********************************'
830 PRINT TAB(20);'*** CONSTANT EVALUATION PROGRAM ***'
840 PRINT TAB(20);'***********************************'
850 PRINT
860 PRINT
870 DIM DATAX(100),DATAY(100),DATX(100),DATY(100),V(100),P(100),AA(20,20)
880 DIM DR(1000),DCENTX(1000),DCENTY(1000),BSUM(10),B(20)
890 DIM RRX(100),RRY(100),DRR(100),RDX(100),RDY(100),DDR(100)
900 PRINT
910 PRINT TAB(14);'INPUT ROLL/STRIP DATA'
920 PRINT TAB(12);'*************************'
930 PRINT
940 PRINT TAB(4);'INPUT RIGID ROLL RADIUS (MM)'
950 INPUT RR
960 PRINT TAB(4);'INPUT STRIP CONTACT WIDTH (MM)'
970 INPUT W
980 PRINT TAB(4);'INPUT INITIAL STRIP THICKNESS (MM)'
990 INPUT H1
1000 PRINT TAB(4);'INPUT FINAL STRIP THICKNESS (MM)'
1010 INPUT H2
1020 PRINT TAB(4);"INPUT YOUNG'S MODULUS OF ROLL MATERIAL (MN MM-2)"
1030 INPUT E
1040 PRINT TAB(4);"INPUT POISSON'S RATIO OF ROLL MATERIAL"
1050 INPUT PO
1060 PRINT TAB(4);'INPUT NUMBER OF SECTIONS ANALYSED'
1070 INPUT NSC
1080 PRINT TAB(4);'INPUT NUMBER OF PASSES PER SECTION'
1090 INPUT NPS
1100 PRINT TAB(4);'INPUT NUMBER OF NODES PER PASS'
1110 INPUT NN
1120 PRINT
1130 PRINT
1140 PRINT TAB(14);'SUMMARY OF ROLL/STRIP DIMENSIONS AND PROPERTIES'
1150 PRINT TAB(12);'**************************************************'
```

```
1160 PRINT
1170 PRINT USING 1180 : RR
1180 FORM '      UNDEFORMED ROLL RADIUS          =',POS39,PIC(ZZ£.£),POS48,&
  & 'MM',SKIP1
1190 PRINT USING 1200 : W
1200 FORM '      STRIP CONTACT WIDTH             =',POS39,PIC(ZZ£.££),POS48,&
  & 'MM',SKIP1
1210 PRINT USING 1220 : H1
1220 FORM '      INITIAL STRIP THICKNESS         =',POS40,PIC(Z£.££),POS48,&
  & 'MM',SKIP1
1230 PRINT USING 1240 : H2
1240 FORM '      FINAL STRIP THICKNESS           =',POS40,PIC(Z£.££),POS48,&
  & 'MM',SKIP1
1250 PRINT USING 1260: E*1000
1260 FORM X5,"YOUNG'S MODULUS                  =",POS39,PIC(Z££.£),POS48,&
  & 'KN MM-2',SKIP1
1270 PRINT USING 1280 : PO
1280 FORM "      POISSON'S RATIO                 =",POS41,PIC(£.£££),SKIP1
1290 PRINT
1300 PRINT
1310 PRINT TAB(15);"* * * * * * * * * * * * * * * *"
1320 PRINT
1330 FOR I = 1 TO 10 : BSUM(I) = 0 : NEXT I
1340 RSUM = 0 : ARSUM = 0 : ADSUM = 0 : CRSUM = 0 : CSUM = 0 : COUNT2 = 0
1350 SCT = 1 : PCT = 1 : PN = NN
1360 IF PCT < = NPS THEN GOTO 1380
1370 SCT = SCT + 1 : PCT = 1
1380 PRINT USING 1390 : SCT ; PCT
1390 FORM '  SECTION ',PIC(Z£),'  PASS ',PIC(Z£),SKIP1
1400 PRINT;' *********************'
1410 PRINT
1420 PRINT TAB(14);'INPUT MEASURED NODAL DATA'
1430 PRINT TAB(8);'( IN THE FORM X(N),Y(N) ON EACH LINE )'
1440 PRINT
1450 FOR I = 1 TO NN : PRINT 'NO.';I
1460 INPUT DATAX(I),DATAY(I) : NEXT I
```

```
1470 PRINT
1480 PRINT
1490 PRINT TAB(20);'MEASURED NODAL DATA'
1500 PRINT TAB(18);"***********************"
1510 PRINT
1520 PRINT "    NODE       X CO-ORDINATE (MM)      Y CO-ORDINATE (MM)"
1530 PRINT
1540 FOR I = 1 TO NN
1550 PRINT USING 1560 : I, DATAX(I),DATAY(I)
1560 FORM POS5,PIC(Z£),POS15,PIC(Z£.£££),POS39,PIC(Z£.££££),SKIP1
1570 NEXT I
1580 PRINT
1590 PRINT 'DO YOU WISH TO ALTER THE DATA ? , 1 IF YES'
1600 INPUT Q1
1610 IF Q1 < > 1 THEN GOTO 1720
1620 PRINT
1630 PRINT 'INPUT NODE NUMBER'
1640 INPUT I
1650 PRINT 'INPUT REVISED DATA'
1660 INPUT DATAX(I),DATAY(I)
1670 GOTO 1480
1680 REM  COMPENSATE FOR PROBING ERRORS
1690 FOR I = 2 TO NN
1700 DATAY(I) = DATAY(I)-0.5*(1-COS((DATAY(I)-DATAY(I-1))/(DATAX(I)-&
  & DATAX(I-1))))
1710 NEXT I
1720 FOR I = NN TO 1 STEP -1 : DATAX(I) = DATAX(I) - DATAX(1)
1730 DATAY(I) = DATAY(I) - DATAY(1)
1740 NEXT I
1750 REM  RADIUS EVALUATION
1760 COUNT = 0 : RSUM = 0 : XSUM = 0 : YSUM = 0
1770 FOR X = 1 TO NN : FOR Y = X+3 TO NN : FOR Z = Y+3 TO NN
1780 DAX = DATAX(X) : DAY = DATAY(X) : DBX = DATAX(Y)
1790 DBY = DATAY(Y) : DCX = DATAX(Z) : DCY = DATAY(Z)
1800 ANGAB = ATN((DBY - DAY)/(DBX - DAX))
1810 ANGBC = ATN((DCY - DBY)/(DCX - DBX)) : ANGAC = ANGBC - ANGAB
```

```
1820 IF ANGAB > = ANGBC THEN GOTO 1950
1830 COUNT = COUNT + 1
1840 LA = SQR(((DCY - DBY)/2)**2 + ((DCX - DBX)/2)**2)
1850 LB = SQR(((DBY - DAY)/2)**2+((DBX - DAX)/2)**2) + LA/COS(ANGAC)
1860 LC = LB/SIN(ANGAC) - LA*TAN(ANGAC)
1870 DR(COUNT) = SQR( LC**2 + LA**2 )
1880 IF DR(COUNT) < 5*RR THEN GOTO 1900
1890 COUNT = COUNT - 1 : GOTO 1950
1900 DBCX = DCX - (( DCX - DBX )/2) : DBCY = DCY - (( DCY - DBY )/2)
1910 DCENTX(COUNT) = DBCX - LC*SIN(ANGBC)
1920 DCENTY(COUNT) = DBCY + LC*COS(ANGBC)
1930 RSUM = RSUM + DR(COUNT) : XSUM = XSUM + DCENTX(COUNT)
1940 YSUM = YSUM + DCENTY(COUNT)
1950 NEXT Z : NEXT Y : NEXT X
1960 RSUM = RSUM / COUNT : XSUM = XSUM / COUNT : YSUM = YSUM / COUNT
1970 J = 0 : RSUMM = 0 : XSUMM = 0 : YSUMM = 0
1980 FOR I = 1 TO COUNT
1990 IF ABS(RSUM - DR(I))/RSUM > 0.1 THEN GOTO 2040
2000 J = J + 1
2010 DR(J) = DR(I) : RSUMM = RSUMM + DR(J)
2020 DCENTX(J) = DCENTX(I) : XSUMM = XSUMM + DCENTX(J)
2030 DCENTY(J) = DCENTY(I) : YSUMM = YSUMM + DCENTY(J)
2040 NEXT I
2050 RMP = RSUMM/J : DX = XSUMM/J : DY = YSUMM/J
2060 PRINT
2070 PRINT ;'PERCENTAGE OF READINGS ACCEPTABLE =';INT((J/COUNT)*100)
2080 PRINT
2090 PRINT ;'MEASURED RADIUS     =';RMP;'MM'
2100 PRINT
2110 REM  ELASTIC RECOVERY COMPENSATION AND DETERMINATION OF DEVIATIONS
2120 REM  BETWEEN RIGID AND DEFORMED ARCS .
2130 DELA = (H2-((EXP(-((0.058*(ABS(LOG(H2/H1)))**1.257)+0.012)))*H2))/2
2140 DELB = (H1-(EXP(-0.012)*H1))/2
2150 AY = DY - RMP
2160 AX = DX - SQR((RMP+DELA)**2 - RMP**2)
2170 BY = AY + (H1 - H2)/2
```

```
2180 BX = DX + SQR((RMP+DELB)**2 - (DY-BY)**2)
2190 B2 = SQR( (BX-AX)**2 + (BY-AY)**2 )/2
2200 ANGAB = ATN(( BY-AY)/(BX-AX))
2210 B3 = SQR( RR**2 - B2**2 )
2220 RX = AX + ( BX-AX )/2 - B3*SIN(ANGAB)
2230 RY = AY + ( BY - AY )/2 + B3*COS(ANGAB)
2240 H = 19 : D5 = (2*B2)/(H-1)
2250 DATX(1) = AX : DATY(1) = AY : DATX(19) = BX : DATY(19) = BY
2260 FOR I = 2 TO H-1 : DATX(I) = AX + (( BX-AX )/( H-1 ))*(I-1)
2270 DATY(I) = AY + (( BY-AY )/( H-1 ))*(I-1) : NEXT I
2280 RRX(1) = AX : RRY(1) = AY : RRX(19) = BX : RRY(19) = BY
2290 DRR(1) = 0 : DRR(19) = 0
2300 FOR I = 2 TO (H-1)/2
2310 XDIST = B2-D5*(I-1) : YDIST = SQR( RR**2 - XDIST**2 )
2320 RRX(I) = RX + YDIST*SIN(ANGAB) - XDIST*COS(ANGAB)
2330 RRY(I) = RY - YDIST*COS(ANGAB) - XDIST*SIN(ANGAB)
2340 DRR(I) = SQR((RRX(I)-DATX(I))**2 + (RRY(I)-DATY(I))**2) : NEXT I
2350 FOR I = ((H-1)/2)+1 TO H-1
2360 XDIST = D5*(I-1)-B2 : YDIST = SQR(RR**2 - XDIST**2 )
2370 RRX(I) = RX + YDIST*SIN(ANGAB) + XDIST*COS(ANGAB)
2380 RRY(I) = RY - YDIST*COS(ANGAB) + XDIST*SIN(ANGAB)
2390 DRR(I) = SQR((RRX(I)-DATX(I))**2 + (RRY(I) - DATY(I))**2) : NEXT I
2400 RDX(1) = AX : RDY(1) = AY : RDX(19) = BX : RDY(19) = BY
2410 DDR(1) = 0 : DDR(19) = 0
2420 BBX = SQR(RMP**2 - (RMP -((H1-H2)/2))**2) + DX
2430 FOR I = 2 TO H-1
2440 IF D5*(I-1) > (DX-AX)*COS(ANGAB) THEN GOTO 2490
2450 RDX(I)=AX+D5*(I-1)/COS(ANGAB)
2460 RDY(I) = DY-SQR((RMP+DELA)**2-(DX-RDX(I))**2)
2470 DDR(I) = SQR((RDX(I)-DATX(I))**2+(RDY(I)-DATY(I))**2)
2480 GOTO 2710
2490 IF D5*(I-1) > (2*B2)-((BX-BBX)*COS(ANGAB)) THEN GOTO 2630
2500 DCABX = DX+(RMP-TAN(ANGAB)*(DX-AX))*COS(ANGAB)*SIN(ANGAB)
2510 DCABY = DY-(RMP-TAN(ANGAB)*(DX-AX))*COS(ANGAB)*COS(ANGAB)
2520 BD2 = SQR((DCABX-AX)**2+(DCABY-AY)**2)
2530 IF D5*(I-1) > BD2 THEN GOTO 2570
```

```
2540 XDIST = BD2-D5*(I-1) : YDIST = SQR(RMP**2-XDIST**2)
2550 RDX(I) = DX + YDIST*SIN(ANGAB)-XDIST*COS(ANGAB)
2560 RDY(I) = DY - YDIST*COS(ANGAB)-XDIST*SIN(ANGAB) : GOTO 2600
2570 XDIST = D5*(I-1)-BD2 : YDIST = SQR(RMP**2 - XDIST**2)
2580 RDX(I) = DX + YDIST*SIN(ANGAB)+XDIST*COS(ANGAB)
2590 RDY(I) = DY - YDIST*COS(ANGAB) + XDIST*SIN(ANGAB)
2600 DDR(I) = SQR((RDX(I)-DATX(I))**2+(RDY(I)-DATY(I))**2)
2610 IF RDY(I) < DATY(I) THEN GOTO 2630
2620 DDR(I) = -1*DDR(I)
2630 HH = H1 - 2*(BY-RDY(I))
2640 DEL = (HH-((EXP(-((0.058*(ABS(LOG(HH/H1)))**1.257)+0.012)))*HH))/2
2650 DDR(I) = DDR(I) + DEL*COS((RDY(I)-AY)/(RDX(I)-AX))
2660 GOTO 2710
2670 RDX(I) = BX-(2*B2-D5*(I-1))/COS(ANGAB): RDY(I)=BY
2680 DDR(I) =-(2*B2-D5*(I-1))*TAN(ANGAB)
2690 DEL = (DELB*((2*B2-D5*(I-1))*TAN(ANGAB)))/(BX-BBX)
2700 DDR(I) = DDR(I)+DEL*COS(ANGAB)
2710 NEXT I
2720 FOR I = 1 TO H : V(I) = DRR(I)-DDR(I)
2730 NEXT I
2740 B(1) = 0 : B(10) = 0
2750 FOR I = 2 TO 9 : B(I) = V((I*2)-1) : NEXT I
2760 R = ((RMP+DELA)+SQR((BX-DX)**2 + (BY-DY)**2))/2
2770 AR = 2*ASIN(B2/RR) : AD = 2*ASIN(B2/R)
2780 CR = RR*AR : C = R*AD
2790 PRINT TAB(20);"CALCULATED ROLL DATA"
2800 PRINT TAB(18);'************************'
2810 PRINT
2820 PRINT USING 2830 : R
2830 FORM X4,'DEFORMED ROLL RADIUS            =',POS39,PIC(ZZ£.£££),X3,&
   & 'MM',SKIP1
2840 PRINT USING 2850 : AR
2850 FORM X4,'RIGID ROLL CONTACT ANGLE        =',POS39,PIC(ZZ£.£££),X3,&
   & 'RADS',SKIP1
2860 PRINT USING 2870 : AD
2870 FORM X4,'DEFORMED ROLL CONTACT ANGLE     =',POS39,PIC(ZZ£.£££),X3,&
```

```
     & 'RADS',SKIP1
2880 PRINT USING 2890 : CR
2890 FORM X4,'RIGID ROLL CONTACT LENGTH        =',POS39,PIC(ZZ£.£££),X3,&
     & 'MM',SKIP1
2900 PRINT USING 2910 : C
2910 FORM X4,'DEFORMED ROLL CONTACT LENGTH     =',POS39,PIC(ZZ£.£££),X3,&
     & 'MM',SKIP1
2920 PRINT
2930 PRINT
2940 PRINT TAB(11);"VERTICAL DEFORMATION OF ROLL ELEMENTS"
2950 PRINT TAB(9);'*****************************************'
2960 PRINT
2970 PRINT "     ELEMENT NO.     DISPLACEMENT (MICRONS)"
2980 PRINT
2990 FOR I = 1 TO 10
3000 PRINT USING 3010 : I , B(I)*1000
3010 FORM POS10,PIC(Z£),POS27,PIC(ZZ£.£),SKIP1
3020 NEXT I
3030 PRINT
3040 FOR I = 1 TO 10 : BSUM(I) = BSUM(I)+B(I) : NEXT I
3050 RRSUM = RRSUM + R : CRRSUM = CRRSUM + CR
3060 CSUM = CSUM + C : ARSUM = ARSUM + AR : ADSUM = ADSUM + AD
3070 COUNT2 = COUNT2 + 1 : PCT = PCT + 1
3080 IF COUNT2 < NSC*NPS THEN GOTO 1360
3090 REM  MEAN OF SECTIONAL PARAMETERS
3100 FOR I = 1 TO 10 : B(I) = BSUM(I)/COUNT2 : NEXT I
3110 R = RRSUM / COUNT2 : CR = CRRSUM / COUNT2 : C = CSUM / COUNT2
3120 AR = ARSUM / COUNT2 : AD = ADSUM / COUNT2
3130 PRINT
3140 PRINT TAB(15);'* * * * * * * * * * * * * * * *'
3150 PRINT
3160 PRINT TAB(20);'MEAN ROLL DATA'
3170 PRINT TAB(18);'*******************'
3180 PRINT
3190 PRINT USING 3200 : R
3200 FORM X4,'DEFORMED ROLL RADIUS             =',POS39,PIC(ZZ£.£££),X3,&
```

```
   & 'MM',SKIP1
3210 PRINT USING 3220 : AR
3220 FORM X4,'RIGID ROLL CONTACT ANGLE        =',POS39,PIC(ZZ£.£££),X3,&
   & 'RADS',SKIP1
3230 PRINT USING 3240 : AD
3240 FORM X4,'DEFORMED ROLL CONTACT ANGLE     =',POS39,PIC(ZZ£.£££),X3,&
   & 'RADS',SKIP1
3250 PRINT USING 3260 : CR
3260 FORM X4,'RIGID ROLL CONTACT LENGTH       =',POS39,PIC(ZZ£.£££),X3,&
   & 'MM',SKIP1
3270 PRINT USING 3280 : C
3280 FORM X4,'DEFORMED ROLL CONTACT LENGTH    =',POS39,PIC(ZZ£.£££),X3,&
   & 'MM',SKIP1
3290 PRINT
3300 PRINT
3310 PRINT TAB(13);'MEAN DEFORMATION OF ROLL ELEMENTS'
3320 PRINT TAB(11);'*************************************'
3330 PRINT
3340 PRINT "     ELEMENT NO.     DISPLACEMENT (MICRONS)"
3350 PRINT
3360 FOR I = 1 TO 10
3370 PRINT USING 3380 : I , B(I)*1000
3380 FORM POS10,PIC(Z£),POS27,PIC(ZZ£.£),SKIP1
3390 NEXT I
3400 PRINT
3410 PRINT TAB(15);'* * * * * * * * * * * * * * * *'
3420 PRINT
3430 PRINT
3440 REM  INFLUENCE CONSTANT EVALUATION
3450 PRINT ;'DO YOU WISH TO CONTINUE ? IF YES TYPE 1'
3460 INPUT CONT
3470 IF CONT < > 1 THEN GOTO 4430
3480 PRINT
3490 PRINT 'INPUT APPLIED LOAD'
3500 INPUT Z6
```

```
3510 PRINT 'INPUT STARTING VALUE OF I.C. ESTIMATE'
3520 INPUT AS
3530 PRINT 'INPUT FINISHING VALUE OF I.C. ESTIMATE'
3540 INPUT AF
3550 PRINT 'INPUT STEP OF INCREMENT OF I.C.'
3560 INPUT AST
3570 FOR A = AS TO AF STEP AST
3580 FOR I = 1 TO 10 : B(I) = BSUM(I)/COUNT2 : NEXT I
3590 S1 = C / 10
3600 S2 = A * S1
3610 M = 10
3620 N = 10
3630 FOR I = 1 TO N
3640 FOR J = 1 TO M
3650 S9 = S1 * ABS( 2 * ABS ( I - J ) - 1 ) / 2
3660 IF I < > J THEN GOTO 3700
3670 AA(I,J) = ((S1-S9) * LOG (S2 / (S1-S9)) + S9 * LOG(S2 / S9))
3680 AA(I,J) = ( 2 * ( AA(I,J)) + ( 1 - PO ) * S1 ) / PI / E
3690 GOTO 3720
3700 AA(I,J) = ((S1+S9) * LOG (S2 / (S1+S9)) - S9 * LOG(S2 / S9))
3710 AA(I,J) = ( 2 * ( AA(I,J)) + ( 1 - PO ) * S1 ) / PI / E
3720 NEXT J
3730 NEXT I
3740 N1 = 10
3750 N = 10
3760 FOR F = 1 TO N1
3770 U = AA(F,F)
3780 F1 = F + 1
3790 REM CHECKING FOR SINGULARITY
3800 IF ABS(U) < 0.000001 THEN GOTO 3960
3810 REM DIVIDE THE ROW BY THE DIAGONAL ELEMENT
3820 FOR J = F1 TO N
3830 AA(F,J) = AA(F,J) / U
3840 NEXT J
3850 B(F) = B(F) / U
3860 REM ELIMINATION BY SUBTRACTION
3870 FOR I = F1 TO N
3880 U = AA(I,F)
```

```
3890 FOR J = F1 TO N
3900 AA(I,J) = AA(I,J) - U * AA(F,J)
3910 NEXT J
3920 B(I) = B(I) - U * B(F)
3930 NEXT I
3940 NEXT F
3950 IF ABS(AA(N,N)) > 0.000001 THEN GOTO 3990
3960 PRINT 'SINGULARITY IN ROW';F
3970 PRINT 'DETERMINANT = 0.0'
3980 GOTO 4430
3990 REM BACK SUBSTITUTION
4000 FOR G = 1 TO N1 - 1
4010 F = N - G
4020 F1 = F + 1
4030 FOR J = F1 TO N
4040 B(F) = B(F) - AA(F,J) * B(J)
4050 NEXT J
4060 NEXT G
4070 D = 1
4080 FOR I = 1 TO N
4090 D = D * AA(I,I)
4100 NEXT I
4110 FOR I = 1 TO N
4120 P(I) = B(I)
4130 NEXT I
4140 U = 0
4150 FOR I = 1 TO N
4160 U = U + P(I)
4170 NEXT I
4180 Q = U / N
4190 W1 = C * Q * W * 1000
4200 IF 0 > W1 THEN GOTO 4220
4210 IF W1 < Z6 THEN GOTO 4230
4220 NEXT A
4230 COUNT3 = COUNT3 + 1
4240 IF COUNT3 = 4 THEN GOTO 4300
```

```
4250 AS = A - AST : AF = A : AST = AST/10
4260 PRINT
4270 PRINT USING 4280 : A , W1
4280 FORM X4,'INF. CONST. =',POS22,PIC(ZZZZ£.£££),POS35,&
  & 'CALC LOAD =',POS48,PIC(ZZZZ£.£££),X3,'KN',SKIP1
4290 GOTO 3570
4300 PRINT
4310 PRINT
4320 PRINT TAB(15);'RESULTS ASSOCIATED WITH INF. CONSTANT'
4330 PRINT TAB(13);'******************************************'
4340 PRINT
4350 PRINT USING 4360 : Z6
4360 FORM X4,'APPLIED LOAD               =',POS32,PIC(ZZZ£.£),X3,'KN',SKIP1
4370 PRINT USING 4380 : W1
4380 FORM X4,'CALCULATED LOAD            =',POS32,PIC(ZZZ£.£),X3,'KN',SKIP1
4390 PRINT USING 4400 : Q*10**6
4400 FORM X4,'MEAN PRESSURE VALUE        =',POS32,PIC(ZZZ£.£),X3,'N MM-2',&
  & SKIP1
4410 PRINT ;'    INFLUENCE CONSTANT      =    ';A
4420 PRINT ;'    LOG INF. CONSTANT       =    ';LOG(A)
4430 STOP
```

APPENDIX III

REPRESENTATIVE SECTIONS OF COMPUTER PRINT-OUT RELATING TO THE ANALYSIS OF A TYPICAL INTERRUPTED-PASS ROLLING TEST

(a) Profile measurement along a typical section (print-out from the Merlin 750M Metrology System).

(b) Curve-fit analysis of a typical section : Influence constant evaluation program.

(c) Mean roll data and influence constant evaluation : Influence constant evaluation program.

(d) Vertical displacement of discretised elements and predicted pressure distribution along a typical section : Pressure distribution program.

(e) Summary of sectional data and separating load evaluation : Pressure distribution program.

(a)

NOMINAL STRIP WIDTH = 60
STRIP CODE = I
REDUCTION NUMBER = 3
SIDE = 2
SECTIONAL STRIP WIDTH = 61.43

SECTION # 1 : POFILE MEASUREMENT

X Z COORDINATES AT .5 WIDTH

No.	Xvalue	Zvalue
1	.005	-.001
2	.515	.006
3	1.016	.009
4	1.511	-.030
5	2.012	-.073
6	2.510	-.114
7	3.010	-.155
8	3.521	-.195
9	4.020	-.249
10	4.521	-.268
11	5.006	-.300
12	5.512	-.334
13	6.015	-.364
14	6.515	-.392
15	7.010	-.416
16	7.511	-.439
17	8.006	-.460
18	8.509	-.481
19	9.007	-.501
20	9.505	-.517
21	10.007	-.535
22	10.506	-.550
23	11.007	-.563
24	11.503	-.576
25	12.005	-.586
26	12.509	-.598
27	13.008	-.607
28	13.510	-.615
29	14.010	-.623
30	14.512	-.630
31	15.007	-.637
32	15.507	-.641
33	16.010	-.645
34	16.510	-.648
35	17.013	-.652
36	17.508	-.656
37	18.009	-.659
38	18.510	-.660
39	19.011	-.658
40	19.509	-.654
41	20.009	-.655

nodes used for profile evaluation

SECTION 6 PASS 1
****

MEASURED NODAL DATA

NODE	X CO-ORDINATE (MM)	Z CO-ORDINATE (MM)
1	0.000	-.5760
2	0.500	-.5630
3	1.000	-.5500
4	1.500	-.5350
5	2.000	-.5170
6	2.500	-.5010
7	3.000	-.4810
8	3.500	-.4600
9	4.000	-.4390
10	4.500	-.4160
11	5.000	-.3920
12	5.500	-.3640
13	6.000	-.3340
14	6.500	-.3000
15	7.000	-.2680
16	7.500	-.2490
17	8.000	-.1950
18	8.500	-.1550
19	9.000	-.1140
20	9.500	-.0730

PERCENTAGE OF READINGS ACCEPTABLE = 31
MEASURED RADIUS = 158.107

CALCULATED ROLL DATA

DEFORMED ROLL RADIUS	=	158.161	MM
RIGID ROLL CONTACT ANGLE	=	0.168	RADS
DEFORMED ROLL CONTACT ANGLE	=	0.134	RADS
RIGID ROLL CONTACT LENGTH	=	21.281	MM
DEFORMED ROLL CONTACT LENGTH	=	21.272	MM

VERTICAL DEFORMATION OF ROLL ELEMENTS

ELEMENT NO.	DISPLACEMENT (MICRONS)
1	0.0
2	32.7
3	56.6
4	72.3
5	80.3
6	80.7
7	73.3
8	58.1
9	34.5
10	0.0

```
DEFORMED ROLL RADIUS            = 153.726   MM
RIGID ROLL CONTACT ANGLE        =   0.165   RADS
DEFORMED ROLL CONTACT ANGLE     =   0.137   RADS
RIGID ROLL CONTACT LENGTH       =  20.971   MM
DEFORMED ROLL CONTACT LENGTH    =  20.964   MM


          MEAN DEFORMATION OF ROLL ELEMENTS
      **************************************

ELEMENT NO.    DISPLACEMENT (MICRONS)

      1                  0.0
      2                 27.8
      3                 47.9
      4                 61.1
      5                 67.9
      6                 68.3
      7                 62.2
      8                 49.4
      9                 29.5
     10                  0.0

           * * * * * * * * * * * * * * * *


DO YOU WISH TO CONTINUE ? IF YES TYPE 1
 ?
1

INPUT APPLIED LOAD
 ?
688
INPUT STARTING VALUE OF I.C. ESTIMATE
 ?
10
INPUT FINISHING VALUE OF I.C. ESTIMATE
 ?
100
INPUT STEP OF INCREMENT OF I.C.
 ?
10

    INF. CONST. =       20.000    CALC LOAD =     400.163    KN

    INF. CONST. =       11.000    CALC LOAD =     672.423    KN

    INF. CONST. =       10.800    CALC LOAD =     686.764    KN


          RESULTS ASSOCIATED WITH INF. CONSTANT
      *****************************************

APPLIED LOAD             =      688.0    KN
CALCULATED LOAD          =      687.5    KN
MEAN PRESSURE VALUE      =      546.6    N MM-2
INFLUENCE CONSTANT       =      10.79
LOG INF. CONSTANT        =      2.37862
```

(d)

SECTION 6 PASS 1

CALCULATED ROLL DATA

DEFORMED ROLL RADIUS	=	146.848	MM
RIGID ROLL CONTACT ANGLE	=	0.161	RADS
DEFORMED ROLL CONTACT ANGLE	=	0.140	RADS
RIGID ROLL CONTACT LENGTH	=	20.503	MM
DEFORMED ROLL CONTACT LENGTH	=	20.497	MM

VERTICAL DEFORMATION OF ROLL ELEMENTS

ELEMENT NO.	DISPLACEMENT (MICRONS)
1	0.0
2	20.1
3	34.5
4	43.9
5	48.8
6	49.1
7	44.9
8	36.0
9	21.8
10	0.0

ESTIMATED ELEMENT PRESSURES

ELEMENT NO.	PRESSURE (N MM-2)
1	- 757.3
2	364.2
3	602.1
4	734.5
5	801.1
6	809.3
7	761.1
8	640.2
9	449.9
10	- 821.7

MEAN PRESSURE ACROSS SECTION = 358.4 N MM-2

(e)

SUMMARY OF SECTIONAL DATA
****

SECTION NO.	MEAN PRESSURE (N MM-2)	CONTACT LENGTH (MM)
1 - 1	225.6	20.0
2 - 1	430.9	20.8
3 - 1	586.3	21.4
4 - 1	400.0	20.7
5 - 1	103.6	19.6
6 - 1	358.4	20.5
7 - 1	539.9	21.2
8 - 1	581.6	21.3
9 - 1	478.8	20.9
10 - 1	191.3	19.9

MEAN PRESSURE ACROSS STRIP = 432.1 N MM-2
MEAN CONTACT LENGTH ACROSS STRIP = 20.62 MM

* * * * * * * * * * * * * * * *
* * * * * * * * * * * * * * *
* * ROLL FORCE = 534.7 KN * *
* * * * * * * * * * * * * * *
* * * * * * * * * * * * * * * *

APPENDIX IV

FINITE ELEMENT ANALYSIS OF THE ELASTIC BEHAVIOUR ALONG THE INDENTOR SURFACE DURING LOADING

Introduction

By imposing the predicted pressure distributions, an attempt was made to theoretically determine the elastic deformation of the indentor body along the interface with the deforming strip. An analysis using the finite element method was employed in which the body of the indentor was discretised into a number of sub-regions, referred to as elements. Adjoining elements were connected together at points, referred to as nodes. A matrix describing the stiffness of each element was created, then merged to form a global stiffness matrix to represent the whole indentor. This was possible since nodes common to more than one element must have the same displacement.

Application of the Finite Element Method Using the PAFEC Computer Package

The PAFEC finite element computer package[55, 56] was used to perform the elastic analysis on the geometry of the indentors whilst subject to static loading conditions. The indentors were modelled three-dimensionally using combinations of twenty noded isoparametric brick elements and fifteen noded isoparametric triangular prism elements. The mesh was generated using the automatic mesh generation facilities in the package, referred to as PAFBLOCKS. Consideration of the symmetrical planes and the regions of pressurisation, reduced the models to a quarter of the actual structure when deforming flat specimens, and half when deforming inclined specimens.

The pressure activities appertaining to each loading configuration were discretised and applied at the appropriate nodes along the indentor surface. Restraint of the nodes along the surface of the roll neck, which represent the points in contact with the ram, allow the solution to proceed. Nodal displacements are determined by relating the stiffness of each element as represented by the global stiffness matrix to the restrained pressure system.

The analysis was performed using the Polytechnic IBM 4341 computer facilities.

Structure of the Models

Schematic representations of the model structures corresponding to both loading configurations are shown in figures AIV.1 and AIV.2.

Figures AIV.3 and AIV.4 show detail of the mesh structures at transverse sections through the centre of the indentor bodies. The relatively fine mesh in the vicinity of the pressurised regions helps reduce computational errors.

Analysis of Results

Finite element models were formulated to represent the indentor structures when subjected to the predicted pressurising conditions appertaining to each static indentation test.

A comparison between the theoretical and empirical interpretations of the elastic behaviour along the indentor surfaces were established by post-processing the finite element results. The appropriate nodal displacements were selected from each finite element solution, and employed in the determination of the deformed indentor radius along the contact arc at the centre of the pressure activity.

To minimise the effects of indentor bending, the nodal displacement in the Y direction diametrically opposite the pressure activity was subtracted from the central node. The amended nodal displacement was related to the rigid indentor configurations to evaluate the deformed indentor radius.

Values of the deformed indentor radius appertaining to both forms of solution are listed in table AIV.1.

<u>Discussions and Conclusions</u>

The finite element method of analysis has proved effective in the modelling of numerous practical engineering components subject to varying loading conditions. However, the current investigation has not effectively adapted the analysis for the reasons discussed later.

Consideration of the deformed indentor radius values listed in table AIV.4 reveal the following salient points:

(i) Indentation of flat specimens : Although investigations were undertaken on a limited scale, the correlation between the deformed indentor radius values derived from the finite element and profile measurement methods was satisfactory.

(ii) Indentation of inclined specimens : Subject of a more rigorous investigation which reveal substantial discrepancies between the deformed indentor radius values derived from the finite element and profile measurement methods. For the 5° inclination angle the finite element values adhere to the trends developed by the profile measurement method. However, for the larger inclination angles these trends were undetectable.

The discrepancies described in (ii) highlight the ineffectiveness of the finite element method in the present application. These can be attributed to the requirement of modelling the indentors using systems of three-dimensional elements. Consequently relatively course meshes were developed to avoid excessive c.p.u. time.

The configurations appertaining to the interrupted-pass rolling conditions have not been attempted using the finite element method during the current investigation. Under these conditions, the depth of work required to develop a satisfactory model can be assessed by considering [21-30] and would constitute a project in its own right.

TABLE AIV.1

A COMPARISON BETWEEN DEFORMED INDENTOR RADIUS VALUES DETERMINED USING THE FINITE ELEMENT AND PROFILE MEASUREMENT METHODS

(I) Deformation of Flat Specimens

STRIP WIDTH /mm	APPLIED LOAD /mm	DEFORMED INDENTOR RADIUS	
		FINITE ELEMENT METHOD /mm	PROFILE MEASUREMENT METHOD /mm
30	300	38.25	38.07
40	300	38.57	38.23
50	300	38.71	38.17
60	300	38.75	38.68
70	300	38.70	38.08

(II) Deformation of Inclined Specimens

(a) 75mm Ø Indentor:

ANGLE OF INCLINE /°	STRIP WIDTH /mm	APPLIED LOAD /kN	DEFORMED INDENTOR RADIUS	
			FINITE ELEMENT METHOD /mm	PROFILE MEASUREMENT METHOD /mm
5	30	200	46.51	43.82
		300	43.35	41.81
		400	42.6	40.35
	40	200	39.66	46.05
		250	39.49	44.02
		300	39.31	42.65
		350	39.17	42.45
		400	39.98	41.86
		450	38.89	41.4
	50	200	39.60	47.63
		300	39.46	44.57

TABLE AIV.1 (cont)

ANGLE OF INCLINE /°	STRIP WIDTH /mm	APPLIED LOAD /kN	DEFORMED INDENTOR RADIUS	
			FINITE ELEMENT METHOD /mm	PROFILE MEASUREMENT METHOD /mm
5	50	400	39.25	43.18
	60	200	39.57	49.95
		300	39.56	46.82
		400	39.46	44.71
10	30	200	41.61	43.13
		300	41.38	41.74
		400	38.36	40.55
	40	200	38.38	45.03
		250	38.36	43.33
		300	38.34	42.01
		350	38.16	41.7
		400	38.27	41.22
		450	38.32	41.38
	50	200	38.36	44.82
		300	38.35	43.25
		400	38.23	42.82
	60	200	38.34	46.98
		300	38.42	43.23
		400	39.89	43.38
15	30	200	40.12	41.62
		300	40.19	40.52
		400	37.93	39.92
	40	200	38.00	43.18
		250	38.00	42.81
		300	38.02	41.54
		350	38.00	42.18
		400	38.14	42.15

TABLE AIV.1 (cont)

ANGLE OF INCLINE /°	STRIP WIDTH /mm	APPLIED LOAD /kN	DEFORMED INDENTOR RADIUS	
			FINITE ELEMENT METHOD /mm	PROFILE MEASUREMENT METHOD /mm
15	40	450	38.09	42.17
	50	200	37.91	47.45
		300	37.96	44.82
		400	38.00	43.4
	60	200	37.86	50.2
		300	37.92	47.16
		400	37.97	44.5

(b) 100mm Ø Indentor:

5	30	400	51.89	54.73
	40	400	52.37	55.37
	50	400	52.58	57.02
	60	400	52.63	59.32
10	30	400	50.87	54.66
	40	400	50.98	56.26
	50	400	51.02	57.16
	60	400		59.98
15	30	400	50.57	54.43
	40	400	50.64	55.22
	50	400	50.66	56.19
	60	400	50.88	59.19

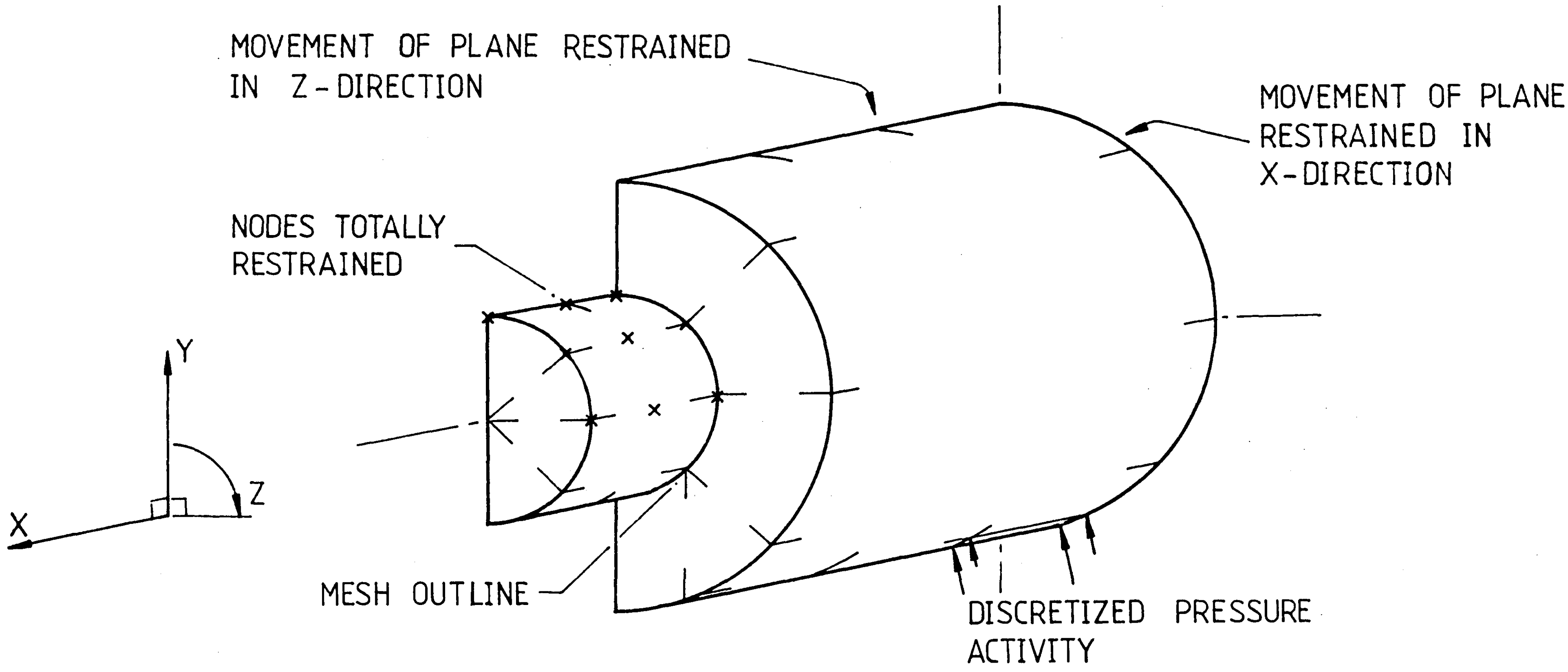

FIG AIV.1 : SCHEMATIC REPRESENTATION OF THE FINITE ELEMENT STRUCTURE OF THE INDENTOR : INDENTATION OF FLAT SPECIMENS

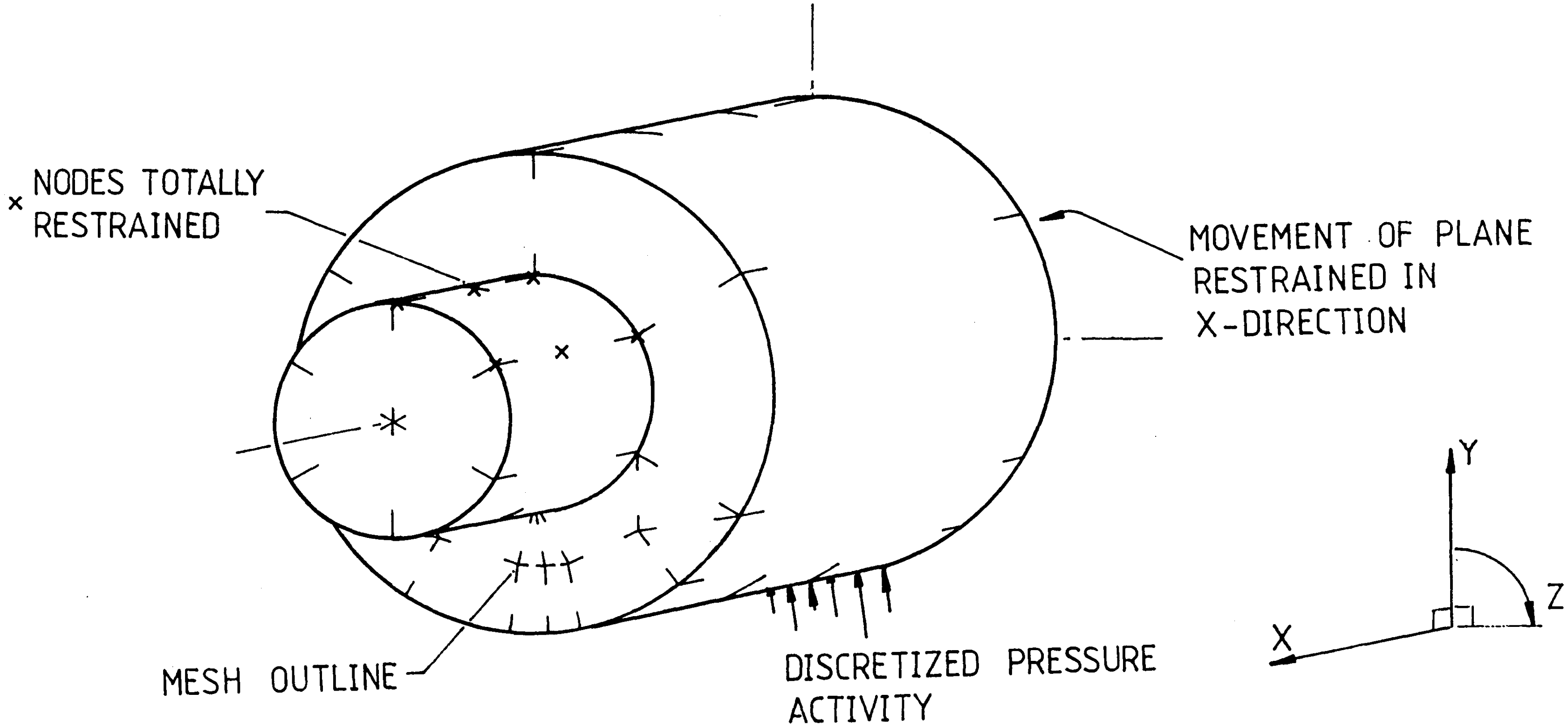

FIG AIV.2 : SCHEMATIC REPRESENTATION OF THE FINITE ELEMENT STRUCTURE OF THE INDENTOR : INDENTATION OF INCLINED SPECIMENS

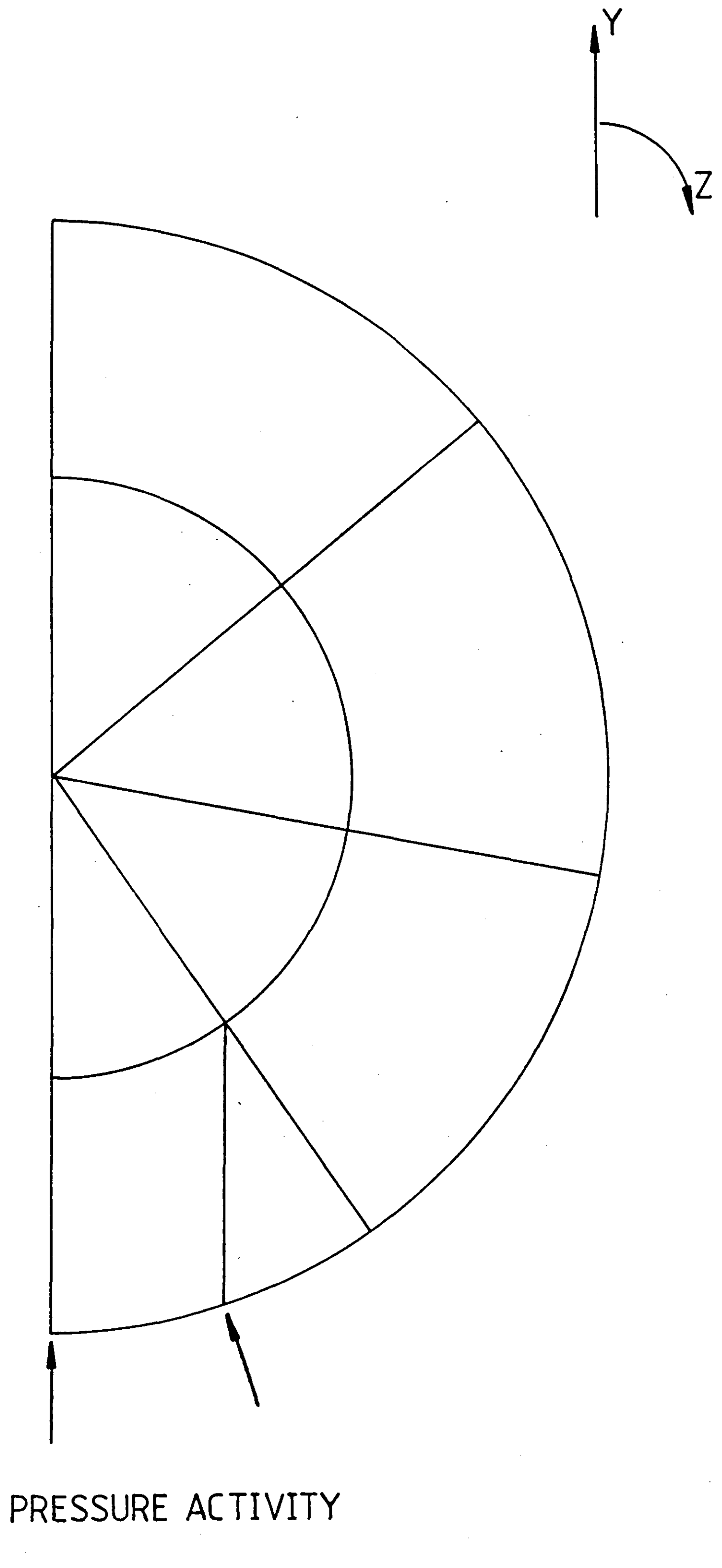

FIG AIV.3 : FINITE ELEMENT MESH OF INDENTOR BODY : INDENTATION OF FLAT SPECIMENS

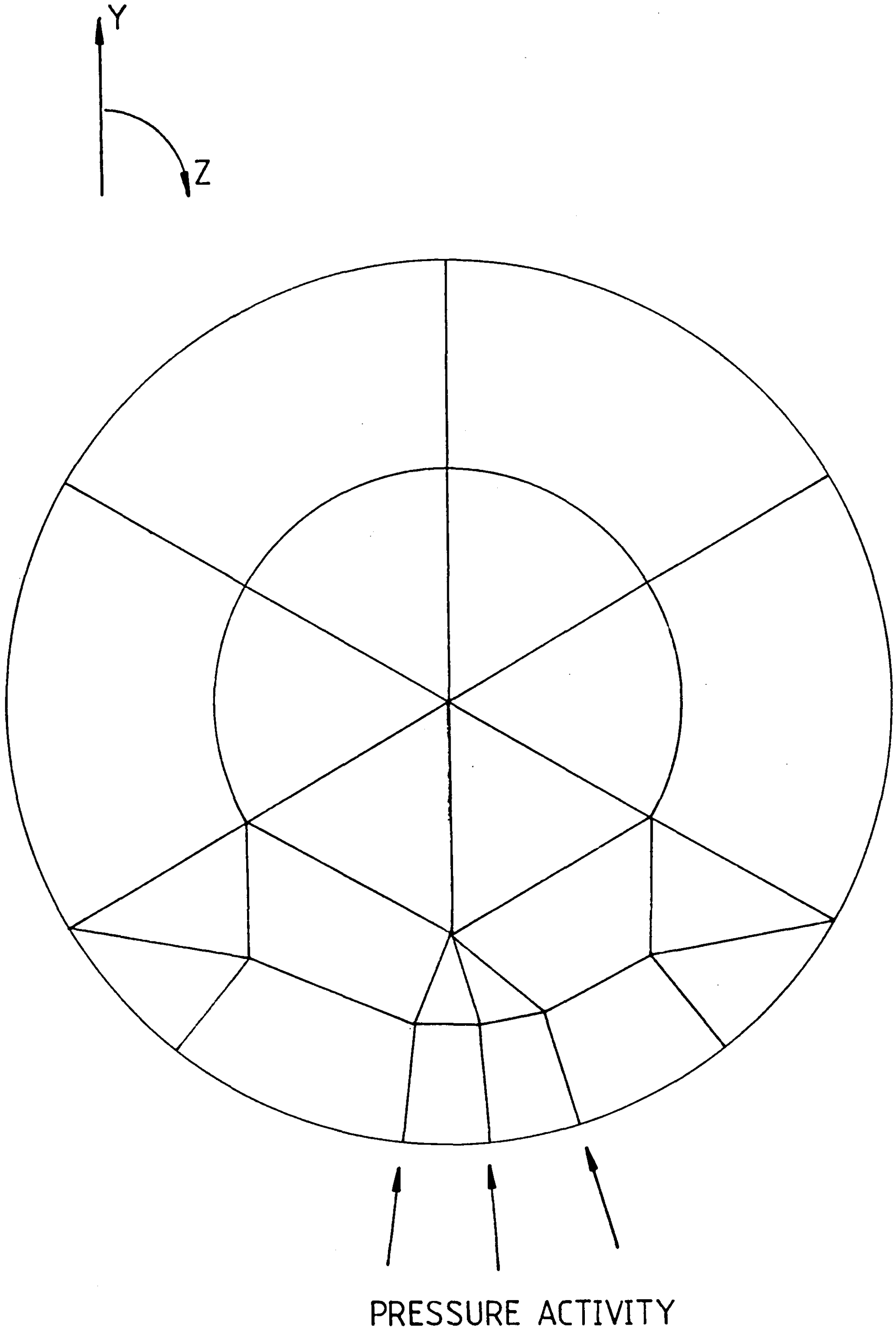

FIG AIV.4 : FINITE ELEMENT MESH OF INDENTOR BODY : INDENTATION OF INCLINED SPECIMENS

APPENDIX V

AN ASSESSMENT OF THE WORKPIECE FORM FOLLOWING A SERIES OF INTERRUPTED ROLLING PASSES

To provide an assessment of the workpiece form following a series of interrupted rolling passes, a detailed inspection of a representative workpiece was performed.

The inspection was undertaken using the Merlin 750M Metrology System in conjunction with the part-program previously formulated for the measurement of imparted roll profiles. Descriptions of the measuring system and the operational procedures are detailed in sections 3.4 and 3.5, respectively.

The format of the measurement sequence remained unaltered from that schematically shown in figure 3.4. However, measurements were established at an increased number of sections across the width of the workpiece. The scan along each section was extended further along the entrance and exit planes with a reduced number of increments. Locations of the nodal measurements on the upper and lower surfaces were symmetric along the longitudinal planes of the workpiece.

Transverse surface profiles were established by relating the probing depths at representative sections across the workpiece. Figures AV.1(a) to (c) show the profiles across both surfaces corresponding to sections through the entry plane, deforming arc region and exit plane, respectively.

Inspection of each pair of representative profiles clearly reveals the effects of 'edge drop'. This term describes the phenomenon in which the workpiece material is thicker at the centre of the strip width than at the edges. This effect occurs when reducing the strip workpiece between parallel sided rolls which are prone to flexural deflection during operation. Considerable efforts have been made over the years to improve the dimensional uniformity of the reduced strip material. The most commonly used method in commercial rolling is to camber the surfaces of the rolls.

The other phenomenon which can be clearly identified by inspecting the profiles is the 'bowing' of the workpiece material across the strip width. This may be attributable to the absence of external tensions being applied to the workpiece during deformation.

WORKPIECE DETAILS.

FIG AV.1 : TRANSVERSE SURFACE PROFILES

Strip Width = 100 mm

Initial Thickness = 8.5 mm

Final Thickness = 7.7 mm

Reduction Number = 4

SECTIONAL DETAILS.

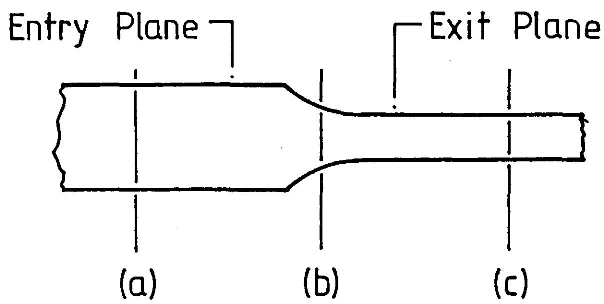

TRANSVERSE SURFACE PROFILES.

Section (a) - Entry Plane

Upper Surface

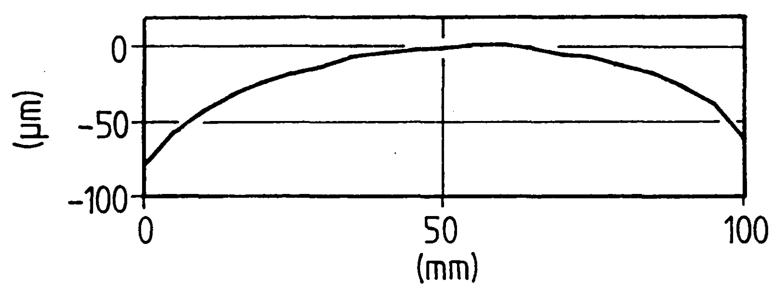

Lower Surface

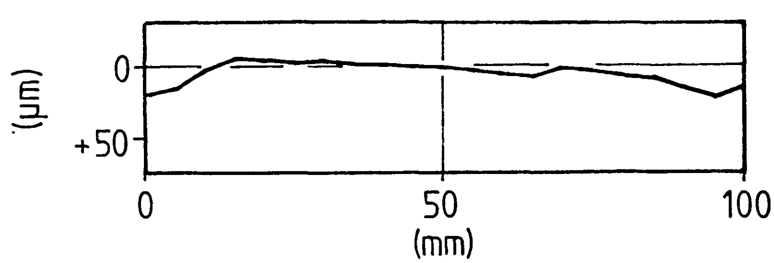

Section (b) - Deforming Arc Region

Upper Surface

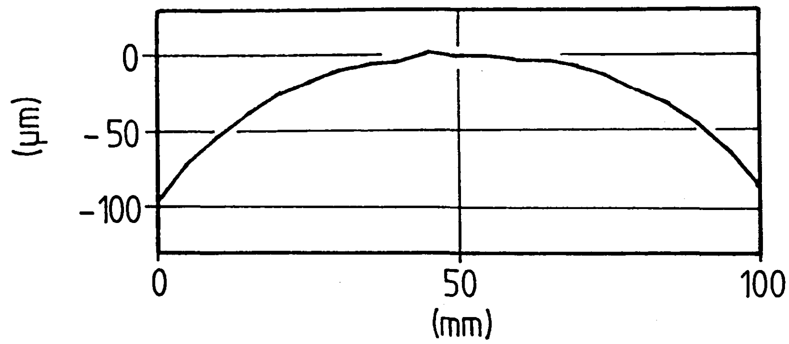

Lower Surface

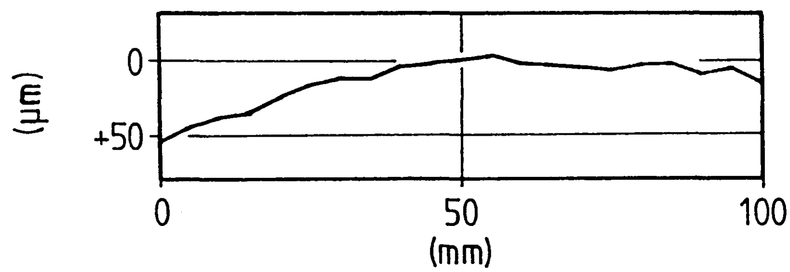

Section (c) - Exit Plane

Upper Surface

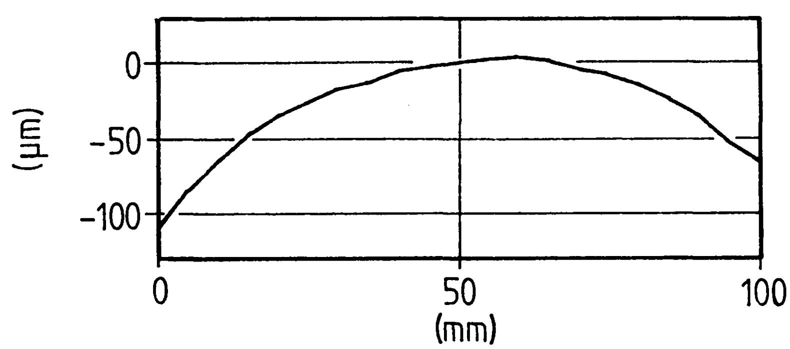

Lower Surface